NIR Absorbing TCBD and DCNQ Functionalized Phenothiazines

Ph.D. Thesis

By

PANKAJ KUMAR GUPTA

DEPARTMENT OF CHEMISTRY
INDIAN INSTITUTE OF TECHNOLOGY INDORE

July 2024

NIR Absorbing TCBD and DCNQ Functionalized Phenothiazines

A THESIS

Submitted in partial fulfillment of the requirements for the award of the degree

of

DOCTOR OF PHILOSOPHY

by

PANKAJ KUMAR GUPTA

DEPARTMENT OF CHEMISTRY
INDIAN INSTITUTE OF TECHNOLOGY INDORE

July 2024

INDIAN INSTITUTE OF TECHNOLOGY INDORE

CANDIDATE'S DECLARATION

I hereby certify that the work which is being presented in the thesis entitled **"NIR Absorbing TCBD and DCNQ Functionalized Phenothiazines"** in the partial fulfillment of the requirements for the award of the degree of **DOCTOR OF PHILOSOPHY** and submitted in the **Department of Chemistry, Indian Institute of Technology Indore**, is an authentic record of my own work carried out during the time period from **July 2019** to **July 2024** under the supervision of **Dr. Rajneesh Misra, Professor, Department of Chemistry, IIT Indore**.

I have not submitted the matter presented in this thesis for the award of any other degree of this or any other institute.

31.07.2024

Signature of the Student with date
(PANKAJ KUMAR GUPTA)

This is to certify that the above statement made by the candidate is correct to the best of my knowledge.

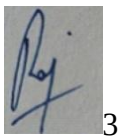
31/7/24

Signature of Thesis Supervisor with date

(Dr. RAJNEESH MISRA)

PANKAJ KUMAR GUPTA has successfully given his Ph.D. Oral Examination held on ……

Signature of Chairperson (OEB)
Date:

Signature of External Examiner
Date:

Signature(s) of Thesis Supervisor(s)
Date:

Signature of PSPC Member #1
Date:

Signature of PSPC Member #2
Date:

ACKNOWLEDGEMENTS

All praise and glory be to the Almighty, the Most Merciful and the embodiment of Satchidananda, Lord **Shri Kanha Ji**. His divine blessings, strength, and patience have granted me the opportunity to complete this study.

The work in this thesis could not have been done without the help of many people who were always there for me when I needed them the most. This is my time to thank them sincerely for their assistance in making it possible for me to complete this long journey of Ph.D.

First and foremost, I would like to express my sincere gratitude to my thesis supervisor, Prof. Rajneesh Misra, for always being there for me, encouraging me during my studies and research, and providing insightful guidance and unwavering support, which have been pivotal in the successful completion of this research. I would like to express my heartfelt gratitude to him for his help in developing my career and for believing in me right from the beginning. He has always helped me get the best out of every situation and his determination to do well even when things are difficult has inspired me to strive for excellence. I would not have been able to complete this task without his excellent leadership, constant encouragement, and careful supervision throughout the journey.

I extend my profound thanks to my PSPC members Dr. Amrendra Kumar Singh and Dr. Umesh A. Kshirsagar, for their guidance, valuable suggestions, and counsel during my journey of Ph.D. as a supervisor. With great respect, I would like to express my special thanks and gratitude to Prof. Suhas S. Joshi [Director, Indian Institute of Technology Indore] for providing and accessing all the facilities at the Indian Institute of Technology Indore.

I am grateful to Prof. Tushar Kanti Mukherjee (Head, Department of Chemistry, Indian Institute of Technology Indore) for his suggestions and guidance in various aspects. I am also grateful to Prof. Suman Mukhopadhyay, Prof. Apurba K. Das, Prof. Sampak Samanta,

Prof. Biswarup Pathak, Prof. Sanjay Kumar Singh, Dr. Tridib Kumar Sarma, Prof. Anjan Chakraborty, Prof. Satya S. Bulusu, Prof. Shaikh M. Mobin, Prof. Chelvam Venkatesh, Dr. Debayan Sarkar, Dr. Abhinav Raghuvanshi, Dr. Dipak Kumar Roy, Dr. Selvakumar Sermadurai, and Dr. Pravarthana Dhanapal for their guidance and help during various activities. I am thankful to the technical staff of Sophisticated Instrumentation Centre (SIC), IIT Indore, Mr. Kinney Pandey, Mr. Ghansyam Bhavsar, Mr. Atul and, to Mr. Manish Kushwaha, Mrs. Vinita Kothari, Mr. Rameshwar and Mr. Souvik for their technical help and support. I would like to extend my gratitude to the Indian Institute of Technology Indore for its excellent infrastructure and to the University Grants Commission (UGC), New Delhi, for providing financial support through the fellowship.

I would like to acknowledge all my teachers who have taught me in some or the other way since my school time. I would have never achieved anything without their guidance, blessing, and support. I am thankful to Mr. Sushil Mishra (Lecturer, RIC College Gonda, U.P.) for his guidance and support. I would like to extend my deepest gratitude to Dr. Saurabh Mishra (Assistant Professor, M.L.K. PG College, Balrampur) who guided me during my post-graduation studies and inspired me to pursue a career in research. I would also like to extend my sincere thanks to the other faculties, Prof. Rajesh Kumar Singh (Professor), Prof. Mohiuddin Ansari (Professor), and Dr. Sunil Kumar Mishra (Assistant Professor) of M.L.K. PG College, Balrampur for their guidance and support. I am thankful to Dr. Sanjeev Kumar Shukla (Sr. Scientist Central Drug Research Institute, Lucknow) for his guidance and support. I am also thankful to Dr. Aniruddh Chaudhary (Assistant Professor Uday Pratap Autonomous College, Varanasi) for his guidance and support.

I would like to personally extend my heartfelt gratitude to my Ph.D. mentor, Dr. Faizal Khan, for his unwavering guidance, support, and assistance throughout my journey, especially during the initial stages of my Ph.D. program and through all my ups and downs. I take this opportunity to express a deep sense of gratitude to my group

members, Dr. Yuvraj Patil, Dr. Madhurima Poddar, Dr. S. Bijesh, Dr. Yogajivan Rout, Dr. Anupama Ekbote, Dr. Indresh Singh Yadav, Dr. Manju Sheokand, Dr. Charu Popli, Dr. Dilip Pinjari, Mr. Mohd. Wazid, Mr. Nikhil Ji Tiwari, Mr. Ramakant Gavale, Mr. Amiy Krishna, Mr. Nitin Rajesh, Ms. Kusum Yadav, Ms. Shivangi Jitendra Tiwari, Ms. Akanksha Dwivedi, Mr. Vivak Kandpal, Ms. Deeksha Gupta, Kusagra, Sandeep, Nitish, Sudhanshu, Ashwani, Pratiksha and Gourav for their kind cooperation and cheerful support.

It has been a wonderful experience working alongside many friends and labmates throughout my Ph.D. journey. I would like to extend my gratitude to Dr. Vasant, Dr. Divya, Dr. Soumitra, Dr. Rishi, Dr. Mahendra, Dr. Reena, Dr. Devraj, Dr. Meher, Dr. Ankit, Dr. Neha, Dr. Bhanu, Dr. Kamal Prakash, Dr. Diptangshu, Mr. Rahul K. Singh, Mr. Shambhu, Mr. Navdeep, Ms. Nida, Ms. Vaishnavi, Ms. Ekta, Ms. Achena, Ms. Likhi, Mr. Naveen, Mr. Shivendu, Mr. Sayantan, Mr. Argha, Mr. Debanjan, Mr. Sanjeev, Mr. Shivendra, Mr. Pawan, Mr. Praveen, Mrs. Meenu, Mrs. Rajni, Ms. Shikha, Mr. Bhanu, Mr. Durgesh, Mr. Rakesh, Mr. Aashu, Mr. Dilip, Mrs. Darakshan, Mr. Kaluram, Mr. Laxman, Mr. Rajesh, Mr. Rahul, Mr. Ramakant, Mr. Hashmat, Mr. Tushar, Mr. Deepak, Mr. Raju, Ms. Priyanka, Ms. Deepti and Mr. Vishal. I would like to extend my gratitude to a few close friends for creating a stimulating and fun-filled environment. My special thanks go to Ms. Suchi, Mr. Sujeet, Mr. Avnish, Mrs. Sandhya, Mrs. Arunima, Ms. Nidhi, Mr. Aashish, Mr. Bashir, Mr. Nageshwar, Mr. Vivek, Mr. Chandan, Mr. Satish, Mr. Shubham, Mr. Rajneesh, Mr. Mukhtar, Mr. Vikrant, Mr. Mohit, Mr. Amit, Mr. Ashtbhuj and Mr. Yogesh.

Most importantly none of these would have been possible without the blessing of my grandfather Late Shri Rangilal Kasaudhan and my grandmother Late Smt. Sumitra Devi. My deepest gratitude and heartfelt thanks to my father-in-law Mr. Jaychand Lal Kasaudhan, my mother-in-law Late Mrs. Sanyogita Devi, my uncles (Mr. Roop Chand Gupta and Mr. Ishwar Chand Gupta), my aunts (Mrs. Maya Devi and Mrs. Suneeta Devi), my brothers (Mr. Rukmesh Gupta, Mr. Mahesh Gupta, Mr. Awdhesh Gupta and Mr. Pradeep Gupta), my sister-in-law

(Mrs. Deepmala Gupta, Mrs. Archana Gupta, Mrs. Aradhana Gupta and Mrs. Chandni Gupta), my sisters (Mrs. Sudha Gupta and Mrs. Muskan Gupta), my brother-in-law (Mr. Sunil Gupta and Mr. Amit Gupta) and the other family members Mr. Mukesh Gupta, Mrs. Sapna Gupta, Mr. Rajesh Gupta, Mrs. Juli Gupta, Mr. Brijesh Gupta, Mrs. Pooja Gupta, Mrs. Archana Gupta, Mr. Ajay Gupta, Mrs. Roli Gupta, Mr. Aditya Gupta, Mr. Umang Gupta, Amit Kasaudhan and Ankush Kasaudhan for their boundless love, support, and guidance have kept me motivated and confident. I must mention the youngest members, Ayush, Piyush, Sonu, Ananya, Shreyanshi, Shivi, Shourya, Shipra, Aradhaya, Aditi, Rimjhim, Mukund, Kanha, Kartik, Vamika, and Raghav, for their smiley and cheerful support. I deeply express my love and gratitude to my beloved family.

Finally, I would like to express my heartfelt gratitude to my parents who mean the world to me. My loving father Late Shri Suresh Chand Gupta and my mother Smt. Janki Devi, whose constant love and support kept me motivated and confident. My achievements and success are a result of their belief in me. I will always be indebted to my parents who gave me the opportunities and experiences that made me who I am today. Thank you both for giving me the strength to pursue my dream. Lastly, I would like to express my deepest gratitude to my beloved wife, Mrs. Pratibha Kasaudhan, whose unwavering support, patience, and love have been my anchor throughout this journey. Her encouragement and understanding have been instrumental in the completion of this work. Thank you for being my rock, my confidant, and my biggest cheerleader. This achievement is as much yours as it is mine. I dedicate this work to my precious son, Aaraj, whose arrival has filled my life with boundless love and inspiration. His presence has been a source of strength and motivation, making this journey even more meaningful.

My Ph.D. journey at IIT Indore was exciting, fulfilling, and rewarding. I am taking a bagful of experiences and memories from here and would like to acknowledge each one who was a part of this beautiful journey.

Thank You…

Pankaj Kumar Gupta

IIT Indore

DEDICATED TO

MY BELOVED PARENTS, MY WIFE AND MY COUNTRY INDIA

-Pankaj

SYNOPSIS

The 10*H*-Phenothiazine has a tricyclic structure consisting of two benzene rings fused to a central thiazine ring. Its chemical structure can be represented in Figure 1. The phenothiazine has a nonplanar shape, good photostability, and thermal stability. The colourless crystalline solid compound 10*H*-phenothiazine has an absorption maximum in dichloromethane at 316 nm. Phenothiazine can be functionalized by the nucleophilic substitution reaction at the nitrogen (N) position or electrophilic substitution reaction at positions 3 and 7. Phenothiazine derivatives exhibit high electron density and low reversible oxidation potential, making them suitable candidates for use in a variety of applications such as chemical sensors, photovoltaic devices, organic light-emitting diodes (OLEDs) and dye-sensitized solar cells (DSSCs).

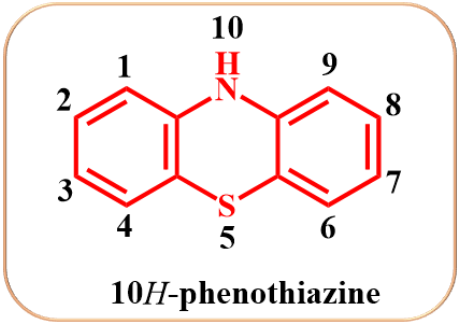

Figure 1. The molecular structure of 10*H*-phenothiazine.

The TCNE (1,1,2,2-tetracyanoethylene) and TCNQ (7,7,8,8-tetracyanoquinodimethane) are strong electron acceptors, and their structures prominently feature cyano groups (–C≡N), which play a crucial role in their electron-accepting properties. (Figure 1.2). TCNE consists of an ethylene backbone (C=C) with four cyano groups attached to the carbon atoms of the double bond and TCNQ consists of a quinodimethane core with four cyano groups attached to the 7 and 8 positions. The cyano groups are highly electronegative and withdraw electron density through their π-conjugated systems. This withdrawal of electron density from the central ethylene moiety and quinodimethane core makes TCNE and TCNQ are very strong electron acceptor, as their reaction with electron-rich alkynes *via* a [2 + 2] cycloaddition (CA)

reaction to produce cyclobutene rings. These cyclobutene intermediates undergo a retroelectrocyclization (RE) reaction resulting in TCBD (1,1,4,4-tetracyanobutadiene) and DCNQ (dicyanoquinodimethane) derivatives (Scheme 1.1). The donor-acceptor (D–A) systems incorporating strong acceptors like TCBD and DCNQ are promising candidates for organic photovoltaic application. Their photonic and electrical characteristics can be tuned by varying the strength of the acceptor or donor units and the π-linker. The cross-conjugated systems with strong electron-acceptor TCBD and DCNQ groups have been used in organic electronic devices due to their strong and wide electronic absorption in the visible to near-IR regions and their ability to tune the lowest unoccupied molecular orbital (LUMO) energy levels. The TCBD and DCNQ functionalized donor-acceptor phenothiazine chromophores exhibit good photochemical stability and excellent solubility in a wide range of solvents. The photonic properties of the TCBD and DCNQ functionalized phenothiazine chromophores can be modified by varying the type of donor, acceptor, and spacer. The tuning of optical and electronic properties in TCBD- and DCNQ-functionalized donor–acceptor phenothiazine chromophores can be utilized in a range of applications, including dye-sensitized solar cells (DSSCs), organic photovoltaics, nonlinear optics (NLOs), organic field-effect transistors (OFETs), organic light-emitting diodes (OLEDs), bulk heterojunction organic solar cells (BHJOSCs), photodynamic therapy, sensing, bioimaging, and single-molecule switches *etc*.

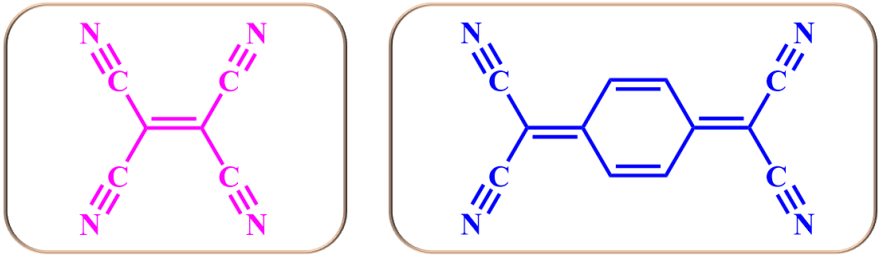

1,1,2,2-tetracyanoethylene (TCNE)

7,7,8,8-tetracyanoquinodimethane (TCNQ)

Figure 2. The molecular structure of TCNE and TCNQ.

We have investigated various donor–acceptor chromophores by incorporating different combinations of electron donors (phenothiazine,

thiophene, triphenylamine, carbazole, and N,4-dimethylbenzenesulfonamide) with strong acceptors (TCNE, TCNQ, and fulleropyrrolidine) to enhance and improve the optical characteristics and the HOMO-LUMO gap. The photophysical, electrochemical, thermal, and computational studies of the TCBD and DCNQ functionalized donor–acceptor phenothiazine chromophores were investigated. The TCBD and DCNQ functionalized donor–acceptor phenothiazine chromophores have strong near-infrared absorption and a low HOMO-LUMO gap, making them promising candidates for optoelectronics applications.

The main objectives of the current study are:

1. To design and synthesize the TCBD and DCNQ functionalized donor–acceptor phenothiazine chromophores for optoelectronic applications.
2. To synthesize symmetrical and unsymmetrical TCBD and DCNQ functionalized donor–acceptor phenothiazine chromophores by varying the donor/acceptor units in a systematic way.
3. To investigate the effect of the cyano-based strong acceptors TCBD and DCNQ incorporated donor–acceptor phenothiazine chromophores on their photophysical, electrochemical, and thermal properties and the energy gap between HOMO and LUMO energy levels.
4. To fine-tune the HOMO-LUMO gap by introducing the donor/acceptor strength or π-linker on the TCBD and DCNQ functionalized donor–acceptor phenothiazine chromophores.
5. To understand the distribution of electron density in the highest occupied molecular orbital (HOMO) and lowest unoccupied molecular orbital (LUMO), the nature of absorption transitions, and the HOMO-LUMO energy gap *via* density functional theory (DFT) and time-dependent density functional theory (TD-DFT) calculations were performed to compare with experimental results.

Chapter 1: Introduction

Chapter 1 describes the design, synthesis, and functionalization of the TCBD and DCNQ moieties and their applications in different fields.

Chapter 2: Materials and experimental techniques

Chapter 2 summarizes the general experimental methods, characterization techniques and details of the instruments used for molecular structure characterization.

Chapter 3: Synthesis and Characterization of NIR absorbing TCBD and DCNQ incorporated donor-acceptor Phenothiazines

In chapter 3, a set of unsymmetrical and symmetrical donor–acceptor-based phenothiazine derivatives **1–18** were designed and synthesized *via* Palladium-catalyzed Sonogashira cross-coupling and followed by [2 + 2] cycloaddition-retroelectrocyclization (CA-RE) reactions. The impact of the incorporation of cyano-based acceptors TCBD and DCNQ in the phenothiazine derivatives **1–18** has been investigated by the photophysical, thermal, and electrochemical properties, and computational studies. The TCBD and DCNQ incorporated phenothiazines **2**, **3**, **5**, **6**, **8**, **9**, **11**, **12**, **14**, **15**, **17**, and **18** exhibit a red-shifted absorption in the near-infrared (NIR) region compared to phenothiazine derivatives **1**, **4**, **7**, **10**, **13**, and **16**. This red-shifted absorption is attributed to the presence of strong intramolecular charge transfer (ICT) transitions.

The electrochemical study suggests that the phenothiazine derivatives **2**, **3**, **5**, **6**, **8**, **9**, **11**, **12**, **14**, **15**, **17**, and **18** exhibited two reduction potentials in the cathodic region which corresponded to the strong TCBD and DCNQ acceptors. The mono-TCBD incorporated phenothiazine derivative **2** displays higher thermal stability in comparison to the other phenothiazine derivatives. The computational studies on phenothiazine derivatives **1–18** reveal that the LUMO is significantly stabilized as the acceptor strength increases, resulting in a reduced HOMO-LUMO gap.

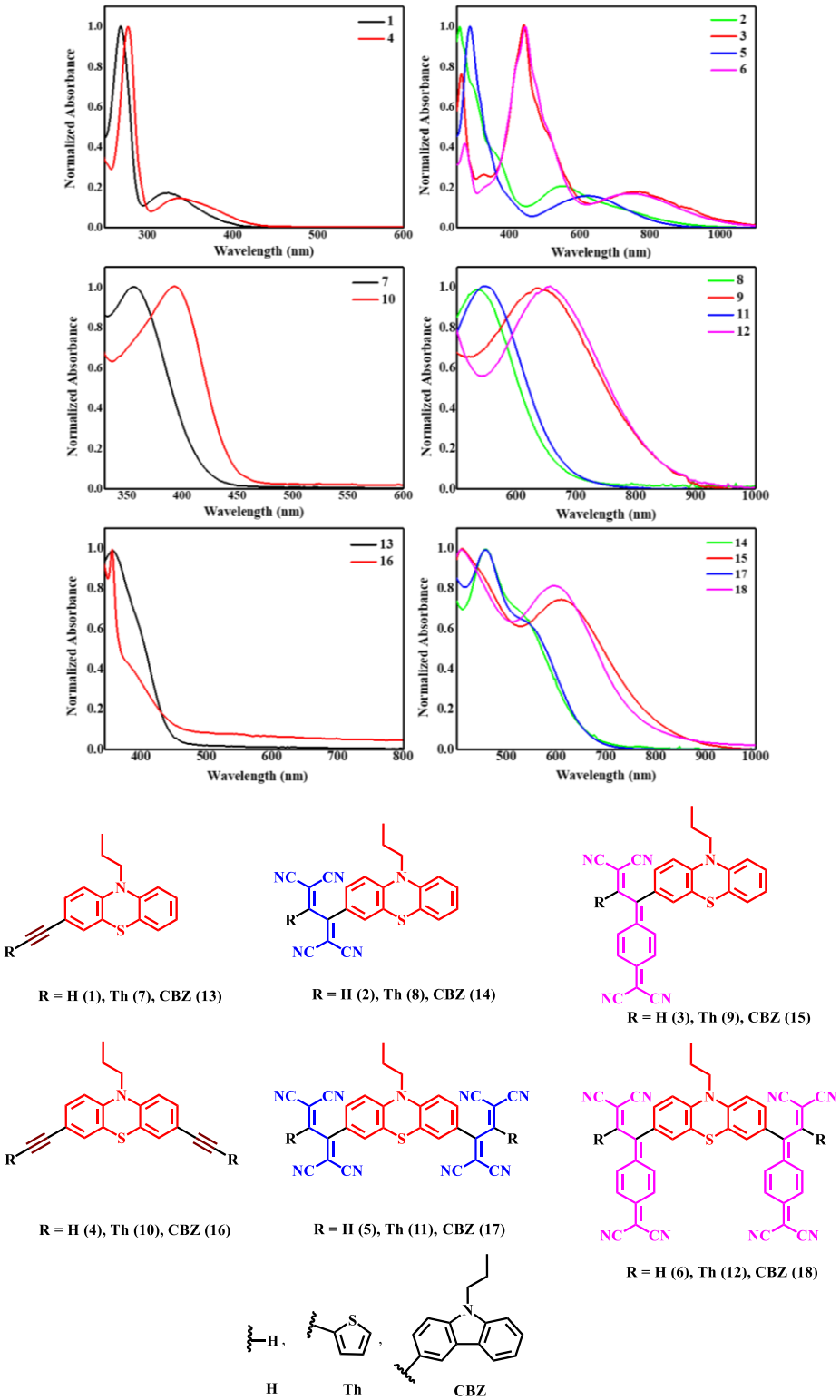

Chapter 4: Near-Infrared Absorbing Donor-Acceptor Based *N*,4-dimethylbenzenesulfonamide Substituted Phenothiazine Derivatives

In chapter 4, symmetrical and unsymmetrical phenothiazine derivatives **1** and **4** were designed and synthesized using the Corey-Fuchs reaction

via Evano′s condition. Furthermore, the symmetrical and unsymmetrical phenothiazine derivatives functionalized with TCBD and DCNQ namely **2**, **3**, **5**, and **6** were synthesized by the [2 + 2] CA-RE reaction with strong electron acceptors TCNE (1,1,2,2-tetracyanoethylene) and TCNQ (7,7,8,8-tetracyanoquinodimethane) units in good yields. The impact of incorporating the strong electron acceptors TCBD and DCNQ moieties in donor-acceptor phenothiazine chromophores **1–6** has been investigated by photophysical, electrochemical, and computational studies. The photophysical properties of the donor–acceptor phenothiazine chromophores **1–6** reveal that the absorption maxima of DCNQ functionalized **3** and **6** exhibit a substantial bathochromic shift of ~100 nm compared to those of TCBD substituted **2** and **5**, due to the strong electron-accepting nature of the DCNQ moiety.

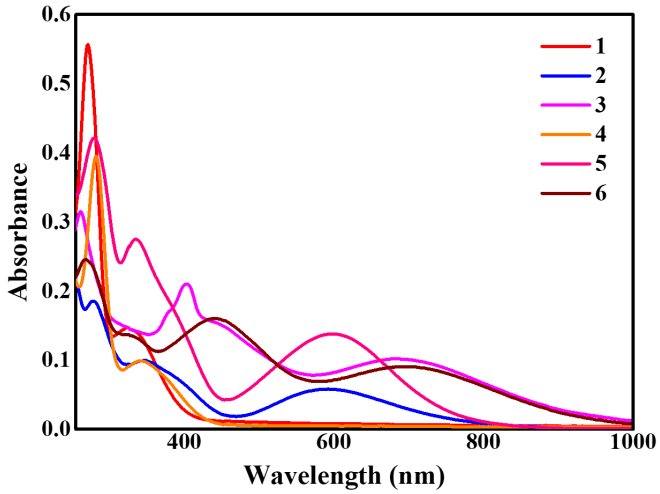

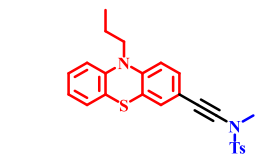

1

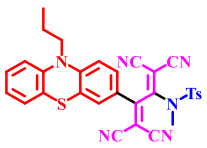

2

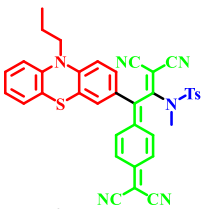

3

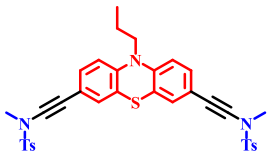

4

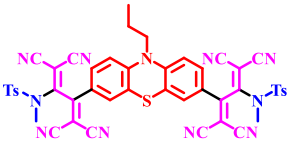

5

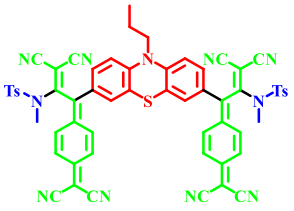

6

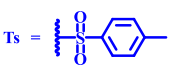

The electrochemical properties reveal that the reduction potential values of **3** and **6** are smaller than those of **2** and **5**, indicating that the DCNQ unit has a greater influence on the electronic properties and contributes more to stabilizing the LUMO energy levels than the TCBD unit. In DFT calculation, the HOMO-LUMO energy gap in DCNQ functionalized **3** and **6** is lower than in TCBD functionalized derivatives **2** and **5**.

Chapter 5: NIR Absorbing TCBD and DCNQ Functionalized Donor-Acceptor Based Symmetrical and Unsymmetrical *N*-Methyl-*p*-toluenesulfonamide-Phenothiazine Derivatives

In chapter 5, a symmetrical phenothiazine derivatives (**PTZ-NTs)$_2$**, **1** was designed and synthesized using the Corey-Fuchs reaction and followed by Evano′s condition. Furthermore, the symmetrical and unsymmetrical phenothiazine derivatives functionalized with TCBD and DCNQ namely (**PTZ-NTs)$_2$-TCBD**, **2**; (**PTZ-NTs)$_2$-(TCBD)$_2$**, **3**; (**PTZ-NTs)$_2$-DCNQ**, **4**; and (**PTZ-NTs)$_2$-(DCNQ)$_2$**, **5** were synthesized by the [2 + 2] CA-RE reaction with strong electron acceptors TCNE (1,1,2,2-tetracyanoethylene) and TCNQ (7,7,8,8-tetracyanoquinodimethane) units in good yields. The phenothiazine derivatives **1–5** were investigated to explore the effects of the incorporation of TCBD and DCNQ moieties on the photophysical, electrochemical, thermal, and computational studies. The photophysical studies suggest that the phenothiazine derivatives **4** and **5** functionalized with DCNQ exhibit a red shift in their absorption spectra in comparison to phenothiazine derivatives **2** and **3** functionalized with TCBD. This shift is attributed to the strong interaction between the donor and acceptor moieties (D-A interaction) and the extended conjugation in the DCNQ moiety.

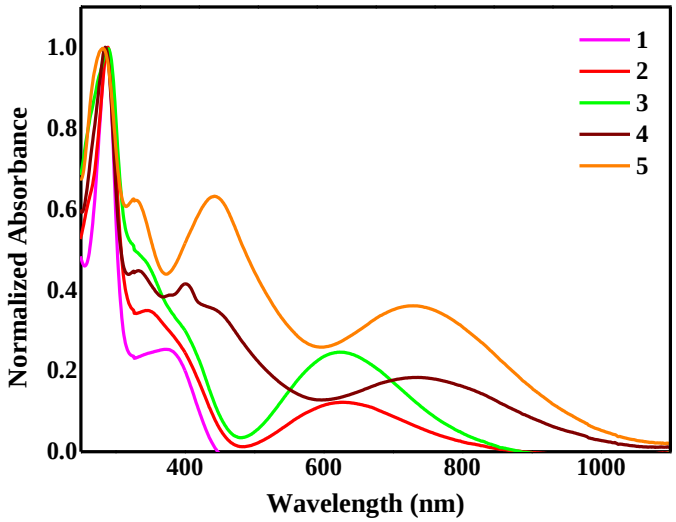

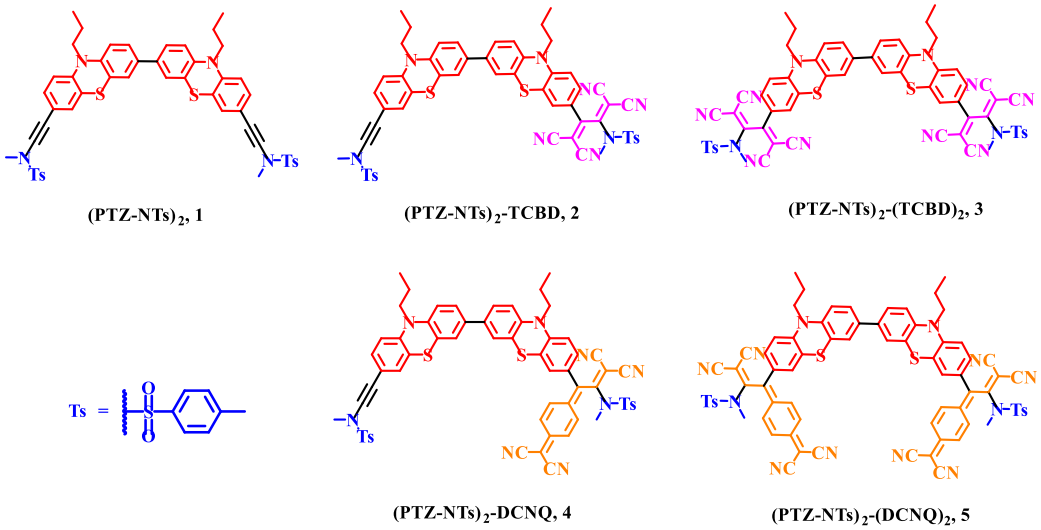

(PTZ-NTs)$_2$, 1 (PTZ-NTs)$_2$-TCBD, 2 (PTZ-NTs)$_2$-(TCBD)$_2$, 3

(PTZ-NTs)$_2$-DCNQ, 4 (PTZ-NTs)$_2$-(DCNQ)$_2$, 5

The electrochemical data indicates that phenothiazine derivatives **2–5** functionalized with TCBD and DCNQ exhibited two reduction waves, which were observed in low potential regions corresponding to the acceptors TCBD and DCNQ moieties. The phenothiazine derivatives **4** and **5** functionalized with DCNQ exhibit higher thermal stability compared to phenothiazine **2** and **3** incorporated with TCBD. The computational studies indicate that the highest occupied molecular orbitals (HOMOs) of the symmetrical and unsymmetrical phenothiazine **1–5** are mainly concentrated on both phenothiazine units, and the lowest unoccupied molecular orbital (LUMO) of symmetrical phenothiazine **1** is mainly localized on the ynamide moiety with some contributions of the centered phenothiazine units.

Chapter 6: Synthesis and Characterization of NIR Absorbing Triphenylamine Substituted Donor–Acceptor Phenothiazine and Fulleropyrrolidine Derivatives

In chapter 6, a series of triphenylamine functionalized phenothiazine derivatives **TPA-PTZ 1–3** and fulleropyrrolidine derivatives **TPA-PTZ-C_{60} 1–3** were designed and synthesized by the Pd-catalyzed Sonogashira cross-coupling reaction *via* [2 + 2] CA-RE reaction followed by Prato reaction. The effect of the fullerene moiety and the strong electron acceptors TCBD and DCNQ on their photophysical, electrochemical, and computational studies have been investigated.

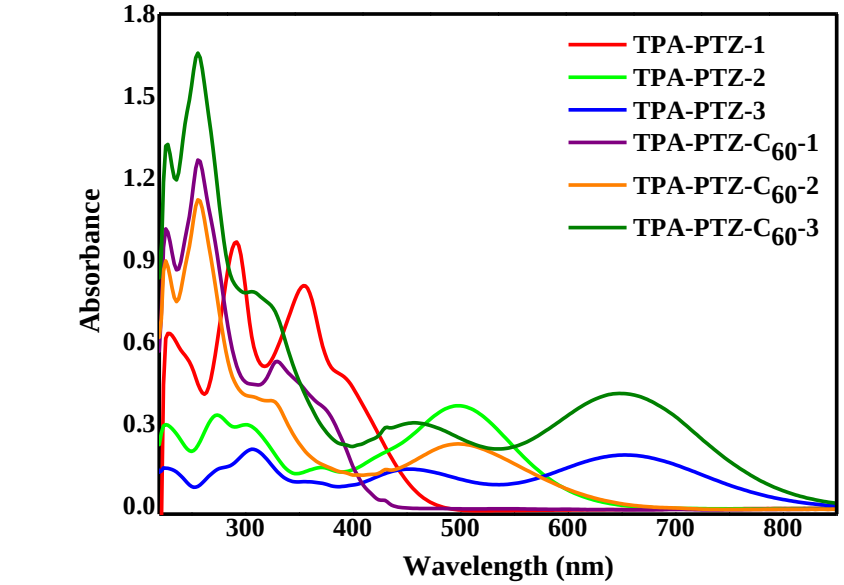

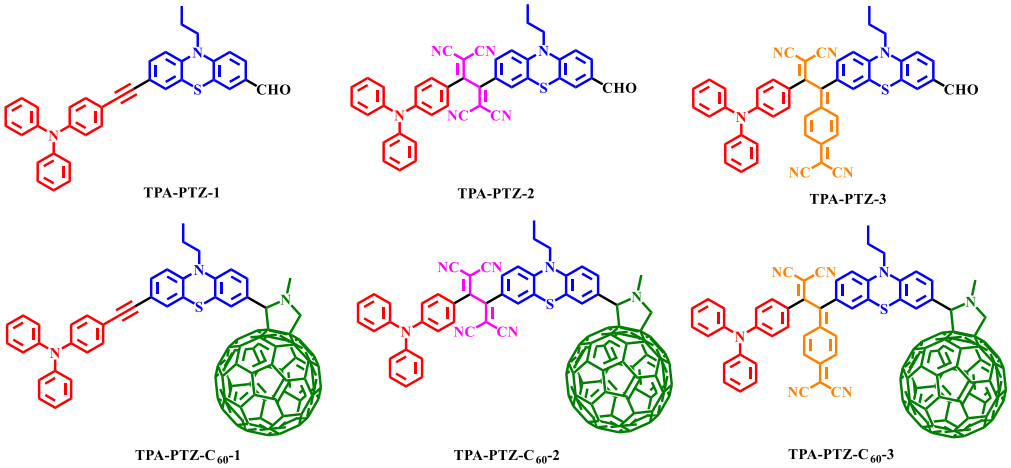

The photophysical spectra of fulleropyrrolidine derivatives **TPA-PTZ-C_{60}-2** and **TPA-PTZ-C_{60}-3** exhibit bathochromic shift because of ICT transition in the NIR region as compared to **TPA-PTZ-**

2 and **TPA-PTZ-3**. The electrochemical characteristics showed that the **TPA-PTZ 1–3** and **TPA-PTZ-C_{60} 1–3** produce multiple redox potentials in cyclic voltammetry because of the availability of various acceptor units (Fullerene, TCBD, and DCNQ), and donor units (Phenothiazine and Triphenylamine). According to the computational study, the addition of the fullerene moiety stabilizes the lowest unoccupied molecular orbital (LUMO) energy level more than the TCBD and DCNQ moieties.

Chapter 7: Design and Synthesis of TCBD and DCNQ Functionalized Phenothiazine and Fulleropyrrolidine Chromophores: Photophysical, Electrochemical and Computational Studies

In chapter 7, a set of phenothiazine chromophores **$(PTZ)_2$ 1–3** were designed and synthesized using the Pd-catalyzed Sonogashira cross-coupling reaction followed by the [2 + 2] CA-RE reaction. Additionally, fulleropyrrolidine derivatives **$(PTZ)_2$-C_{60} 1–3** were synthesized *via* the 1,3-dipolar cycloaddition reaction (Prato reaction) in good yields. The impact of incorporating fullerene moiety along with strong electron acceptors such as TCBD and DCNQ has been examined on their photophysical, electrochemical, and computational studies.

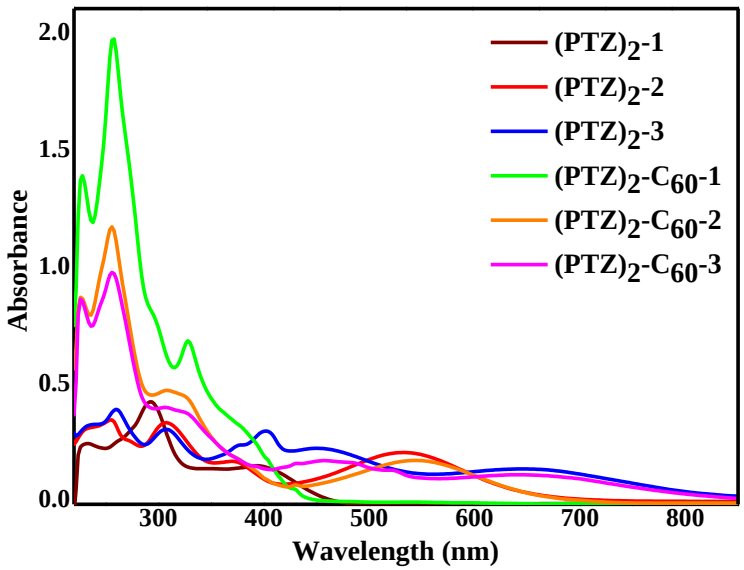

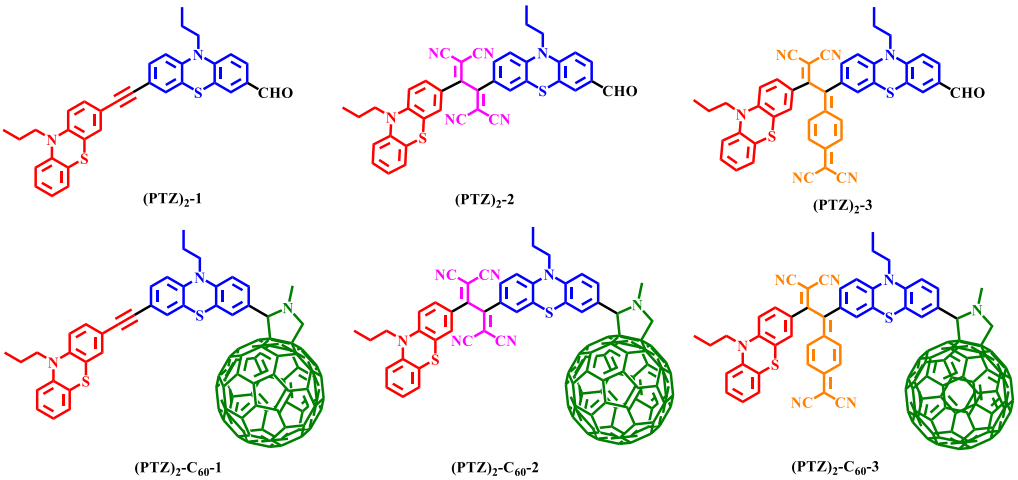

The photophysical properties clearly show that the DCNQ-functionalized donor-acceptor chromophores **(PTZ)$_2$-3** and **(PTZ)$_2$-C$_{60}$-3** resulted in a redshifted band with a low optical bandgap compared to the TCBD-functionalized **(PTZ)$_2$-2** and **(PTZ)$_2$-C$_{60}$-2**. This shift is due to the intramolecular charge transfer (ICT) transition. The electrochemical studies of the phenothiazine chromophores **(PTZ)$_2$ 1–3** and fulleropyrrolidine derivatives **(PTZ)$_2$-C$_{60}$ 1–3** show multiple redox potentials correspond to redox-active PTZ, TCBD, DCNQ, and fullerene moieties. The computational studies suggest that the electron density of HOMO energy levels of **(PTZ)$_2$-2** and **(PTZ)$_2$-3** are mostly delocalized over the phenothiazine unit whereas, the electron density in LUMO energy levels are concentrated over the acceptors TCBD and DCNQ moieties.

Chapter 8: Conclusions and Future Scope

Chapter 8 summarizes the salient features of the work and future perspectives for developing new donor-acceptor materials for optoelectronic applications.

List of Publications

[1] **Gupta, P. K.**, Khan, F., & Misra, R. (2023). NIR-Absorbing 1,1,4,4-Tetracyanobuta-1,3-diene- and Dicyanoquinodimethane-Functionalized Donor-Acceptor Phenothiazine Derivatives: Synthesis and Characterization. *The Journal of Organic Chemistry*, *88*(20), 14308–14322. https://doi.org/10.1021/ACS.JOC.3C01029. (Impact Factor = 3.6)†

[2] **Gupta, P. K.**,[$] Das, S.,[$] Misra, R., & D'Souza, F. (2024). Near-IR Capturing N-Methylbenzene Sulfonamide-Phenothiazine Incorporating Strong Electron Acceptor Push-Pull Systems: Photochemical Ultrafast Carrier Dynamics. *Chemistry – A European Journal*, e202304313. https://doi.org/10.1002/CHEM.202304313. (Impact Factor = 4.353)†

[3] **Gupta, P. K.**,[$] Kandpal, S.,[$] Kumar, R., & Misra, R. (2024). Ferrocene-Functionalized Fulleropyrrolidine Derivative: A Performance Enhancer for Solid-State Electrochromic Devices. *ACS Applied Optical Materials*, *2*(1), 158–165. https://doi.org/10.1021/ACSAOM.3C00384.

[4] Khan, F., Mahmoudi, M., **Gupta, P. K.**, Volyniuk, D., Grazulevicius, J. V., & Misra, R. (2023). Mechanochromic Materials Based on Tetraphenylethylene-Substituted Phenothiazines: Substituent-Dependent Hypsochromic and Bathochromic Switching of Emission. *Journal of Physical Chemistry C*, *127*(3), 1643–1654. https://doi.org/10.1021/ACS.JPCC.2C07010 (Impact Factor = 3.7)

[5] **Gupta, P. K.**,[$] Das, S.,[$] Misra, R., & D'Souza, F. (2025). Acceptor-Dependent Intervalence Charge Transfer and Separation Dynamics in Broad-Band-Capturing Push–Pull Chromophores. *Journal of Physical Chemistry C*, *129*(14), 6924–6942. https://doi.org/10.1021/acs.jpcc.5c01681 (Impact Factor = 3.7)†

[6] **Gupta, P. K.**, Bansal, L., Kumar, R., & Misra, R. (2025). Design, Synthesis, and Characterization of a Phenothiazine Functionalized Triazine Derivative for Electrochromic Device. *ACS Applied Optical Materials*, *3*(1), 14−21. https://doi.org/10.1021/acsaom.4c00345.

[7] **Gupta, P. K.**,[$] Ileperuma, C. V.,[$] Misra, R., & D'Souza, F. Strong acceptor incorporated phenothiazine-C60 multi-redox push-pull conjugates: Demonstration of C60's superior electron acceptor characteristics, (Manuscript Under Preparation).†

[8] **Gupta, P. K.**,[$] Ileperuma, C. V.,[$] Misra, R., & D'Souza, F. Synthesis and Characterization of NIR absorbing Triphenylamine substituted donor-acceptor Phenothiazine and fulleropyrrolidine derivatives, (Manuscript Under Preparation).†

†Papers pertaining to the thesis.

$Authors having equal contribution.

CONFERENCE/SYMPOSIUM PRESENTATION

1. **P. K. Gupta**, Y. Rout, P. Gautam, R. Misra, Synthesis and Characterization of NIR absorbing Triphenylamine substituted donor-acceptor Phenothiazines, Royal Society of Chemistry and IIT Indore Symposium on Materials Science Towards New Horizons-2023, (January 19-20, 2023); Poster Presentation.
2. **P. K. Gupta**, Y. Rout, P. Gautam, R. Misra, Synthesis and Characterization of NIR absorbing Triphenylamine substituted donor-acceptor Phenothiazines, International Conference on Molecules and Materials Technology (MMT-2023), National Institute of Technology Kurukshetra, India (April 21-22, 2023); Poster Presentation.
3. **P. K. Gupta**, Y. Rout, P. Gautam, R. Misra, Synthesis and Characterization of NIR absorbing Triphenylamine substituted donor-acceptor Phenothiazines, IEEE Student Research Symposium (SRS'23), Indian Institute of Technology Indore, India (October 10-11, 2023); One Slide Presentation.
4. **P. K. Gupta**, F. Khan, R. Misra, NIR-Absorbing 1,1,4,4-Tetracyanobuta-1,3-diene- and Dicyanoquinodimethane-Functionalized Donor−Acceptor Phenothiazine Derivatives: Synthesis and Characterization, In-house Chemistry Symposium "CHEM-2024", Indian Institute of Technology Indore, India (21st March 2024); Poster Presentation.
5. **P. K. Gupta**, R. Misra, Near-Infrared Absorbing Donor-Acceptor Based N,4 dimethylbenzenesulfonamide Substituted Phenothiazine Derivatives, International Conference on Multidisciplinary Approaches to Chemical Sciences (InCoMAC-2024), National P G College Lucknow, Uttar Pradesh, India (November 24-26, 2024); Poster Presentation.

TABLE OF CONTENTS

LIST OF FIGURES

Chapter 1. Introduction

LIST OF SCHEMES

LIST OF TABLES

LIST OF CHARTS

ACRONYMS

D–A	Donor–acceptor
PPh_3	Triphenylphosphine
DMF	Dimethylformamide
DCM	Dichloromethane
DCE	Dichloroethane
PTZ	Phenothiazine
CBZ	Carbazole
TPA	Triphenylamine
NTs	*N*-Methyl-*p*-toluenesulfonamide
C_{60}	Fullerene
DMEDA	*N*,*N*-dimethylethylenediamine
TCNE	1,1,2,2-tetracyanoethylene
TCNQ	7,7,8,8-tetracyanoquinodimethane
EtOH	Ethanol
MeOH	Methanol
THF	Tetrahydrofuran
TLC	Thin Layer Chromatography
TEA	Triethylamine
Ph	Phenyl
IR	Infrared
UV-Vis	UV-Visible Spectroscopy
ICT	Intramolecular Charge Transfer
Calcd.	Calculated
$CDCl_3$	Chloroform-d
ESI-MS	Electrospray Ionization-Mass Spectrometry
HRMS	High-Resolution Mass Spectrometry
NMR	Nuclear Magnetic Resonance
DFT	Density Functional Theory
TD-DFT	Time-dependent Density Functional Theory
HOMO	Highest Occupied Molecular Orbital
LUMO	Lowest Unoccupied Molecular Orbital
CARE	Cycloaddition-retroelectrocyclization

CV	Cyclic voltammetry
DPV	Differential pulse voltammetry
$TBAPF_6$	Tetrabutylammonium hexafluorophosphate
TGA	Thermogravimetric analysis
T_d	Decomposition temperature
TCBD	1,1,4,4-tetracyanobutadiene
DCNQ	Dicyanoquinodimethane
MALDI	Matrix Assisted Laser Desorption Ionization

NOMENCLATURE

λ	Wavelength
ε	Extinction coefficient
α	Alfa
β	Beta
γ	Gamma
π	Pi
ϕ	Fluorescence quantum yield
σ	Sigma
Å	Angstrom
nm	Nanometer
cm	Centimeter
°	Degree
°C	Degree Centigrade
mmol	Millimole
mL	Milliliter
µL	Microliter
V	Volt
eV	electron Volt
µA	Microampere
a. u.	Arbitrary Unit

Chapter 1

Introduction

1.1. General Introduction

Over the past few decades, the development of donor–acceptor (D–A) molecular systems for optoelectronic applications have progressed significantly.[1, 2] The D–A frameworks in small organic compounds with π-bridging (D–π–A) are desirable owing to their low HOMO–LUMO band gap and broad absorption.[3–5] The scientific community has shown significant interest in the design and synthesis of novel multi-modular π-conjugated D–A chromophores. These compounds hold great potential for various applications in the field of organic photovoltaics (OPVs), organic solar cells (OSCs), organic light-emitting diodes (OLEDs), thermally activated delayed fluorescence (TADF) and biological research.[6–10]

1.2. Donor–Acceptor Systems

A donor–acceptor system is a molecular or chemical arrangement, wherein the donor component is electron-rich, and donates electrons to the acceptor component which is an electron-deficient species (Figure 1.1), this leads to charge transfer with unique electronic properties.[11–13] These D–A systems are essential in many areas, such as photovoltaics, OLEDs, organic electronics, sensors, OFETs, and photodynamic therapy. The design, synthesis, and characterization of D–A systems are essential for optimizing their performance and exploring their potential applications.[14–16] Ongoing research on D–A systems aims to enhance their performance, stability, and explore new applications driven by advances in materials science, synthetic chemistry, and device development.[17–20]

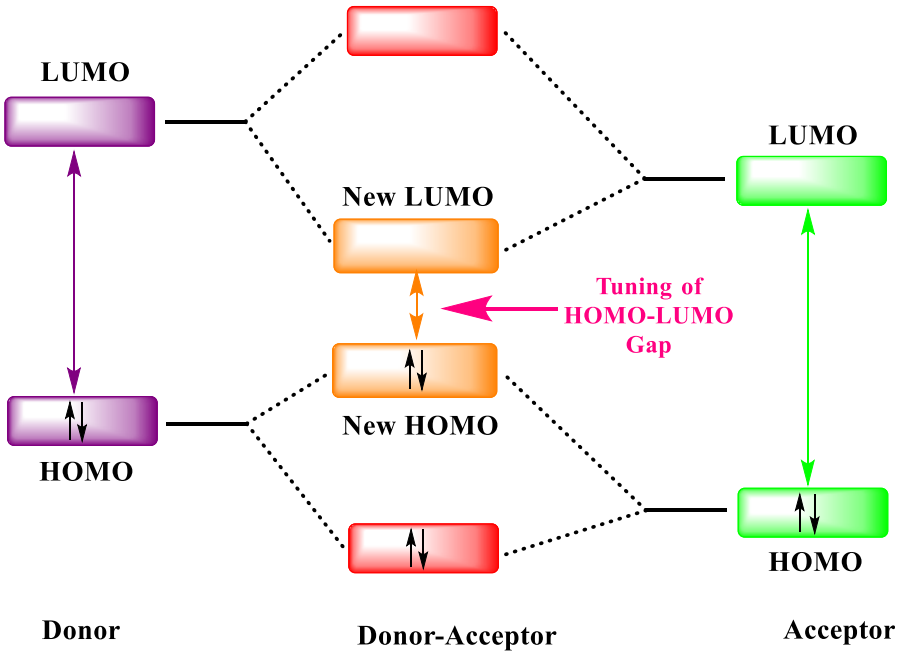

Figure 1.1. Schematic representation of the HOMO and LUMO energy levels in the D–A system.

1.2.1. Donor

The molecule possesses ability to donate the electron to another molecule is known as a donor, for example, the groups containing heteroatoms with lone pairs of electrons, such as amines (NH_2), hydroxyl (OH), sulphides, *etc*. Other aromatic carbocycles include metallocene derivatives such as ferrocene and well-known donors (Chart 1.1). The donor ability of a donor is crucial for charge transfer and electronic properties in any D–A systems. Phenothiazine (PTZ), carbazole (CBZ), triphenylamine (TPA), and ferrocene are widely used donors for designing molecular systems with low HOMO–LUMO gap.[21–24]

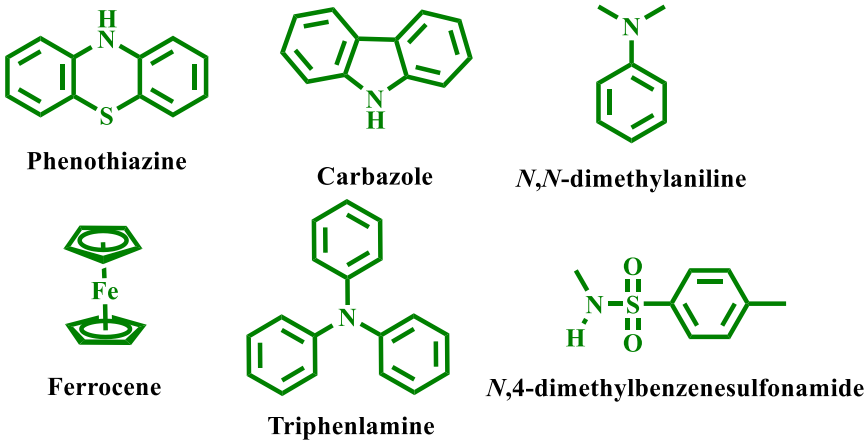

Chart 1.1. Chemical structures of electron donor moieties.

1.2.2. Acceptor

The molecule which accepts electrons from another molecule is called an acceptor. The acceptor's strength to withdraw electrons depends on the LUMO and is stronger when the lowest occupied molecular orbital (LOMO) is low-lying. In many cases the acceptors include amides, nitrogen-rich heterocycles, nitriles, boron complexes, fulleropyrrolidines, tetracyano acceptors, *etc*. (Chart 1.2).[25–28]

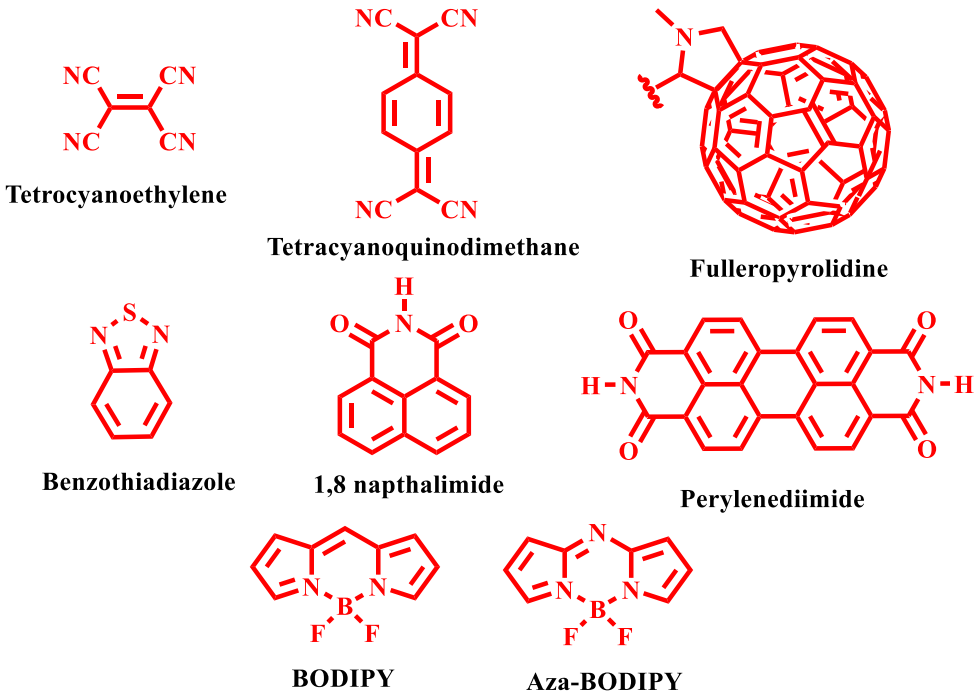

Chart 1.2. Chemical structures of electron acceptor moieties.

In the D–A system, the LUMO is more stabilized, while the HOMO is destabilized, compared to those of the individual donor (D) and acceptor (A) units (Figure 1.1).[29] When a donor and acceptor are appropriately linked with an appropriate linker, such as a double, triple, or aromatic ring, the absorption spectra are found to be redshifted with decreased HOMO–LUMO gap[30] The strength of the donor–acceptor (D–A) interaction depends on the individual strengths of both the donor and the acceptor.[31] Additionally, the nature of the linker between them plays a crucial role in determining the overall strength of the donor–acceptor system. These strong D–A systems have various applications in different fields including organic solar cells (OSCs), non-linear optics (NLO), OLEDs, mechanochromism, OFETs, and photodynamic therapy.[32–37]

1.3. Phenothiazine

The 10*H*-Phenothiazine possesses a tricyclic structure, consisting of two benzene rings fused to a central thiazine ring (Chart 1.3), synthesized by Bernthsen in 1883 with the reaction of diphenylamine and sulfur.[38] The phenothiazine is a colourless crystalline solid that has a nonplanar shape, good photostability, and thermal stability, exhibiting absorption maximum at 316 nm in dichloromethane. The phenothiazine exhibits strong electron-donating properties due to the electron-rich sulfur (S) and nitrogen (N) atoms in its structure. Moreover, it can be functionalized by the nucleophilic substitution reaction at the nitrogen (N) position or electrophilic substitution reaction at positions C-3 and C-7.[39–43] The sulfur atom in the phenothiazine unit can be readily oxidized to sulfoxide (oxidation state +4) and sulfone (oxidation state +6) upon reaction with suitable oxidizing agents, such as (H_2O_2) hydrogen peroxide or (m-CPBA) 3-chloroperbenzoic acid.[44–46] Phenothiazine derivatives exhibit high electron density and low reversible oxidation potential, making them suitable candidates for variety of applications such as chemical sensors, photovoltaic devices, OLEDs, DSSCs, OFETs, perovskite solar cells (PSCs), batteries, and many more.[47, 48] Some previous reports have mainly explored the

optoelectronic applications of phenothiazines in solar cells, the potential of the phenothiazine core in the development of organic fluorescent materials has not yet been extensively examined.[49, 50]

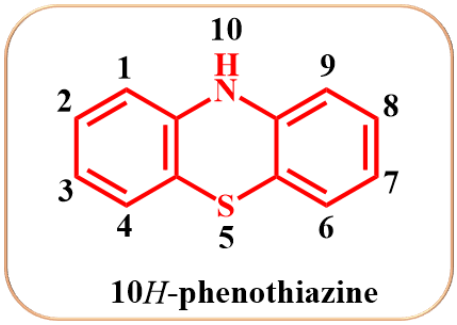

Chart 1.3. The molecular structure of phenothiazine core, showing its complete numbering.

1.3.1. Synthesis of Phenothiazine core

The following principal methods can synthesize the phenothiazine:

1.3.1.1. From diphenylamines

10*H*-Phenothiazine can be synthesized by reacting diphenylamine with sulfur at 250–260 °C (Scheme 1.1). This method was first described by Bernthsen[38] and was later improved by adding a small amount of iodine as a catalyst. The addition of iodine lowers reaction temperatures, reduces reaction times, and improves yields.[51]

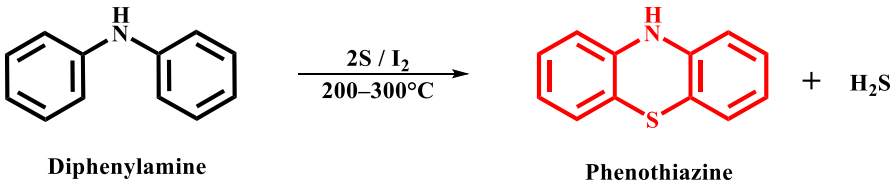

Scheme 1.1. Synthetic route of 10*H*-phenothiazine from diphenylamine.

1.3.1.2. From 2-bromobenzenethiol

(i) The Pd-catalyzed coupling reaction of 1-bromo-2-iodobenzene with 2-bromobenzenethiol and primary amine to form *N*,*N*-dimethyl-3-(10*H*-phenothiazin-10-yl)propan-1-amine in 74% yield (Scheme 1.2).[52]

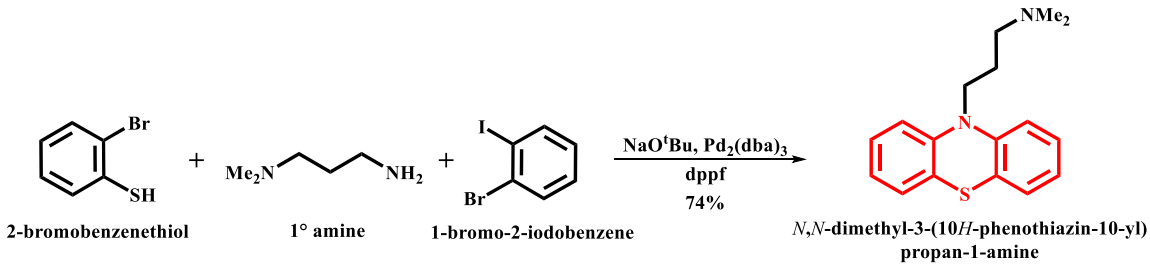

Scheme 1.2. Synthetic route of *N*,*N*-dimethyl-3-(10*H*-phenothiazin-10-yl)propan-1-amine from 1-bromo-2-iodobenzene, primary amine and 2-bromobenzenethiol.

(ii) The reaction of 2-iodoaniline with 2-bromobenzenethiol in the presence of copper iodide (CuI) and L-proline catalyst to give 10*H*-phenothiazine in 66% yield (Scheme 1.3).[53]

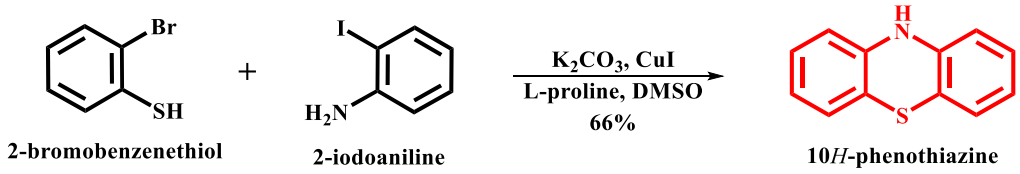

Scheme 1.3. Synthetic route of 10*H*-phenothiazine from 2-iodoaniline and 2-bromobenzenethiol.

1.3.1.3. From 2-aminobenzenethiol

(i) The condensation reaction of cyclohexanone and 2-aminobenzenethiol in the presence of 10 mol% thiol additives to form 10*H*-phenothiazine with a 35% yield (Scheme 1.4).[54]

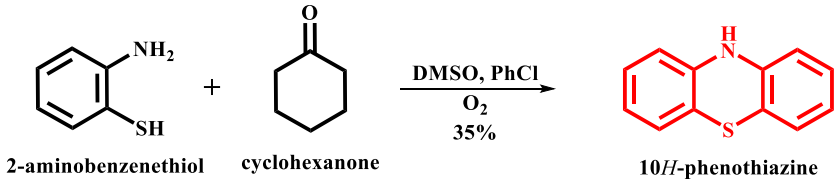

Scheme 1.4. Synthetic route of 10*H*-phenothiazine from cylcohexanone and 2-aminobenzenethiol.

(ii) A metal-catalyzed coupling reaction of 1-bromo-2-chlorobenzene with 2-aminobenzenethiol led to the formation of 10*H*-phenothiazine in a 67% yield (Scheme 1.5).[55]

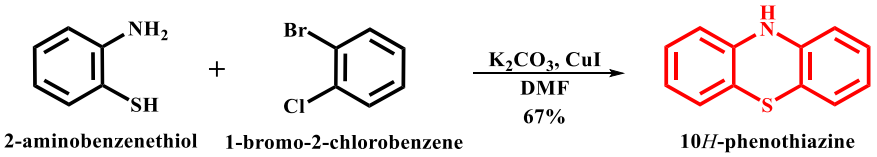

Scheme 1.5. Synthetic route of 10*H*-phenothiazine from 1-bromo-2-chlorobenzene and 2-aminobenzenethiol.

1.3.1.4. From diphenylaminosulfinic acids

(i) A solution of 5-nitro-2-(phenylamino)benzenesulfinic acid, when reacted with sulfuric acid (H_2SO_4) for 30 minutes, forms 3-nitro-10*H*-phenothiazine with the evolution of sulfur dioxide (SO_2) gas (Scheme 1.6).[56]

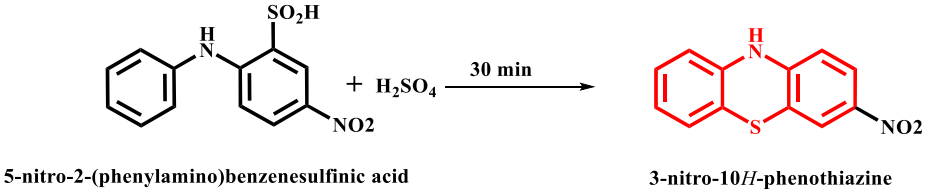

Scheme 1.6. Synthetic route of 3-nitro-10*H*-phenothiazine from 5-nitro-2-(phenylamino)benzenesulfinic acid and sulfuric acid.

(ii) The warm aqueous solution of 5-nitro-2-(phenylamino)benzenesulfinic acid, upon addition of hydriodic acid (HI), also leads to the formation of 3-nitro-10*H*-phenothiazine (Scheme 1.7).[57]

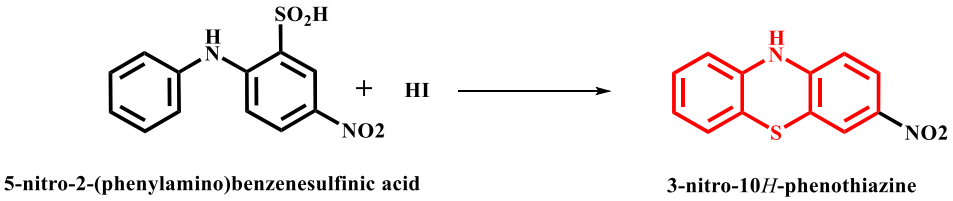

Scheme 1.7. Synthetic route of 3-nitro-10*H*-phenothiazine from 5-nitro-2-(phenylamino)benzenesulfinic acid and hydriodic acid.

1.3.1.5. From diphenylsulfides

The reaction of 2-((2-iodo-4-nitrophenyl)thio-5-nitroaniline with sodium carbonate (Na_2CO_3) and cuprous iodide (CuI) at 220–230 °C for

30 hours to give 2,8-dinitro-10*H*-phenothiazine in 51% yield (Scheme 1.8). This reaction was reported by Michels and Amstutz.[58]

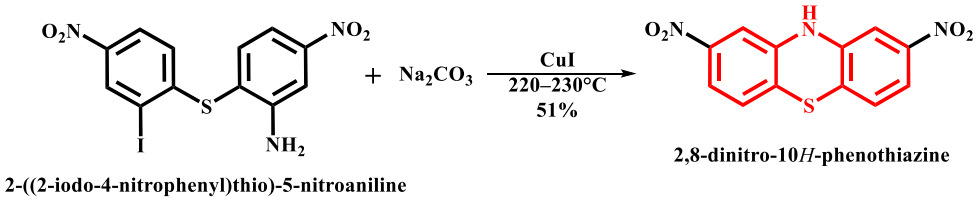

2-((2-iodo-4-nitrophenyl)thio)-5-nitroaniline

2,8-dinitro-10*H*-phenothiazine

Scheme 1.8. Synthetic route of 2,8-dinitro-10*H*-phenothiazine from diphenylsulfides.

1.3.1.6. Smiles rearrangement

The reaction of 2-aminobenzenethiol hydrochloride with 2-chloro-1,3,5-trinitrobenzene furnished an intermediate 2-((2,4,6-trinitrophenyl)thio)aniline, which upon treatment with NaOH undergoes Smiles rearrangement to form 1,3-dinitro-10*H*-phenothiazine with the liberation of nitrous acid (HNO_2) (Scheme 1.9).[59]

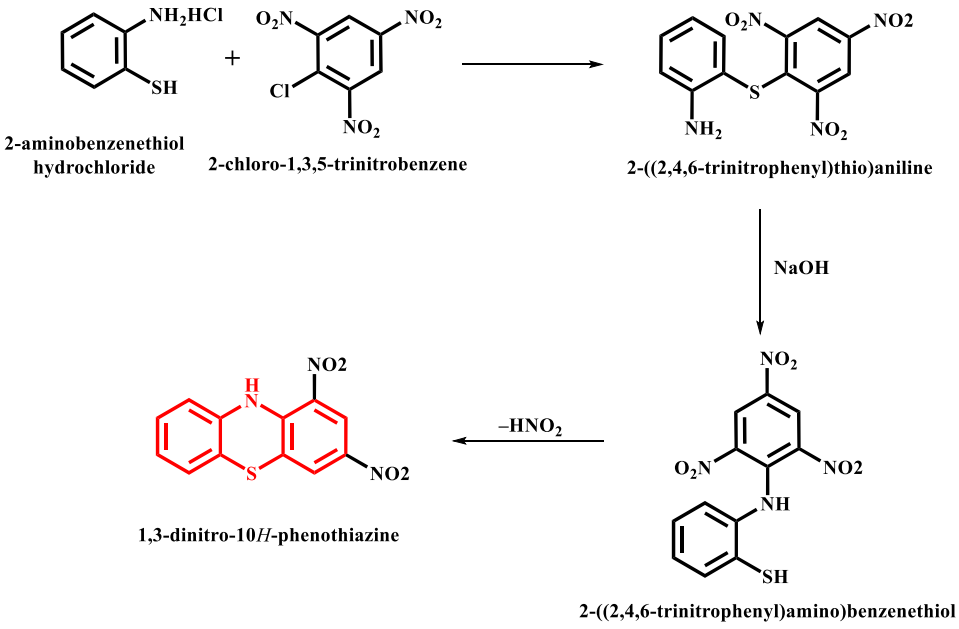

2-aminobenzenethiol hydrochloride

2-chloro-1,3,5-trinitrobenzene

2-((2,4,6-trinitrophenyl)thio)aniline

2-((2,4,6-trinitrophenyl)amino)benzenethiol

1,3-dinitro-10*H*-phenothiazine

Scheme 1.9. Synthetic route of 1,3-dinitro-10*H*-phenothiazine by Smiles rearrangement.

1.4. TCNE (1,1,2,2-tetracyanoethylene) and TCNQ (7,7,8,8-tetracyanoquinodimethane)

The TCNE (1,1,2,2-tetracyanoethylene) and TCNQ (7,7,8,8-tetracyanoquinodimethane) are known to be strong electron acceptors, and their structures prominently feature cyano groups (–C≡N), which play a crucial role in their electron-accepting properties. (Figure 1.2).[60, 61] TCNE consists of an ethylene backbone (C=C) with four cyano groups attached to the carbon atoms of the double bond and TCNQ consists of a quinodimethane core with four cyano groups attached to the 7 and 8 positions (Figure 1.2). The cyano groups are highly electronegative and withdraw electron density through their π-conjugated systems, makes TCNE and TCNQ very strong electron acceptors,[62, 63]. Moreover, the reaction of TCNE and TCNQ with electron-rich alkynes *via* a [2 + 2] cycloaddition (CA) reaction to furnish cyclobutene rings, which further undergo a retroelectrocyclization (RE) reaction resulting in TCBD (1,1,4,4-tetracyanobutadiene) and DCNQ (dicyanoquinodimethane) derivatives (Scheme 1.10).[64–66] The TCBD and DCNQ incorporated donor–acceptor (D–A) systems are promising candidates for organic photovoltaic application.[67] Their photonic and electrical characteristics can be tuned by varying the strength of the acceptor or donor units and the π-linker.[68, 69] The electroactive units TCBD and DCNQ display two single-electron reduction waves which are stable and reversible. The cross-conjugated systems having TCBD and DCNQ acceptors exhibited applications in organic electronic devices. These systems can tune the LUMO energy levels and have a strong and broad electronic absorption spectrum from visible to near-infrared (NIR) regions.[70–73] The synthetic pathway of the [2 + 2] CA–RE reaction of TCNE and TCNQ with donor-substituted alkynes are shown in Scheme 1.10.

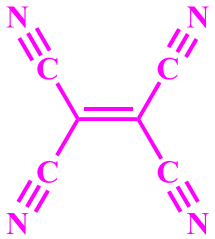

1,1,2,2-tetracyanoethylene (TCNE)

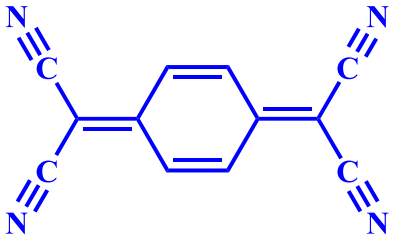

7,7,8,8-tetracyanoquinodimethane (TCNQ)

Figure 1.2. The molecular structure of TCNE and TCNQ.

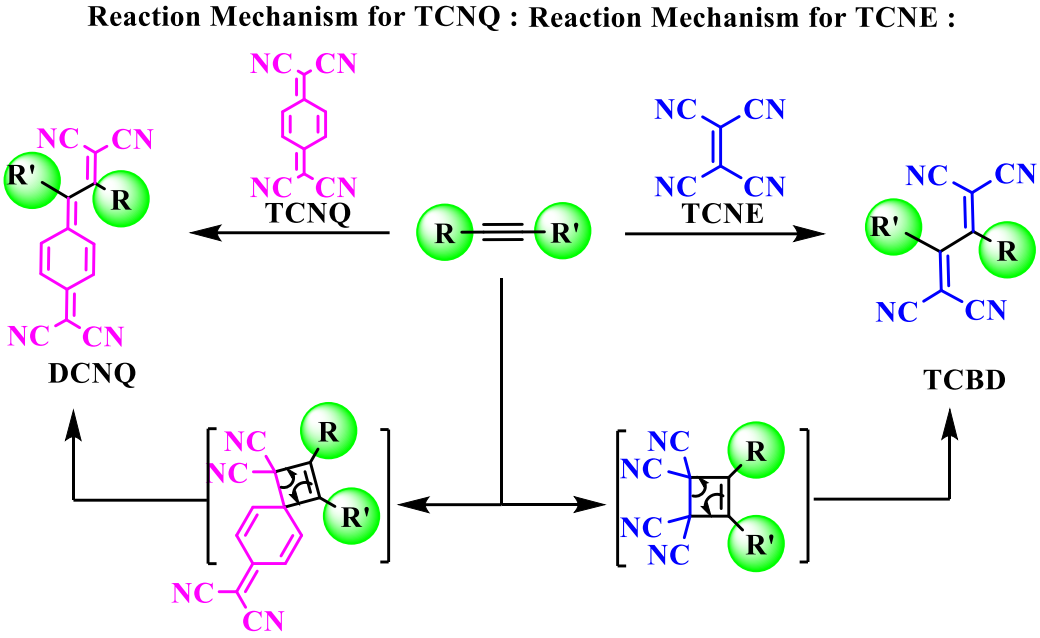

Scheme 1.10. Synthetic pathway for the [2 + 2] Cycloaddition-Retroelectrocyclization (CA-RE) reaction of TCNE and TCNQ with donor-substituted alkynes, yielding a novel class of donor–acceptor nonplanar charge transfer chromophores.

1.4.1. Synthesis of TCNE and TCNQ

TCNE and TCNQ can be synthesized by the following methods:

1.4.1.1. Synthesis of TCNE

In 1959, Carboni *et al*. reported the synthesis of **TCNE** using malononitrile and potassium bromide, with the gradual addition of bromine in an ice-water bath, resulting in the formation of a dibromomalononitrile-potassium bromide (T1) complex precipitate. Subsequently, the T1 complex and copper powder were reacted in dry benzene to produce **TCNE** in good yields (Scheme 1.11).[74]

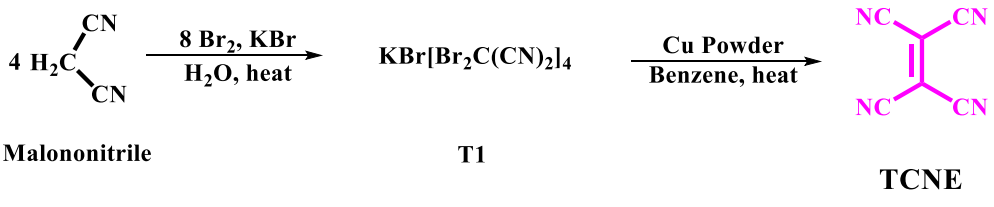

Scheme 1.11. Synthetic route of TCNE.

1.4.1.2. Synthesis of TCNQ

In 1962, Acker *et al*. reported the synthesis of **TCNQ** by condensing malononitrile with cyclohexane-1,4-dione in a benzene solution, yielding a mixture of T2 and T3 intermediates. Subsequently, T2 and T3 were combined with pyridine and either *N*-bromosuccinimide or bromine to produce **TCNQ** in good yields. Other oxidizing agents, such as selenium dioxide, have also been employed for this conversion to TCNQ, but with less favorable results (Scheme 1.12).[75]

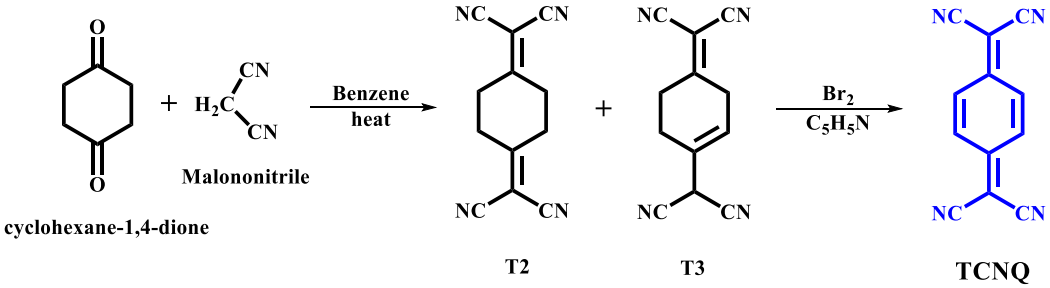

Scheme 1.12. Synthetic route of TCNQ.

Bruce *et al*. introduced the CA-RE reaction in organometallic chemistry for the first time in 1981, involving the combination of metal-acetylide complexes with an electron-deficient olefin.[76] Diederich *et al*. synthesized charge-transfer chromophores by reacting the strong acceptors TCNE and TCNQ with various acetylenic donors through a [2 + 2] CA–RE reaction.[77] Michinobu *et al*. have conducted extensive research on TCBD and DCNQ functionalized derivatives, identifying these compounds as promising candidates for solar applications.[78, 79] Shoji, Paul, Trolez, and Kato *et al*. have reported redox-active ICT chromophores based on TCBD and DCNQ-incorporated donor–acceptor derivatives, highlighting their potential for various optoelectronic applications.[80–83] Nakamura *et al*. have investigated carbazole-based TCBD compounds for applications in DSSCs, OPVs, and nonlinear optics (NLOs).[84] Holger and coworkers reported a series of 1,1′-dialkynylferrocenes functionalized with TCBD for application in molecular electronics.[85] Our research group (Misra *et*

al.) has reported the synthesis of TCBD- and DCNQ-incorporated derivatives using phenothiazine, carbazole, thiophene, triphenylamine, N-methylbenzene sulfonamide, and ferrocene as terminal donors in phenothiazine derivatives.[86–90] The variety and number of substituents added to the alkyne significantly affects its reactivity with TCNE and TCNQ, as well as the overall yield of the reaction. Notably, the [2 + 2] cycloaddition-retroelectrocyclization (CA-RE) reaction is distinguished by its high product yield and the absence of byproduct formation.

1.5. Reactions of TCBD and DCNQ

1.5.1. Phenothiazine-based TCBD and DCNQ Derivatives

The phenothiazine has a nonplanar shape, good photostability, and thermal stability.[91, 92] The colourless crystalline solid compound 10*H*-phenothiazine has an absorption maximum in dichloromethane at 316 nm. Phenothiazine can be functionalized by the nucleophilic substitution reaction at the nitrogen (N) position, or electrophilic substitution reaction at positions 3 and 7.[24, 93, 94] Phenothiazine derivatives exhibit high electron density and a low reversible oxidation potential, making them suitable candidates for use in a variety of applications such as chemical sensors, photovoltaic devices, OLEDs and DSSCs.[95–99]

The thiophene, carbazole, *N*,4-dimethylbenzenesulfonamide, triphenylamine, phenothiazine, and ferrocenyl-based TCBD and DCNQ incorporated phenothiazine derivatives **1–38** were synthesized by using the [2 + 2] CA–RE (Figure 1.3).[86–89, 100], wherein the nature and the number of the end-capping donor and acceptor moieties were changed inside the molecule.

The mono-TCBD-incorporated phenothiazine derivatives **1–5** exhibited absorption maxima at 545, 538, 542, 591, and 531 nm, respectively, attributed to the intramolecular charge transfer (ICT) transition resulting from the strong donor–acceptor (D–A) interactions. On the other hand, the mono-DCNQ incorporated phenothiazine

derivatives **6–10** showed absorption maxima at 760, 640, 613, 686, and 454 nm, respectively. The higher wavelength regions correspond to the ICT transition from the donors (carbazole, thiophene, *N*,4-dimethylbenzenesulfonamide, phenothiazine, and ferrocene) to the acceptors (TCNE/TCNQ) entities. The mono-DCNQ incorporated derivatives **6–10** showed red-shifted absorption spectra as compared to the mono-TCBD integrated derivatives **1–5**, because of the excellent electron-accepting characteristics of the DCNQ unit. In the case of unsymmetrical substituted phenothiazine derivatives **11–16**, the TCBD-incorporated derivatives **11** and **12** show absorption maxima at 498 and 547 nm, respectively, whereas DCNQ-incorporated derivatives **13** and **14** display absorption maxima at 450 and 468 nm, respectively attributed to the intramolecular charge transfer transition. The DCNQ-incorporated phenothiazine derivatives **13** and **14** display blue-shifted absorption spectra in comparison to TCBD-incorporated phenothiazines **11** and **12**. The incorporation of TCNQ into the compounds **11** and **12** resulted in the formation of **15** and **16**. The triphenylamine substituted phenothiazine derivative **15** shows absorption maxima at 636 nm and exhibits a red-shifted absorption by 138 nm as compared to compound **11**. In contrast, ferrocenyl functionalized phenothiazine derivative **16** showed absorption maxima at 524 nm, hypsochromically shifted by 23 nm compared to derivative **12**. Subsequently, the di-TCBD incorporated phenothiazine derivatives **17–22** displayed the absorption maxima at 620, 548, 552, 599, 537, and 492 nm, respectively. Although, the di-DCNQ incorporated phenothiazine derivatives **23–28** showed absorption maxima at 745, 665, 597, 702, 448, and 650 nm, respectively. These absorption maxima are attributed to ICT transitions from the donor (D) to acceptor (A) moieties. The di-DCNQ incorporated ferrocenyl functionalized phenothiazine derivative **27** displays hypsochromic shifted absorption as compared to di-TCBD incorporated ferrocenyl functionalized phenothiazine derivative **21**. The ICT band of absorption maxima for phenothiazine derivatives **29–33** incorporated with TCBD were found at 564, 564, 541, 548, and 549 nm. Conversely, in the case of DCNQ-incorporated phenothiazine derivatives **34–38**, the

ICT band of absorption maxima was observed at 753, 857, 858, 860, and 675 nm (Table 1.1). This difference is attributed to the strong donor–acceptor (D–A) interaction between the donor phenothiazine and the acceptor DCNQ moiety. The DCNQ-incorporated derivatives exhibit bathochromically-shifted absorption in comparison to the TCBD-incorporated derivatives due to the strong electron accepting character of the DCNQ unit.

The TCBD and DCNQ incorporated phenothiazine derivatives **1–28** revealed multi-reversible reduction potentials ranging from −0.05 to −1.11 V on the cathodic regions, which are attributed to the mono ($TCBD^{0/\cdot-}$ and $DCNQ^{0/\cdot-}$) and di ($TCBD^{\cdot-/2-}$ and $DCNQ^{\cdot-/2-}$) anions formation of the TCBD and DCNQ moieties. Additionally, on the anodic side, the TCBD and DCNQ incorporated phenothiazine derivatives **1–28** exhibited multi-oxidation potentials in the 0.24–1.65 V range, corresponding to the donors (thiophene, carbazole, *N*,4-dimethylbenzenesulfonamide, phenothiazine, and ferrocene) entities. On the other hand, the TCBD-incorporated phenothiazines **29–32** and DCNQ-incorporated phenothiazine derivatives **34–37** exhibited two reduction potentials on the cathodic side in the range of –0.72 to –0.83 V and –0.31 to –0.33 V, respectively, attributed to the mono ($TCBD^{0/\cdot-}$ and $DCNQ^{0/\cdot-}$) and di ($TCBD^{\cdot-/2-}$ and $DCNQ^{\cdot-/2-}$) anions formation of the TCBD and DCNQ moieties. The oxidation potentials of phenothiazine have been affected by electron-deficient TCBD or DCNQ due to induced electronic effects. On the anodic side, the TCBD-incorporated phenothiazine derivatives **29–32** and DCNQ-incorporated phenothiazine derivatives **34–37** showed two oxidation potentials in the range of 0.35–1.00 V, which corresponds to the donor phenothiazine entity. In the case of **29–32**, the first oxidation process was difficult by ~150 mV, whereas in **34–37**, the effect was significantly less, at ~50 mV considering DCNQ being an excellent electron acceptor. The phenothiazine derivatives **33** and **38** incorporated with TCBD and DCNQ exhibit a single reversible oxidation potential at 0.99 V and 0.09 V, respectively corresponding to the strong donor ability of the phenothiazine entity. The reduction potentials of derivatives **33** and **38**

appear in the low potential region at –0.20 V and –0.59 V, and –0.10 V and –0.27 V, respectively, corresponding to the formation of monoanions and dianions of the TCBD and DCNQ moieties (Table 1.1). The addition of cyano-based strong electron acceptors such as TCBD and DCNQ lowers the LUMO energy levels, resulting in a bathochromic shift in the UV-vis spectra. The DCNQ functionalized phenothiazine derivatives showed lower HOMO–LUMO energy gap compared to that of TCBD, owing to the strong accepting nature of the DCNQ moiety.

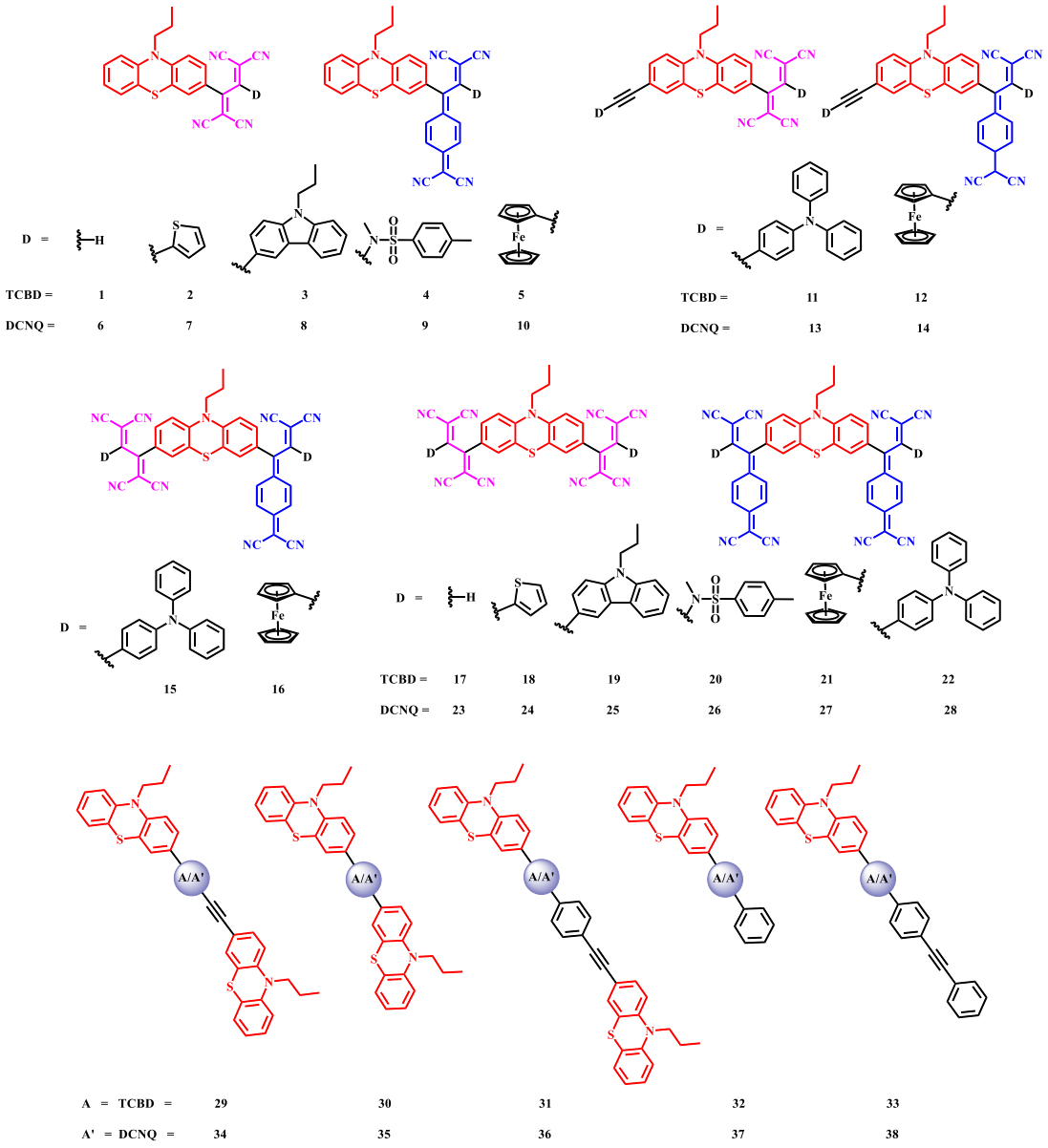

Figure 1.3. Chemical structures of phenothiazine derivatives **1–38** incorporated with TCBD or DCNQ units.

Table 1.1. Summary of photophysical, electrochemical, and theoretically obtained data of phenothiazine derivatives **1–38**.

Compounds	λ_{max} **(nm)**[a]	**ε / 10^4 (M^{-1}cm^{-1})**[a]	E_{ox} **(V)**[b]	E_{red} **(V)**[b]	E_g **(eV)**[c]
1	545	1.96	1.01	–0.05, –0.69	1.62
2	538	0.91	0.91, 1.65	–0.45, –0.75	2.32
3	542	0.76	0.82	–0.52, –0.89	2.51
4	591	0.58	1.02, 1.58	–0.27, –0.75	2.42
5	531	6.53	0.71	–0.75, –1.04	2.64
6	760	1.77	0.94	–0.07, –0.23	1.37
7	640	0.43	0.24, 1.01	–0.26, –0.85	1.85
8	613	2.33	0.83	–0.38, –0.95	1.89
9	686	1.01	0.89, 1.47	–0.16, –0.29	1.81
10	454	6.02	0.55, 0.65	–0.56	2.22
11	498	1.70	0.76, 0.89, 1.08	–0.58, –0.88	2.07
12	547	6.80	0.33, 0.68, 0.81	–0.76, –1.06	2.49
13	450	2.00	0.67, 0.79, 1.06	–0.45, –0.55	1.63
14	468	7.73	0.32, 0.55, 0.68	–0.55	2.03
15	636	2.80	0.79, 0.97	–0.37, –0.48, –0.64, –0.93	1.77
16	524	7.71	0.56, 0.68, 0.85	–0.54, –0.83, –1.11	2.28
17	620	2.18	1.02	–0.21, –0.86	1.78

18	548	1.13	0.91, 1.46	–0.47, –0.75	2.62
19	552	1.98	1.11	–0.48, –0.84	2.60
20	599	1.38	1.23, 1.65	–0.28, –0.78	2.19
21	537	7.01	0.68, 0.95	–0.72, –1.07	2.63
22	492	4.00	1.10	–0.52, –0.87	2.37
23	745	3.61	0.85	–0.10, –0.36	1.50
24	665	0.71	0.11, 0.76	–0.28, –0.45	2.02
25	597	1.99	1.38	–0.44, –0.86	1.89
26	702	0.90	1.01, 1.55	–0.13, –0.27	1.78
27	448	8.03	0.54, 0.79	–0.56	2.24
28	650	3.60	0.77, 0.90	–0.37, –0.49	1.71
29	564	–	0.47, 0.95	–0.72, –1.12	2.28
30	564	–	0.45, 0.90	–0.72, –1.13	2.42
31	541	–	0.45, 0.95	–0.78, –1.56	2.38
32	548	–	0.47, 0.94	–0.83, –1.23	2.37
33	549	0.48	0.99	–0.20, –0.59	2.35
34	753	–	0.37, 0.70	–0.33, –0.80	1.77
35	857	–	0.40, 0.78	–0.32, –0.73	1.87
36	858	–	0.35, 1.00	–0.31, –0.65	1.82
37	860	–	0.38, 0.91	–0.32, –0.92	1.79
38	675	0.39	0.09	–0.10, –0.27	1.82

[a]Absorbance measured in DCM and benzonitrile at 1×10^{-5} M concentration. λ_{max}: absorption maxima. ε: extinction coefficient. [b]Electrochemical analysis was estimated by DPV in 0.1 M solution of ($TBAPF_6$ in DCM) and ($TBAClO_4$ in o-dichlorobenzene) at a 100 mVs^{-1}

scan rate *versus* saturated calomel electrode, Fc/Fc^+ electrode and Ag/AgCl electrode. ^cE_g = HOMO–LUMO band gap as calculated by DFT at B3LYP/6-31G**/ B3LYP/6-31G*/ B3LYP/6-31G(d,p) basis set level for C, H and N.

1.5.2. Phenothiazine-5,5-dioxide-based TCBD and DCNQ Derivatives

The phenothiazine can be oxidized to phenothiazine-5,5-dioxide (*i.e.* sulfone), which lowers the electron density of the molecule, makes it more difficult to oxidize and subsequently tune its electronic properties.[101, 102] When the sulfur atom in the phenothiazine unit is oxidized to form sulfoxide and sulfone groups, the dihedral angle (the angle between the planes of the benzene rings) is significantly reduced. However, the fundamental structure of the phenothiazine unit remains unchanged.[103] The phenothiazine-5,5-dioxide possesses a non-planar structure have been considered a potential candidate for the luminophores family due to its high photoluminescence, phosphorescence, and room temperature phosphorescence (RTP) properties, and is also used in optoelectronic applications.[104–106]

The phenothiazine-5,5-dioxide derivatives **39–48** functionalized with TCBD and DCNQ were designed and synthesized *via* the [2 + 2] CA–RE reaction of the ethynyl-linked phenothiazine-5,5-dioxide derivatives with the strong acceptor TCNE/TCNQ units resulting in yields of 43–75% (Figure 1.4).[90, 107, 108] The phenothiazine-5,5-dioxide derivatives **39** and **40** functionalized with TCBD and DCNQ showed two absorption bands in the UV-vis spectra at 342, 427 nm and 373, 535 nm, respectively which is associated with ICT transition from the weak donor phenothiazine-5,5-dioxide to the acceptors TCBD/DCNQ moieties. The DCNQ substituted phenothiazine-5,5-dioxide derivative **40** exhibited absorption at higher wavelength regions than TCBD incorporated derivative **39**. The absorption spectra of mono- and di-TCBD incorporated phenothiazine-5,5-dioxide derivatives **41**, **42**, **45**, and **46** showed numerous absorption bands in the shorter wavelength region *i.e.* 250−430 nm, corresponding to the π−π*

transitions, and at the band at longer wavelength regions *i.e.* 437, 570, 446, and 546 nm, respectively, corresponding to the ICT transitions arising from D−A interactions. Additionally, the mono- and di-DCNQ incorporated phenothiazine-5,5-dioxide derivatives **43**, **44**, **47**, and **48** exhibited a broad absorption band in the longer wavelength region *i.e.* from 525−1000 nm (absorption maxima at 663, 660, 665 and 663 nm, respectively), which could be ascribed to the ICT transitions and in the shorter wavelength region from 300–500 nm, attributed to the π−π* transitions (Table 1.2). The ICT band of the DCNQ-incorporated phenothiazine-5,5-dioxide derivatives **40**, **43**, **44**, **47**, and **48** were bathochromically shifted by 90–150 nm in comparison to TCBD-incorporated phenothiazine-5,5-dioxide derivatives **39**, **41**, **42**, **45** and **46,** which are corresponding to the strong accepting nature of the DCNQ moiety.

The electrochemical studies were evaluated by the cyclic voltammogram, the TCBD and DCNQ incorporated phenothiazine-5,5-dioxide derivatives **39** and **40** revealed one reversible oxidation potential at 1.74 V and 1.41 V, respectively, corresponding to the weak donor ability of the phenothiazine-5,5-dioxide entity. Whereas the reduction waves of the phenothiazine-5,5-dioxide functionalized TCBD and DCNQ derivatives **39** and **40** occur at –0.09, –0.41 V and –0.11, –0.24 V, respectively, due to the formation of the mono and di anions of the TCBD and DCNQ moieties in the low potential region. In the case of the mono- and di-TCBD incorporated phenothiazine-5,5-dioxide derivatives **41**, **42**, **45**, and **46,** the two reduction potentials were observed in the range of –0.14 to –0.80 V, corresponding to mono ($TCBD^{0/\bullet-}$) and di ($TCBD^{-\bullet/2-}$) anion formation of the TCBD moiety in the cathodic region. Similarly, the mono- and di-DCNQ incorporated phenothiazine-5,5-dioxide derivatives **43**, **44**, **47**, and **48** revealed two oxidation potentials in the –0.01 to –0.66 region, which attributed to the formation of the mono and di anions of the electron-deficient DCNQ moiety in the anodic side. On the other hand, the TCBD and DCNQ incorporated triphenylamine substituted phenothiazine-5,5-dioxide derivatives **41**, **43**, **45**, and **47** revealed two oxidation potentials at 0.65,

1.25 V; 0.67, 1.27 V; 0.69, 1.04 V and 0.81, 1.30 V, respectively (Table 1.2). The first oxidation potential relates to the triphenylamine unit, while the second oxidation potential is associated with the phenothiazine-5,5-dioxide unit. For compound **42**, the two oxidation potentials were observed at 0.88 V and 1.06 V. The first oxidation corresponds to the phenothiazine group which is distant from TCBD, and the second potential is attributed to the phenothiazine group which is close to TCBD. Similarly, in the case of **44**, **46** and **48** only one oxidation potential was observed at 0.95, 1.07 and 0.90 V, respectively, corresponding to phenothiazine moieties (overlap of two anodic waves).

The DCNQ-incorporated phenothiazine-5,5-dioxide derivatives **40**, **43**, **44**, **47** and **48** show a lower HOMO–LUMO energy gap in comparison to TCBD functionalized phenothiazine-5,5-dioxide derivatives **39**, **41**, **42**, **45** and **46** corresponding to the strong acceptor character of the DCNQ unit.

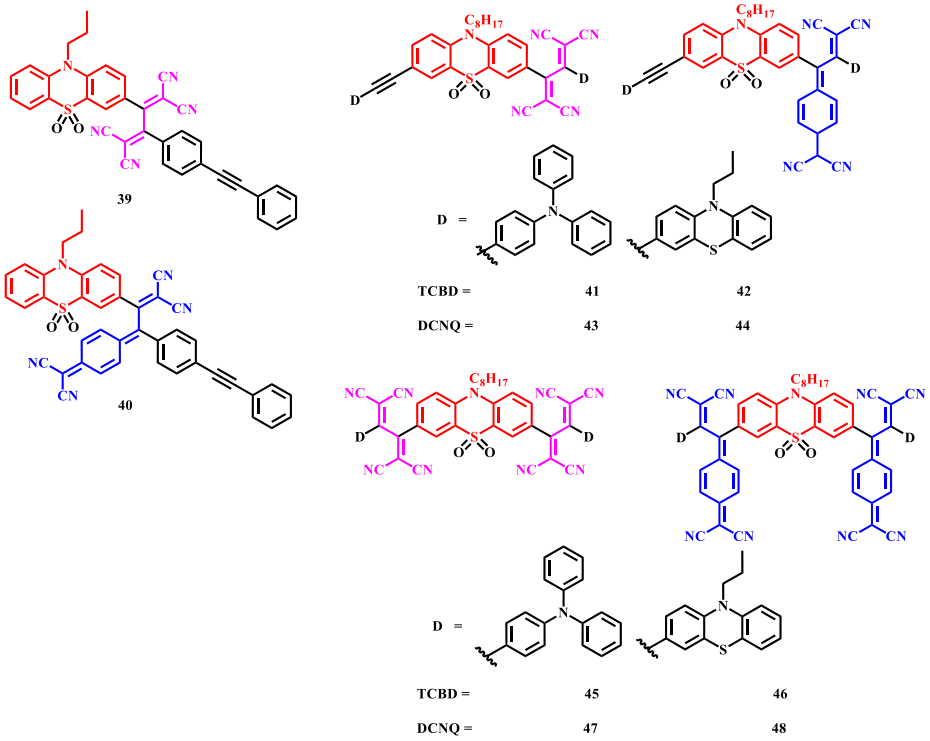

Figure 1.4. Chemical structures of phenothiazine-5,5-dioxide derivatives **39–48** incorporated with TCBD or DCNQ units.

Table 1.2. Summary of photophysical, electrochemical, and theoretically obtained data of phenothiazine-5,5-dioxide derivatives **39–48**.

Compounds	λ_{max} (nm)[a]	ε / 10^4 ($M^{-1}cm^{-1}$)[a]	E_{ox} (V)[b]	E_{red} (V)[b]	E_g (eV)[c]
39	427	0.78	1.74	–0.09, –0.41	2.77
40	535	0.88	1.41	–0.11, –0.24	2.19
41	437	–	0.65, 1.25	–0.17 to –0.80	1.80
42	570	1.01	0.88, 1.06	–0.16, –0.54	2.09
43	663	–	0.67, 1.27	–0.33, –0.66	1.41
44	660	1.42	0.95	–0.03, –0.13	1.46
45	446	–	0.69, 1.04	–0.17 to –0.80	2.22
46	546	1.84	1.07	–0.14, –0.57	2.05
47	665	–	0.81, 1.30	–0.13, –0.27	1.66
48	663	0.78	0.90	–0.01, –0.13	1.62

[a]Absorbance measured in DCM at 1×10^{-5} M concentration; λ_{max}: absorption maxima; ε: extinction coefficient. [b]Electrochemical analysis was estimated by DPV in 0.1 M solution of tetrabutylammonium hexafluorophosphate ($TBAPF_6$) in DCM and $TBA(ClO)_4$ in DCB at a 100 mVs^{-1} scan rate *versus* Ag/AgCl electrode. [c]E_g = HOMO–LUMO band gap as calculated by DFT at B3LYP/6-31G(d,p) and B3LYP/6-31G** basis set level for C, H, and N.

1.5.3. TCBD and DCNQ Derivatives Based on BODIPY

The BODIPY dyes, often known as 4,4-Difluoro-4-bora-3a,4a-diaza-s-indacene dyes, have attracted significant interest over recent years due to their excellent chemical and photophysical properties. These include strong absorption, high molar absorption coefficients, long fluorescence lifetimes, high fluorescence quantum yields, low toxicity, and as well as good photochemical stability.[109–112] The optical and electronic

characteristics of BODIPYs can be tuned by extending the conjugation and introducing suitable donor/acceptor (D/A) units at the meso and pyrrolic (α and β) positions.[113, 114] Consequently, BODIPY-based π-conjugated dyes have found widespread application in the development of laser dyes, fluorescent imaging agents, chemosensors, molecular switches, photosensitizers, light-emitting devices, and optoelectronic materials.[115–117]

In 2017, 2020 and 2024, Misra *et al*. reported the TCBD and DCNQ incorporated meso BODIPYs **49–54,** which were synthesized by the [2 + 2] CA–RE reaction resulted in 60–85% yields (Figure 1.5).[118–120] The absorption spectra showed that TCBD-incorporated BODIPYs **49**, **50**, and **53** showed substantial broadening in the S0→S1 transition, as well as a broad shoulder peak in the 530–700 nm region. Similarly, DCNQ-incorporated BODIPYs **51**, **52**, and **54** had the same trend, showing a broadening of the S0→S1 peak with a new broad peak covering the 560–900 nm range. The DCNQ-incorporated BODIPYs **51**, **52**, and **54** exhibit a red-shifted ICT band in the lower energy region in comparison to TCBD-incorporated BODIPYs **49**, **50**, and **53** corresponding to stronger electronic communication between the D and A units (Table 1.3).

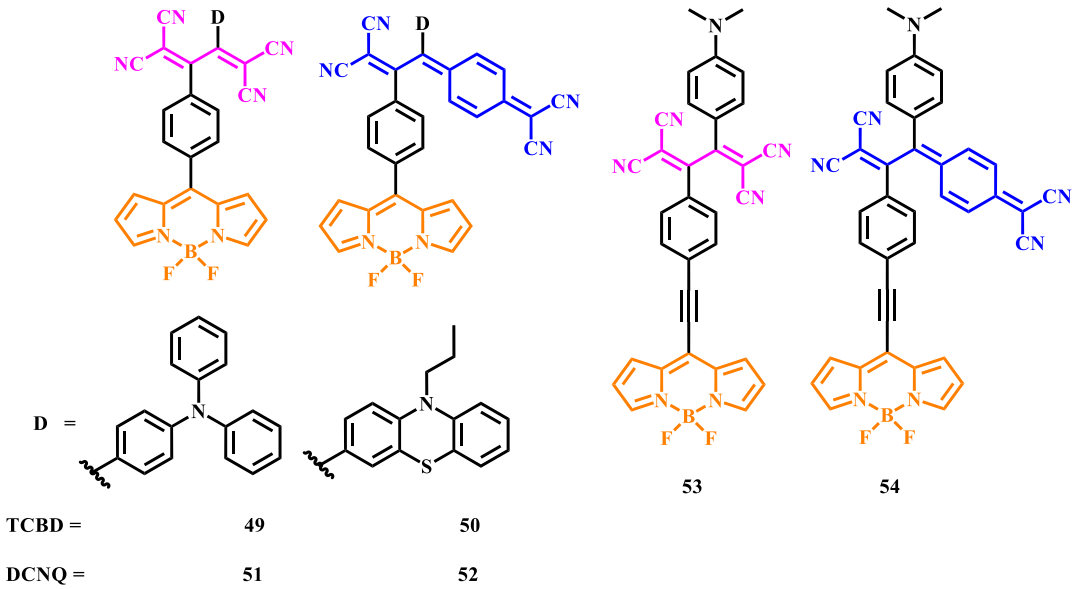

Figure 1.5. Chemical structures of BODIPY derivatives **49–54** functionalized with TCBD or DCNQ moieties.

The electrochemical studies suggest that the TCBD incorporated BODIPYs **49** and **50** exhibited three reduction potentials at (–0.20, –0.56 and –0.91V) and (–0.10, –0.47 and –0.79 V), respectively. The first two one-electron reduction potentials were attributed to the formation of the mono ($TCBD^{0/\cdot-}$) and di ($TCBD^{\cdot-/2-}$) anions of the TCBD moiety and the last reduction potential was due to the anion formation of the BODIPY unit. Similarly, the DCNQ incorporated BODIPYs **51** and **52** exhibits two reduction potentials observed at (–0.05 and –0.18 V) and (–0.05 and –0.11 V), respectively, corresponding to the formation of the mono ($DCNQ^{0/\cdot-}$) and di ($DCNQ^{\cdot-/2-}$) anions of the DCNQ moiety, and another reduction potential which were cathodically shifted and appeared at –0.78 and –0.70 V, respectively which is due to the reduction of the BODIPY. On the other hand, the oxidation potentials of the TCBD/DCNQ incorporated BODIPYs **49–52** were observed at (1.36, 1.71 V), (1.04, 1.67 V), (1.09, 1.72 V), and (0.99, 1.61 V), respectively. The first oxidation wave corresponds to the oxidation of the triphenylamine and phenothiazine entities, while the second oxidation wave is attributed to the cation formation of the BODIPY unit (Figure 1.6 and Table 1.3). These findings indicate that while reducing the TCBD-incorporated BODIPYs **49** and **50** is more challenging compared to DCNQ-incorporated BODIPYs **51** and **52**, it demonstrates a superior ability to disrupt the electronic characteristics of phenothiazine, triphenylamine, and BODIPY entities within the conjugates.

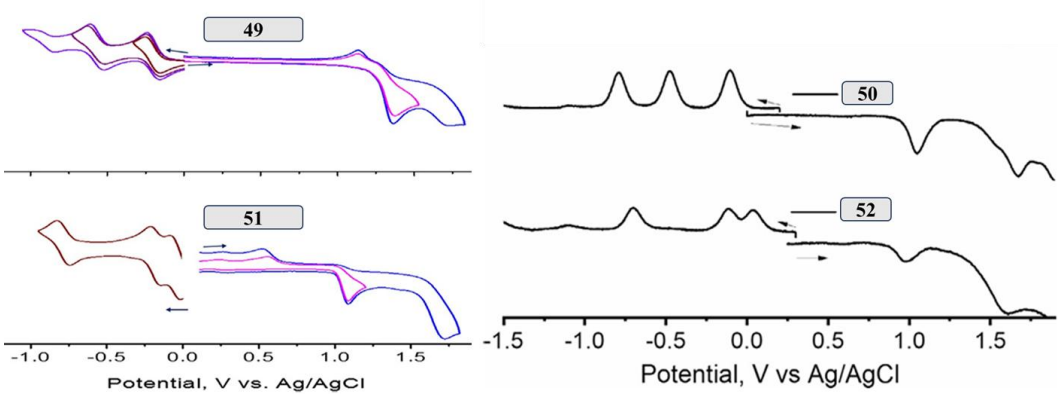

Figure 1.6. Cyclic voltammograms of BODIPYs **49** and **51**, and differential pulse voltammograms of BODIPYs **50** and **52** in benzonitrile containing 0.1 M (TBA)ClO_4 were recorded at a scan rate of 100 mVs^{-1}.

The *N*,*N*-dimethylanilne functionalized donor−acceptor BODIPYs **53** and **54** showed oxidation potential at 1.51 and 0.99 V, due to the formation of $NND^{\cdot+}$ on the cathodic region. Four reduction potentials were observed at (–0.32, –0.43, –0.82, –1.55 V) and (–0.12, –0.25, –0.52, –1.44 V) respectively, the initial first two reduction potentials were observed due to the mono and di anion formation of the TCBD and DCNQ moieties. The last two reduction potentials were observed due to the formation of the BODIPY mono and di anions.[121] Each step corresponds to a one-electron transfer. The BODIPY **54** was easier to reduce in comparison to BODIPY **53** because the DCNQ has better electron acceptor nature (Table 1.3 and Figure 1.7).

The DFT calculations suggest that the DCNQ-incorporated BODIPYs lower the HOMO–LUMO gap as compared to TCBD-incorporated BODIPYs because of the strong accepting capability of the DCNQ.

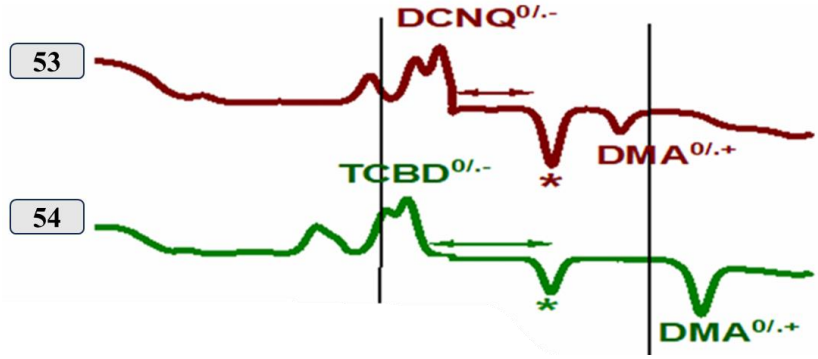

Figure 1.7. Differential pulse voltammograms of *N*,*N*-dimethylanilne functionalized BODIPYs **53** and **54** in DCB containing 0.1 M (TBA)ClO_4 supporting electrolyte at 298 K. *indicates ferrocene oxidation used as an internal standard.

Table 1.3. Summary of photophysical, electrochemical, and theoretically obtained data of BODIPY derivatives **49–54**.

Compounds	λ_{max} (nm)[a]	E_{ox} (V)[b]	E_{red} (V)[b]	E_g (eV)[c]
49	–	1.36, 1.71	–0.20, –0.56, –0.91	–
50	–	1.04, 1.67	–0.10, –0.47, –0.79	1.97
51	–	1.09, 1.72	–0.05, –0.18, –0.78	–
52	–	0.99, 1.61	–0.05, –0.11, –0.70	1.57
53	561	1.51	–0.32, –0.43, –0.82, –1.55	2.41
54	689	0.99	–0.12, –0.25, –0.52, –1.44	1.82

[a]Absorbance measured in (benzonitrile, toluene, and DCB) at 1×10^{-5} M concentration. λ_{max}: absorption maxima. [b]Electrochemical analysis was estimated by DPV in 0.1 M solution of $(TBA)ClO_4$ in benzonitrile and $TBAPF_6$ in DCM at a 100 mVs^{-1} scan rate *versus* Ag/AgCl electrode. [c]E_g = HOMO–LUMO band gap as calculated by DFT at B3LYP/6-31G (d,p) basis set level.

1.5.4. Isoindigo-based TCBD and DCNQ Derivatives

Isoindigo is used as a strong acceptor to improve in push-pull organic chromophores due to its versatile acceptor nature. Its photochemical stability, planar structure, and potential for structural modification.[122–124] It has been used as an antiproliferative agent in pharmaceutical applications and applied in the design of small molecules and polymers that are donor–acceptor (D–A) based.[125, 126] Isoindigo-based materials are promising in organic semiconductors and photovoltaics due to their high absorption coefficients and good charge transport properties in the visible spectrum.[127, 128]

In 2020, Misra *et al*. reported the synthesis of four triphenylamine (TPA) substituted mono- and di-TCBD and DCNQ-incorporated isoindigo derivatives, namely **55** (90%), **56** (93%), **57**

(83%), and **58** (87%) *via* the CA-RE reaction as shown in Figure 1.8.[129]

The mono-TCBD incorporated isoindigo derivative **55** exhibited two distinct absorption bands in its electronic absorption spectrum, the band at lower wavelength region *i.e.* 457 nm corresponds to the π–π* transition, while the band at higher wavelength region *i.e.* 594 nm is associated with the ICT transition. Similarly, the di-TCBD incorporated isoindigo derivative **56** shows two absorption bands at 475 nm and 554–710 nm, which are due to the π–π* transition and the ICT transition, respectively. Notably, the absorption spectrum of isoindigo derivative **55** with mono-TCBD displays a red shift compared to isoindigo derivative **56** with di-TCBD. This shift is attributed to the more twisted backbone structure of isoindigo **56** followed by the incorporation of an additional TCBD unit. Additionally, the DCNQ-incorporated isoindigo derivatives **57** and **58** exhibit two distinct electronic absorption bands, with high-energy bands at approximately 428 nm and 430 nm, and low-energy bands at 628 nm and 619 nm, respectively, as shown in Table 1.4. The high-energy bands are caused by the π−π* transition, while the low-energy bands are due to the ICT transition.

The three reduction potentials were observed in the isoindigo derivatives **55–58** that are incorporated with mono- and di-TCBD and DCNQ. The first two reduction potentials in isoindigo derivatives occur at –0.30 and –0.57 V (for **55**), –0.17 and –0.76 V (for **56**), –0.15 and –0.26 V (for **57**) and –0.15 and –0.26 V (for **58**), corresponding to the TCBD and DCNQ moieties. The isoindigo derivatives **55–58** undergo the third reduction at around –0.85 V, –0.87 V, –0.86 V, and –0.89 V, respectively, attributed to the isoindigo moiety (Table 1.4). The strong acceptor character of the DCNQ moiety is indicated by its lower reduction values compared to the TCBD and isoindigo units. The mono-TCBD and DCNQ substituted isoindigo derivatives **55** and **57** exhibit two oxidation potentials at 0.97 V and 1.25 V, and 0.92 V and 1.72 V, respectively, attributed to the TPA moiety. The di-TCBD and DCNQ incorporated isoindigo derivatives **56** and **58** display a single oxidation potential ~ 1.25 V and 0.99 V, respectively. The photophysical and DFT

investigations indicate a red shift in the absorption spectra of mono- and di-DCNQ functionalized isoindigo derivatives. These derivatives also exhibit low HOMO–LUMO gap values.

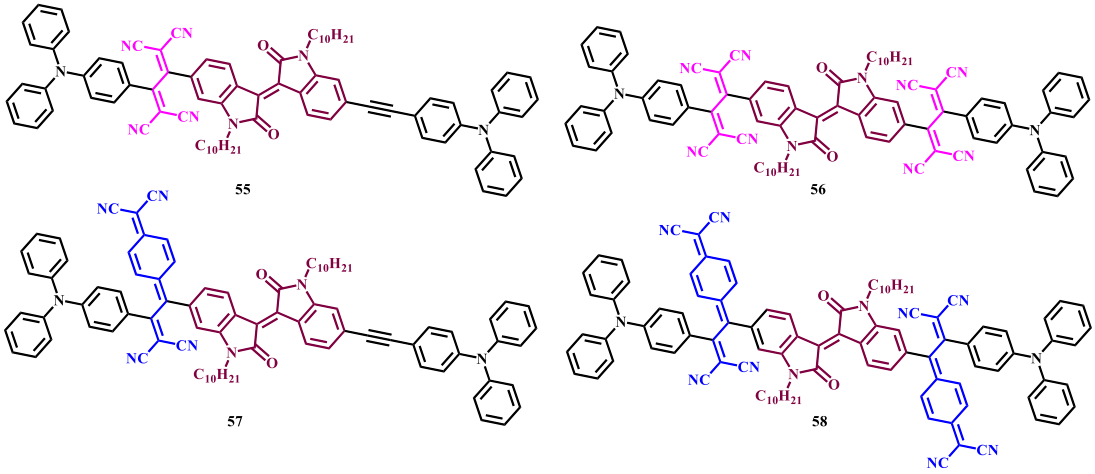

Figure 1.8. Chemical structures of isoindigo derivatives **55–58** functionalized with TCBD or DCNQ moieties.

Table 1.4. Summary of photophysical, electrochemical, and theoretically obtained data of isoindigo derivatives **55–58**.

Compounds	λ_{max} **(nm)**[a]	ε **($M^{-1}cm^{-1}$)**[a]	E_{ox} **(V)**[b]	E_{red} **(V)**[b]	E_g **(eV)**[c]
55	594	23720	0.97 1.25	–0.30 –0.57 –0.85	1.81
56	475	55620	1.25	–0.17 –0.76 –0.87	1.95
57	628	33720	0.92 1.72	–0.15 –0.26 –0.86	1.78

58	619	33240	0.99	–0.15 –0.26 –0.89	1.55

[a]Absorbance measured in DCM at 1×10^{-5} M concentration. λ_{max}: absorption maxima. ε: extinction coefficient. [b]Electrochemical analysis was estimated by DPV in 0.1 M solution of tetrabutylammonium hexafluorophosphate ($TBAPF_6$) in DCM at a 100 mVs^{-1} scan rate *versus* saturated calomel electrode. [c]E_g = HOMO–LUMO band gap as calculated by DFT at B3LYP/6-31G** basis set level for C, H and N.

1.5.5. TCBD and DCNQ Derivatives Based on Truxene

Truxene is a planar heptacyclic aromatic compound that can be regarded as a cyclotrimer of fluorene.[130] Truxene is a star-shaped molecule, plays key role in the construction of extended π-conjugated molecular systems.[131] Truxene has excellent solubility, thermal and chemical stability, and ease of functionalization making it an essential building block for the design of π-conjugated derivatives in a variety of applications, such as OFETs, OPVs, chemical sensors, OLEDs, organic fluorescent probes, organic solar cells (OSCs), nonlinear optics, liquid crystals, and bioimaging.[132–136] Jian Pei *et al*. have invested significant synthetic effort in developing a range of π-conjugated truxene-based molecular systems with a star shape that have potential uses in optoelectronics.[137]

The tri-TCBD/DCNQ incorporated truxene derivatives **59** (71%), **60** (65%), **61** (65%), and **62** (60%), were synthesized by the [2 + 2] CA–RE reaction (Figure 1.9).[138, 139] The photonic and electronic characteristics of tri-TCBD/DCNQ incorporated truxenes with end-capping moieties of triphenylamine (**59**, **61**) and phenothiazine (**60**, **62**) were investigated. The photophysical properties of the truxene derivatives **59** and **60** incorporated with TCBD display absorption maxima at 433 nm and 545 nm, respectively, while the DCNQ-incorporated truxene derivatives **61** and **62** displayed absorption maxima at 655 nm and 637 nm, respectively. These lower energy

regions are caused by ICT transition corresponding to strong D–A interactions between donors (triphenylamine and phenothiazine) to acceptors (TCBD and DCNQ) moieties. The DCNQ-incorporated truxene derivatives **61** and **62** exhibit a red-shifted absorption and low HOMO–LUMO gap comparison to TCBD-incorporated truxenes **59** and **60**. This suggests that truxenes **61** and **62** have strong donor–acceptor (D–A) interactions. The electron-deficient TCBD incorporated truxene derivative **60** exhibits two reduction potentials at –0.80 V and –1.18 V, with the oxidation of PTZ anodically shifted by 210 mV to 0.51 V. The DCNQ-incorporated truxene **62** showed two reduction potentials at –0.62 and –0.78 V corresponding to DCNQ moiety while the oxidation of phenothiazine exhibited at 0.39 V. The TCBD/DCNQ incorporated truxene derivatives **59** and **61** display a one reduction wave at –1.49 and –1.46 V due to the strong acceptor TCNE and TCNQ moieties. The oxidation wave at 1.30 and 1.25 V, respectively, attributed to the donor moiety (Table 1.5). The stronger charge transfer observed in derivatives **61** and **62** compared to **59** and **60** is attributed to the superior electron acceptor ability of the DCNQ moiety.

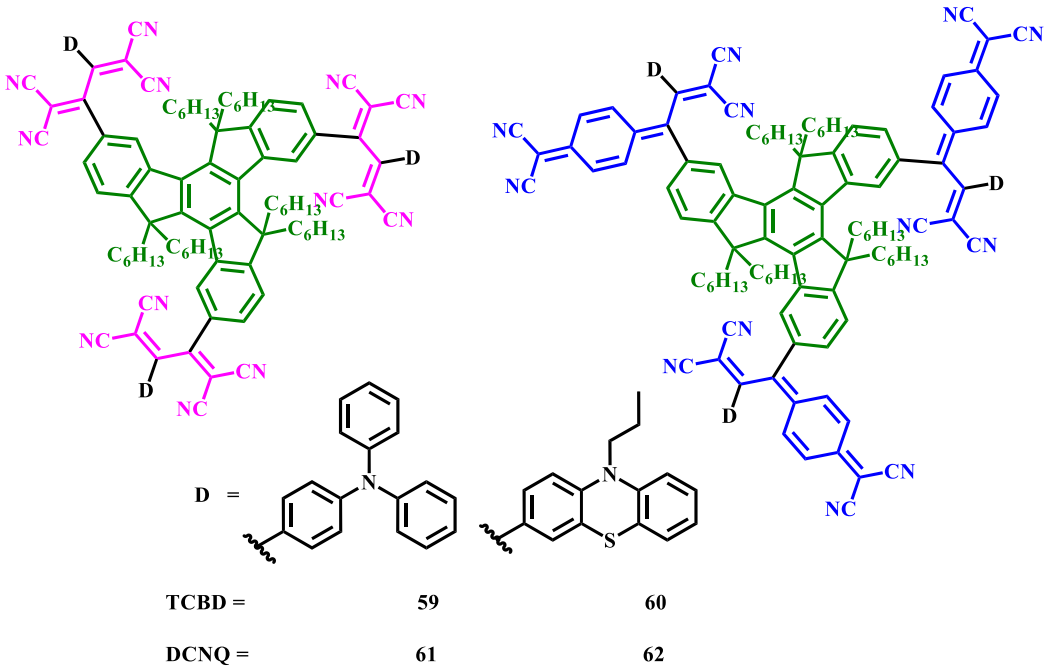

Figure 1.9. Chemical structures of truxene derivatives **59–62** functionalized with TCBD or DCNQ moieties.

Table 1.5. Summary of photophysical, electrochemical, and theoretically obtained data of truxene derivatives **59–62**.

Compounds	λ_{max} **(nm)**[a]	ε **/ 10^5 (M^{-1}cm^{-1})**[a]	E_{ox} **(V)**[b]	E_{red} **(V)**[b]	E_g **(eV)**
59	433	1.5	1.30	–1.49	2.34[c]
60	545	–	0.51	–0.80 –1.18	1.31[b]
61	655	1.8	1.25	–1.46	1.92[c]
62	637	–	0.39	–0.62 –0.78	1.01[b]

[a]Absorbance measured in DCM (**59**, **61**) and toluene (**60**, **62**) at 1×10^{-5} M concentration. λ_{max}: absorption maxima; ε = extinction coefficient. [b]Electrochemical analysis was estimated by DPV in 0.1 M solution of tetrabutylammonium hexafluorophosphate ($TBAPF_6$) in DCM (**59**, **61**) and benzonitrile (**60**, **62**) at a 100 mVs^{-1} scan rate *versus* Fc/Fc^+ electrode. [c]E_g = HOMO–LUMO band gap as calculated by DFT at B3LYP/6-31G** basis set level in the gas phase.

1.5.6. Naphthalenediimide-based TCBD and DCNQ Derivatives

Naphthalenediimide (NDI) can function as a subunit that withdraws electrons in a D-π-A chromophore system. NDIs are known for their excellent light absorption, high electron mobility, outstanding thermal stability, and favorable photochemical properties, making them ideal for various optoelectronic applications.[140–142] As significant electron-accepting (n-type) semiconductors, NDIs are utilized in OPVs, OTFTs, OLEDs, and OSCs applications.[143–145]

In 2021, Rao *et al*. reported the synthesis of symmetrical and unsymmetrical donor–acceptor based on TPA donor and NDI acceptor chromophores **63–67**. These chromophores were synthesized *via* a [2 +

2] CA-RE reaction with the strong electron acceptors TCNE (1,1,2,2-tetracyanoethylene) and TCNQ (7,7,8,8-tetracyanoquinodimethane), resulting in yields of 41–81% (Figure 1.10).[146] The TCBD and DCNQ naphthalenediimide derivatives **63–67** exhibit absorption bands in the range of 280–400 nm, attributed to the π-π* transition. While in the longer wavelength regions displayed at 486 nm, 484 nm, 650 nm, 651 nm, and 650 nm, respectively, corresponding to ICT transitions. (Table 1.6). The two cross-conjugated DCNQ incorporated derivatives **65** (650 nm), **66** (651 nm), and **67** (650 nm) exhibited red-shifted absorption band when compared to the TCBD functionalized derivatives **63** (486 nm) and **64** (484 nm). These results show that the DCNQ moiety is a stronger acceptor than the TCBD moiety.

The TCBD and DCNQ naphthalenediimide derivatives **63–67** display multiple redox potentials with onset values of oxidation (E_{ox}) and (E_{red}) shown in Table 1.6. The onset values of the oxidation (E_{ox}) of naphthalenediimide derivatives **63–67** are at 1.19, 0.91, 0.96, 0.92, and 0.89 V, and the onset values of the reduction (E_{red}) are –0.31, –0.24, –0.26, –0.41, and –0.24 V, respectively. The estimated HOMO/LUMO energy levels of naphthalenediimide derivatives **63–67** from the equation (HOMO = –e[E_{ox} + 4.7] eV and LUMO = –e[E_{red} + 4.7] eV)[147] are –5.89/–4.39, –5.61/–4.46, –5.66/–4.44, –5.62/–4.29, and –5.59/–4.46 eV, respectively. The naphthalenediimide derivatives **67** showed a significant LUMO energy level because of the increased electron-withdrawing ability of the TCBD and DCNQ moieties. According to electrochemical properties, reducing the LUMO energy level of chromophores is the most efficient strategy to prevent electron entrapment by moisture or oxygen.

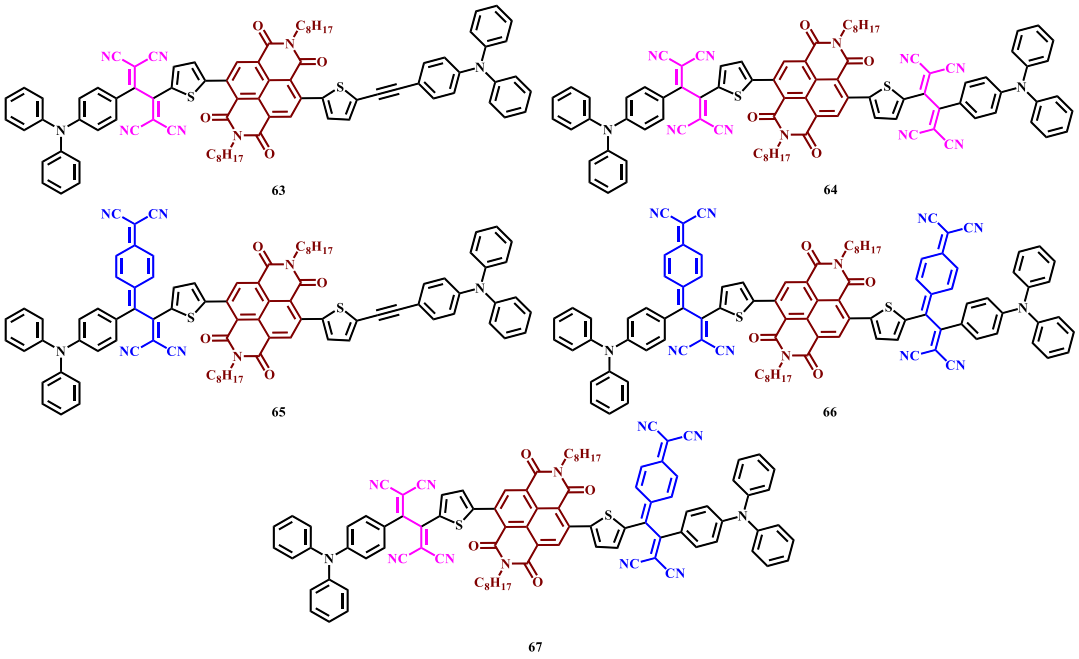

Figure 1.10. Chemical structures of naphthalenediimide derivatives **63–67** functionalized with TCBD or DCNQ moieties.

The performance of optoelectronic materials is determined by the energy gap between the HOMO and LUMO, known as the HOMO–LUMO energy gap (E_g). Additionally, the distribution of electron density in the frontier molecular orbitals is influenced by the electron-donating strength of the various NDI-based chromophores. Figure 1.11 represents the frontier molecular orbitals of **63–67** as calculated using DFT. The results suggest that the HOMO electron density is mainly concentrated on the triphenylamine moiety, whereas the LUMO is dispersed over the NDI component. After introducing the TCNE and TCNQ electron-accepting groups into the molecular structures transfers the electron density of the LUMO to these groups and moves away from the NDI core. The theoretically calculated HOMOs of the NDI derivatives **63–67** are –5.46 eV, –6.06 eV, –5.44 eV, –6.03 eV, and –5.96 eV and the corresponding LUMOs are –3.91 eV, –4.30 eV, –4.03 eV, –4.22 eV, and –4.21 eV, respectively. The theoretically calculated energy gaps (E_g) for **63–67** are 1.55 eV, 1.76 eV, 1.41 eV, 1.81 eV, and 1.75 eV, respectively (Figure 1.11). The LUMO energy levels of the chromophores are lowered by electron acceptor subunits like TCBD and DCNQ, which can be used to tune the bandgap.

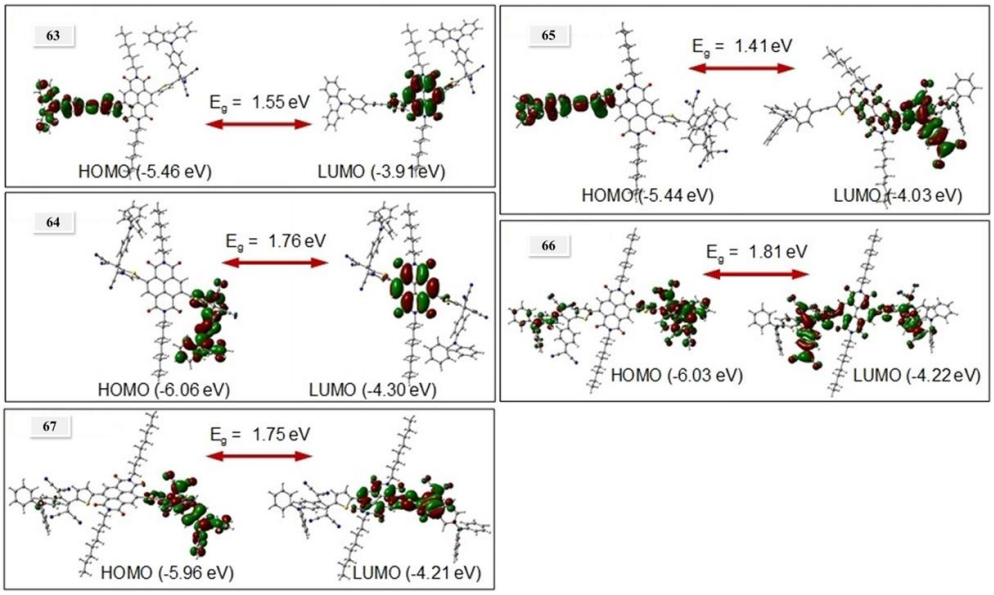

Figure 1.11. Frontier molecular orbitals of push-pull **63** to **65** chromophores, calculated at B3LYP/6-31G(d,p)//B3LYP/6-311G(d,p) and **66** to **67** chromophores, calculated at B3LYP/6-31G(d,p)//B3LYP/6-311+G(d,p) basis set level.

Table 1.6. Summary of photophysical, electrochemical, and theoretically obtained data of naphthalenediimide derivatives **63–67**.

Compounds	λ_{max} **(nm)**[a]	ε **/ 10^4 (M^{-1}cm^{-1})**[a]	E_{ox}^{onset} **(V)**[b]	E_{red}^{onset} **(V)**[b]	E_g **(eV)**[b]	E_g **(eV)**[c]
63	486	3.67	1.19	–0.31	1.50	1.55
64	484	5.76	0.91	–0.24	1.15	1.76
65	650	3.14	0.96	–0.26	1.22	1.41
66	651	9.81	0.92	–0.41	1.33	1.81
67	650	2.49	0.89	–0.24	1.13	1.75

[a]Absorbance measured in DCM at 1 × 10^{-5} M concentration. λ_{max}: absorption maxima; ε = extinction coefficient. [b]Electrochemical analysis was estimated by CV in 0.1 M solution of tetrabutylammonium hexafluorophosphate ($TBAPF_6$) in DCM at a 100 mVs^{-1} scan rate *versus* Ag/AgCl electrode. [c]E_g = HOMO–LUMO band gap as calculated by

DFT at B3LYP/6-31G(d,p)//B3LYP/6-311G(d,p) (for **63** to **65**) and B3LYP/6-31G(d,p)//B3LYP/6-311+G(d,p) (for **66** to **67**).

1.5.7. Benzothiadiazole-based TCBD and DCNQ Derivatives

Benzothiadiazole is a heterocyclic compound consisting of a benzene ring fused with a thiadiazole ring. It has an electron-deficient nature and the ability to enhance charge transport properties.[148–151] Benzothiadiazole derivatives are used as fluorescent probes, photoinduced intramolecular charge transfer (ICT), solar cells, materials science, OLEDs, pharmaceuticals, and nonlinear optics.[152–155] Lee *et al*. developed non-fullerene acceptors for organic solar cells based on 2,1,3-benzothiadiazole (BTD) functionalized with rhodamine, resulting in 8.19% power conversion efficiency.[156] Yang *et al*. investigated 2,1,3-benzothiadiazole (BTD) chromophores based on diketopyrrolopyrrole and isoindigo for use in high-performance ambipolar semiconducting materials.[157]

The TCBD and DCNQ incorporated benzothiadiazole derivatives **68–78** were designed and synthesized *via* [2 + 2] CA-RE reaction with ethynyl linked donor functionalized benzothiadiazole derivatives and strong acceptors TCNE and TCNQ resulting in 50–85% yields (Figure 1.12).[158–160] The TCBD and DCNQ incorporated benzothiadiazole derivatives **68–78** show absorption bands in shorter wavelength regions at 275–400 nm range attributed to the π-π* transition, whereas, in the longer wavelength region the absorption maxima occur at 455–690 nm range, corresponding to the ICT transition. The DCNQ-incorporated derivatives show a substantial bathochromic shift compared to the TCBD-incorporated derivatives because of the strong D–A interaction of the DCNQ moieties.

The electrochemical studies suggest that the TCBD-incorporated benzothiadiazole derivatives **68** and **70** show three reversible reduction potentials in the range of –0.21 V to –1.03 V. The first and second reduction potentials correspond to the mono- and di-anion formation of the TCBD moiety and the third reduction potential is attributed to the benzothiazole unit. The DCNQ-incorporated benzothiadiazole

derivatives **69** and **71** exhibit three reversible reduction potentials on the cathodic side in the range of −0.21 V to −0.99 V corresponding to the DCNQ and benzothiadiazole acceptor moieties. On the anodic side, the benzothiadiazole derivatives **68–71** showed two oxidation potentials in the region of 0.92–1.34 V corresponding to the triphenylamine entity.

In case of mono-TCBD and DCNQ incorporated benzothiadiazole derivatives **72** and **73** exhibit two reversible reduction potentials at (−0.61, −1.04 V) and (−0.59, −0.72 V), respectively, attributed to the reduction of TCBD and DCNQ moieties and third reduction potential observed at −1.92 V and −1.98 V corresponding to the benzothiadiazole entity. On the anodic side, the benzothiadiazole derivatives **72** and **73** showed two quasi-reversible oxidation potentials at (0.62, 0.80 V) and (0.57, 0.72 V), respectively corresponding to the donor triphenylamine unit. On the other hand, the di-TCBD incorporated benzothiadiazole derivative **74** exhibits three reduction potentials at –0.15, –0.30 and –0.96 V. The first two reduction potentials corresponds to the TCBD moiety and the third reduction potential is attributed to the benzothiadiazole unit. The di-DCNQ incorporated benzothiadiazole derivative **75** exhibits multiple reversible reduction potentials in the region of −0.12 to −1.06 V, due to the DCNQ and benzothiadiazole acceptor moieties. In the case of benzothiadiazole derivative **76** which has both TCBD and DCNQ electron acceptors, four reduction potentials were observed on the cathodic regions at −0.52, −0.66, −0.85, and −1.32 V corresponding to strong acceptor TCBD/DCNQ and benzothiadiazole moieties. On the anodic side, the benzothiadiazole derivative **76** exhibits two oxidation potentials at 0.57 and 0.80 V, due to the TPA unit.

The benzothiadiazole derivatives **77** and **78** functionalized with TCBD and DCNQ display four reduction potentials on the cathodic side. The first two reduction potentials occurring between –0.2 V and –0.85 V are attributed to the TCBD and DCNQ moieties. The subsequent two reduction potentials ranging from –0.95 V to –1.40 V correspond to the naphthalimide and benzothiadiazole acceptor units. On the anodic side, the TCBD and DCNQ incorporated benzothiadiazole derivatives **77** and

78 exhibits one oxidation potential at 1.10 and 0.83 V corresponding to the donor triphenylamine unit (Table 1.7). A comparison of the first reduction potentials of benzothiadiazole derivatives **68–78** reveals that the DCNQ-incorporated derivatives **69**, **71**, **73**, **75**, **76**, and **78** are more easily reduced than the TCBD- incorporated derivatives **68**, **70**, **72**, **74**, and **77**. This difference can correspond to the stronger electron-accepting character of the DCNQ moiety.

The DFT calculations show that the electron density of HOMOs for benzothiadiazole derivatives **68–78** are mainly delocalized over the donor triphenylamine (TPA) entity and adjacent to the TCBD/DCNQ moieties or directly linked to the benzothiadiazole core. Whereas the LUMOs are mainly concentrated on the electron acceptors such as benzothiadiazole, TCBD, and DCNQ moieties. The DCNQ-incorporated benzothiadiazole derivatives lower the LUMO energy level, which leads to a low HOMO–LUMO gap and bathochromic shift in the electronic absorption spectra as compared to TCBD-incorporated benzothiadiazole derivatives.

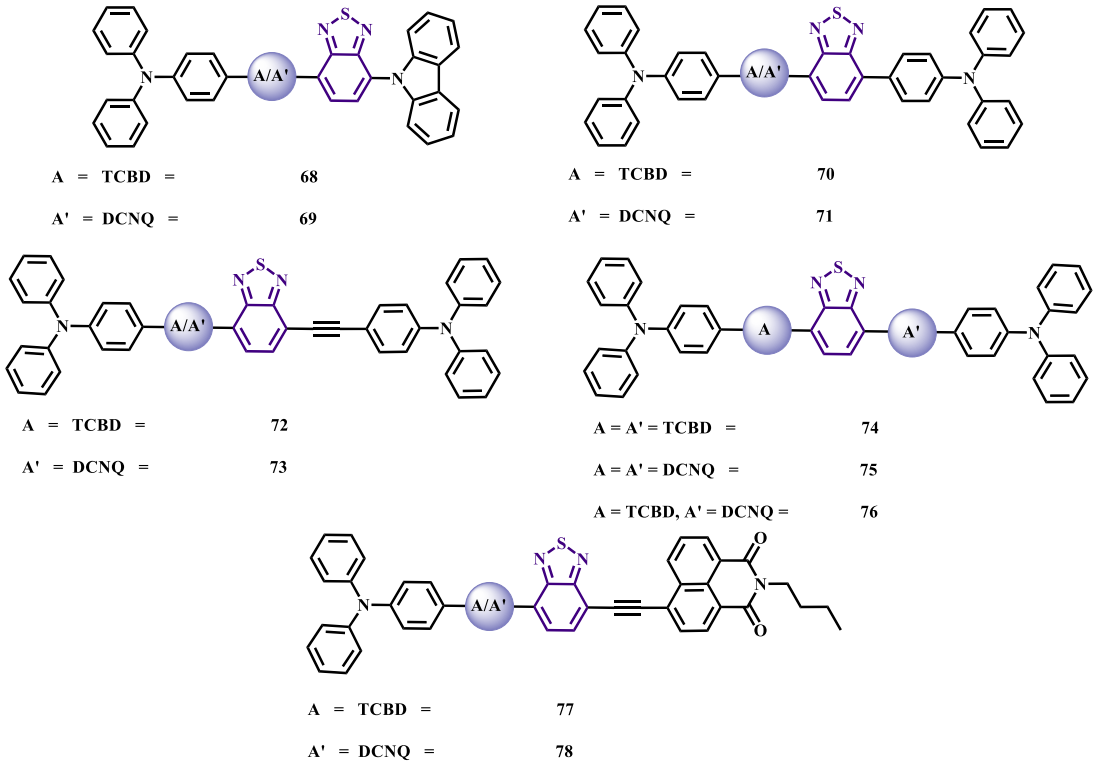

Figure 1.12. Chemical structures of benzothiadiazole derivatives **68–78** functionalized with TCBD or DCNQ moieties.

Table 1.7. Summary of photophysical, electrochemical, and theoretically obtained data of benzothiadiazole derivatives **68–78**.

Compounds	λ_{max} **(nm)**[a]	ε **/ 10^4 (M^{-1}cm^{-1})**[a]	E_{ox} **(V)**[b]	E_{red} **(V)**[b]	E_g **(eV)**[c]
68	518	4.86	0.97 1.18	–0.36 –0.83 –1.03	2.46
69	665	5.11	0.92 1.34	–0.21 –0.35 –0.99	2.31
70	560	3.38	0.94 1.15	–0.43 –0.81 –1.02	2.40
71	683	5.66	0.92 1.07	–0.22 –0.36 –0.99	2.18
72	–	–	0.62 0.80	–0.61 –1.04 –1.92	1.23[b]
73	–	–	0.57 0.72	–0.59 –0.72 –1.98	1.16[b]
74	490	6.02	1.04	–0.15 –0.30	2.03

				–0.96	
75	637	5.14	0.91	–0.12 –0.22 –0.35 –0.45 –1.06	1.86
76	–	–	0.57 0.80	–0.52 –0.66 –0.85 –1.32	1.07[b]
77	455	3.7	1.10	–0.45 –0.84 –1.19 –1.40	4.44
78	690	1.3	0.83	–0.29 –0.74 –0.95 –1.25	4.17

[a]Absorbance measured in (benzonitrile and DCM) at 1×10^{-5} M concentration. λ_{max}: absorption maxima; ε: extinction coefficient. [b]Electrochemical analysis was estimated by DPV in 0.1 M solution of [(TBA)ClO_4 in benzonitrile and $TBAPF_6$ in DCM] at a 100 mVs^{-1} scan rate *versus* [Fc/Fc^+ electrode and SCE electrode]. [c]E_g = HOMO–LUMO band gap as calculated by DFT at B3LYP/6-31G*// B3LYP/6-31G** basis set level.

1.5.8. Fullerene-based TCBD and DCNQ Derivatives

Fullerene (C_{60}) has a strong electron-accepting nature due to its electron-deficient π system and good charge-transporting. Fullerenes and their derivatives have a high electron affinity and low reorganization energy during electron transfer. They also possess an exceptional capacity to transport charge, making them suitable electron acceptor components in organic photosynthetic and photovoltaic systems. Fullerene-based acceptors with high LUMO levels need to produce a high voltage in organic photovoltaic systems.[161–164]

In 2014, Yamada *et al*. reported the TCBD and DCNQ incorporated diethylamine and octamethylferrocenyl functionalized fulleropyrrolidine derivatives **79–82** which were synthesized *via* the Prato reaction followed by [2 + 2] CA–RE reaction resulting in 96%, 73%, 25%, and 86% yields, respectively (Figure 1.13).[165]

The absorption spectra of fulleropyrrolidine-based derivatives **79–82** are the result of contributions from fullerene (C_{60}) and the donor–acceptor structure. The absorption maxima of the pyrrolidinofullerene-based derivatives **79–82** show at 475, 707, 401, and 554 nm, respectively which corresponds to ICT transition. The cyclic voltammograms of compounds **79–82** displayed a one-electron reversible oxidation potential at 0.90, 1.00, 1.02, and 1.07 V, respectively. This oxidation potential corresponds to the *N*,*N*-diethylaniline and octamethylferrocenyl moiety. Additionally, five distinct and well-separated one-electron reversible reduction potentials were observed ranging from –0.72 to –2.19 V corresponding to the TCBD/DCNQ and fullerene acceptor units (Table 1.8). The quantum yields of fulleropyrrolidine-based derivatives **80**, **81**, and **82** are diminished to 4.0×10^{-5}, 2.0×10^{-5}, and 1.0×10^{-5}, respectively. This is in comparison to the reference quantum yield of 6.0×10^{-4} when excited by C_{60} at a wavelength of 330 nm, with N-methylfulleropyrrolidine as the reference compound. In contrast, the quantum yield of **79** remains at 6.0×10^{-4}, indicating that there is no reduction in the fluorescence of fullerene. Substituting with N,N-

diethylaniline may result in a longer lifetime compared to octamethylferrocenyl due to the greater distance and the characteristics of the Marcus inverted region.[166]

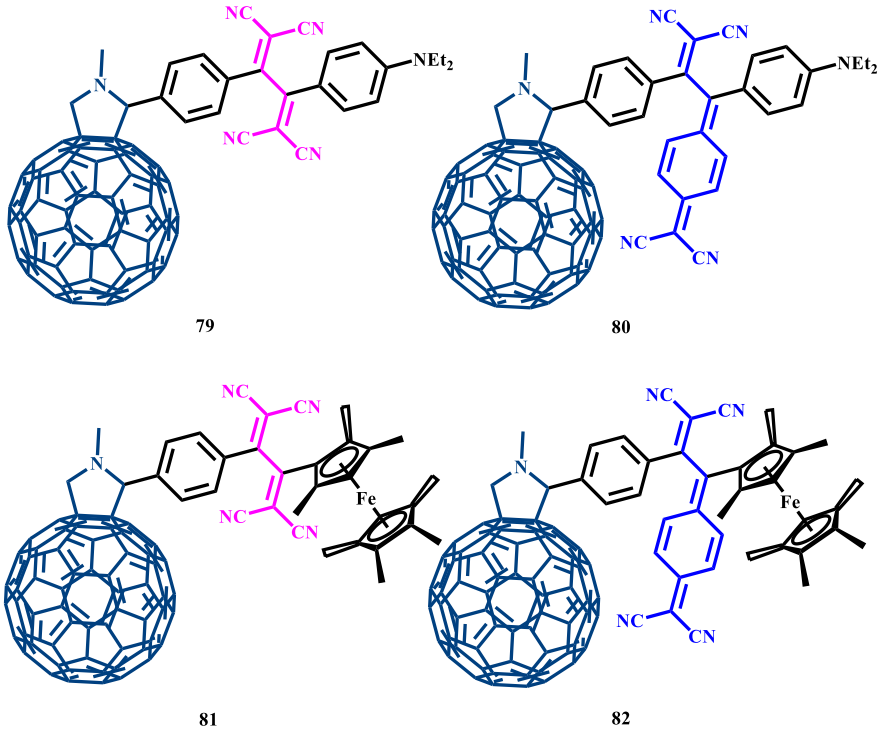

Figure 1.13. Chemical structures of fulleropyrrolidine derivatives **79–82** functionalized with TCBD or DCNQ moieties.

Table 1.8. Summary of photophysical, and electrochemical obtained data of fullerene derivatives **79–82**.

Compounds	λ_{max} **(nm)**[a]	ε **/ 10^4 (M^{-1}cm^{-1})**[a]	E_{ox} **(V)**[b]	E_{red} **(V)**[b]	E_g^{opt} **(eV)**[a]
79	475	2.68	0.90	–0.95 –1.15 –1.24 –1.55 –2.19	2.61
80	707	3.55	1.00	–0.70	1.75

				–0.84 –1.15 –1.52 –2.05	
81	401	1.90	1.02	–0.94 –1.11 –1.34 –1.52 –2.06	3.09
82	554	2.0	1.07	–0.72 –0.82 –1.12 –1.51 –2.05	2.24

[a]Absorbance measured in CH_2Cl_2 at 6×10^{-6} M concentration. λ_{max}: absorption maxima. ε: extinction coefficient, E_g^{opt}: optical bandgap. [b]Electrochemical analysis in 0.1 M solution of tetrabutylammonium hexafluorophosphate ($TBAPF_6$) in DCM at a 100 mVs^{-1} scan rate *versus* Fc^+/Fc (ferrocenium/ferrocene).

1.5.9. Quinoxaline-based TCBD and DCNQ Derivatives

Quinoxalines are a class of heterocyclic compounds containing a fused ring system composed of a benzene ring and a pyrazine ring. Quinoxaline functionalized compounds have significant importance in organic synthesis, medicinal chemistry, and materials science due to their diverse biological and pharmacological activities.[167] Burrows *et al*. synthesized bipolar materials incorporating quinoxalines as the electron-transporting unit and arylamine as the hole-transporting

unit.[168] The photophysical properties of aza-derivatives of 1,2-diaryl-ethylenes, including quinoxaline, have garnered significant attention due to the influence of the n-π* states introduced by nitrogen atoms.[169] The quinoxaline-based D–A systems are found useful in studying electron transfer and seeking applications for aggregation-induced emission.[170–173] The quinoxaline derivatives **83** and **84** were synthesized by [2 + 2] CA-RE reaction in good yields (Figure 1.14).[174]

The absorption maximum of quinoxaline derivative **83** is located at 467 nm, attributed to an ICT transition from donor (D) to acceptor (A) TCBD moiety. In case of compound **84**, two absorption bands were observed at 463 nm and 658 nm corresponding to the π−π* transition and ICT transition, respectively (Figure 1.15). The compound **84** shows a red-shifted absorption by 191 nm compared to compound **83** indicating the strong electron-accepting character of the DCNQ moiety. The electrochemical properties of quinoxaline derivatives **83** and **84** functionalized with TCBD and DCNQ were examined using cyclic voltammetry. Both derivatives display a single oxidation potential at 0.45 V and 0.44 V, respectively, corresponding to the triphenylamine unit. The quinoxaline derivatives **83** and **84** reveal three reduction potentials observed at (−0.68, −1.04, and −2.26V) and (−0.32, −0.54, and −1.96 V), respectively (Table 1.9). The first two reduction potentials correspond to electron-deficient TCBD and DNCQ moieties and the third reduction potential is attributed to the quinoxaline unit. In compounds **83** and **84**, the HOMO was mainly localized on the triphenylamine units that are directly attached to the quinoxaline moiety. On the other hand, the LUMO was mainly located on the quinoxaline and TCBD unit in compound **83** and on the quinoxaline and DCNQ unit in compound **84**.

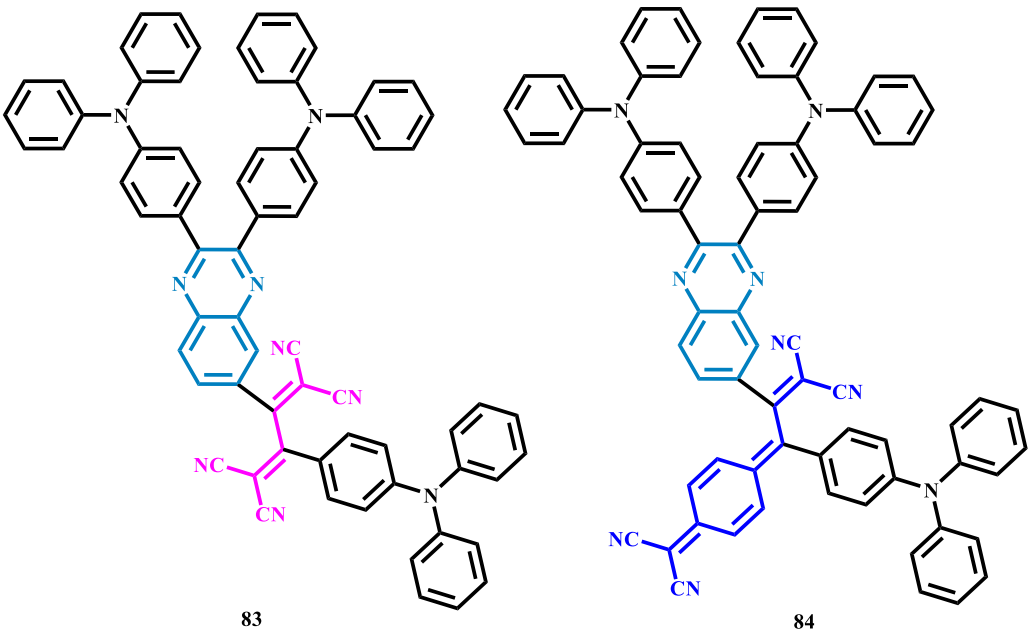

Figure 1.14. Chemical structures of Quinoxaline derivatives **83** and **84** functionalized with TCBD or DCNQ moieties.

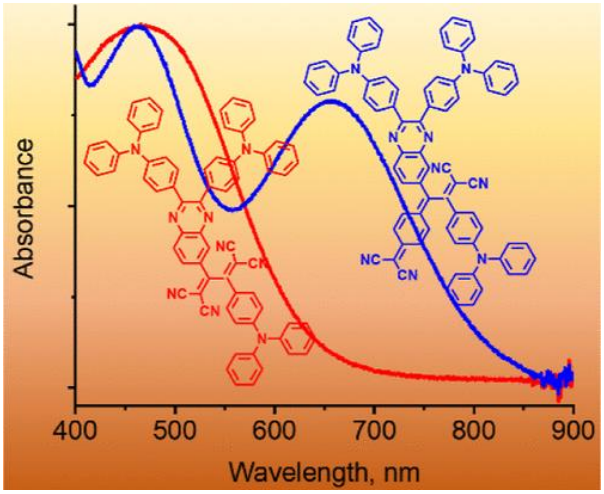

Figure 1.15. Absorption spectra of Quinoxaline derivatives **83** and **84** in benzonitrile.

Table 1.9. Summary of photophysical, electrochemical, and theoretically obtained data of Quinoxaline derivatives **83** and **84**.

Compounds	λ_{max} **(nm)**[a]	E_{ox} **(V)**[b]	E_{red} **(V)**[b]	E_g **(eV)**[c]
83	467	0.45	–0.68	2.01

			–1.04 –2.26	
84	463 658	0.44	–0.32 –0.54 –1.96	1.60

[a]Absorbance measured in benzonitrile at 1×10^{-5} M concentration. λ_{max}: absorption maxima. [b]Electrochemical analysis was estimated by DPV in 0.1 M solution of tetrabutylammonium hexafluorophosphate ($TBAPF_6$) in DCM at a 100 mVs^{-1} scan rate *versus* Fc/Fc^+ electrode. [c]E_g = HOMO–LUMO band gap as calculated by DFT at B3LYP/6-31G* basis set level in the gas phase.

1.5.10. 3-Alkynylindole-based TCBD and DCNQ Derivatives

Indole is a bicyclic structure consisting of a five-membered nitrogen-containing pyrrole ring fused with a six-membered benzene ring.[175, 176] It is widely recognized for its structural characteristics and versatile properties, making it a promising candidate in various fields such as organic synthesis, materials science, and pharmaceuticals.[177, 178] The 3-Alkynylindole is a compound in which an alkynyl group is attached to the third position of an indole ring. Researchers are interested in the various electrical and photonic properties that can be achieved by structurally modifying 3-alkynylindole. It is possible to precisely modify its electrical structure by changing the substituents and functional groups, thus enabling the development of specialized applications in molecular electronics, sensors, and optoelectronics.[179–181]

The 3-alkynylindole-based TCBD and DCNQ derivatives **85–102** were synthesized *via* the [2 + 2] CA-RE reaction of ethynyl-linked 3-alkynylindole derivatives with strong acceptor TCNE and TCNQ. The yields of the corresponding 3-alkynylindole derivatives **85–102** are shown in Figure 1.16.[182] The extensive structural variation seen in this investigation provides an understanding of the relationship between

the structure and optical properties of the nonplanar push-pull chromophores. The chromophores functionalized with TCBD (**85–93**) have absorption maxima (λ_{max}) values ranging from 395 to 442 nm, but the chromophores incorporated with TCNQ (**94–102**) have λ_{max} values close to the near-infrared spectrum, between 612 and 658 nm (Table 1.10). The low-energy absorption bands correspond to ICT transitions between electron-poor cyano-rich acceptor units and electron-rich indole groups. Compared to those induced by TCNE, chromophores containing TCNQ exhibit significantly red-shifted low-energy absorption bands. These observations align with the calculated energy band gap values for chromophores **85–102** (Figure 1.17). The calculated band gap values for TCBD incorporated derivatives **85–93** range from 2.52 to 2.89 eV, whereas DCNQ incorporated derivatives **94–102** have lower band gap values ranging from 1.78 to 2.33 eV compared to TCBD incorporated derivatives **85–93**. Notably, derivatives with nitrobenzene-containing chromophores **89** and **98** exhibit the lowest band gap values. This can be attributed to the strong electron-accepting properties of nitrobenzene relative to other substituent groups studied. In all cases, the electron density distribution in the HOMOs is primarily located on the donor indole moiety, while the LUMOs are predominantly concentrated on the electron-deficient cyano-rich regions. Both HOMO and LUMO depictions reveal small but discernible overlaps, illustrating the electron transfer from the electron-rich indole to the electron-deficient cyano-rich core. These findings indicate the potential of indole-containing push−pull systems for applications in optoelectronics.

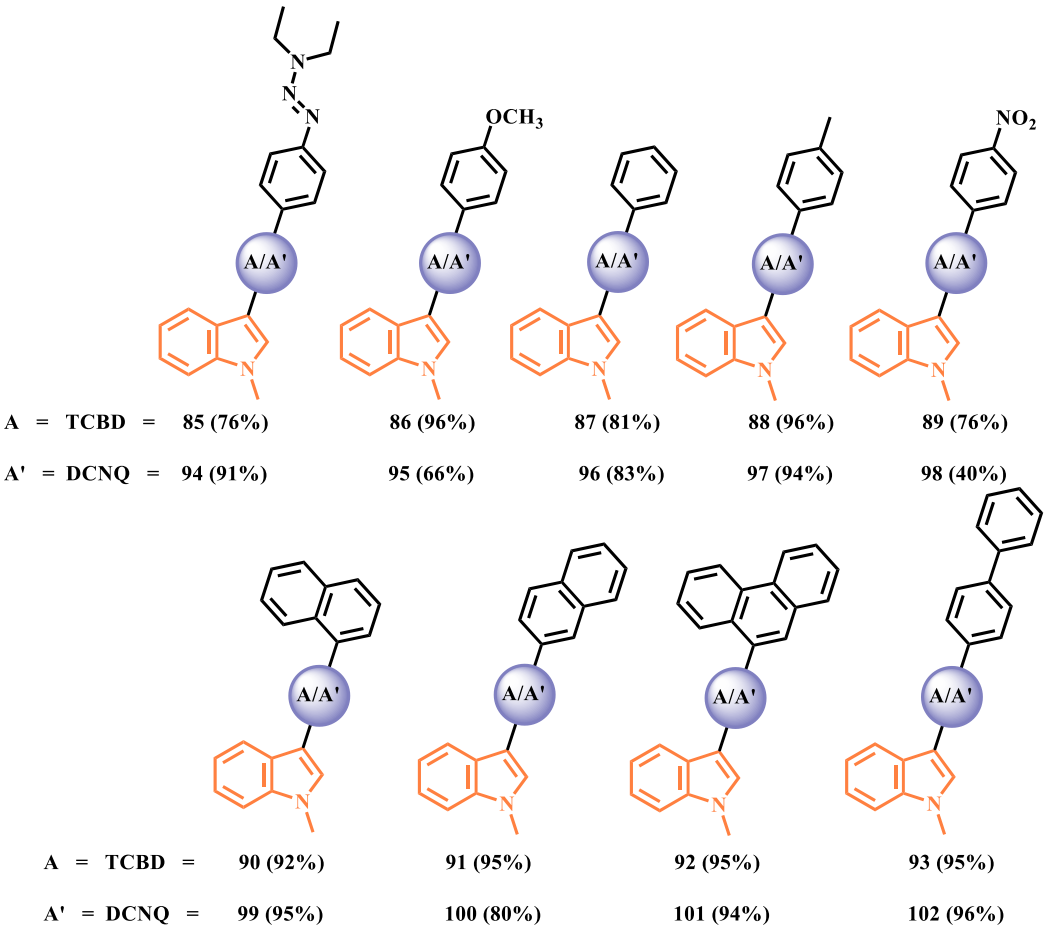

Figure 1.16. Chemical structures of 3-alkynylindole derivatives **85–102** functionalized with TCBD or DCNQ moieties.

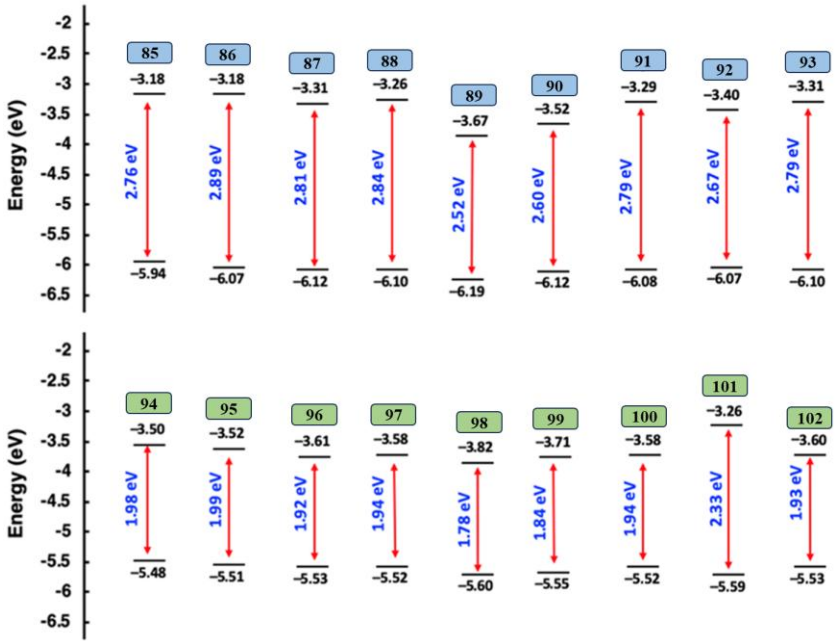

Figure 1.17. Energy-level diagram of the HOMOs and LUMOs of TCBD functionalized 3-alkynylindole derivatives **85–93** and DCNQ

functionalized 3-alkynylindole derivatives **94−102** estimated by DFT studies using B3LYP/6-31G* basis set level.

Table 1.10. Summary of photophysical and theoretically obtained data of 3-alkynylindole derivatives **85–102**.

Compounds	λ_{max} **(nm)**[a]	ε **/ 10^4 (M^{-1}cm^{-1})**[a]	E_{HOMO} **(V)**[b]	E_{LUMO} **(V)**[b]	E_g **(eV)**[b]
85	442	3.73	–5.94	–3.18	2.76
86	428	1.4	–6.07	–3.18	2.89
87	426	1.53	–6.12	–3.31	2.81
88	427	0.85	–6.10	–3.26	2.84
89	407	1.45	–6.19	–3.67	2.52
90	431	1.06	–6.12	–3.52	2.60
91	395	1.72	–6.08	–3.29	2.79
92	434	0.97	–6.07	–3.40	2.67
93	390	3.8	–6.10	–3.31	2.79
94	612	2.84	–5.48	–3.50	1.98
95	610	3.2	–5.51	–3.52	1.99
96	614	1.88	–5.53	–3.61	1.92
97	614	2.32	–5.52	–3.58	1.94
98	635	2.2	–5.60	–3.82	1.78
99	653	1.88	–5.55	–3.71	1.84
100	617	1.95	–5.52	–3.58	1.94
101	658	1.40	–5.59	–3.26	2.33
102	626	2.4	–5.53	–3.60	1.93

[a]Absorbance measured in dichloromethane solvent at 25 °C. λ_{max}: absorption maxima; ε: extinction coefficient. [b]HOMO and LUMO and energy band gap calculated by DFT calculations using B3LYP/6-31G* basis set level.

1.5.11. Silafluorene-based TCBD and DCNQ Derivatives

Silafluorene is a derivative of fluorene where a silicon atom replaces one of the carbon atoms in the five-membered ring because of its high thermal stability, fast electron transport, and excellent photoluminescence.[183, 184] Silafluorene derivatives have numerous uses as organic functional materials, including OFETs, OPVs, OLEDs, and molecular wires.[185–187] Moon *et al*. have developed two new donor–acceptor (D–A) type polymers utilizing silafluorenes as electron donors, which exhibit significant solubility and high thermal stability.[188] Shimizu *et al*. summarized the progress in utilizing various substituted silafluorenes as solid-state emitters.[189]

The TCBD and DCNQ incorporated silafluorene derivatives **103–108** were synthesized by the [2 + 2] CA-RE reaction of ethynyl-bridged silafluorenes with three equivalents of TCNE and TCNQ (Figure 1.18).[190] The DCNQ-incorporated silafluorene derivatives **106–108** exhibit red-shifted absorption spectra with lower HOMO–LUMO energy gap in comparison to the TCBD-incorporated silafluorene derivatives **103–105**.

The TCBD-incorporated silafluorene derivatives **103–105** containing amino electron-donating groups display distinct absorption maxima at 457 nm, 459 nm, and 439 nm, respectively, with shoulder bands extending to approximately 550 nm. These bands correspond to the ICT transitions involving the lone pairs electrons of the amino groups. Conversely, the DCNQ-incorporated silafluorene derivatives **106–108**, which also incorporate amino donors, exhibit two distinct absorption bands at (458 nm, 696 nm), (449 nm, 672 nm), and (450 nm, 676 nm), respectively. These absorption bands indicate strong multi-ICT transitions and highlight stronger donor−acceptor interactions in silafluorene derivatives **106–108** (Table 1.11). The silafluorene

derivative **107** exhibited a slightly red-shifted ICT transition compared to compounds **106** and **108**. This suggests that the *N*,*N*-dimethylamino groups have a greater ability to donate electrons than the triphenylamino groups. The absorption maxima of silafluorene derivative **107** remains unchanged compared to compound **108**, suggesting that the substituents on the Si atom do not significantly affect the absorption spectra. Overall, symmetrical silafluorene derivatives **103−108**, characterized by a D−A−D′−A−D structural motif, exhibit variable absorption bands ranging from 300 to 900 nm across the UV-vis and NIR spectral regions.

The electrochemical investigation of silafluorene derivatives **103–108** reveals distinct oxidation potentials ranging from 0.58 to 1.82 V, attributed to the respective terminal *N*,*N*-dimethylaniline and triphenylamine donor moieties. TCBD derivatives **103–105** exhibit three oxidation potentials at (0.74 V, 1.31 V), (0.75 V, 1.31 V), and (0.79 V, 1.33 V), corresponding to the donor silafluorene, NND, and TPA units, respectively. In contrast, DCNQ derivatives **106–108** display oxidation potentials at 0.84 V, 1.03 V, and 1.03 V, respectively, which are 0.47 V, 0.28 V, and 0.30 V lower than their TCNE counterparts. Both TCBD and DCNQ silafluorene derivatives **103–108** show two reversible reduction potentials ranging from −0.89 to −0.16 V, associated with TCNE and TCNQ acceptor units, suggesting two-electron transfers potentially forming tetraanionic species.[191] The reduction potentials of **103–108** are exhibited at (−0.31 V, −0.72 V), (−0.19 V, −0.67 V), (−0.16 V, −0.68 V), (−0.33 V, −0.82 V), (−0.27 V, −0.85 V), and (−0.25 V, −0.69 V), respectively (Table 1.11). Comparative analysis of the first reduction potential among the symmetrical silafluorene derivatives indicates that TCNQ derivatives **106–108** are more readily reduced compared to TCNE derivatives **103–105**. This is attributed to the stronger electron-withdrawing nature of TCNQ units. The HOMO energy levels predominantly exhibit electron density localized on the silafluorene or phenyl moieties, whereas the LUMO energy levels generally show delocalization on the TCBD and DCNQ acceptor moieties. The TCBD derivatives **103–105** display π−π* transitions in the shorter wavelength region and ICT transitions in the

longer wavelength region. Similarly, DCNQ derivatives **106–108** exhibit ICT transitions with lower HOMO–LUMO energy gaps, consistent with experimental observations.

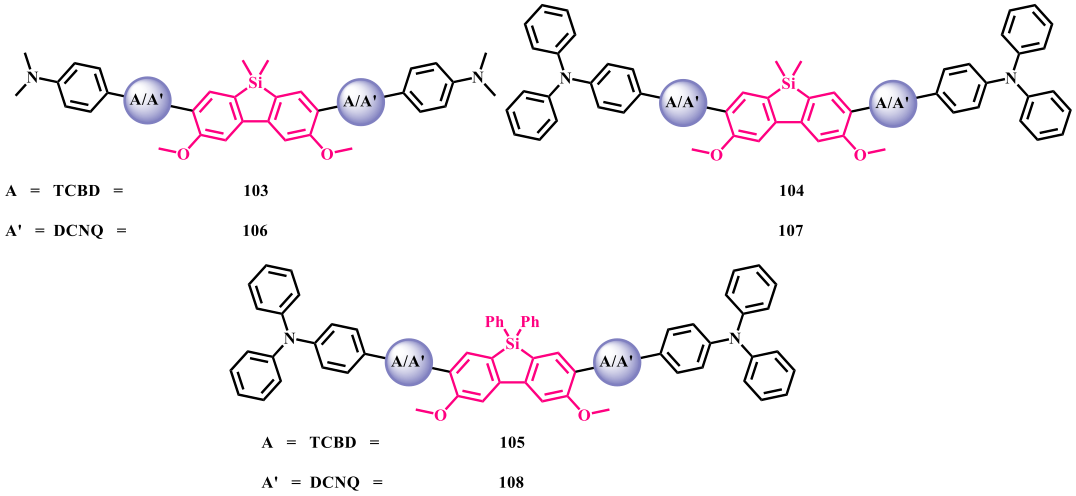

Figure 1.18. Chemical structures of TCBD/DCNQ functionalized Silafluorene derivatives **103–108**.

Table 1.11. Summary of photophysical, electrochemical, and theoretically obtained data of Silafluorene derivatives **103–108**.

Compounds	λ_{max} **(nm)**[a]	ε **/ 10^4 (M^{-1}cm^{-1})**[a]	E_{ox} **(V)**[b]	E_{red} **(V)**[b]	E_g **(eV)**[c]
103	457	6.18	0.74 1.31	–0.31 –0.72	2.28
104	459	3.81	0.75 1.31	–0.19 –0.67	2.03
105	439	5.68	0.79 1.33	–0.16 –0.68	2.01
106	696	6.64	0.84	–0.33 –0.82	1.88
107	672	5.1	1.03	–0.27	1.75

				–0.85	
108	676	4.27	1.03	–0.25 –0.69	1.75

[a]The absorption maxima estimated from the UV−vis absorption spectra (1.0×10^{-5} M in DCM). λ_{max}: absorption maxima; ε: extinction coefficient. [b]Electrochemical analysis in 0.1 M solution of tetrabutylammonium hexafluorophosphate ($TBAPF_6$) in DCM at a 100 mVs^{-1} scan rate *versus* saturated calomel electrode. [c]Energy band gap calculated by DFT calculations using B3LYP/6-31G** basis set level.

1.5.12. Tetraphenylethylene-based TCBD and DCNQ Derivatives

Tetraphenylethylene (TPE) has been used as a weak electron donor in organic frameworks with D–A and D–A–D structures.[192, 193] TPE is a commonly used AIE fluorophore and has been effectively utilized for developing various AIE-active stimuli-responsive materials.[194–196] AIEs are utilized in bioimaging, biological process elucidation, innovative therapies including photothermal therapy (PTT), cocktail therapy, photodynamic therapy (PDT), and sonodynamic therapy enhancement.[197–205] The TCBD and DCNQ functionalized tetraphenylethylene derivatives **109** and **110** were synthesized using an excess of tetracyano derivatives (TCNE and TCNQ) *via* [2 + 2] CA-RE reaction in 71% and 47% yields, respectively (Figure 1.19).[206] The tetraphenylethylene derivatives functionalized with DCNQ and TCBD were studied for their photophysical and electrochemical properties.

The TCBD functionalized tetraphenylethylene derivative **109** exhibits two absorption bands at 307 nm ($\varepsilon = 4.56 \times 10^4\ M^{-1}cm^{-1}$) and 469 nm ($\varepsilon = 1.13 \times 10^5\ M^{-1}cm^{-1}$). The absorption band at lower wavelength region is due to the π–π* transition, while the absorption band at higher wavelength region corresponds to the ICT transition due to the involvement of dicyanovinylic moieties. On the other hand, the DCNQ-incorporated TPE derivative **110** exhibits three different absorption bands at 337 nm ($\varepsilon = 1.14 \times 10^5\ M^{-1}cm^{-1}$), 468 nm ($\varepsilon = 7.85 \times 10^4\ M^{-1}cm^{-1}$) and 688 nm ($\varepsilon = 1.55 \times 10^5\ M^{-1}cm^{-1}$). The first

absorption band is due to the π–π* transition, while the second absorption band corresponds to a less intense CT band because of the involvement of the dicyanovinylic moieties, and the third band is attributed to an intense charge transfer band involving the dicyanoquinoïd moieties.

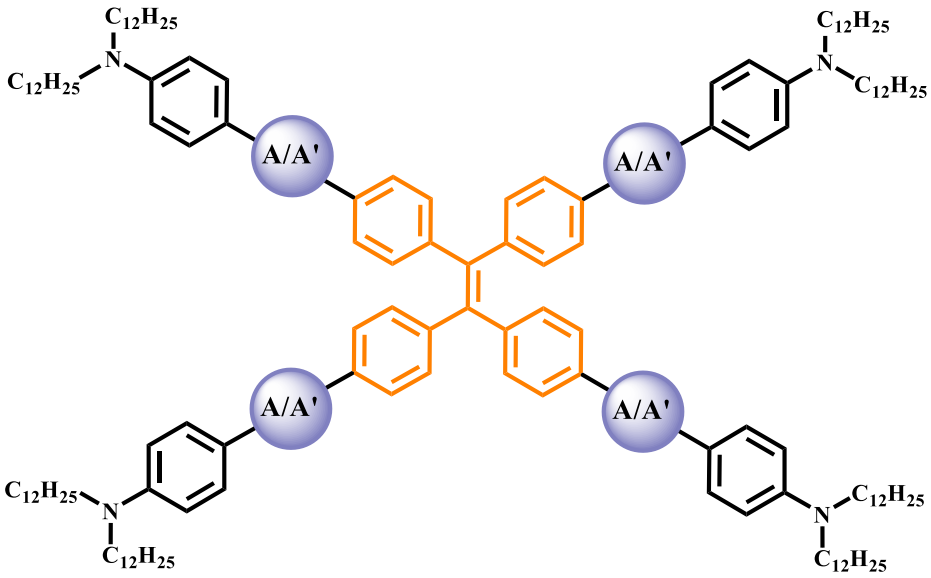

Figure 1.19. Chemical structures of tetraphenylethylene derivatives **109** and **110** functionalized with TCBD or DCNQ moieties.

Table 1.12. Summary of photophysical, electrochemical, and theoretically obtained data of tetraphenylethylene derivatives **109** and **110**.

Compounds	λ_{max} **(nm)**[a]	ε **/ 10**^{5} **(M**$^{-1}$**cm**$^{-1}$**)**[a]	E_{ox} **(V)**[b]	E_{red} **(V)**[b]	E_g^{opt} **(eV)**[a]
109	469	1.13	1.31	–0.45 –0.88	2.30
110	688	1.55	0.88	–0.23 –0.46	1.38

[a]Absorbance measured in THF at 6 × 10^{-6} M concentration. λ_{max}: absorption maxima. ε: extinction coefficient E_g^{opt}: optical bandgap. [b]Electrochemical analysis in 0.1 M solution of tetrabutylammonium hexafluorophosphate ($TBAPF_6$) in DCM at a 100 mVs^{-1} scan rate *versus* saturated calomel electrode.

The electrochemical properties of TPE derivatives **109** and **110** incorporated with TCBD and DCNQ were investigated using cyclic voltammetry (CV) (Figure 1.20). The TPE derivatives **109** and **110** exhibit one oxidation potential at 1.31 and 0.88 V respectively, which corresponds to the oxidation of the four anilines. The reduction potentials are significantly affected by the presence of electron-accepting groups. The TPE derivatives **109** and **110** incorporated TCBD and DCNQ exhibit two reduction potentials at (–0.45 V, –0.88 V) and (–0.23 V, –0.46 V) vs. SCE, respectively (Table 1.12). These potentials correspond to the mono-anion and di-anion formation of the TCBD and DCNQ moieties.

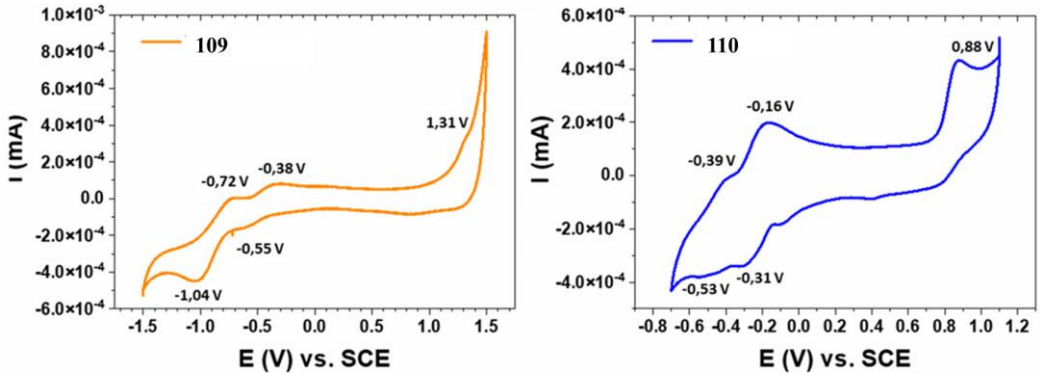

Figure 1.20. Cyclic voltammograms of **109** and **110** in 0.1 M solution of tetrabutylammonium hexafluorophosphate (Bu_4NPF_6) in DCM at 100 $mV.s^{-1}$ scan rate *versus* SCE.

1.5.13. Azulene-based TCBD and DCNQ Derivatives

Azulene is a natural colouring ingredient in cosmetics and skin care products because of its bright blue colour.[207] It is a common ingredient in skincare products, particularly those designed for sensitive or irritated skin due to its soothing and anti-inflammatory properties. Azulene ($C_{10}H_8$) has attracted the interest of several research groups because of its unique properties.[208, 209]

In 2008 and 2009, Shoji *et al*. reported that the mono- and di-TCBD/DCNQ incorporated phenyl and thiophene linkage azulene derivatives **111–118** were designed and synthesized by the [2 + 2] CA–RE reaction using one and two equivalents of TCNE and TCNQ acceptor moieties resulted in the 70–90% yields (Figure 1.21).[80, 210] The UV-visible spectra of mono- and di-TCBD incorporated azulene derivatives **111** and **112** (phenyl linkage) exhibited two strong and weak charge transfer (CT) absorption at 462, 534 nm and 444, 540 nm, respectively. The charge transfer (CT) absorption wavelength of compound **112** exhibited a red shift of 6 nm as compare to compound **111**, attributable to the extension of the π-conjugation in compound **112**. Additionally, the **115** and **116** (thiophene linkage) exhibit the absorption maxima at 460 and 434 nm, respectively. The phenyl linkage mono- and di-TCBD incorporated azulene derivatives **111** and **112** exhibit bathochromic shifts by around 100 nm in comparison to thiophene-linked derivatives **115** and **116**. The mono-DCNQ incorporated azulene derivative **113** (phenyl linkage) showed weak and strong absorption spectra at 393 and 641 nm, respectively, and a significant solvent effect could be seen when the solvent had been changed from DCM to hexane and in this case, absorption maxima observed at 598 nm. The mono-DCNQ incorporated azulene derivative **117** with a thiophene linkage, exhibited strong absorption maxima at 626 nm and a hypsochromic shift of 31 nm when measured in hexane. In contrast, the di-DCNQ incorporated azulene derivative **114** (with a phenyl linkage) showed a strong charge transfer (CT) absorption maxima at 627 nm. The CT absorption of **114** exhibited a 14 nm hypsochromic shift compared to compound **113**, which was inconsistent with the expected expansion of the π-conjugation. Additionally, when the solvent for compound **114** was changed to hexane, the CT absorption maxima showed a bathochromic shift of 9 nm, with the broad absorption band extending towards the near-infrared spectrum. The two absorption bands in the di-DCNQ-incorporated azulene derivative **118** (thiophene linkage) were seen in all solvents, and a hypsochromic shift could be observed again when the solvent was changed to hexane.

The electrochemical analysis of the mono-TCBD incorporated azulene derivative **111** (with a phenyl linkage) exhibits two reversible reduction potentials at –0.61 V and –1.03 V, corresponding to the formation of anionic and dianionic radical species. In contrast, the di-TCBD incorporated azulene derivative **112** (with a phenyl linkage) shows four reversible reduction potentials at –0.45 V, –0.63 V, –1.00 V, and –1.09 V, indicating the formation of a tetraanionic species. On the other hand, the mono- and di-DCNQ incorporated azulenes **113** and **114** (phenyl linkage) revealed two reversible reduction potentials at (–0.44, –0.59 V) and (–0.38, –0.55 V), respectively which are due the formation of the dianionic and tetraanionic species. Additionally, the mono- and di-TCBD incorporated azulenes **115** and **116** (thiophene linkage) exhibited three reversible reduction potentials at (–0.64, –1.03, and –1.95 V) and (–0.31, –0.54, and –1.10 V), respectively attributed to the formation of trianionic and tetraanionic species. The mono-DCNQ incorporated azulene derivative **117** (thiophene linkage) also revealed two reversible reduction waves at –0.44 V and –0.58 V which corresponds to the dianionic formation. The di-DCNQ incorporated azulene derivatives **118** (thiophene linkage) showed four reversible reduction waves observed at –0.31 V, –0.43 V, –0.61 V, and –1.94 V, corresponding to two-electron transfer in one step and the formation of pentaanionic species (Table 1.13).

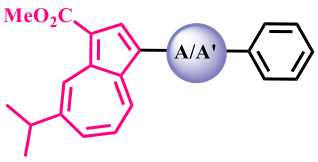

A = TCBD = 111

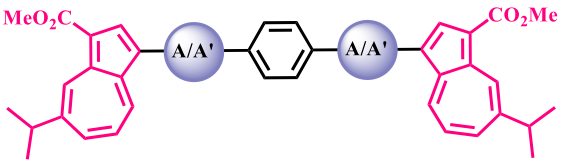

112

A' = DCNQ = 113

114

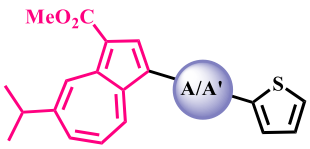

A = TCBD = 115

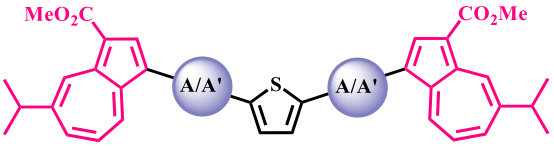

116

A' = DCNQ = 117

118

Figure 1.21. Chemical structures of azulene derivatives **111–118** functionalized with TCBD or DCNQ moieties.

Table 1.13. Summary of photophysical and electrochemical obtained data of azulene derivatives **111–118**.

Compounds	λ_{max} **(nm)**[a]	ε **/ 10^4 ($M^{-1}cm^{-1}$)**[a]	E_{red} **(V)**[b]
111	534	3.88	–0.61, –1.03
112	540	4.10	–0.46, –0.64, –1.01, –1.11
113	641	4.42	–0.43, –0.59
114	627	4.70	–0.38, –0.55
115	460	4.18	–0.64, –1.03, –1.95
116	434	4.67	–0.31, –0.54, –1.10
117	626	4.47	–0.44, –0.58
118	590	4.69	–0.31, –0.43, –0.61, –1.90

[a]Absorbance measured in DCM. λ_{max}: absorption maxima; ε: extinction coefficient. [b]Electrochemical analysis in 0.1 M solution of tetraethylammonium perchlorate Et_4NClO_4 in benzonitrile at a 100 mVs^{-1} scan rate *versus* Fc/Fc^+.

1.5.14. Imidazole-based TCBD and DCNQ Derivatives

Imidazole is a heterocyclic aromatic organic compound characterized by a five-membered ring with three carbon atoms and two nitrogen atoms, exhibiting an amphoteric nature.[211, 212] Imidazole and its derivatives exhibit various biological activities and are present in numerous natural compounds. It finds extensive usage in organic synthesis, chemosensors, pharmaceuticals, and acts as a coordinating ligand in coordination chemistry. Its aromatic character of imidazole makes it an essential building block in medicinal chemistry and facilitates drug design.[213–215]

In 2023, Guragain *et al*. reported the TCBD and DCNQ incorporated triphenylamine substituted imidazole derivatives **119** and **120** which were synthesized by [2 + 2] CA-RE reaction of ethyne-linked triphenylamine functionalized imidazole with TCNE and TCNQ as a strong acceptor, resulted in 88% and 80% yield, respectively (Figure 1.22).[216] The absorption spectra of the triphenylamine functionalized imidazole derivatives **119** and **120** incorporated with TCBD and DCNQ exhibited the absorption maxima at 495 nm and 668 nm, respectively attributed to ICT transitions. The absorption spectra of the DCNQ-incorporated imidazole derivatives **120** exhibits a red-shift in comparison to the TCBD-incorporated imidazole derivative **119** because the molecular structure of **120** is more twisted backbones after the DCNQ moiety is incorporated.

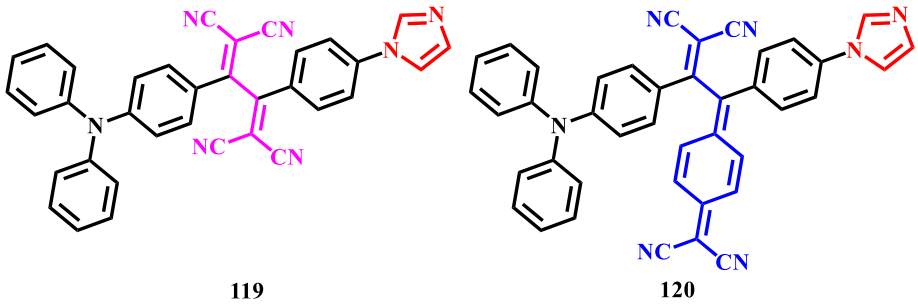

Figure 1.22. Chemical structures of imidazole derivatives **119** and **120** functionalized with TCBD or DCNQ moieties.

The DPVs of compounds **119** and **120** were conducted in DCB using 0.1 M (TBA)ClO_4 as shown in Figure 1.23. At the anodic potential one reversible oxidation wave was observed for **119** and **120** at 0.65 and 0.52 V which corresponds to donor triphenylamine moiety. Similarly, at the cathodic potential the three reversible reduction waves were observed for **119** and **120** at (–0.88, –1.28 and –1.95 V) and (–0.34, –0.68 and –0.96 V), respectively, corresponding to the acceptor TCBD, DCNQ, and imidazole moieties (Table 1.14). The photophysical and electrochemical studies demonstrated that the DCNQ-incorporated triphenylamine functionalized imidazole derivatives **120** exhibited red-shifted absorption by approximately 170 nm along with lower HOMO–LUMO gap values.

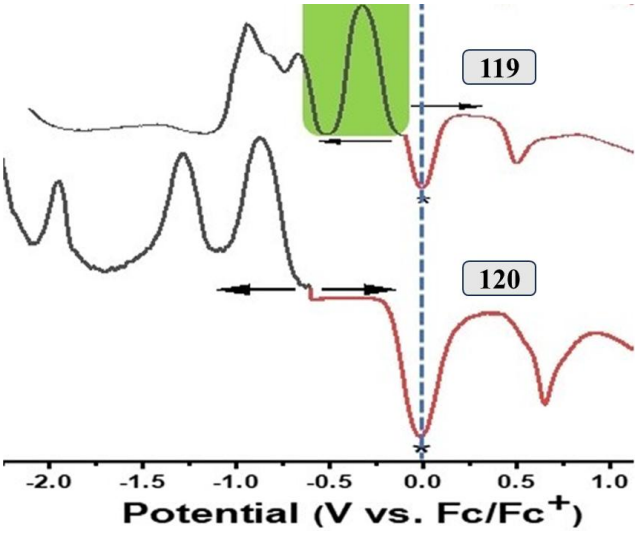

Figure 1.23. Differential pulse voltammograms of TCBD/DCNQ functionalized imidazole derivatives **119** and **120** in DCB containing 0.1 M $(TBA)ClO_4$. The peak denoted by '*' is due to ferrocene oxidation used as an internal standard.

Table 1.14. Summary of photophysical and electrochemical obtained data of imidazole derivatives **119** and **120**.

Compounds	λ_{max} **(nm)**[a]	ε **/ 10^4 ($M^{-1}cm^{-1}$)**[a]	E_{ox} **(V)**[b]	E_{red} **(V)**[b]	E_g **(eV)**[b]
119	495	4.19	0.65	–0.88 –1.28 –1.95	1.53
120	668	4.00	0.52	–0.34 –0.68 –0.96	0.86

[a]Absorbance measured in DCB. λ_{max}: absorption maxima. ε: extinction coefficient. [b]Electrochemical analysis in 0.1 M solution of tetrabutylammonium perchlorate $(TBA)ClO_4$ in DCB at a 100 mVs^{-1} scan rate *versus* Fc/Fc^+.

1.5.15. Naphthalimide-based TCBD and DCNQ Derivatives

The 1,8-naphthalimide moiety is a versatile fluorescent compound that exhibits high electron affinity and acts as an acceptor unit with high charge carrier mobility.[217] The photonic and electronic properties of the donor–acceptor (D–A) naphthalimide derivatives can be influenced at the C–4 or C–5 positions.[218] The chemistry of 1,8-Naphthalimide derivatives has attracted significant attention from researchers in various fields, including fluorescent dyes, laser dyes, pH sensors, metal sensors, bioimaging, optoelectronic materials, *etc*.[219–224]

In 2017, Gautam *et al*. reported the TCBD and DCNQ functionalized Naphthalimide derivatives **121** and **122**, synthesized by the [2 + 2] CA-RE reaction of ethynyl linked triphenylamine substituted naphthalimide with strong acceptors TCNE and TCNQ in 65% and 60% yields, respectively (Figure 1.24).[225] The naphthalimide derivatives **121** and **122** incorporated with TCBD and DCNQ show significant absorption in the visible spectrum. This is indicated by a high-energy band observed between 330 and 414 nm, which corresponds with the π-π* transition. Furthermore, an ICT transition has been observed at wavelengths greater than 450 nm in the near-infrared (NIR) region.

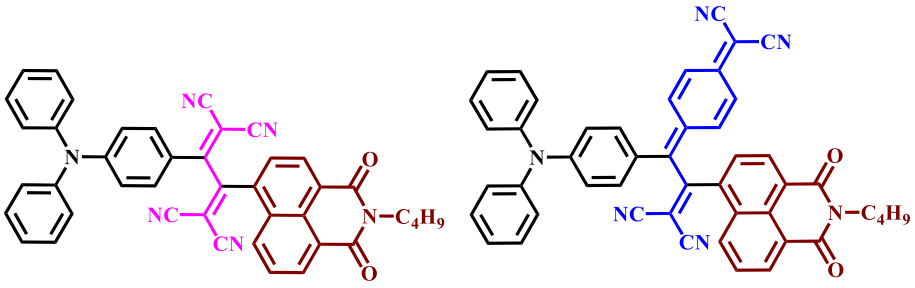

Figure 1.24. Chemical structures of functionalized naphthalimide derivatives **121** and **122** functionalized with TCBD or DCNQ moieties.

The naphthalimides **121** and **122** show multiple redox potentials corresponding to the naphthalimide, TCBD, and DCNQ acceptors moieties, and the oxidation of the donor TPA moiety. The naphthalimides **121** and **122** exhibit one oxidation at 1.14 and 0.98 V, respectively, corresponding to the triphenylamine moiety. Meanwhile,

they exhibit three reduction potentials at (–0.32, –0.76, and –1.01 V) and (–0.10, –0.29, and –1.10 V), respectively (Figure 1.25 and Table 1.15). The first two correspond to TCBD and DCNQ moieties, while the last corresponds to the acceptor naphthalimide unit.

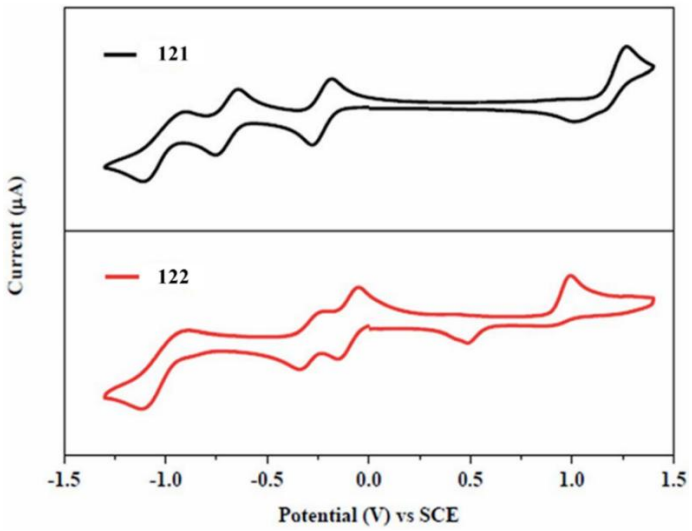

Figure 1.25. Cyclic voltammogram of **121** and **122** at 0.01 M concentration in 0.1 M Bu_4NPF_6 in chloroform recorded at a scan rate of 100 mV s^{-1}.

The density functional theory (DFT) was employed for investigating the naphthalimide derivatives **121** and **122** at the B3LYP/6-31G** basis set level. The electron density of the HOMOs for compounds **121** and **122** are mainly localized over the triphenylamine donor moiety. On the other hand, the LUMOs are mainly delocalized on the acceptor TCBD, DCNQ, and 1,8-naphthalimide moieties (Figure 1.26). The compound **122** exhibits a red shift in absorption and lower the HOMO–LUMO gap as compared to the compound **121** due to the strong electron accepting character of DCNQ moiety. The TCBD and DCNQ-incorporated naphthalimides exhibit broad absorption spectra, multiple reduction potentials, and low HOMO–LUMO gap values, which make them promising candidates for organic photovoltaics.

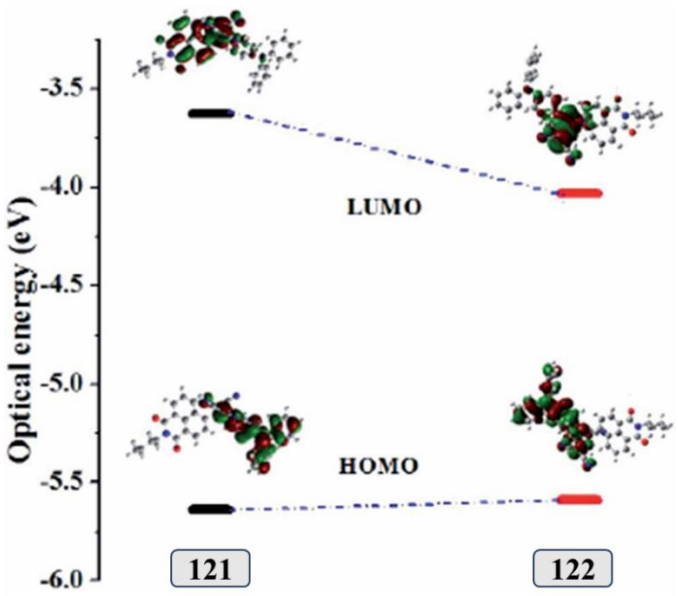

Figure 1.26. The correlation diagram of the HOMO and LUMO frontier molecular orbitals and energies of **121** and **122** are calculated by DFT calculations at the B3LYP/6 31G** basis set level.

Table 1.15. Summary of photophysical and electrochemically obtained data of naphthalimide derivatives **121** and **122**.

Compounds	λ_{max} **(nm)**[a]	ε **/ 10^4 (M^{-1}cm^{-1})**[a]	E_{ox} **(V)**[b]	E_{red} **(V)**[b]	E_g **(eV)**[b]
121	451	3.46	1.14	–0.32 –0.76 –1.01	1.44
122	722	1.86	0.98	–0.10 –0.29 –1.10	1.30

[a]Absorbance measured in chloroform at 1 × 10^{-5} M concentration; λ_{max}: absorption maxima; ε: extinction coefficient. [b]E_{ox} and E_{red} are oxidation and reduction potentials. E_g is the electrochemical band gap calculated by using the onset values of the oxidation and reduction potential.

1.5.16. Ferrocene-based TCBD and DCNQ Derivatives

Ferrocene is an excellent electron donor and has a sandwich-like structure. Ferrocene and its derivatives exhibit high thermal and photochemical stability, essential for the development of materials used in nonlinear optics (NLOs), superconductors, semiconductors, OFETs, OSCs, redox catalysts, sensing, organic synthesis, and biochemistry. [226–229]

In 2024, Popli *et al*. reported the *N*,*N*-dimethylaniline functionalized mono- and di-TCBD/DCNQ incorporated ferrocene derivatives **123–126** synthesized by using 1 and 2 equivalents of TCNE and TCNQ *via* [2 + 2] CA–RE reaction in 33%, 80%, 56% and 95% yields, respectively (Figure 1.27).[230] The mono- and di-TCBD incorporated ferrocenes **123** and **124** show two absorption bands at (313 and 467 nm), and (360 and 467 nm), respectively. On the other hand, the mono- and di-DCNQ incorporated ferrocenes **125** and **126** exhibits two absorption bands at (323 and 651 nm) and (334 and 647 nm), respectively. The absorption band at longer wavelengths is attributed to intramolecular charge transfer (ICT), while the absorption band at shorter wavelengths is corresponds to the π–π * transition. The ICT band of DCNQ-incorporated ferrocenes **125** and **126** has a stronger and broader absorption band. It shows a redshift absorption of around 185 nm when compared to TCBD-incorporated ferrocene **123** and **124** because of the presence of the acceptor DCNQ moiety. Ferrocene **126** shows a blue-shifted band compared to **125**, presumably due to the twisted backbone in the molecular structure after the incorporation of an additional DCNQ moiety.

The mono- and di-TCBD/DCNQ incorporated ferrocenes **123**–**126** exhibit two oxidation potentials at (0.82, 1.17 V), (0.82, 1.30 V) (0.15, 0.93 V) and (0.38, 0.80 V), respectively. The first oxidation potential corresponds to donor ferrocene and the second one is attributed to *N*,*N*-dimethylaniline unit. The mono- and di-TCBD incorporated ferrocenes **123** and **124** show two reduction potentials at –0.64, –0.87 V

and –0.53, –0.69 V, respectively, attributed to the TCBD moieties. Additionally, mono- and di-TCBD incorporated ferrocenes **125** and **126** showed two reduction waves at –0.37, –0.62 V and –0.26, –0.37 V, respectively, indicating the reduction of the DCNQ moieties (Table 1.16). The *N*,*N*-dimethylaniline functionalized mono- and di-TCBD and DCNQ incorporated ferrocene derivatives **123–126** exhibit high thermal stability with decomposition temperatures ranging from 373 to 513 °C (Table 1). The order of the thermal stability is as follows **125** > **123** > **126** > **124**. According to the results, the mono and di-DCNQ incorporated ferrocene derivatives (**125** and **126**) are more stable than the mono- and di-TCBD incorporated ferrocene derivatives (**123** and **124**), respectively. The DFT calculations show that in the mono- and di-TCBD/DCNQ incorporated ferrocene derivatives **123–126** the electron density of the HOMO is mainly localized over the donor moieties *N*,*N*-dimethylaniline and ferrocene, whereas the LUMO orbitals are mainly concentrated on the acceptors TCBD and DCNQ moieties (Figure 1.28).

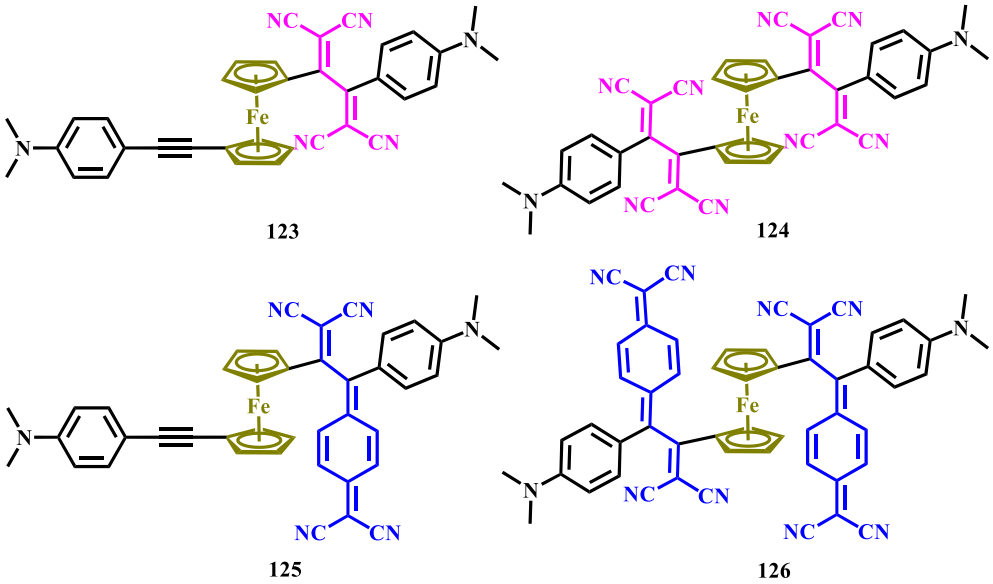

Figure 1.27. Chemical structures of ferrocene derivatives **123–126** functionalized with TCBD or DCNQ moieties.

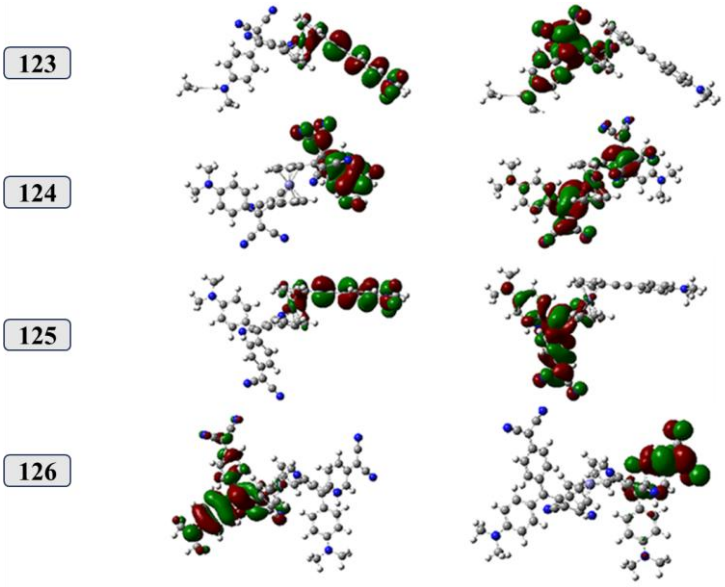

Figure 1.28. The frontier molecular orbitals of ferrocene derivatives **123–126** are calculated by DFT calculations at the (B3LYP/ 6–31G** for C, H, N and Lanl2DZ for Fe) basis set level.

Table 1.16. Summary of photophysical, electrochemical, and theoretically obtained data of ferrocene derivatives **123–126**.

Compounds	λ_{max} **(nm)**[a]	ε **/ 10^4 (M^{-1}cm^{-1})**[a]	E_{ox} **(V)**[b]	E_{red} **(V)**[b]	E_g **(eV)**[c]	T_d **(°C)**
123	467	4.45	0.82 1.17	–0.64 –0.87	2.40	455
124	467	5.49	0.82 1.30	–0.53 –0.69	2.62	373
125	651	1.38	0.15 0.93	–0.37 –0.62	1.65	513
126	647	6.14	0.38 0.80	–0.26 –0.37	1.41	383

[a]Absorbance measured in DCM at 1 × 10^{-5} M concentration; λ_{max}: absorption maxima; ε: extinction coefficient. [b]Electrochemical analysis

was estimated by DPV in 0.1 M solution of tetrabutylammonium hexafluorophosphate ($TBAPF_6$) in DCM at a 100 mVs^{-1} scan rate *versus* Ag/AgCl electrode. $^{c}E_g$ = HOMO–LUMO band gap as calculated by DFT at B3LYP/6-31G** for C, H, N, and Lanl2DZ for Fe basis set level of theory. T_d: Decomposition temperature at 10% weight loss.

1.6. Applications of TCBD and DCNQ Bridged Molecular Framework

The TCBD and DCNQ-based donor–acceptor (D–A) molecular framework have been investigated for a variety of applications. Here, we discuss some of the key applications:

1.6.1. Solar Cells

The solar cell utilizes organic materials, primarily carbon-based molecules or polymers to transform sunlight into electricity.[231, 232] Compared to traditional silicon-based solar cells, organic solar cells (OSCs) manifest several advantages, including flexibility, lightweight properties, and the potential for lower manufacturing costs, which makes OSCs particularly promising for a variety of applications.[233–237]

1.6.1.1. Bulk Heterojunction Organic Solar Cells (BHJOSCs)

Organic solar cells (OSCs) have been investigated as a renewable energy source due to their ability to convert sunlight into the electricity at a low cost.[238, 239] Significant improvements in the performance of OSCs have been achieved with bulk heterojunction (BHJ) architectures, which incorporate a conjugated polymer as the electron donor and a fullerene as the electron acceptor.[240, 241] The TCBD and DCNQ functionalized derivatives **121** and **122** were used for bulk heterojunction organic solar cells (Figure 1.24)[225] To demonstrate the potential applications of compounds **121** and **122** as acceptors in the polymer solar cells, they were combined with the donor–acceptor (D–A) copolymer **P**. Subsequently, bulk heterojunction polymer solar cells (BHJ-PSCs) were fabricated with the following device structure:

ITO/PEDOT:PSS/P:121 or 122/PFN/Al.[242]. The copolymer **P** has a D–A structure, with dibromide 2-hexyl-4,7-dibromo-5-fluorobenzo-1,2,3-triazole as the acceptor unit and 4,4′-bis(2-ethylhexyl)-5,5′-bis(trimethyltin)-dithieno[3,2-b:2′,3′-d]silole as the donor unit. The copolymer **P** shows a strong absorption band with maximum absorption at 578 nm in thin films. The absorption profile of copolymer **P** complements that of **121** and **122**, making it suitable for enhancing light harvesting efficiency when blended with **121** and **122** as acceptors. The absorption spectra of the BHJ active layer cast from chloroform are displayed in Figure 1.29. The impact of various D/A weight ratios and the additive's concentration were examined to optimize device performance. Figure 1.30 displays the optimized PSC's current-voltage characteristic. Table 1.17 provides a summary of the relevant data. The devices based on **P:121** (1:1) and **P:122** exhibited overall power conversion efficiencies (PCEs) of 2.34% (J_{sc} = 6.14 mA cm^{-2}, V_{oc} = 1.06 V and FF = 0.36) and 3.14% (J_{sc} = 8.02 mA cm^{-2}, V_{oc} = 0.98 V and FF = 0.40), respectively, without the use of an additive. The device's performance improved significantly to 4.94% (J_{sc} = 9.15 mA cm^{-2}, V_{oc} = 1.02 V and FF = 0.54) for device **121** and 6.11% (J_{sc} = 11.25 mA cm^{-2}, V_{oc} = 0.92 V and FF = 0.59) for device **122** after a 3% DIO additive was added.

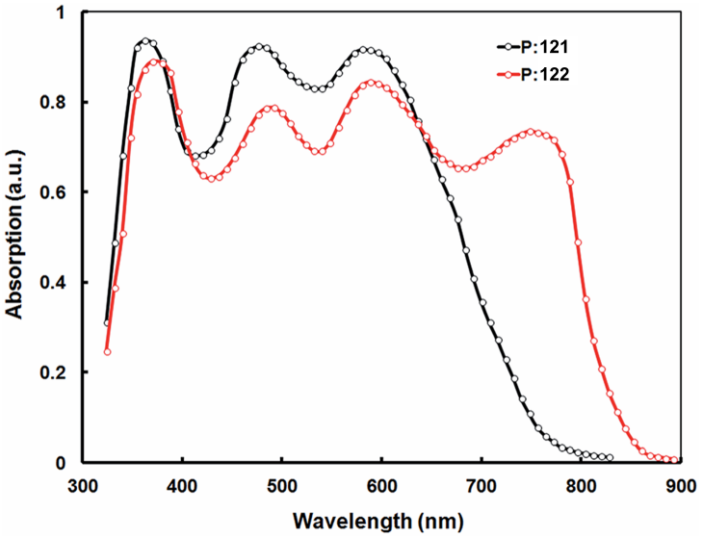

Figure 1.29. Normalized absorption spectra of thin films of **P:121** and **P:122** cast from chloroform.

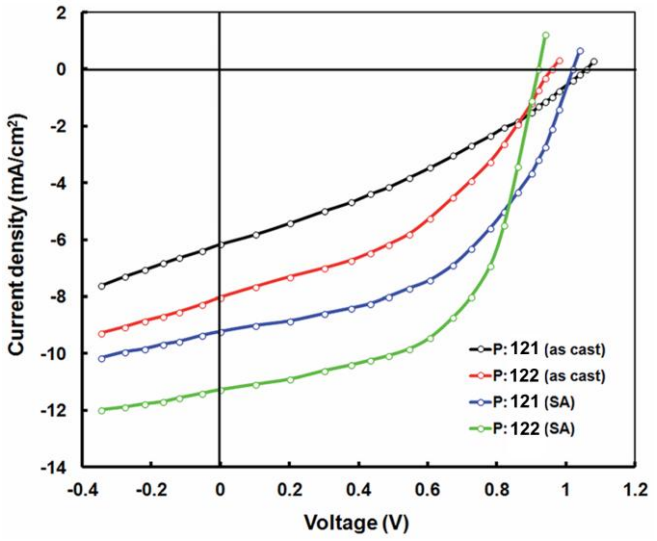

Figure 1.30. Current-voltage (J-V) characteristics of devices with **P:121** and **P:122** illumination spectra.

Table 1.17. Photovoltaic parameters of the organic solar cells based on **P:121** and **P:122**.

Active layer	J_{SC} **(mA cm^{-2})**	V_{OC} **(V)**	**FF**	**PCE (%)**
P:121 (as cast)	6.14	1.06	0.36	2.34 (2.23)[a]
P:122 (as cast)	8.02	0.98	0.40	3.14 (3.06)[a]
P:121 (SA)	9.15	1.02	0.54	4.94 (4.86)[a]
P:122 (SA)	11.26	0.92	0.59	6.11 (6.07)[a]

[a]Average of eight devices.

1.6.1.2. Dye-sensitized solar cells (DSSCs)

Dye-sensitized solar cells (DSSCs) have garnered significant attention of the scientific community due to its potential as a promising renewable energy source, offering high power conversion efficiency and low production costs.[243, 244] The TCBD and DCNQ functionalized derivatives **127–130** were used as a photosensitizer for DSSCs (Figure 1.31).[245]

The DSSC devices were fabricated using FTO conducting glass substrates, which were screen-printed with a 15 µm transparent layer of 20 nm titania particles and a 10 µm scattering layer of 400 nm titania particles. The chemically adsorbed derivatives **127–130** on TiO_2 produced J–V curves in DSSCs (Figure 1.32, Table 1.18). The TCBD-incorporated triphenylamine derivative **129** achieved a J_{sc} of 0.65 mA cm^{-2}, which is higher than the 0.12 mA cm^{-2} of the TCBD-functionalized dimethylaniline derivative **127**. Similarly, the DCNQ-incorporated triphenylamine derivative **130** showed a J_{sc} of 1.71 mA cm^{-2}, compared to 1.41 mA cm^{-2} for the DCNQ-functionalized dimethylaniline derivative **128**, indicating the effectiveness of triphenylamine as a donor unit. DCNQ-incorporated derivatives also exhibited higher V_{oc} values than TCBD counterparts, attributed to their energy levels and larger molecular sizes. The device sensitized by DCNQ-incorporated derivative **128** had twice the V_{oc} of the TCBD-functionalized derivative **127**. The highest PCE of 0.25% was achieved with the DCNQ-incorporated triphenylamine derivative **130**.

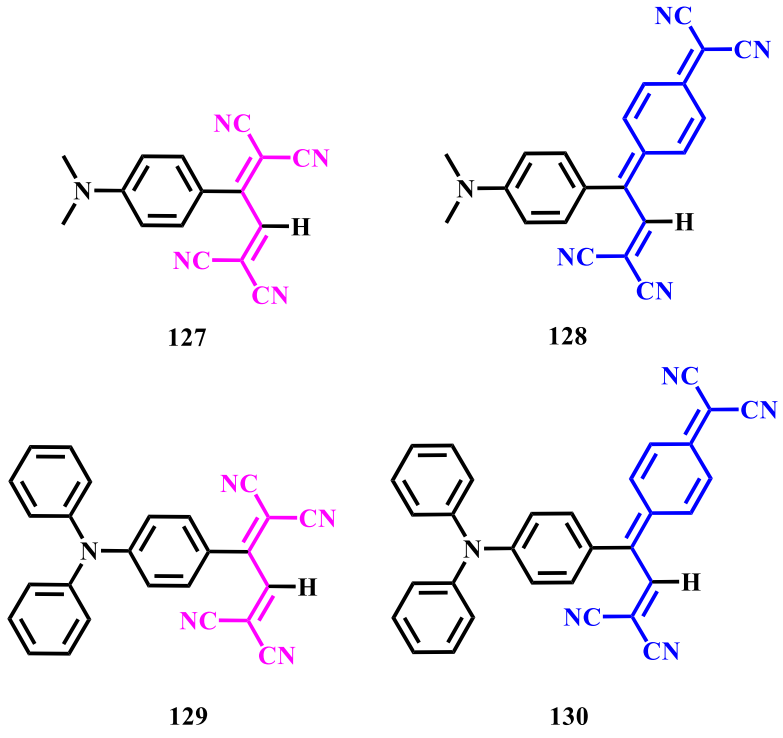

Figure 1.31. Chemical structures of TCBD and DCNQ functionalized derivatives **127–130** for dye-sensitized solar cells.

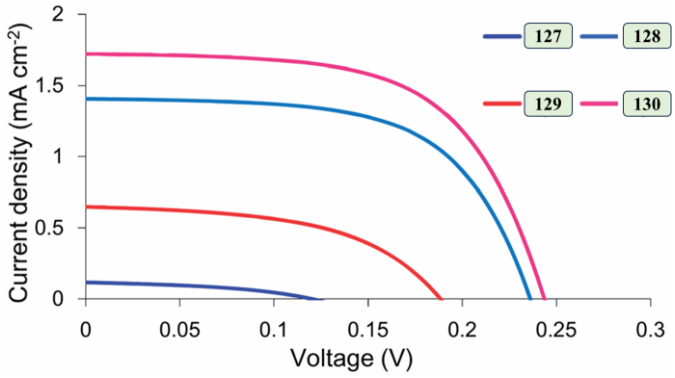

Figure 1.32. Photocurrent density–photovoltage (J–V) curves of DSSCs based on **127–130**.

Table 1.18. Summary of DSSC performances[a].

Compounds	***J*SC (mA cm^{-2})**	***V*OC (V)**	**FF**	**PCE (%)**
127	0.12	0.12	0.42	0.0058
128	1.41	0.24	0.61	0.20
129	0.65	0.19	0.52	0.063
130	1.71	0.24	0.61	0.25

[a]0.25 cm^2 TiO_2 electrode composed of a transparent layer (15 µm) and scattering layer (10 µm) in CH_3CN containing 2 M LiI and 0.025 M I_2.

1.6.2. Photoacoustic Imaging (PAI)

Photoacoustic imaging is a hybrid technique that combines the high contrast of optical imaging with the high spatial resolution of ultrasound imaging, enabling detailed visualization of biological tissues. Photoacoustic imaging a non-invasive real-time technique benefits from materials absorbing light in the near-infrared (NIR) region. NIR-absorbing low molecular weight organic dyes are promising as PA contrast agents due to their good biodegradability and lower potential toxicity compared to inorganic agents.[248–251] In 2022, Misra *et al*. reported DCNQ-incorporated derivatives **131** and **132** for photoacoustic imaging (Figure 1.33).[252] These derivatives exhibited NIR absorption

and were evaluated for their photoacoustic applications. The photoacoustic spectra of **131** and **132** were measured in DMF using tube phantoms, with ICG as a reference, using a Vevo LAZR 2100 device across 680–970 nm. Both dyes produced detectable PA signals at 5 nmol/mL, with peaks around 695–700 nm, and had a detection limit of 2 nmol/mL. The PA spectra closely matched their absorption spectra (Figure 1.34), suitable for spectral unmixing. In aqueous solutions with cremophor EL,[253] both dyes were detectable at 12.5 µM, showing a slight 10 nm red-shift in PA maxima compared to DMF solutions, indicating *J*-aggregation.

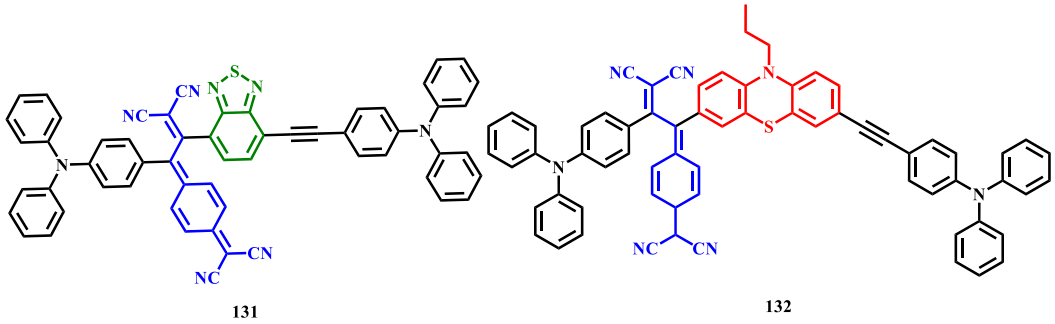

Figure 1.33. Chemical structures of the DCNQ functionalized derivatives **131** and **132** for photoacoustic imaging.

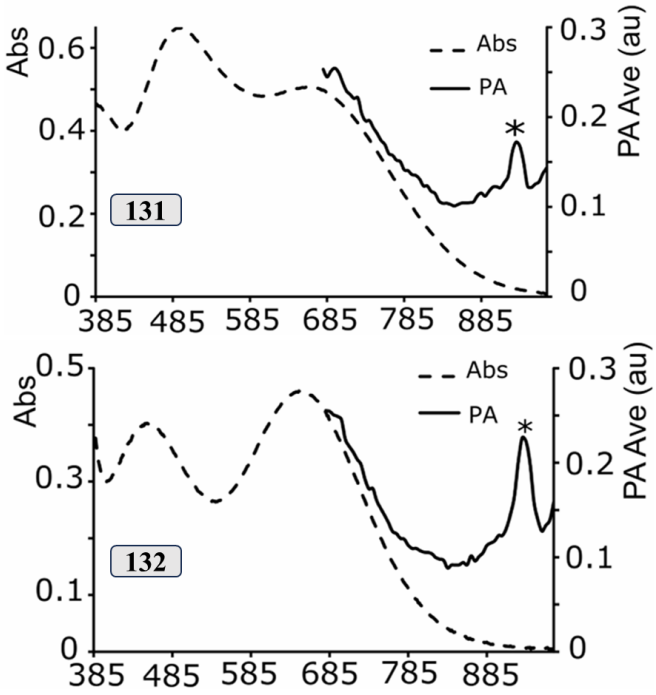

Figure 1.34. Overlay of UV–vis spectra (in DCM) and photoacoustic (PA) spectra (in DMF) of DCNQ-functionalized derivatives **131** and **132** at 10 μM (*background signal from the tube).

In 2019, Zhao *et al*. reported the application of DCNQ-incorporated derivatives **133** and **134** for photoacoustic imaging (Figure 1.35).[254] Figure 1.36a shows that all the NIR-absorbing derivatives exhibited a good photoacoustic effect. The molar extinction coefficients (ε) of fullerene derivatives **133** and **134** were measured to understand their photoacoustic intensities. According to the photothermal mechanism equation for the photoacoustic effect:

$$q \propto \Gamma \varepsilon \eta F \qquad (1)$$

where Γ is the Gruneisen parameter, η is the thermal conversion efficiency, ε is the optical absorption coefficient, and F is the local optical fluence.[255] The thermal conversion efficiencies (η) were calculated from the cooling curves in Figure 1.36b. Despite DCNQ-functionalized derivatives **133** and **134** showing optical absorption coefficients of 1.1×10^4 and 2.5×10^4 L mol^{-1} cm^{-1}, respectively, their thermal conversion efficiencies (η) did not match the photoacoustic intensities. The DCNQ incorporated derivative **133** had the highest thermal conversion efficiency (52.3%) compared to **134** (43.8%). However, the photoacoustic intensity of **134** with a phenyl group was higher than that of **133** with a thienyl group (Table 1.19).

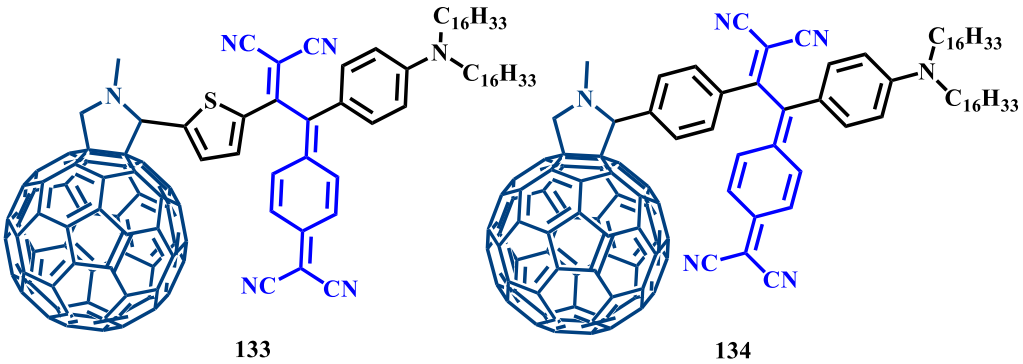

Figure 1.35. Chemical structures of the DCNQ functionalized derivatives **133** and **134** for photoacoustic imaging.

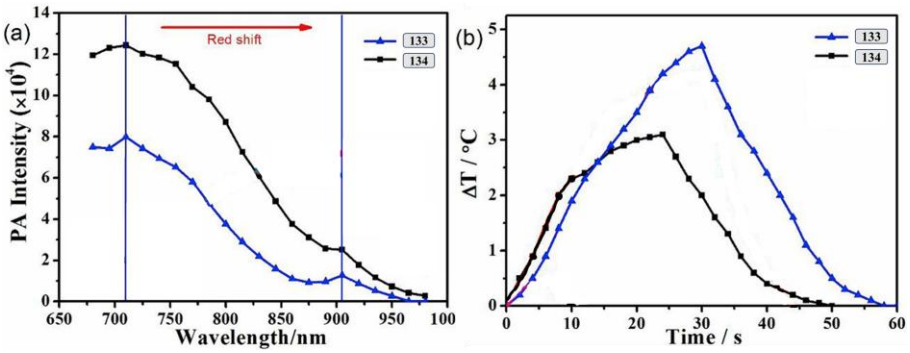

Figure 1.36. (a) PA intensities of the DCNQ functionalized derivatives **133** and **134** in THF (3×10^{-5} M); (b) Heating and cooling curves of DCNQ functionalized derivatives **133** and **134** as a function of time.

Table 1.19. Summary of PA intensity, ε, ΔT, τ_s, and η of the DCNQ functionalized derivatives **133** and **134**.

Compounds	**PA (10^4)**	**ε (10^4L/mol/cm)**	**ΔT (°C)**	**τ_s**	**η (%)**
133	8.0	1.1	4.7	4.6	52.3
134	12.4	2.5	3.1	4.6	43.8

1.7. Current Work

The π-conjugated donor–acceptor molecular systems with a low HOMO–LUMO band gap are an interesting class of materials owing to their wide application in the field of optoelectronics. A large variety of electron donors (phenothiazine, thiophene, triphenylamine, carbazole, and *N*,4-dimethylbenzenesulfonamide) and strong acceptors (TCNE, TCNQ, and fulleropyrrolidine) have been incorporated into the donor–acceptor chromophores to enhance the optical characteristics and HOMO–LUMO band gap. The photophysical, electrochemical, thermal, and computational studies of the TCBD and DCNQ functionalized donor–acceptor chromophores were investigated.

The main objectives of the current work are as follows:

1. To design and synthesize the TCBD and DCNQ functionalized donor–acceptor phenothiazine chromophores for optoelectronic applications.
2. To synthesize symmetrical and unsymmetrical TCBD and DCNQ functionalized donor–acceptor phenothiazine chromophores by varying the donor/acceptor units in a systematic way.
3. To investigate the effect of the cyano-based strong acceptors TCBD and DCNQ incorporated phenothiazine chromophores on their photophysical, electrochemical, thermal properties and the energy gap between HOMO and LUMO energy levels.
4. To fine-tune the HOMO–LUMO gap by altering the donor/acceptor strength or π-linker on the TCBD and DCNQ functionalized phenothiazine based donor–acceptor chromophores.
5. To understand the distribution of electron density in the highest occupied molecular orbital (HOMO) and lowest unoccupied molecular orbital (LUMO), the nature of absorption transitions, and the HOMO–LUMO energy gap *via* density functional theory (DFT) and time-dependent density functional theory (TD-DFT) calculations.

1.8. Organization of thesis

Chapter 1 describes the general introduction of the donor–acceptor system, followed by the design, synthesis, and functionalization of the TCBD and DCNQ moieties as well as their application in different fields.

Chapter 2 summarizes the instrumentation and general methods used in the present study.

Chapter 3 describes the design and synthesis of the NIR absorbing 1,1,4,4-tetracyanobuta-1,3-diene (TCBD) and dicyanoquinodimethane (DCNQ) functionalized phenothiazine based donor–acceptor chromophores. The photophysical, electrochemical, thermal, and theoretical studies were investigated to analyze the effect of strong acceptors TCBD and DCNQ in the donor–acceptor chromophores.

Chapter 4 describes the design and synthesis of the Near-IR capturing *N,4*-dimethyl-benzenesulfonamide phenothiazine-based TCBD and DCNQ incorporated donor–acceptor chromophores and investigated their photophysical, electrochemical, and computational studies.

Chapter 5 describes the synthesis and characterization of NIR absorbing TCBD and DCNQ functionalized symmetrical and unsymmetrical *N*-methyl-*p*-toluenesulfonamide-phenothiazine based donor–acceptor chromophores. The photophysical, electrochemical, thermal, and computational studies were studied to understand the effect of strong acceptors TCBD and DCNQ moieties in the donor–acceptor chromophores.

Chapter 6 describes the synthesis and characterization of NIR absorbing triphenylamine substituted TCBD and DCNQ incorporated phenothiazine and fulleropyrrolidine based donor–acceptor chromophores, exploring their photophysical, electrochemical, and computational studies.

Chapter 7 describes the design and synthesis of TCBD and DCNQ functionalized phenothiazine and fulleropyrrolidine based donor–acceptor chromophores, exploring their photophysical, electrochemical, and computational studies.

Chapter 8 summarizes the salient features of the work and their future prospectus to develop the donor–acceptor (D–A) materials for optoelectronic applications.

1.9. References

[1] Patil, Y., Jadhav, T., Dhokale, B., & Misra, R. (2016). Tuning of the HOMO–LUMO Gap of Symmetrical and Unsymmetrical Ferrocenyl-Substituted Diketopyrrolopyrroles. *European Journal of Organic Chemistry*, *2016*(4), 733–738. (DOI: 10.1002/ejoc.201501123).

[2] Wong, W.-Y., Wong, W.-K., & Raithby, P. R. (1998). Synthesis, characterisation and properties of platinum(II) acetylide complexes of ferrocenylfluorene: novel soluble donor–acceptor heterometallic materials. *Journal of the Chemical Society, Dalton Transactions*, (16), 2761–2766. (DOI: 10.1039/a803168a).

[3] Patil, Y., Misra, R., Chen, F. C., & Sharma, G. D. (2016). Small molecule-based N-phenyl carbazole substituted diketopyrrolopyrroles as donors for solution-processed bulk heterojunction organic solar cells. *Physical Chemistry Chemical Physics*, *18*(33), 22999–23005. (DOI: 10.1039/C6CP03767D).

[4] Blankevoort, N., Bastante, P., Davidson, R. J., Salthouse, R. J., Daaoub, A. H. S., Cea, P., … Sadeghi, H. (2024). Exploring the Impact of the HOMO–LUMO Gap on Molecular Thermoelectric Properties: A Comparative Study of Conjugated Aromatic, Quinoidal, and Donor–Acceptor Core Systems. *ACS Omega*. (DOI: 10.1021/acsomega.3c09760).

[5] Paramasivam, M., Gupta, A., Raynor, A. M., Bhosale, S. V., Bhanuprakash, K., & Jayathirtha Rao, V. (2014). Small band gap D-π-A-π-D benzothiadiazole derivatives with low-lying HOMO levels as potential donors for applications in organic photovoltaics: a combined experimental and theoretical investigation. *RSC Adv.*, *4*(67), 35318–35331. (DOI: 10.1039/C4RA02700K).

[6] Cappello, D., Buguis, F. L., & Gilroy, J. B. (2022). Tuning the Properties of Donor–Acceptor and Acceptor–Donor–Acceptor Boron Difluoride Hydrazones *via* Extended π-Conjugation. *ACS*

Omega, *7*(36), 32727–32739. (DOI: 10.1021/acsomega.2c04401).

[7] Geramita, K., Tao, Y., Segalman, R. A., & Tilley, T. D. (2010). Synthesis and Characterization of Fluorinated Heterofluorene-Containing Donor−Acceptor Systems. *The Journal of Organic Chemistry*, *75*(6), 1871–1887. (DOI: 10.1021/jo902488w).

[8] Li, G., Chen, Y., Qiao, Y., Lu, Y., & Zhou, G. (2018). Charge Transfer Switching in Donor–Acceptor Systems Based on BN-Fused Naphthalimides. *The Journal of Organic Chemistry*, *83*(10), 5577–5587. (DOI: 10.1021/acs.joc.8b00597).

[9] Bijesh, S., & Misra, R. (2018). Triphenylamine Functionalized Unsymmetrical Quinoxalines. *Asian Journal of Organic Chemistry*, *7*(9), 1882–1892. (DOI: 10.1002/ajoc.201800384).

[10] Funabiki, K., Yamada, K., Arisawa, Y., Watanabe, A., Agou, T., Kubota, Y., … Kutsumizu, S. (2022). Design, Regioselective Synthesis, and Photophysical Properties of Perfluoronaphthalene-Based Donor–Acceptor–Donor Fluorescent Dyes. *The Journal of Organic Chemistry*, *87*(17), 11751–11765. (DOI: 10.1021/acs.joc.2c01446).

[11] Franca, L. G., Danos, A., & Monkman, A. (2023). Donor, Acceptor, and Molecular Charge Transfer Emission All in One Molecule. *The Journal of Physical Chemistry Letters*, *14*(11), 2764–2771. (DOI: 10.1021/acs.jpclett.2c03925).

[12] Crisenza, G. E. M., Mazzarella, D., & Melchiorre, P. (2020). Synthetic Methods Driven by the Photoactivity of Electron Donor–Acceptor Complexes. *Journal of the American Chemical Society*, *142*(12), 5461–5476. (DOI: 10.1021/jacs.0c01416).

[13] Mathur, C., Gupta, R., & Bansal, R. K. (2024). Organic Donor-Acceptor Complexes As Potential Semiconducting Materials. *Chemistry – A European Journal*, *30*(23). (DOI: 10.1002/chem.202304139).

[14] Najare, M. S., Patil, M. K., Garbhagudi, M., Yaseen, M., Inamdar, S. R., & Khazi, I. A. M. (2021). Design, synthesis and characterization of π-conjugated 2,5-diphenylsubstituted-1,3,4-

oxadiazole-based D-π-A-π'-D′ form of efficient deep blue functional materials: Photophysical properties and fluorescence "Turn-off" chemsensors approach. *Journal of Molecular Liquids*, *328*, 115443. (DOI: 10.1016/j.molliq.2021.115443).

[15] Belavagi, N. S., Deshapande, N., Pujar, G. H., Wari, M. N., Inamdar, S. R., & Khazi, I. A. M. (2015). Design, Synthesis and Optoelectronic Properties of Unsymmetrical Oxadiazole Based Indene Substituted Derivatives as Deep Blue Fluoroscent Materials. *Journal of Fluorescence*, *25*(5), 1323–1330. (DOI: 10.1007/s10895-015-1620-3).

[16] Zhang, Y., Du, H., Yin, Y., Dong, Y., Zhao, J., & Xu, Z. (2020). Synthesis and characterization of soluble donor–acceptor type copolymers based on benzotriazole, quinoxaline and benzene units with multicolor electrochromism. *Organic Electronics*, *77*, 105514. (DOI: 10.1016/j.orgel.2019.105514).

[17] Khelifi, W., & Luscombe, C. K. (2024). Recent developments in indacenodithiophene and indacenodithienothiophene-based donor–acceptor conjugated polymers: From design to device performance in organic electronics. *Progress in Polymer Science*, *151*, 101804. (DOI: 10.1016/j.progpolymsci.2024.101804).

[18] van Mullekom, H. (2001). Developments in the chemistry and band gap engineering of donor–acceptor substituted conjugated polymers. *Materials Science and Engineering: R: Reports*, *32*(1), 1–40. (DOI: 10.1016/S0927-796X(00)00029-2).

[19] Wang, L., & Zhu, W. (2024). Organic Donor–Acceptor Systems for Photocatalysis. *Advanced Science*, *11*(10), 2307227. (DOI: 10.1002/advs.202307227).

[20] Holliday, S., Li, Y., & Luscombe, C. K. (2017). Recent advances in high performance donor–acceptor polymers for organic photovoltaics. *Progress in Polymer Science*, *70*, 34–51. (DOI: 10.1016/j.progpolymsci.2017.03.003).

[21] Zhang, L., Zeng, S., Yin, L., Ji, C., Li, K., Li, Y., & Wang, Y. (2013). The synthesis and photovoltaic properties of A–D–A-

type small molecules containing diketopyrrolopyrrole terminal units. *New J. Chem.*, *37*(3), 632–639. (DOI: 10.1039/C2NJ40963A)

[22] Maligaspe, E., Pundsack, T. J., Albert, L. M., Zatsikha, Y. V., Solntsev, P. V., Blank, D. A., & Nemykin, V. N. (2015). Synthesis and Charge-Transfer Dynamics in a Ferrocene-Containing Organoboryl aza-BODIPY Donor–Acceptor Triad with Boron as the Hub. *Inorganic Chemistry*, *54*(8), 4167–4174. (DOI: 10.1021/acs.inorgchem.5b00494).

[23] Leliège, A., Blanchard, P., Rousseau, T., & Roncali, J. (2011). Triphenylamine/Tetracyanobutadiene-Based D-A-D π-Conjugated Systems as Molecular Donors for Organic Solar Cells. *Organic Letters*, *13*(12), 3098–3101. (DOI: 10.1021/ol201002j).

[24] Khan, F., & Misra, R. (2023). Recent advances in the development of phenothiazine and its fluorescent derivatives for optoelectronic applications. *Journal of Materials Chemistry C*, *11*(8), 2786–2825. (DOI: 10.1039/D2TC04326B).

[25] Chen, W., Yang, X., Long, G., Wan, X., Chen, Y., & Zhang, Q. (2015). A perylene diimide (PDI)-based small molecule with tetrahedral configuration as a non-fullerene acceptor for organic solar cells. *Journal of Materials Chemistry C*, *3*(18), 4698–4705. (DOI: 10.1039/C5TC00865D).

[26] Reutenauer, P., Kivala, M., Jarowski, P. D., Boudon, C., Gisselbrecht, J.-P., Gross, M., & Diederich, F. (2007). New strong organic acceptors by cycloaddition of TCNE and TCNQ to donor-substituted cyanoalkynes. *Chemical Communications*, (46), 4898. (DOI: 10.1039/b714731g).

[27] Brothers, P. J. (2011). Boron Complexes of Pyrrolyl Ligands. *Inorganic Chemistry*, *50*(24), 12374–12386. (DOI: 10.1021/ic2011919).

[28] Prato, M., Maggini, M., & Scorrano, G. (1996). Synthesis and applications of fulleropyrrolidines. *Synthetic Metals*, *77*(1–3), 89–91. (DOI: 10.1016/0379-6779(96)80065-8).

[29] Zhang, D., & Heeney, M. (2020). Organic Donor–Acceptor Systems. *Asian Journal of Organic Chemistry*, *9*(9), 1251–1251. (DOI: 10.1002/ajoc.202000465).

[30] Narsaria, A. K., Poater, J., Fonseca Guerra, C., Ehlers, A. W., Lammertsma, K., & Bickelhaupt, F. M. (2018). Rational design of near-infrared absorbing organic dyes: Controlling the HOMO–LUMO gap using quantitative molecular orbital theory. *Journal of Computational Chemistry*, *39*(32), 2690–2696. (DOI: 10.1002/jcc.25731).

[31] Khalid, M., Hussain, R., Hussain, A., Ali, B., Jaleel, F., Imran, M., … Jahrukh Tariq, C. (2019). Electron Donor and Acceptor Influence on the Nonlinear Optical Response of Diacetylene-Functionalized Organic Materials (DFOMs): Density Functional Theory Calculations. *Molecules*, *24*(11), 2096. (DOI: 10.3390/molecules24112096).

[32] Chi, Z., Zhang, X., Xu, B., Zhou, X., Ma, C., Zhang, Y., … Xu, J. (2012). Recent advances in organic mechanofluorochromic materials. *Chemical Society Reviews*, *41*(10), 3878. (DOI: 10.1039/c2cs35016e).

[33] Chen, L. X. (2019). Organic Solar Cells: Recent Progress and Challenges. *ACS Energy Letters*, *4*(10), 2537–2539. (DOI: 10.1021/acsenergylett.9b02071).

[34] Zhao, Y., Zhang, Z., Lu, Z., Wang, H., & Tang, Y. (2019). Enhanced Energy Transfer in a Donor–Acceptor Photosensitizer Triggers Efficient Photodynamic Therapy. *ACS Applied Materials & Interfaces*, *11*(42), 38467–38474. (DOI: 10.1021/acsami.9b12375).

[35] Chen, R., Lu, R.-Q., Shi, K., Wu, F., Fang, H.-X., Niu, Z.-X., … Cao, X.-Y. (2015). Corannulene derivatives with low LUMO levels and dense convex–concave packing for n-channel organic field-effect transistors. *Chemical Communications*, *51*(72), 13768–13771. (DOI: 10.1039/C5CC03550C).

[36] Dini, D., Calvete, M. J. F., & Hanack, M. (2016). Nonlinear Optical Materials for the Smart Filtering of Optical Radiation.

Chemical Reviews, *116*(22), 13043–13233. (DOI: 10.1021/acs.chemrev.6b00033).

[37] Han, X., Bai, Q., Yao, L., Liu, H., Gao, Y., Li, J., … Yang, B. (2015). Highly Efficient Solid-State Near-Infrared Emitting Material Based on Triphenylamine and Diphenylfumaronitrile with an EQE of 2.58% in Nondoped Organic Light-Emitting Diode. *Advanced Functional Materials*, *25*(48), 7521–7529. (DOI: 10.1002/adfm.201503344).

[38] Bernthsen, A. (1883). Zur Kenntniss des Methylenblau und verwandter Farbstoffe. *Berichte der deutschen chemischen Gesellschaft*, *16*(2), 2896–2904. (DOI: 10.1002/cber.188301602249).

[39] Revoju, S., Matuhina, A., Canil, L., Salonen, H., Hiltunen, A., Abate, A., & Vivo, P. (2020). Structure-induced optoelectronic properties of phenothiazine-based materials. *Journal of Materials Chemistry C*, *8*(44), 15486–15506. (DOI: 10.1039/D0TC03421E).

[40] Gangadhar, P. S., Reddy, G., Prasanthkumar, S., & Giribabu, L. (2021). Phenothiazine functional materials for organic optoelectronic applications. *Physical Chemistry Chemical Physics*, *23*(28), 14969–14996. (DOI: 10.1039/D1CP01185E).

[41] Al-Busaidi, I. J., Haque, A., Al Rasbi, N. K., & Khan, M. S. (2019). Phenothiazine-based derivatives for optoelectronic applications: A review. *Synthetic Metals*, *257*, 116189. (DOI: 10.1016/j.synthmet.2019.116189).

[42] Kim, G., Yeom, H. R., Cho, S., Seo, J. H., Kim, J. Y., & Yang, C. (2012). Easily Attainable Phenothiazine-Based Polymers for Polymer Solar Cells: Advantage of Insertion of *S*,*S*-dioxides into its Polymer for Inverted Structure Solar Cells. *Macromolecules*, *45*(4), 1847–1857. (DOI: 10.1021/ma202661b).

[43] Taurand, G. (2000). Phenothiazine and Derivatives. In Wiley-VCH Verlag GmbH & Co. KGaA (Ed.), *Ullmann's Encyclopedia of Industrial Chemistry* (p. a19_387). Weinheim,

Germany: Wiley-VCH Verlag GmbH & Co. KGaA. (DOI: 10.1002/14356007.a19_387)

[44] Rout, Y., Montanari, C., Pasciucco, E., Misra, R., & Carlotti, B. (2021). Tuning the Fluorescence and the Intramolecular Charge Transfer of Phenothiazine Dipolar and Quadrupolar Derivatives by Oxygen Functionalization. *Journal of the American Chemical Society*, *143*(26), 9933–9943. (DOI: 10.1021/jacs.1c04173).

[45] Huang, P., Manju, Kazim, S., Lezama, L., Misra, R., & Ahmad, S. (2021). Tailoring of a Phenothiazine Core for Electrical Conductivity and Thermal Stability: Hole-Selective Layers in Perovskite Solar Cells. *ACS Applied Materials & Interfaces*, *13*(28), 33311–33320. (DOI: 10.1021/acsami.1c08470).

[46] Rout, Y., Ekbote, A., & Misra, R. (2021). Recent development on the synthesis, properties and applications of luminescent oxidized phenothiazine derivatives. *Journal of Materials Chemistry C*, *9*(24), 7508–7531. (DOI: 10.1039/D1TC00695A).

[47] Tang, G., Sukhanov, A. A., Zhao, J., Yang, W., Wang, Z., Liu, Q., … Jacquemin, D. (2019). Red Thermally Activated Delayed Fluorescence and the Intersystem Crossing Mechanisms in Compact Naphthalimide–Phenothiazine Electron Donor/Acceptor Dyads. *The Journal of Physical Chemistry C*, *123*(50), 30171–30186. (DOI: 10.1021/acs.jpcc.9b09335).

[48] Duvva, N., Eom, Y. K., Reddy, G., Schanze, K. S., & Giribabu, L. (2020). Bulky Phenanthroimidazole–Phenothiazine D−π–A Based Organic Sensitizers for Application in Efficient Dye-Sensitized Solar Cells. *ACS Applied Energy Materials*, *3*(7), 6758–6767. (DOI: 10.1021/acsaem.0c00892).

[49] Luo, J.-S., Wan, Z.-Q., & Jia, C.-Y. (2016). Recent advances in phenothiazine-based dyes for dye-sensitized solar cells. *Chinese Chemical Letters*, *27*(8), 1304–1318. (DOI: 10.1016/j.cclet.2016.07.002).

[50] Thokala, S., & Singh, S. P. (2020). Phenothiazine-Based Hole Transport Materials for Perovskite Solar Cells. *ACS Omega*, *5*(11), 5608–5619. (DOI: 10.1021/acsomega.0c00065).

[51] Knoevenagel, E. (1914). Über die Katalytischen Wirkungen des Jods. *Journal für Praktische Chemie*, *89*(1), 1–50. (DOI: 10.1002/prac.19130890101).

[52] Dahl, T., Tornøe, C. W., Bang-Andersen, B., Nielsen, P., & Jørgensen, M. (2008). Palladium-Catalyzed Three-Component Approach to Promazine with Formation of One Carbon–Sulfur and Two Carbon–Nitrogen Bonds. *Angewandte Chemie International Edition*, *47*(9), 1726–1728. (DOI: 10.1002/anie.200705209).

[53] Ma, D., Geng, Q., Zhang, H., & Jiang, Y. (2010). Assembly of Substituted Phenothiazines by a Sequentially Controlled CuI/ <scp>L</scp> -Proline-Catalyzed Cascade C–S and C–N Bond Formation. *Angewandte Chemie International Edition*, *49*(7), 1291–1294. (DOI: 10.1002/anie.200905646).

[54] Liao, Y., Jiang, P., Chen, S., Xiao, F., & Deng, G.-J. (2013). Synthesis of phenothiazines from cyclohexanones and 2-aminobenzenethiols under transition-metal-free conditions. *RSC Advances*, *3*(40), 18605. (DOI: 10.1039/c3ra43989e).

[55] Dai, C., Sun, X., Tu, X., Wu, L., Zhan, D., & Zeng, Q. (2012). Synthesis of phenothiazines *via* ligand-free CuI-catalyzed cascade C–S and C–N coupling of aryl ortho-dihalides and ortho-aminobenzenethiols. *Chemical Communications*, *48*(43), 5367. (DOI: 10.1039/c2cc30814b).

[56] Krishna, S., Jain, M. S. (1928) *Proc. 15th Indian Sci. Cong*., 153; Chem. Abstracts 26, 3001.

[57] Evans, W. J., & Smiles, S. (1935). 42. A rearrangement of o-acetamido-sulphones and -sulphides. *Journal of the Chemical Society (Resumed)*, 181. (DOI: 10.1039/jr9350000181).

[58] Michels, J. G., & Amstutz, E. D. (1950). Studies in the Sulfone Series. V. [1] 2,8-Diaminophenothiazine-5-dioxide. *Journal of the American Chemical Society*, *72*(2), 888–892. (DOI: 10.1021/ja01158a064).

[59] Kehrmann, F., & Steinberg, J. (1911). Über einige Derivate des 1.3-Diamino-phenazthioniums. *Berichte der deutschen chemischen Gesellschaft*, 44(3), 3011-3017.

[60] Patil, Y., Butenschön, H., & Misra, R. (2023). Tetracyanobutadiene Bridged Push-Pull Chromophores: Development of New Generation Optoelectronic Materials. *The Chemical Record*, *23*(1). (DOI: 10.1002/tcr.202200208).

[61] Zhang, Z., Gou, G., Wan, J., Li, H., Wang, M., & Li, L. (2022). Synthesis, Structure, and Significant Energy Gap Modulation of Symmetrical Silafluorene-Cored Tetracyanobutadiene and Tetracyanoquinodimethane Derivatives. *The Journal of Organic Chemistry*, *87*(5), 2470–2479. (DOI: 10.1021/acs.joc.1c02382).

[62] Reutenauer, P., Kivala, M., Jarowski, P. D., Boudon, C., Gisselbrecht, J.-P., Gross, M., & Diederich, F. (2007). New strong organic acceptors by cycloaddition of TCNE and TCNQ to donor-substituted cyanoalkynes. *Chemical Communications*, (46), 4898. (DOI: 10.1039/b714731g).

[63] Kivala, M., Boudon, C., Gisselbrecht, J. P., Seiler, P., Gross, M., & Diederich, F. (2007). Charge-transfer chromophores by cycloaddition-retro-electrocyclization: Multivalent systems and cascade reactions. *Angewandte Chemie - International Edition*, *46*(33), 6357–6360. (DOI: 10.1002/anie.200701733).

[64] Philippe, C., Bui, A. T., Beau, M., Bloux, H., Riobé, F., Mongin, O., … Trolez, Y. (2022). Synthesis and Photophysical Properties of 1,1,4,4-Tetracyanobutadienes Derived from Ynamides Bearing Fluorophores. *Chemistry – A European Journal*, *28*(23). (DOI: 10.1002/chem.202200025).

[65] Neethu, K. M., Nag, K., Dar, A. H., Bajaj, A., Gopal, S. A., Gowri, V., … Jayamurugan, G. (2023). A study of [2 + 2] cycloaddition–retroelectrocyclization in water: observation of substrate-driven transient-nanoreactor-induced new reactivity. *Organic & Biomolecular Chemistry*, *21*(14), 2922–2929. (DOI: 10.1039/D3OB00053B).

[66] Michinobu, T., Boudon, C., Gisselbrecht, J., Seiler, P., Frank, B., Moonen, N. N. P., … Diederich, F. (2006). Donor-Substituted 1,1,4,4-Tetracyanobutadienes (TCBDs): New Chromophores with Efficient Intramolecular Charge-Transfer Interactions by Atom-Economic Synthesis. *Chemistry – A European Journal*, *12*(7), 1889–1905. (DOI: 10.1002/chem.200501113).

[67] Leliège, A., Blanchard, P., Rousseau, T., & Roncali, J. (2011). Triphenylamine/Tetracyanobutadiene-Based D-A-D π-Conjugated Systems as Molecular Donors for Organic Solar Cells. *Organic Letters*, *13*(12), 3098–3101. (DOI: 10.1021/ol201002j).

[68] Bureš, F., Schweizer, W. B., May, J. C., Boudon, C., Gisselbrecht, J., Gross, M., … Diederich, F. (2007). Property Tuning in Charge-Transfer Chromophores by Systematic Modulation of the Spacer between Donor and Acceptor. *Chemistry – A European Journal*, *13*(19), 5378–5387. (DOI: 10.1002/chem.200601735).

[69] Wang, J.-L., Xiao, Q., & Pei, J. (2010). Benzothiadiazole-Based D−π-A−π-D Organic Dyes with Tunable Band Gap: Synthesis and Photophysical Properties. *Organic Letters*, *12*(18), 4164–4167. (DOI: 10.1021/ol101754q).

[70] Zatsikha, Y. V., Maligaspe, E., Purchel, A. A., Didukh, N. O., Wang, Y., Kovtun, Y. P., … Nemykin, V. N. (2015). Tuning Electronic Structure, Redox, and Photophysical Properties in Asymmetric NIR-Absorbing Organometallic BODIPYs. *Inorganic Chemistry*, *54*(16), 7915–7928. (DOI: 10.1021/acs.inorgchem.5b00992).

[71] Jordan, M., Kivala, M., Boudon, C., Gisselbrecht, J., Schweizer, W. B., Seiler, P., & Diederich, F. (2011). Switching the Regioselectivity in Cycloaddition-Retro-Electrocyclizations between Donor-Activated Alkynes and the Electron-Accepting Olefins TCNE and TCNQ. *Chemistry – An Asian Journal*, *6*(2), 396–401. (DOI: 10.1002/asia.201000539).

[72] Mammadova, F., Inyurt, F. C., Barsella, A., & Dengiz, C. (2023). Cyano-rich donor–acceptor–donor type NLOphores containing dialkylated triazene and aniline groups. *Dyes and Pigments*, *209*, 110894. (DOI: 10.1016/j.dyepig.2022.110894).

[73] Philippe, C., Melan, J., Barsella, A., Vives, T., Leroux, Y. R., Robin-Le Guen, F., … Trolez, Y. (2023). A comprehensive study of tetracyanobutadiene push-pull chromophores derived from γ-pyranylidene. *Tetrahedron Chem*, *5*, 100036. (DOI: 10.1016/j.tchem.2023.100036).

[74] Carboni, R. A. (1959). Tetracyanoethylene. *Organic Syntheses*, *39*, 64. (DOI: 10.15227/ORGSYN.039.0064).

[75] Acker, D. S., & Hertler, W. R. (1962). Substituted Quinodimethans. I. Preparation and Chemistry of 7, 7, 8, 8-Tetracyano Quino Dimethan. *Journal of the American Chemical Society*, *84*(17), 3370–3374. (DOI: 10.1021/JA00876A028).

[76] Bruce, M. I., Rodgers, J. R., Snow, M. R., & Swincer, A. G. (1981). Cyclopentadienyl-ruthenium and -osmium chemistry. Cleavage of tetracyanoethylene under mild conditions: X-ray crystal structures of [Ru{η^3-$C(CN)_2CPhC{=}C(CN)_2$}(PPh_3)(η-C_5H_5)] and [Ru{$C[{=}C(CN)_2]CPh{=}C(CN)_2$}-($CNBu^t$)($PPh_3$)(η-$C_5H_5$)]. *Journal of the Chemical Society, Chemical Communications*, (6), 271–272. (DOI: 10.1039/C39810000271).

[77] Kivala, M., Boudon, C., Gisselbrecht, J. P., Seiler, P., Gross, M., & Diederich, F. (2007). A novel reaction of 7,7,8,8-tetracyanoquinodimethane (TCNQ): Charge-transfer chromophores by [2 + 2] cycloaddition with alkynes. *Chemical Communications*, (45), 4731–4733. (DOI: 10.1039/b713683h).

[78] Michinobu, T. (2011). Adapting semiconducting polymer doping techniques to create new types of click postfunctionalization. *Chemical Society Reviews*, *40*(5), 2306–2316. (DOI: 10.1039/c0cs00205d).

[79] Michinobu, T. (2008). Click-type reaction of aromatic polyamines for improvement of thermal and optoelectronic

properties. *Journal of the American Chemical Society*, *130*(43), 14074–14075. (DOI: 10.1021/JA8061612).

[80] Shoji, T., Ito, S., Toyota, K., Yasunami, M., & Morita, N. (2008). Synthesis, Properties, and Redox Behavior of Mono-, Bis-, and Tris[1,1,4,4,-tetracyano-2-(1-azulenyl)-3-butadienyl] Chromophores Binding with Benzene and Thiophene Cores. *Chemistry – A European Journal*, *14*(27), 8398–8408. (DOI: 10.1002/chem.200701981).

[81] Bui, A. T., Philippe, C., Beau, M., Richy, N., Cordier, M., Roisnel, T., … Trolez, Y. (2020). Synthesis, characterization and unusual near-infrared luminescence of 1,1,4,4-tetracyanobutadiene derivatives. *Chemical Communications*, *56*(24), 3571–3574. (DOI: 10.1039/C9CC09560H).

[82] Kato, S. I., Noguchi, H., Kobayashi, A., Yoshihara, T., Tobita, S., & Nakamura, Y. (2012). Bicarbazoles: Systematic structure-property investigations on a series of conjugated carbazole dimers. *Journal of Organic Chemistry*, *77*(20), 9120–9133. (DOI: 10.1021/JO3016538).

[83] Jordan, M., Kivala, M., Boudon, C., Gisselbrecht, J. P., Schweizer, W. B., Seiler, P., & Diederich, F. (2011). Switching the regioselectivity in cycloaddition-retro-electrocyclizations between donor-activated alkynes and the electron-accepting olefins TCNE and TCNQ. *Chemistry, an Asian journal*, *6*(2), 396–401. (DOI: 10.1002/ASIA.201000539).

[84] Kato, S. ichiro, Noguchi, H., Jin, S., & Nakamura, Y. (2016). Synthesis and Electronic, Optical, and Electrochemical Properties of a Series of Tetracyanobutadiene-Substituted Carbazoles. *Asian Journal of Organic Chemistry*, *5*(2), 246–256. (DOI: 10.1002/ajoc.201500431).

[85] Krauße, N., Kielmann, M., Ma, J., & Butenschön, H. (2015). Reactions of Alkynyl- and 1,1′-Dialkynylferrocenes with Tetracyanoethylene – Unanticipated Addition at the Less Electron-Rich of Two Triple Bonds. *European Journal of*

Organic Chemistry, *2015*(12), 2622–2631. (DOI: 10.1002/ejoc.201500105).

[86] Poddar, M., & Misra, R. (2017). NIR-Absorbing Donor–Acceptor Based 1,1,4,4-Tetracyanobuta-1,3-Diene (TCBD)- and Cyclohexa-2,5-Diene-1,4-Ylidene-Expanded TCBD-Substituted Ferrocenyl Phenothiazines. *Chemistry – An Asian Journal*, *12*(22), 2908–2915. (DOI: 10.1002/asia.201700879).

[87] Rout, Y., Gautam, P., & Misra, R. (2017). Unsymmetrical and Symmetrical Push–Pull Phenothiazines. *The Journal of Organic Chemistry*, *82*(13), 6840–6845. (DOI: 10.1021/acs.joc.7b00991).

[88] Gupta, P. K., Khan, F., & Misra, R. (2023). NIR-Absorbing 1,1,4,4-Tetracyanobuta-1,3-diene- and Dicyanoquinodimethane-Functionalized Donor–Acceptor Phenothiazine Derivatives: Synthesis and Characterization. *The Journal of Organic Chemistry*, *88*(20), 14308–14322. (DOI: 10.1021/acs.joc.3c01029).

[89] Kumar Gupta, P., Das, S., Misra, R., & D'Souza, F. (2024). Near-IR Capturing N-Methylbenzene Sulfonamide-Phenothiazine Incorporating Strong Electron Acceptor Push-Pull Systems: Photochemical Ultrafast Carrier Dynamics. *Chemistry – A European Journal*, *30*(25), e202304313. (DOI: 10.1002/chem.202304313).

[90] Yadav, I. S., & Misra, R. (2022). Phenothiazine and phenothiazine-5,5-dioxide-based push–pull derivatives: synthesis, photophysical, electrochemical and computational studies. *New Journal of Chemistry*, *46*(33), 15999–16006. (DOI: 10.1039/D2NJ03089F).

[91] Hauck, M., Schönhaber, J., Zucchero, A. J., Hardcastle, K. I., Müller, T. J. J., & Bunz, U. H. F. (2007). Phenothiazine Cruciforms: Synthesis and Metallochromic Properties. *The Journal of Organic Chemistry*, *72*(18), 6714–6725. (DOI: 10.1021/jo070922l).

[92] Khan, F., Mahmoudi, M., Gupta, P. K., Volyniuk, D., Grazulevicius, J. V., & Misra, R. (2023). Mechanochromic Materials Based on Tetraphenylethylene-Substituted Phenothiazines: Substituent-Dependent Hypsochromic and Bathochromic Switching of Emission. *The Journal of Physical Chemistry C*, *127*(3), 1643–1654. (DOI: 10.1021/acs.jpcc.2c07010).

[93] Michinobu, T., Satoh, N., Cai, J., Li, Y., & Han, L. (2014). Novel design of organic donor–acceptor dyes without carboxylic acid anchoring groups for dye-sensitized solar cells. *Journal of Materials Chemistry C*, *2*(17), 3367. (DOI: 10.1039/c3tc32165g).

[94] Zhang, H., Wan, X., Xue, X., Li, Y., Yu, A., & Chen, Y. (2010). Selective Tuning of the HOMO–LUMO Gap of Carbazole-Based Donor–Acceptor–Donor Compounds toward Different Emission Colors. *European Journal of Organic Chemistry*, *2010*(9), 1681–1687. (DOI: 10.1002/ejoc.200901167).

[95] Hauck, M., Stolte, M., Schönhaber, J., Kuball, H., & Müller, T. J. J. (2011). Synthesis, Electronic, and Electro-Optical Properties of Emissive Solvatochromic Phenothiazinyl Merocyanine Dyes. *Chemistry – A European Journal*, *17*(36), 9984–9998. (DOI: 10.1002/chem.201100592).

[96] Müller, T. J. J. (1999). First synthesis and electronic properties of ring-alkynylated phenothiazines. *Tetrahedron Letters*, *40*(36), 6563–6566. (DOI: 10.1016/S0040-4039(99)01402-1).

[97] Krämer, C. S., & Müller, T. J. J. (2003). Synthesis and Electronic Properties of Alkynylated Phenothiazines. *European Journal of Organic Chemistry*, *2003*(18), 3534–3548. (DOI: 10.1002/ejoc.200300250).

[98] Tian, H., Yang, X., Chen, R., Pan, Y., Li, L., Hagfeldt, A., & Sun, L. (2007). Phenothiazine derivatives for efficient organic dye-sensitized solar cells. *Chemical Communications*, (36), 3741. (DOI: 10.1039/b707485a).

[99] Sailer, M., Gropeanu, R.-A., & Müller, T. J. J. (2003). Practical Synthesis of Iodo Phenothiazines. A Facile Access to Electrophore Building Blocks. *The Journal of Organic Chemistry*, *68*(19), 7509–7512. (DOI: 10.1021/jo034555z).

[100] Yadav, I. S., Jang, Y., Rout, Y., Thomas, M. B., Misra, R., & D'Souza, F. (2022). Near-IR Intramolecular Charge Transfer in Strongly Interacting Diphenothiazene-TCBD and Diphenothiazene-DCNQ Push-Pull Triads. *Chemistry – A European Journal*, *28*(25). (DOI: 10.1002/chem.202200348).

[101] Kim, G., Yeom, H. R., Cho, S., Seo, J. H., Kim, J. Y., & Yang, C. (2012). Easily attainable phenothiazine-based polymers for polymer solar cells: Advantage of insertion of S,S-dioxides into its polymer for inverted structure solar cells. *Macromolecules*, *45*(4), 1847–1857. (DOI: 10.1021/MA202661B).

[102] Ojha, M., Banerjee, M., Ray, S., Singh, A. K., Anoop, A., & Singh, N. D. P. (2022). Switching photorelease to singlet oxygen generation by oxygen functionalization of phenothiazine photocages. *Chemical Communications*, *58*(16), 2754–2757. (DOI: 10.1039/D1CC06950K).

[103] Umezono, S., & Okuno, T. (2017). Systematic study of intermolecular C–X···OS (X = Cl, Br, I) halogen bonds in (E)-10-(1,2-dihalovinyl)-10H-phenothiazine 5,5-dioxides. *Journal of Molecular Structure*, *1147*, 636–642. (DOI: 10.1016/J.MOLSTRUC.2017.06.135).

[104] Ding, X., Chen, C., Sun, L., Li, H., Chen, H., Su, J., … Cheng, M. (2019). Highly efficient phenothiazine 5,5-dioxide-based hole transport materials for planar perovskite solar cells with a PCE exceeding 20%. *Journal of Materials Chemistry A*, *7*(16), 9510–9516. (DOI: 10.1039/C9TA00654K).

[105] Rout, Y., Ekbote, A., & Misra, R. (2021). Recent development on the synthesis, properties and applications of luminescent oxidized phenothiazine derivatives. *Journal of Materials Chemistry C*, *9*(24), 7508–7531. (DOI: 10.1039/D1TC00695A).

[106] Shanmugasundaram, K., Chitumalla, R. K., Jang, J., & Choe, Y. (2017). Phenothiazine based blue emitter for light-emitting electrochemical cells. *New Journal of Chemistry*, *41*(18), 9668–9673. (DOI: 10.1039/C7NJ00976C).

[107] Sheokand, M., Alsaleh, A. Z., D'Souza, F., & Misra, R. (2023). Excitation Wavelength-Dependent Charge Stabilization in Highly Interacting Phenothiazine Sulfone-Derived Donor–Acceptor Constructs. *The Journal of Physical Chemistry B*, *127*(12), 2761–2773. (DOI: 10.1021/acs.jpcb.2c08472).

[108] Sheokand, M., Ji Tiwari, N., & Misra, R. (2023). Near-IR absorbing 1,1,4,4-tetracyanobutadiene-functionalized phenothiazine sulfones. *Organic & Biomolecular Chemistry*, *21*(18), 3896–3905. (DOI: 10.1039/D3OB00361B)

[109] Zatsikha, Y. V., Didukh, N. O., Swedin, R. K., Yakubovskyi, V. P., Blesener, T. S., Healy, A. T., … Kovtun, Y. P. (2019). Preparation of Viscosity-Sensitive Isoxazoline/Isoxazolyl-Based Molecular Rotors and Directly Linked BODIPY–Fulleroisoxazoline from the Stable *meso* -(Nitrile Oxide)-Substituted BODIPY. *Organic Letters*, *21*(14), 5713–5718. (DOI: 10.1021/acs.orglett.9b02082).

[110] Nguyen, V.-N., Ha, J., Koh, C. W., Ryu, B., Kim, G., Park, J. H., … Yoon, J. (2021). Access to the Triplet Excited States of Heavy-Atom-Free Boron-Dipyrromethene Photosensitizers *via* Radical Pair Intersystem Crossing for Image-Guided Tumor-Targeted Photodynamic Therapy. *Chemistry of Materials*, *33*(19), 7889–7896. (DOI: 10.1021/acs.chemmater.1c02776).

[111] Carlotti, B., Poddar, M., Elisei, F., Spalletti, A., & Misra, R. (2019). Energy-Transfer and Charge-Transfer Dynamics in Highly Fluorescent Naphthalimide–BODIPY Dyads: Effect of BODIPY Orientation. *The Journal of Physical Chemistry C*, *123*(40), 24362–24374. (DOI: 10.1021/acs.jpcc.9b05851).

[112] Shinde, J., Thomas, M. B., Poddar, M., Misra, R., & D'Souza, F. (2021). Does Location of BF_2-Chelated Dipyrromethene (BODIPY) Ring Functionalization Affect Spectral and Electron

Transfer Properties? Studies on α-, β-, and Meso-Functionalized BODIPY-Derived Donor–Acceptor Dyads and Triads. *The Journal of Physical Chemistry C*, *125*(43), 23911–23921. (DOI: 10.1021/acs.jpcc.1c06704).

[113] Gapare, R. L., & Thompson, A. (2022). Substitution at boron in BODIPYs. *Chemical Communications*, *58*(53), 7351–7359. (DOI: 10.1039/D2CC02362H).

[114] Nenavath, S., Duvva, N., Kaswan, R. R., Lim, G. N., D'Souza, F., & Giribabu, L. (2023). Intramolecular Photoinduced Energy and Electron Transfer Reactions in Phenanthroimidazole–Boron Dipyromethane Donor–Acceptor Dyads. *The Journal of Physical Chemistry A*, *127*(32), 6779–6790. (DOI: 10.1021/acs.jpca.3c04141).

[115] Duan, C., Zhou, Y., Shan, G.-G., Chen, Y., Zhao, W., Yuan, D., … Niu, G. (2019). Bright solid-state red-emissive BODIPYs: facile synthesis and their high-contrast mechanochromic properties. *Journal of Materials Chemistry C*, *7*(12), 3471–3478. (DOI: 10.1039/C8TC06421K).

[116] Wei, Z., Sharma, S., Philip, A. M., Sengupta, S., & Grozema, F. C. (2021). Excited state dynamics of BODIPY-based acceptor–donor–acceptor systems: a combined experimental and computational study. *Physical Chemistry Chemical Physics*, *23*(14), 8900–8907. (DOI: 10.1039/D1CP00453K).

[117] Thompson, B. L., Kieffer, I. A., & Heiden, Z. M. (2022). Utilization of BODIPY-based redox events to manipulate the Lewis acidity of fluorescent boranes. *Chemical Communications*, *58*(16), 2646–2649. (DOI: 10.1039/D1CC06400B).

[118] Yadav, I. S., Kaswan, R. R., Liyanage, A., Misra, R., & D'Souza, F. (2024). Dimethylaniline-Tetracyanobutadiene and Dimethylaniline-Extended-Tetracyanobutadiene Functionalized BODIPYs Witnessing Ultrafast Charge Transfer. *The Journal of Physical Chemistry C*, *128*(12), 4934–4945. (DOI: 10.1021/acs.jpcc.4c00072).

[119] Poddar, M., Jang, Y., Misra, R., & D'Souza, F. (2020). Excited-State Electron Transfer in 1,1,4,4-Tetracyanobuta-1,3-diene (TCBD)- and Cyclohexa-2,5-diene-1,4-diylidene-Expanded TCBD-Substituted BODIPY-Phenothiazine Donor–Acceptor Conjugates. *Chemistry – A European Journal*, *26*(30), 6869–6878. (DOI: 10.1002/chem.202000346).

[120] Gautam, P., Misra, R., Thomas, M. B., & D'Souza, F. (2017). Ultrafast Charge-Separation in Triphenylamine-BODIPY-Derived Triads Carrying Centrally Positioned, Highly Electron-Deficient, Dicyanoquinodimethane or Tetracyanobutadiene Electron-Acceptors. *Chemistry – A European Journal*, *23*(38), 9192–9200. (DOI: 10.1002/chem.201701604).

[121] Patil, Y., Popli, C., & Misra, R. (2018). Near-infrared absorbing tetracyanobutadiene-bridged diketopyrrolopyrroles. *New Journal of Chemistry*, *42*(5), 3892–3899. https://doi.org/10.1039/C7NJ05162J

[122] Wee, X. K., Yeo, W. K., Zhang, B., Tan, V. B. C., Lim, K. M., Tay, T. E., & Go, M. L. (2009). Synthesis and evaluation of functionalized isoindigos as antiproliferative agents. *Bioorganic & Medicinal Chemistry*, *17*(21), 7562–7571. (DOI: 10.1016/J.BMC.2009.09.008).

[123] Lei, T., Wang, J.-Y., & Pei, J. (2014). Design, Synthesis, and Structure–Property Relationships of Isoindigo-Based Conjugated Polymers. *Accounts of Chemical Research*, *47*(4), 1117–1126. (DOI: 10.1021/ar400254j).

[124] Goswami, S., Gish, M. K., Wang, J., Winkel, R. W., Papanikolas, J. M., & Schanze, K. S. (2015). π-Conjugated Organometallic Isoindigo Oligomer and Polymer Chromophores: Singlet and Triplet Excited State Dynamics and Application in Polymer Solar Cells. *ACS Applied Materials & Interfaces*, *7*(48), 26828–26838. (DOI: 10.1021/acsami.5b09041).

[125] Song, H., Deng, Y., Jiang, Y., Tian, H., & Geng, Y. (2018). π-Conjugation expanded isoindigo derivatives and the donor–

acceptor conjugated polymers: synthesis and characterization. *Chemical Communications*, *54*(7), 782–785. (DOI: 10.1039/C7CC08603B).

[126] Aumaitre, C., Rodriguez-Seco, C., Jover, J., Bardagot, O., Caffy, F., Kervella, Y., … Demadrille, R. (2018). Visible and near-infrared organic photosensitizers comprising isoindigo derivatives as chromophores: synthesis, optoelectronic properties and factors limiting their efficiency in dye solar cells. *Journal of Materials Chemistry A*, *6*(21), 10074–10084. (DOI: 10.1039/C8TA01826J).

[127] Ren, Y., Hailey, A. K., Hiszpanski, A. M., & Loo, Y. L. (2014). Isoindigo-containing molecular semiconductors: Effect of backbone extension on molecular organization and organic solar cell performance. *Chemistry of Materials*, *26*(22), 6570–6577. (DOI: 10.1021/CM503312C).

[128] Stalder, R., Mei, J., Graham, K. R., Estrada, L. A., & Reynolds, J. R. (2014). Isoindigo, a versatile electron-deficient unit for high-performance organic electronics. *Chemistry of Materials*, *26*(1), 664–678. (DOI: 10.1021/CM402219V).

[129] Rout, Y., Chauhan, V., & Misra, R. (2020). Synthesis and Characterization of Isoindigo-Based Push–Pull Chromophores. *The Journal of Organic Chemistry*, *85*(7), 4611–4618. (DOI: 10.1021/acs.joc.9b03267).

[130] Ventura, B., Barbieri, A., Barigelletti, F., Diring, S., & Ziessel, R. (2010). Energy Transfer Dynamics in Multichromophoric Arrays Engineered from Phosphorescent $Pt^{II}/Ru^{II}/Os^{II}$ Centers Linked to a Central Truxene Platform. *Inorganic Chemistry*, *49*(18), 8333–8346. (DOI: 10.1021/ic1008413).

[131] Cao, X. Y., Zhang, W. Bin, Wang, J. L., Zhou, X. H., Lu, H., & Pei, J. (2003). Extended pi-conjugated dendrimers based on truxene. *Journal of the American Chemical Society*, *125*(41), 12430–12431. (DOI: 10.1021/JA037723D).

[132] Zong, X., Liang, M., Fan, C., Tang, K., Li, G., Sun, Z., & Xue, S. (2012). Design of Truxene-Based Organic Dyes for High-

Efficiency Dye-Sensitized Solar Cells Employing Cobalt Redox Shuttle. *The Journal of Physical Chemistry C*, *116*(20), 11241–11250. (DOI: 10.1021/jp301406x).

[133] Ma, L., Wu, Z., Zhou, G., Yuan, F., Yu, Y., Yao, C., … Gong, Q. (2015). The molecular picture of amplified spontaneous emission of star-shaped functionalized-truxene derivatives. *Journal of Materials Chemistry C*, *3*(27), 7004–7013. (DOI: 10.1039/C5TC01040C).

[134] Misra, R., & Gautam, P. (2014). Tuning of the HOMO–LUMO gap of donor-substituted symmetrical and unsymmetrical benzothiadiazoles. *Organic & Biomolecular Chemistry*, *12*(29), 5448–5457. (DOI: 10.1039/c4ob00629a).

[135] Xie, Y., Zhang, X., Xiao, Y., Zhang, Y., Zhou, F., Qi, J., & Qu, J. (2012). Fusing three perylenebisimide branches and a truxene core into a star-shaped chromophore with strong two-photon excited fluorescence and high photostability. *Chemical Communications*, *48*(36), 4338–4340. (DOI: 10.1039/c2cc31261a).

[136] Yao, C., Yu, Y., Yang, X., Zhang, H., Huang, Z., Xu, X., … Wu, Z. (2015). Effective blocking of the molecular aggregation of novel truxene-based emitters with spirobifluorene and electron-donating moieties for furnishing highly efficient non-doped blue-emitting OLEDs. *Journal of Materials Chemistry C*, *3*(22), 5783–5794. (DOI: 10.1039/C5TC01018G).

[137] Pei, J., Wang, J.-L., Cao, X.-Y., Zhou, X.-H., & Zhang, W.-B. (2003). Star-Shaped Polycyclic Aromatics Based on Oligothiophene-Functionalized Truxene: Synthesis, Properties, and Facile Emissive Wavelength Tuning. *Journal of the American Chemical Society*, *125*(33), 9944–9945. (DOI: 10.1021/ja0361650).

[138] Sharma, R., Thomas, M. B., Misra, R., & D'Souza, F. (2019). Strong Ground- and Excited-State Charge Transfer in C_3-Symmetric Truxene-Derived Phenothiazine-Tetracyanobutadine

and Expanded Conjugates. *Angewandte Chemie*, *131*(13), 4394–4399. (DOI: 10.1002/ange.201814388).

[139] Sharma, R., Maragani, R., & Misra, R. (2018). C_3 -Symmetric star shaped donor–acceptor truxenes: synthesis and photophysical, electrochemical and computational studies. *New Journal of Chemistry*, *42*(2), 882–890. (DOI: 10.1039/C7NJ03934D).

[140] Das, A., & Ghosh, S. (2016). H-bonding directed programmed supramolecular assembly of naphthalene-diimide (NDI) derivatives. *Chemical Communications*, *52*(42), 6860–6872. (DOI: 10.1039/C6CC01983H).

[141] Yan, C., Barlow, S., Wang, Z., Yan, H., Jen, A. K.-Y., Marder, S. R., & Zhan, X. (2018). Non-fullerene acceptors for organic solar cells. *Nature Reviews Materials*, *3*(3), 18003. (DOI: 10.1038/natrevmats.2018.3).

[142] Nowak-Król, A., Shoyama, K., Stolte, M., & Würthner, F. (2018). Naphthalene and perylene diimides – better alternatives to fullerenes for organic electronics? *Chemical Communications*, *54*(98), 13763–13772. (DOI: 10.1039/C8CC07640E).

[143] Rao, P. S., Gupta, A., Srivani, D., Bhosale, S. V., Bilic, A., Li, J., … Bhosale, S. V. (2018). An efficient non-fullerene acceptor based on central and peripheral naphthalene diimides. *Chemical Communications*, *54*(40), 5062–5065. (DOI: 10.1039/C8CC01779D).

[144] Higginbotham, H. F., Pander, P., Rybakiewicz, R., Etherington, M. K., Maniam, S., Zagorska, M., … Data, P. (2018). Triphenylamine disubstituted naphthalene diimide: elucidation of excited states involved in TADF and application in near-infrared organic light emitting diodes. *Journal of Materials Chemistry C*, *6*(30), 8219–8225. (DOI: 10.1039/C8TC02936A).

[145] Zhou, N., & Facchetti, A. (2018). Naphthalenediimide (NDI) polymers for all-polymer photovoltaics. *Materials Today*, *21*(4), 377–390. (DOI: 10.1016/j.mattod.2018.02.003).

[146] Srinivasa Rao, P., Brixi, S., Shaikh, D. B., Al Kobaisi, M., Lessard, B. H., Bhosale, S. V., & Bhosale, S. V. (2021). The Effect of TCNE and TCNQ Acceptor Units on Triphenylamine-Naphthalenediimide Push-Pull Chromophore Properties. *European Journal of Organic Chemistry*, *2021*(18), 2615–2624. (DOI: 10.1002/ejoc.202100198).

[147] Bard, A. J., & Faulkner, L. R. (2001). Polarography and Pulse Voltammetry. *Electrochemical Methods: Fundamentals and Applications*, 261–304.

[148] Winterfeld, K. A., Lavarda, G., Guilleme, J., Sekita, M., Guldi, D. M., Torres, T., & Bottari, G. (2017). Subphthalocyanines Axially Substituted with a Tetracyanobuta-1,3-diene–Aniline Moiety: Synthesis, Structure, and Physicochemical Properties. *Journal of the American Chemical Society*, *139*(15), 5520–5529. (DOI: 10.1021/jacs.7b01460).

[149] Gautam, P., Misra, R., Thomas, M. B., & D'Souza, F. (2017). Ultrafast Charge-Separation in Triphenylamine-BODIPY-Derived Triads Carrying Centrally Positioned, Highly Electron-Deficient, Dicyanoquinodimethane or Tetracyanobutadiene Electron-Acceptors. *Chemistry – A European Journal*, *23*(38), 9192–9200. (DOI: 10.1002/chem.201701604).

[150] Xu, H., Yang, Y., Zhong, C., Zhan, X., & Chen, X. (2018). Narrow bandgap non-fullerene acceptor based on a thiophene-fused benzothiadiazole unit with a high short-circuit current density of over 20 mA cm^{-2}. *Journal of Materials Chemistry A*, *6*(15), 6393–6401. (DOI: 10.1039/C8TA00704G).

[151] Zhou, J., Xie, S., Amond, E. F., & Becker, M. L. (2013). Tuning Energy Levels of Low Bandgap Semi-Random Two Acceptor Copolymers. *Macromolecules*, *46*(9), 3391–3394. (DOI: 10.1021/ma400531v).

[152] Rohwer, E. J., Akbarimoosavi, M., Meckel, S. E., Liu, X., Geng, Y., Lawson Daku, L. M., … Feurer, T. (2018). Dipole Moment and Polarizability of Tunable Intramolecular Charge Transfer States in Heterocyclic π-Conjugated Molecular Dyads

Determined by Computational and Stark Spectroscopic Study. *The Journal of Physical Chemistry C*, *122*(17), 9346–9355. (DOI: 10.1021/acs.jpcc.8b02268).

[153] Akbarimoosavi, M., Rohwer, E., Rondi, A., Hankache, J., Geng, Y., Decurtins, S., … Cannizzo, A. (2019). Tunable Lifetimes of Intramolecular Charge-Separated States in Molecular Donor–Acceptor Dyads. *The Journal of Physical Chemistry C*, *123*(14), 8500–8511. (DOI: 10.1021/acs.jpcc.8b11066).

[154] Cheng, Y.-J., Chen, C.-H., Ho, Y.-J., Chang, S.-W., Witek, H. A., & Hsu, C.-S. (2011). Thieno[3,2- *b*]pyrrolo Donor Fused with Benzothiadiazolo, Benzoselenadiazolo and Quinoxalino Acceptors: Synthesis, Characterization, and Molecular Properties. *Organic Letters*, *13*(20), 5484–5487. (DOI: 10.1021/ol202199v).

[155] Hu, Y., Dössel, L. F., Wang, X., Mahesh, S., Pisula, W., De Feyter, S., … Narita, A. (2017). Synthesis, Photophysical Characterization, and Self-Assembly of Hexa- *peri* -hexabenzocoronene/Benzothiadiazole Donor–Acceptor Structure. *ChemPlusChem*, *82*(7), 1030–1033. (DOI: 10.1002/cplu.201700162).

[156] Ahn, J., Oh, S., Lee, H., Lee, S., Song, C. E., Lee, H. K., … Lee, J.-C. (2019). Simple and Versatile Non-Fullerene Acceptor Based on Benzothiadiazole and Rhodanine for Organic Solar Cells. *ACS Applied Materials & Interfaces*, *11*(33), 30098–30107. (DOI: 10.1021/acsami.9b09256).

[157] Kim, J., Han, A.-R., Hong, J., Kim, G., Lee, J., Shin, T. J., … Yang, C. (2014). Ambipolar Semiconducting Polymers with π-Spacer Linked Bis-Benzothiadiazole Blocks as Strong Accepting Units. *Chemistry of Materials*, *26*(17), 4933–4942. (DOI: 10.1021/cm500800u).

[158] Rout, Y., Jang, Y., Gobeze, H. B., Misra, R., & D'Souza, F. (2019). Conversion of Large-Bandgap Triphenylamine–Benzothiadiazole to Low-Bandgap, Wide-Band Capturing Donor–Acceptor Systems by Tetracyanobutadiene and/or

Dicyanoquinodimethane Insertion for Ultrafast Charge Separation. *The Journal of Physical Chemistry C*, *123*(38), 23382–23389. (DOI: 10.1021/acs.jpcc.9b06632).

[159] Rout, Y., & Misra, R. (2021). Design and synthesis of 1,8-naphthalimide functionalized benzothiadiazoles. *New Journal of Chemistry*, *45*(22), 9838–9845. (DOI: 10.1039/D1NJ00919B).

[160] Misra, R., & Gautam, P. (2014). Tuning of the HOMO–LUMO gap of donor-substituted symmetrical and unsymmetrical benzothiadiazoles. *Organic & Biomolecular Chemistry*, *12*(29), 5448. (DOI: 10.1039/c4ob00629a).

[161] Bruno, C., Doubitski, I., Marcaccio, M., Paolucci, F., Paolucci, D., & Zaopo, A. (2003). Electrochemical Generation of C_{60}^{2+} and C_{60}^{3+}. *Journal of the American Chemical Society*, *125*(51), 15738–15739. (DOI: 10.1021/ja0388515).

[162] Anthopoulos, T. D., Singh, B., Marjanovic, N., Sariciftci, N. S., Montaigne Ramil, A., Sitter, H., … de Leeuw, D. M. (2006). High performance n-channel organic field-effect transistors and ring oscillators based on C60 fullerene films. *Applied Physics Letters*, *89*(21), 213504. (DOI: 10.1063/1.2387892).

[163] Arias, F., Echegoyen, L., Wilson, S. R., Lu, Q., & Lu, Q. (1995). Methanofullerenes and Methanofulleroids Have Different Electrochemical Behavior at Negative Potentials. *Journal of the American Chemical Society*, *117*(4), 1422–1427. (DOI: 10.1021/ja00109a029).

[164] Echegoyen, L., & Echegoyen, L. E. (1998). Electrochemistry of Fullerenes and Their Derivatives. *Accounts of Chemical Research*, *31*(9), 593–601. (DOI: 10.1021/ar970138v).

[165] Yamada, M., Tancini, F., Sekita, M., Guldi, D. M., Boudon, C., Gisselbrecht, J.-P., … Diederich, F. (2014). Ground and Excited State Electronic Interactions in Push–Pull-Chromophore–[60]Fullerene Conjugates. *Fullerenes, Nanotubes and Carbon Nanostructures*, *22*(1–3), 99–127. (DOI: 10.1080/1536383X.2013.794342).

[166] Marcus, R. A. (1956). On the Theory of Oxidation-Reduction Reactions Involving Electron Transfer. I. *The Journal of Chemical Physics*, *24*(5), 966–978. (DOI: 10.1063/1.1742723).

[167] Chung, W. S., & Liu, J. H. (1997). Quinoxalino-fused sultines and their application in Diels–Alder reactions. *Chemical Communications*, (2), 205–206. (DOI: 10.1039/A606764F).

[168] Burrows, H. D., Fonseca, S. M., Gigante, B., Esteves, M. A., & Guerreiro, A. M. (2006). Fluorescence Study of Dehydroabietic Acid-Based Bipolar Arylamine-Quinoxalines. *Journal of Fluorescence*, *16*(2), 227–231. (DOI: 10.1007/s10895-005-0048-6).

[169] Schmitz, C., Pösch, P., Thelakkat, M., Schmidt, H.-W., Montali, A., Feldman, K., … Weder, C. (2001). Polymeric Light-Emitting Diodes Based on Poly(p-phenylene ethynylene), Poly(triphenyldiamine), and Spiroquinoxaline. *Advanced Functional Materials*, *11*(1), 41–46. (DOI: 10.1002/1616-3028(200102)11:1<41::AID-ADFM41>3.0.CO;2-S).

[170] Wen, Z., Yang, T., Zhang, D., Wang, Z., Dong, S., Xu, H., … Wang, H. (2022). A multifunctional luminescent material based on quinoxaline and triphenylamine groups: polymorphism, mechanochromic luminescence, and applications in high-efficiency fluorescent OLEDs. *Journal of Materials Chemistry C*, *10*(9), 3396–3403. (DOI: 10.1039/D1TC04285H).

[171] Boxi, S., Jana, D., & Ghorai, B. K. (2019). Synthesis and optical properties of bipolar quinoxaline-triphenylamine based stilbene compounds. *Optical Materials: X*, *1*, 100013. (DOI: 10.1016/j.omx.2019.100013).

[172] Gupta, S., & Milton, M. D. (2022). Novel Y-shaped AIEE-TICT active π-extended quinoxalines-based donor–acceptor molecules displaying acidofluorochromism and temperature dependent emission. *Journal of Photochemistry and Photobiology A: Chemistry*, *424*, 113630. (DOI: 10.1016/j.jphotochem.2021.113630).

[173] Wang, X., Zhou, Y., Lei, T., Hu, N., Chen, E.-Q., & Pei, J. (2010). Structural−Property Relationship in Pyrazino[2,3-g]quinoxaline Derivatives: Morphology, Photophysical, and Waveguide Properties. *Chemistry of Materials*, *22*(12), 3735–3745. (DOI: 10.1021/cm100798q).

[174] Jang, Y., Sekaran, B., Singh, P. P., Misra, R., & D'Souza, F. (2023). Accelerated Intramolecular Charge Transfer in Tetracyanobutadiene- and Expanded Tetracyanobutadiene-Incorporated Asymmetric Triphenylamine–Quinoxaline Push–Pull Conjugates. *The Journal of Physical Chemistry A*, *127*(20), 4455–4462. (DOI: 10.1021/acs.jpca.3c01732).

[175] Thorley, K. J., Hales, J. M., Kim, H., Ohira, S., Brédas, J., Perry, J. W., & Anderson, H. L. (2013). Cyanine-Like Dyes with Large Bond-Length Alternation. *Chemistry – A European Journal*, *19*(31), 10370–10377. (DOI: 10.1002/chem.201300609).

[176] Zhang, L., Zhu, Y., Yin, G., Lu, P., & Wang, Y. (2012). 3-alkenylation or 3-alkylation of indole with propargylic alcohols: Construction of 3,4-dihydrocyclopenta[b]indole and 1,4-dihydrocyclopenta[b]indole in the presence of different catalysts. *Journal of Organic Chemistry*, *77*(21), 9510–9520. (DOI: 10.1021/JO300339A).

[177] Damodiran, M., Muralidharan, D., & Perumal, P. T. (2009). Regioselective synthesis and biological evaluation of bis(indolyl)methane derivatized 1,4-disubstituted 1,2,3-bistriazoles as anti-infective agents. *Bioorganic & Medicinal Chemistry Letters*, *19*(13), 3611–3614. (DOI: 10.1016/j.bmcl.2009.04.131).

[178] Kaushik, N., Kaushik, N., Attri, P., Kumar, N., Kim, C., Verma, A., & Choi, E. (2013). Biomedical Importance of Indoles. *Molecules*, *18*(6), 6620–6662. (DOI: 10.3390/molecules18066620).

[179] Keller, N., & Bein, T. (2021). Optoelectronic processes in covalent organic frameworks. *Chemical Society Reviews*, *50*(3), 1813–1845. (DOI: 10.1039/D0CS00793E).

[180] Budania, S., Shelke, G. M., & Kumar, A. (2017). Synthesis of 3-alkenylated indole and bis(indol-3-yl) derivatives catalyzed by sulfonic acid-functionalized ionic liquid under ultrasound irradiation. *Synthetic Communications*, *47*(7), 646–654 (DOI: 10.1080/00397911.2016.1278232).

[181] Girgis, A. S., Panda, S. S., Srour, A. M., Abdelnaser, A., Nasr, S., Moatasim, Y., … Soliman, A. A. F. (2021). 3-Alkenyl-2-oxindoles: Synthesis, antiproliferative and antiviral properties against SARS-CoV-2. *Bioorganic Chemistry*, *114*, 105131. (DOI: 10.1016/J.BIOORG.2021.105131).

[182] Erden, K., & Dengiz, C. (2022). 3-Alkynylindoles as Building Blocks for the Synthesis of Electronically Tunable Indole-Based Push–Pull Chromophores. *The Journal of Organic Chemistry*, *87*(6), 4385–4399. (DOI: 10.1021/acs.joc.2c00067).

[183] Gou, G., Zhang, Z., Yuan, B., Fan, T., & Li, L. (2021). Synthesis, photophysical properties and optical stabilities of dimethylthio modified dibenzosiloles: High quantum yield emitters. *Dyes and Pigments*, *194*, 109642. (DOI: 10.1016/j.dyepig.2021.109642).

[184] Furukawa, S., Kobayashi, J., & Kawashima, T. (2009). Development of a Sila-Friedel−Crafts Reaction and Its Application to the Synthesis of Dibenzosilole Derivatives. *Journal of the American Chemical Society*, *131*(40), 14192–14193. (DOI: 10.1021/ja906566r).

[185] Dang, T. T., Nguyen, H. M. T., Nguyen, H., Dung, T. N., Nguyen, M. T., & Dehaen, W. (2020). Advances in Synthesis of π-Extended Benzosilole Derivatives and Their Analogs. *Molecules*, *25*(3), 548. (DOI: 10.3390/molecules25030548).

[186] Zheng, Y., Wang, Z., Wang, X., Li, J., Feng, X. J., He, G., … Lu, H. (2021). Bipolar Arylsilane: Synthesis, Photoelectronic Properties, and High-Performance Deep Blue Organic Light-Emitting Diodes. *ACS Applied Electronic Materials*, *3*(1), 422–429. (DOI: 10.1021/acsaelm.0c00960).

[187] Zheng, Y., Zhu, X., Ni, Z., Wang, X., Zhong, Z., Feng, X. J., … Lu, H. (2021). Bipolar Molecules with Hybridized Local and

Charge-Transfer State for Highly Efficient Deep-Blue Organic Light-Emitting Diodes with EQE of 7.4% and CIE $_y$ ∼ 0.05. *Advanced Optical Materials*, *9*(21), 2100965. (DOI: 10.1002/adom.2021009650).

[188] Song, H. J., Lee, J. Y., Lee, E. J., & Moon, D. K. (2013). Conjugated polymer consisting of dibenzosilole and quinoxaline as donor materials for organic photovoltaics. *European Polymer Journal*, *49*(10), 3261–3270. (DOI: 10.1016/j.eurpolymj.2013.06.032).

[189] Shimizu, M. (2015). Dibenzosiloles and 12*H* -Indololo[3,2-*d*]naphtho[1,2-*b*][1]siloles: Exploration of Organic Chromophores Exhibiting Efficient Solid-State Fluorescence. *The Chemical Record*, *15*(1), 73–85. (DOI: 10.1002/tcr.201402084).

[190] Zhang, Z., Gou, G., Wan, J., Li, H., Wang, M., & Li, L. (2022). Synthesis, Structure, and Significant Energy Gap Modulation of Symmetrical Silafluorene-Cored Tetracyanobutadiene and Tetracyanoquinodimethane Derivatives. *The Journal of Organic Chemistry*, *87*(5), 2470–2479. (DOI: 10.1021/acs.joc.1c02382).

[191] Shoji, T., Ito, S., Okujima, T., & Morita, N. (2012). Synthesis of push–pull chromophores by the sequential [2 + 2] cycloaddition of 1-azulenylbutadiynes with tetracyanoethylene and tetrathiafulvalene. *Organic & Biomolecular Chemistry*, *10*(41), 8308–8313. (DOI: 10.1039/c2ob26028j).

[192] Khan, F., Ekbote, A., & Misra, R. (2019). Reversible mechanochromism and aggregation induced enhanced emission in phenothiazine substituted tetraphenylethylene. *New Journal of Chemistry*, *43*(41), 16156–16163. (DOI: 10.1039/C9NJ03290H).

[193] Jiang, M., Gu, X., Kwok, R. T. K., Li, Y., Sung, H. H. Y., Zheng, X., … Tang, B. Z. (2018). Multifunctional AIEgens: Ready Synthesis, Tunable Emission, Mechanochromism, Mitochondrial, and Bacterial Imaging. *Advanced Functional Materials*, *28*(1), 1704589. (DOI: 10.1002/ADFM.201704589).

[194] Ekbote, A., Jadhav, T., & Misra, R. (2017). T-Shaped donor–acceptor–donor type tetraphenylethylene substituted quinoxaline derivatives: aggregation-induced emission and mechanochromism. *New Journal of Chemistry*, *41*(17), 9346–9353. (DOI: 10.1039/C7NJ01531C).

[195] Xiong, J., Wang, K., Yao, Z., Zou, B., Xu, J., & Bu, X. H. (2018). Multi-Stimuli-Responsive Fluorescence Switching from a Pyridine-Functionalized Tetraphenylethene AIEgen. *ACS Applied Materials and Interfaces*, *10*(6), 5819–5827. (DOI: 10.1021/ACSAMI.7B18718).

[196] Khan, F., Mahmoudi, M., Gupta, P. K., Volyniuk, D., Grazulevicius, J. V., & Misra, R. (2023). Mechanochromic Materials Based on Tetraphenylethylene-Substituted Phenothiazines: Substituent-Dependent Hypsochromic and Bathochromic Switching of Emission. *The Journal of Physical Chemistry C*, *127*(3), 1643–1654. (DOI: 10.1021/acs.jpcc.2c07010).

[197] Lin, Y., Yi, M., Guan, X., Chen, E., Yang, L., Li, S., … Zhang, L. (2023). “Two birds with one stone” strategy for the lung cancer therapy with bioinspired AIE aggregates. *Journal of Nanobiotechnology*, *21*(1), 49. (DOI: 10.1186/s12951-023-01799-1).

[198] Liu, S., Li, Y., Kwok, R. T. K., Lam, J. W. Y., & Tang, B. Z. (2021). Structural and process controls of AIEgens for NIR-II theranostics. *Chemical Science*, *12*(10), 3427–3436. (DOI: 10.1039/D0SC02911D).

[199] Wu, M., Chen, L., Chen, Q., Hu, R., Xu, X., Wang, Y., … Gu, M. (2023). Engineered Phage with Aggregation-Induced Emission Photosensitizer in Cocktail Therapy against Sepsis. *Advanced Materials*, *35*(6), 2208578. (DOI: 10.1002/adma.202208578).

[200] Jiang, W., Cheng, C., Qiu, X., Chen, L., Guo, X., Luo, Y., … Ren, J. (2023). Peptide Supramolecular Assembly-Instructed In Situ Self-Aggregation for Stratified Targeting Sonodynamic

Therapy Enhancement of AIE Luminogens. *Advanced Science*, *10*(4), 2204989. (DOI: 10.1002/advs.202204989).

[201] Zhou, L., Chen, L., Chen, S., Pu, Z., Gu, M., & Shen, Y. (2023). Highly Efficient Photodynamic Therapy with Mitochondria-Targeting Aggregation-Induced Emission Photosensitizer for Retinoblastoma. *Advanced Healthcare Materials*, *12*(3), 2202219. (DOI: 10.1002/adhm.202202219).

[202] Wang, X., Xue, K., Wang, X., Zhao, Y., Deng, J., Yang, L., … Qi, Z. (2023). An aggregation-induced emission photosensitizer with efficient singlet oxygen generation capacity for mitochondria targeted photodynamic therapy. *Dyes and Pigments*, *213*, 111181. (DOI: 10.1016/j.dyepig.2023.111181).

[203] Arribat, M., Rémond, E., Richeter, S., Gerbier, P., Clément, S., & Cavelier, F. (2019). Silole Amino Acids with Aggregation-Induced Emission Features Synthesized by Hydrosilylation. *European Journal of Organic Chemistry*, *2019*(12), 2275–2281. (DOI: 10.1002/ejoc.201801869).

[204] Huang, X., Zhang, S., Liu, Z., Cao, W., Li, G., Gao, W., & Tang, B. (2023). Novel AIE Probe for In Situ Imaging of Protein Sulfonation to Assess Cigarette Smoke-Induced Inflammatory Damage. *Analytical Chemistry*, *95*(3), 1967–1974. (DOI: 10.1021/acs.analchem.2c04267).

[205] Yang, J., Wang, Z., Ge, J., Deng, Y., Ding, F., Hu, L., & Wang, H. (2023). A deep-red emission AIE fluorescent probes based on coumarin for imaging lipid droplets in living cells. *Journal of Molecular Structure*, *1277*, 134847. (DOI: 10.1016/j.molstruc.2022.134847).

[206] Roger, M., Bretonnière, Y., Trolez, Y., Vacher, A., Arbouch, I., Cornil, J., … Gerbier, P. (2023). Synthesis and Characterization of Tetraphenylethene AIEgen-Based Push–Pull Chromophores for Photothermal Applications: Could the Cycloaddition–Retroelectrocyclization Click Reaction Make Any Molecule Photothermally Active? *International Journal of Molecular Sciences*, *24*(10), 8715. (DOI: 10.3390/ijms24108715).

[207] Wang, L., Yan, J., Fu, P. P., Parekh, K. A., & Yu, H. (2003). Photomutagenicity of cosmetic ingredient chemicals azulene and guaiazulene. *Mutation Research - Fundamental and Molecular Mechanisms of Mutagenesis*, *530*(1–2), 19–26. (DOI: 10.1016/S0027-5107(03)00131-3)

[208] Ito, S., Morita, N., & Kubo, T. (1985). Azulene. *Houben-Weyl, Methoden der Organischen Chemie*, *0*(2), 127–418. (DOI: 10.5059/YUKIGOSEIKYOKAISHI.62.766).

[209] Liu, R. S. H. (2002). Colorful Azulene and Its Equally Colorful Derivatives. *Journal of Chemical Education*, *79*(2), 183. (DOI: 10.1021/ed079p183).

[210] Shoji, T., Ito, S., Toyota, K., Iwamoto, T., Yasunami, M., & Morita, N. (2009). Reactions between 1-Ethynylazulenes and 7,7,8,8-Tetracyanoquinodimethane (TCNQ): Preparation, Properties, and Redox Behavior of Novel Azulene-Substituted Redox-Active Chromophores. *European Journal of Organic Chemistry*, *2009*(25), 4316–4324. (DOI: 10.1002/ejoc.200900539).

[211] Narasimhan, B., Sharma, D., & Kumar, P. (2011). Biological importance of imidazole nucleus in the new millennium. *Medicinal Chemistry Research*, *20*(8), 1119–1140. (DOI: 10.1007/s00044-010-9472-5).

[212] K, S. P. (n.d.). A Review on "Imidazoles": Their Chemistry and Pharmacological Potentials. *International Journal of PharmTech Research CODEN*, *3*(1), 268–282.

[213] Rha, C. J., Lee, H., & Kim, C. (2020). An effective phthalazine-imidazole-based chemosensor for detecting Cu^{2+}, Co^{2+} and S^{2-} *via* the color change. *Inorganica Chimica Acta*, *511*, 119788. (DOI: 10.1016/j.ica.2020.119788).

[214] Zheng, X., Ma, Z., & Zhang, D. (2020). Synthesis of Imidazole-Based Medicinal Molecules Utilizing the van Leusen Imidazole Synthesis. *Pharmaceuticals*, *13*(3), 37. (DOI: 10.3390/ph13030037).

[215] Gaba, M., & Mohan, C. (2016). Development of drugs based on imidazole and benzimidazole bioactive heterocycles: recent advances and future directions. *Medicinal Chemistry Research*, *25*(2), 173–210. (DOI: 10.1007/s00044-015-1495-5).

[216] Guragain, M., Pinjari, D., Misra, R., & D'Souza, F. (2023). Zinc Tetrapyrrole Coordinated to Imidazole Functionalized Tetracyanobutadiene or Cyclohexa-2,5-diene-1,4-diylidene-expanded-tetracyanobutadiene Conjugates: Dark vs. Light-Induced Electron Transfer. *Chemistry – A European Journal*, *29*(68). (DOI: 10.1002/chem.202302665).

[217] Poddar, M., Sivakumar, G., & Misra, R. (2019). Donor–acceptor substituted 1,8-naphthalimides: design, synthesis, and structure–property relationship. *Journal of Materials Chemistry C*, *7*(47), 14798–14815. (DOI: 10.1039/C9TC02634G).

[218] Zhang, J., Zhang, X., Li, G., Xiao, H., Li, W., Xie, S., … Bo, Z. (2015). A nonfullerene acceptor for wide band gap polymer based organic solar cells. *Chemical Communications*, *52*(3), 469–472. (DOI: 10.1039/C5CC08023A).

[219] Kotowicz, S., Korzec, M., Pająk, A. K., Golba, S., Małecki, J. G., Siwy, M., … Schab-Balcerzak, E. (2021). New Acceptor–Donor–Acceptor Systems Based on Bis-(Imino-1,8-Naphthalimide). *Materials*, *14*(11), 2714. (DOI: 10.3390/ma14112714).

[220] Langdon-Jones, E. E., Williams, C. F., Hayes, A. J., Lloyd, D., Coles, S. J., Horton, P. N., … Pope, S. J. A. (2017). Luminescent 1,8-Naphthalimide-Derived ReI Complexes: Syntheses, Spectroscopy, X-ray Structure and Preliminary Bioimaging in Fission Yeast Cells. *European Journal of Inorganic Chemistry*, *2017*(44), 5279–5287. (DOI: 10.1002/EJIC.201700549).

[221] Georgiev, N. I., Krasteva, P. V., Bakov, V. V., & Bojinov, V. B. (2022). A Highly Water-Soluble and Solid State Emissive 1,8-Naphthalimide as a Fluorescent PET Probe for Determination of pHs, Acid/Base Vapors, and Water Content in Organic Solvents. *Molecules*, *27*(13). (DOI: 10.3390/MOLECULES27134229).

[222] Wu, H.-L., Dong, J.-P., Sun, F.-G., Li, R. X., & Jiang, Y.-X. (2022). New Selective Fluorescent “Turn-On” Sensor for Detection of Hg^{2+} Based on a 1,8-Naphthalimide Schiff Base Derivative. *Journal of Applied Spectroscopy*, *89*(3), 487–494. (DOI: 10.1007/S10812-022-01384-8).

[223] Yang, S., Meng, F., Tian, H., & Chen, K. (2002). Photostability of novel copolymers functionalized with laser dyes based on modified rhodamine 6G and 1,8-naphthalimide. *European Polymer Journal*, *38*(5), 911–919. (DOI: 10.1016/S0014-3057(01)00265-8).

[224] Xia, T., Wang, L., Qu, Y., Rui, Y., Cao, J., Hu, Y., … Xu, J. (2016). A thermoresponsive fluorescent rotor based on a hinged naphthalimide for a viscometer and a viscosity-related thermometer. *Journal of Materials Chemistry C*, *4*(24), 5696–5701. (DOI: 10.1039/C6TC01241H).

[225] Gautam, P., Sharma, R., Misra, R., Keshtov, M. L., Kuklin, S. A., & Sharma, G. D. (2017). Donor–acceptor–acceptor (D–A–A) type 1,8-naphthalimides as non-fullerene small molecule acceptors for bulk heterojunction solar cells. *Chemical Science*, *8*(3), 2017–2024. (DOI: 10.1039/C6SC04461A).

[226] Dhokale, B., Gautam, P., Mobin, S. M., & Misra, R. (2013). Donor–acceptor, ferrocenyl substituted BODIPYs with marvelous supramolecular interactions. *Dalton Transactions*, *42*, 1512–1518. (DOI: 10.1039/c2dt31632c).

[227] Green, M. L. H., Marder, S. R., Thompson, M. E., Bandy, J. A., Bloor, D., Kolinsky, P. V., & Jones, R. J. (1987). Synthesis and structure of (cis)-[1-ferrocenyl-2-(4-nitrophenyl)ethylene], an organotransition metal compound with a large second-order optical nonlinearity. *Nature*, *330*(6146), 360–362. (DOI: 10.1038/330360a0).

[228] Jawaria, R., Khan, M. U., Hussain, M., Muhammad, S., Sagir, M., Hussain, A., & Al-Sehemi, A. G. (2022). Synthesis and characterization of ferrocene-based thiosemicarbazones along with their computational studies for potential as inhibitors for

SARS-CoV-2. *Journal of the Iranian Chemical Society*, *19*(3), 839–846. (DOI: 10.1007/S13738-021-02346-1).

[229] Gong, G., Cao, Y., Qian, H., Zhou, Y., Zhao, H., Li, L., … Zhao, G. (2018). Assessment of the antitumor activity of a cyclopalladated ferrocene compound assisted by a dual-targeting drug delivery system. *Chemical Communications*, *54*(60), 8312–8315. (DOI: 10.1039/C8CC03308K).

[230] Popli, C., Misra, R., & Butenschön, H. (2024). NIR-absorbing TCBD and cyclohexa-2,5-diene-1,4-diylidene-expanded TCBD bridged derivatives of 1,1′-bis(N,N-dimethylaniline)-substituted ferrocene. *Journal of Organometallic Chemistry*, *1006*, 122998. (DOI: 10.1016/j.jorganchem.2023.122998).

[231] Solak, E. K., & Irmak, E. (2023). Advances in organic photovoltaic cells: a comprehensive review of materials, technologies, and performance. *RSC Advances*, *13*(18), 12244–12269. (DOI: 10.1039/D3RA01454A).

[232] Hösel, M., Angmo, D., & Krebs, F. C. (2013). Organic solar cells (OSCs). In *Handbook of Organic Materials for Optical and (Opto)electronic Devices* (pp. 473–507). Elsevier. (DOI: 10.1533/9780857098764.3.473).

[233] Li, S., Li, Z., Wan, X., & Chen, Y. (2023). Recent progress in flexible organic solar cells. *eScience*, *3*(1), 100085. (DOI: 10.1016/j.esci.2022.10.010).

[234] Ye, L., Xiong, Y., Zhang, M., Guo, X., Guan, H., Zou, Y., & Ade, H. (2020). Enhanced efficiency in nonfullerene organic solar cells by tuning molecular order and domain characteristics. *Nano Energy*, *77*, 105310. (DOI: 10.1016/j.nanoen.2020.105310).

[235] Søndergaard, R., Hösel, M., Angmo, D., Larsen-Olsen, T. T., & Krebs, F. C. (2012). Roll-to-roll fabrication of polymer solar cells. *Materials Today*, *15*(1–2), 36–49. (DOI: 10.1016/S1369-7021(12)70019-6).

[236] Ye, L., Hu, H., Ghasemi, M., Wang, T., Collins, B. A., Kim, J.-H., … Ade, H. (2018). Quantitative relations between interaction

parameter, miscibility and function in organic solar cells. *Nature Materials*, *17*(3), 253–260. (DOI: 10.1038/s41563-017-0005-1).

[237] Hou, J., Inganäs, O., Friend, R. H., & Gao, F. (2018). Organic solar cells based on non-fullerene acceptors. *Nature Materials*, *17*(2), 119–128. (DOI: 10.1038/nmat5063).

[238] Jin, H., Stoltzfus, D. M., Saghaei, J., Burn, P. L., & Shaw, P. E. (2020). A three-dimensional multi-chromophore naphthalene diimide acceptor for polymer bulk heterojunction solar cells. *Synthetic Metals*, *268*, 116505. (DOI: 10.1016/j.synthmet.2020.116505).

[239] Lin, Y., Li, Y., & Zhan, X. (2012). Small molecule semiconductors for high-efficiency organic photovoltaics. *Chemical Society Reviews*, *41*(11), 4245. (DOI: 10.1039/c2cs15313k).

[240] Patil, Y., & Misra, R. (2018). Diketopyrrolopyrrole-Based and Tetracyano-Bridged Small Molecules for Bulk Heterojunction Organic Solar Cells. *Chemistry – An Asian Journal*, *13*(3), 220–229. (DOI: 10.1002/asia.201701493).

[241] Espinosa, N., Hösel, M., Angmo, D., & Krebs, F. C. (2012). Solar cells with one-day energy payback for the factories of the future. *Energy Environ. Sci.*, *5*(1), 5117–5132. (DOI: 10.1039/C1EE02728J).

[242] Keshtov, M. L., Kholhlov, A. R., Kuklin, S. A., Ostapov, I. E., Nikolaey, A. Yu., Konstantinov, I. O., Sharma, A., Koukaras, E. N., & Sharma, G. D. (2016). Synthesis and photophysical properties of regioregular low bandgap copolymers with controlled 5-fluorobenzotriazole orientation for photovoltaic application. *Polymer Chemistry*, *7*, 5849-5861. (DOI: 10.1039/C6PY01173J).

[243] Pakravesh, F., Izadyar, M., & Arkan, F. (2021). Effect of electron donor and acceptor on the photovoltaic properties of organic dyes for efficient dye-sensitized solar cells. *Physica B: Condensed Matter*, *609*, 412815. (DOI: 10.1016/j.physb.2021.412815).

[244] Qin, C., Wong, W., & Han, L. (2013). Squaraine Dyes for Dye-Sensitized Solar Cells: Recent Advances and Future Challenges. *Chemistry – An Asian Journal*, *8*(8), 1706–1719. (DOI: 10.1002/asia.201300185).

[245] Michinobu, T., Satoh, N., Cai, J., Li, Y., & Han, L. (2014). Novel design of organic donor–acceptor dyes without carboxylic acid anchoring groups for dye-sensitized solar cells. *Journal of Materials Chemistry C*, *2*(17), 3367. (DOI: 10.1039/c3tc32165g).

[246] Reynal, A., Forneli, A., Martinez-Ferrero, E., Sánchez-Díaz, A., Vidal-Ferran, A., O'Regan, B. C., & Palomares, E. (2008). Interfacial Charge Recombination Between e^{-}−TiO_2 and the I^{-}/I_3^{-} Electrolyte in Ruthenium Heteroleptic Complexes: Dye Molecular Structure−Open Circuit Voltage Relationship. *Journal of the American Chemical Society*, *130*(41), 13558–13567. (DOI: 10.1021/ja800513m).

[247] Miyashita, M., Sunahara, K., Nishikawa, T., Uemura, Y., Koumura, N., Hara, K., … Mori, S. (2008). Interfacial Electron-Transfer Kinetics in Metal-Free Organic Dye-Sensitized Solar Cells: Combined Effects of Molecular Structure of Dyes and Electrolytes. *Journal of the American Chemical Society*, *130*(52), 17874–17881. (DOI: 10.1021/ja803534u).

[248] Borg, R. E., & Rochford, J. (2018). Molecular Photoacoustic Contrast Agents: Design Principles & Applications. *Photochemistry and Photobiology*, *94*(6), 1175–1209. (DOI: 10.1111/php.12967).

[249] Zhu, W., Miao, Z., Chu, Y., Li, L., Wang, L., & Wang, D. (2022). Photoacoustic Effect of Near-Infrared Absorbing Organic Molecules *via* Click Chemistry. *Molecules*, *27*(7), 2329. (DOI: 10.3390/molecules27072329).

[250] Kim, C., Favazza, C., & Wang, L. V. (2010). In Vivo Photoacoustic Tomography of Chemicals: High-Resolution Functional and Molecular Optical Imaging at New Depths.

Chemical Reviews, *110*(5), 2756–2782. (DOI: 10.1021/cr900266s).

[251] Ntziachristos, V., & Razansky, D. (2010). Molecular Imaging by Means of Multispectral Optoacoustic Tomography (MSOT). *Chemical Reviews*, *110*(5), 2783–2794. (DOI: 10.1021/cr9002566).

[252] Rout, Y., Michel Merkes, J., Banala, S., & Misra, R. (2022). Dicyanoquinodimethane (DCNQ) linked benzothiadiazole and phenothiazine derivatives for photoacoustic imaging. *Journal of Photochemistry and Photobiology A: Chemistry*, *429*, 113935. (DOI: 10.1016/j.jphotochem.2022.113935).

[253] Gelderblom, H., Verweij, J., Nooter, K., & Sparreboom, A. (2001). Cremophor EL. *European Journal of Cancer*, *37*(13), 1590–1598. (DOI: 10.1016/S0959-8049(01)00171-X).

[254] Zhao, Z., Wang, D., Gao, H., Yang, Z., Cao, H., & He, W. (2019). Photoacoustic effect of near-infrared absorbing fullerene derivatives with click moieties. *Dyes and Pigments*, *164*, 182–187. (DOI: 10.1016/j.dyepig.2019.01.022).

[255] Ahn, H.-Y., Yao, S., Wang, X., & Belfield, K. D. (2012). Near-Infrared-Emitting Squaraine Dyes with High 2PA Cross-Sections for Multiphoton Fluorescence Imaging. *ACS Applied Materials & Interfaces*, *4*(6), 2847–2854. (DOI: 10.1021/am300467w).

Chapter 2

Materials and Experimental Techniques

2.1. Introduction

This chapter addresses about the instrumentation, materials, computational calculations, and spectroscopic techniques utilized in the characterization of synthesized molecules.

2.2. Chemicals for synthesis

The common solvents used for syntheses were purified according to well-known procedures.[1] 10*H*-phenothiazine, 9*H*-carbazole, n-propyl iodide, sodium hydroxide, potassium hydroxide, anhydrous sodium sulphate, glacial acetic acid, bromine, hydrogen peroxide, bis(pinacolato)diboron, potassium acetate, ferrocene, *N*-Bromosuccinimide, hydrochloric acid, triphenylamine, carbon tetrabromide, and triphenylphosphine were obtained from S. D. Fine chem. Ltd. and Spectrochem India. Copper iodide (CuI), cesium carbonate, Bis(triphenylphosphine)palladium(II) dichloride ($PdCl_2(PPh_3)_2$), [1,1′-Bis(diphenylphosphino)ferrocene]dichloropalladium(II) (Pd(dppf)Cl), tetrakis(triphenylphosphine)palladium(0) ($Pd(PPh_3)_4$), tetrabutylammonium hexafluorophosphate ($TBAPF_6$), 4-ethynyl-*N*,*N*-dimethylaniline and *N*-methylglycine (sarcosine) were purchased from Aldrich chemicals USA and Spectrochem India. 1,2-Dimethylethylenediamine (DMEDA), N,4-dimethylbenzenesulfonamide, 1,1,2,2-tetracyanoethylene (TCNE) and 7,7,8,8-tetracyanoquinodimethane (TCNQ) was obtained from TCI chemicals. Fullerene (C_{60}) was obtained from Aldrich chemicals USA and SES research USA.

Dry solvents dichloromethane (DCM), 1,2-dichloroethane (DCE), chloroform ($CHCl_3$), *N*,*N*-dimethylformamide (DMF), triethylamine (TEA), tetrahydrofuran (THF), acetone, toluene, 1,4-dioxane, acetonitrile, isopropanol, ethanol, and methanol were obtained

from S. D. Fine chem. Ltd, Advent Chembio Pvt. Ltd. and Spectrochem India. All moisture sensitive reactions were performed under nitrogen/argon atmosphere using standard schlenk method. The *N*-Bromosuccinimide was recrystallized from hot water before use. The solvents and reagents were used as received unless otherwise indicated. Photophysical and electrochemical studies were performed using spectroscopic grade solvents. Silica gel (100–200 mesh and 230–400 mesh) were purchased from Rankem chemicals, India. TLC pre-coated silica gel plates (Kieselgel 60F254, Merck) were obtained from Merck, India.

2.3. Spectroscopic Measurements

2.3.1. NMR Spectroscopy

^{1}H NMR (400 MHz and 500 MHz), and ^{13}C NMR (100 MHz and 125 MHz) spectra were recorded on the Bruker Avance (III) 400 MHz and Model AVNACE NEO500 Ascend Bruker 500 MHz FT-NMR spectrometer, using $CDCl_3$ as solvent. Chemical shifts in ^{1}H, and ^{13}C NMR spectra were reported in parts per million (ppm). In ^{1}H NMR chemical shifts are reported relative to the residual solvent peak ($CDCl_3$, 7.26 ppm). Multiplicities are given as: s (singlet), d (doublet), t (triplet), q (quartet), m (multiplet). ^{13}C NMR chemical shifts are reported relative to the solvent residual peak ($CDCl_3$, 77.02 ppm).

2.3.2. Mass Spectrometry

High resolution mass spectra (HRMS) were recorded on Brucker-Daltonics, micrOTOF-Q II mass spectrometer using positive and negative mode electrospray ionizations.

2.3.3. UV-Vis Spectroscopy

UV-Vis absorption spectra were recorded using a Varian Cary100 Bio UV-Vis and PerkinElmer LAMBDA 35 UV/Vis spectrophotometer.

2.4. Electrochemical Studies

The cyclic voltammograms (CVs) and differential pulse voltammograms (DPVs) were recorded on PalmSens 4 electrochemical analyzer using Glassy carbon as working electrode and Pt wire as the counter electrode, Ag/AgCl electrode as the reference electrode. The scan rate was 100 mVs^{-1}. A solution of 0.1 M tetrabutylammonium hexafluorophosphate (Bu_4NPF_6) in dichloromethane (CH_2Cl_2) was used as the supporting electrolyte. The CV and DPV plotting convention is the IUPAC convention. The polishing material is a commercially available polishing pad and alumina(Al_2O_3).

2.5. Thermal Analysis

Thermogravimetric analysis was performed on the Mettler Toledo thermal analysis system at a heating rate of 10 ℃ min^{-1} under the nitrogen atmosphere.

2.6. Computational Calculations

The density functional theory (DFT) calculation was performed at the B3LYP/6-31G (d,p) level for C, H, N, O, and S in the Gaussian 09W program.[2]

2.7. References

[1] (a) Vogel A. I., Tatchell A. R., Furnis B. S., Hannaford A. J., Smith, P. W. G. (1996). Vogel's Textbook of Practical Organic Chemistry (5th Edition) (5th ed.). (b) Wei Ssberger A. Proskraner E. S. Riddick J. A., Toppos Jr. E. F. (1970). Organic Solvents in Techniques of Organic Chemistry, Vol. IV, 3rd Edition, Inc. New York.

[2] (a) Frisch, M. J.; Trucks, G. W.; Schlegel, H. B.; Scuseria, G. E.; Robb, M. A.; Cheeseman, J. R.; Scalmani, G.; Barone, V.; Mennucci, B.; Petersson, G. A.; Nakatsuji, H.; Caricato, M.; Li, X.; Hratchian, H. P.; Izmaylov, A. F.; Bloino, J.; Zheng, G.; Sonnenberg, J. L.; Hada, M.; Ehara, M.; Toyota, K.; Fukuda, R.; Hasegawa, J.; Ishida, M.; Nakajima, T.; Honda, Y.; Kitao, O.;

Nakai, H.; Vreven, T.; Montgomery, J. A. Jr.; Peralta, J. E.; Ogliaro, F.; Bearpark, M.; Heyd, J. J.; Brothers, E.; Kudin, K. N.; Staroverov, V. N.; Kobayashi, R.; Normand, J.; Raghavachari, K.; Rendell, A.; Burant, J. C.; Iyengar, S. S.; Tomasi, J.; Cossi, M.; Rega, N.; Millam, N. J.; Klene, M.; Knox, J. E.; Cross, J. B.; Bakken, V.; Adamo, C.; Jaramillo, J.; Gomperts, R.; Stratmann, R. E.; Yazyev, O.; Austin, A. J.; Cammi, R.; Pomelli, C.; Ochterski, J. W.; Martin, R. L.; Morokuma, K.; Zakrzewski, V. G.; Voth, G. A.; Salvador, P.; Dannenberg, J. J.; Dapprich, S.; Daniels, A. D.; Farkas, O.; Foresman, J. B.; Ortiz, J. V.; Cioslowski, J.; Fox, D. J. (2009). Gaussian 09, revision A.02; *Gaussian, Inc*.: Wallingford, CT.; (b) Lee, C., Yang, W., & Parr, R. G. (1988). Development of the Colle-Salvetti correlation-energy formula into a functional of the electron density. *Physical Review B, 37*(2), 785–789. https://doi.org/10.1103/PhysRevB.37.785; (c) Becke, A. D. (1993). A new mixing of Hartree-Fock and local density-functional theories. *The Journal of Chemical Phys*ics, *98*(2), 1372–1377. https://doi.org/10.1063/1.464304.

Chapter 3

Synthesis and Characterization of NIR Absorbing TCBD and DCNQ Incorporated Donor-Acceptor Phenothiazines

3.1. Introduction

The π-conjugated small molecules which contain *S* and *N*-atom based heterocyclic units such as thiazoles, benzothiazoles, benzothiadiazole, carbazole, thiophene, and phenothiazines are of wide interest due to their potential applications in the field of organic light emitting diodes (OLEDs), non-linear optics (NLO), organic photovoltaics (OPVs) and organic field-effect transistors (OFETs).[1–4] Phenothiazine is a heterocyclic compound which has a non-planar geometry and exhibits excellent photo and thermal stability.[5–7] The 10*H*-phenothiazine is a colorless crystalline solid with an absorption maxima at 316 nm in dichloromethane. Phenothiazine can be easily functionalized by electrophilic substitution reactions at the -3 and -7 positions and nucleophilic substitution reactions at the *N*-position.[8–10] The high electron density and good electron donor ability of phenothiazine make it a suitable candidate to be used in various applications such as chemical sensors, photovoltaic devices, and light-emitting diodes (LEDs).[11, 12] Thiophene is one of the most widely used heterocyclic compound and is widely explored as a donor material in organic solar cells (OSC).[13] The high polarizability of the sulphur atoms in the thiophene ring contributes significantly to the electron-donating and charge-transport behaviour of the thiophene derivatives.[14, 15] Thiophene derivatives are widely used in organic solar cells, organic light-emitting diodes (OLEDs), and organic field-effect transistors (OFETs).[16] Carbazole is an essential component frequently used as an electron-donating (D) group in π-conjugated molecules. It is used for excellent hole-transporting capabilities, luminescence efficiency, optical properties, thermal and chemical stability, and easy structural modification.[17] Several carbazole-containing oligomers have been used as essential functional components in different systems, such as organic field-effect

transistors, organic light-emitting diodes (OLEDs), and organic photovoltaics.[18]

The cyano-based electron acceptors 1,1,2,2-tetracyanoethylene (TCNE) and 7,7,8,8-tetracyanoquinodimethane (TCNQ) are well-known strong electron acceptors[19] and are highly reactive towards electron-rich alkynes and undergo [2 + 2] cycloaddition reaction to form cyclobutene rings followed by retroelectrocyclization reaction (CA-RE reaction)[20] to give 1,1,4,4-tetracyanobutadiene (TCBD) and cyclohexa-2,5-diene-1,4-diylidene-expanded TCBD or DCNQ (dicyanoquinodimethane) derivatives.[21] The donor-acceptor systems containing TCBD and DCNQ acceptors are potential candidates for organic photovoltaics.[22] Tuning the photonic properties for donor-acceptor systems can be achieved by changing the strength of donor or acceptor units and the connecting π-linker.[23–25] The cross-conjugated systems with strong electron-acceptor TCBD and DCNQ groups have recently been used in organic electronic devices due to their strong and wide electronic absorption in the visible to near-IR regions and their ability to tune the lowest unoccupied molecular orbital (LUMO) energy levels.[26]

Diederich *et al.* used [2 + 2] cycloaddition–retroelectrocyclization reaction to produce charge-transfer chromophores by reacting TCNE and TCNQ acceptors with a variety of acetylenic donors.[27] Michinobu *et al.* have extensively explored the TCBD and DCNQ substituted derivatives which are considered as promising materials for photovoltaic applications.[28] Shoji, Kato, Paul and Trolez *et al.* have reported the donor–acceptor based TCNE and TCNQ substituted derivatives as redox-active ICT chromophores for various optoelectronic applications.[29, 30] Nakamura *et al.* explored carbazole based TCBD derivatives for application in nonlinear optics (NLOs), organic photovoltaics (OPVs) and dye-sensitized solar cells (DSSCs).[31] A series of 1,1'-disubstituted ferrocenyl TCBD compounds have been reported by Holger and coworkers.[32] Our group has reported TCBD and expanded TCBD (DCNQ) incorporated phenothiazine derivatives with ferrocenyl and triphenylamine donors at

the terminal position.[33, 34] Herein, we have investigated the optoelectronic, thermal, and computational studies by introducing hydrogen, thiophene and carbazole at the terminal position (Scheme 3.1).

In this manuscript, we describe the design and synthesis of symmetrical and unsymmetrical TCBD and DCNQ functionalized phenothiazines with terminal donors (H, thiophene, and carbazole). The phenothiazine derivatives **1–18** were synthesized by the Pd-catalyzed Sonogashira cross-coupling reaction followed by [2 + 2] cycloaddition retroelectrocyclic ring-opening reaction (Scheme 3.2, 3.3 and 3.4). Herein, our objective was to investigate the photophysical and electrochemical properties of unsubstituted, thiophene and carbazole functionalized phenothiazine derivatives by incorporating strong electron acceptors TCNE and TCNQ moieties. The DCNQ derivatives exhibit more pronounced intramolecular charge transfer (ICT) transition and reduced HOMO-LUMO energy gaps compared to TCBD derivatives. This difference is due to the stronger electron-accepting character of the DCNQ compared to the TCBD moiety, as there is excessive electronic conjugation in the former molecular structure owing to the presence of a six-membered quinone ring.[4(a), 4(b), 33, 34, 35(a)]

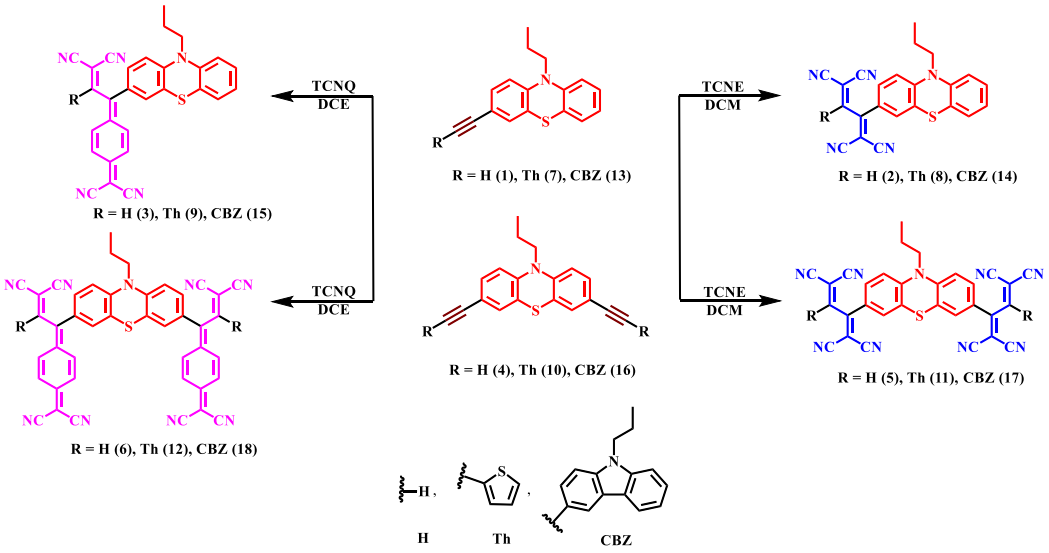

Scheme 3.1. General synthetic scheme for phenothiazine derivatives **1–18**.

3.2 Result and Discussion

The ethynyl phenothiazines **1** and **4** were synthesized according to the literature procedure.[1(a)] The [2 + 2] cycloaddition−retroelectro-cyclization reaction of ethynyl phenothiazine **1** and **4** with TCNE and TCNQ resulted in the formation of TCBD and DCNQ functionalized phenothiazine derivatives **2**, **3**, **5**, and **6** (Scheme 3.2). The reaction of **1** with 1.1 equivalents of TCNE in dichloromethane solvent at room temperature for 2 hours resulted in the formation of **2** in 70% yield, whereas the reaction of **4** with 2.1 equivalents of TCNE in dichloromethane solvent at room temperature for 8 hours resulted in the formation of **5** in 65% yield. The reaction of ethynyl phenothiazines **1** and **4** with 1.1 and 2.1 equivalents of TCNQ in dichloromethane at room temperature for 18 and 24 hours, respectively resulted in the formation of **3** and **6** in 80% and 70% yield, respectively.

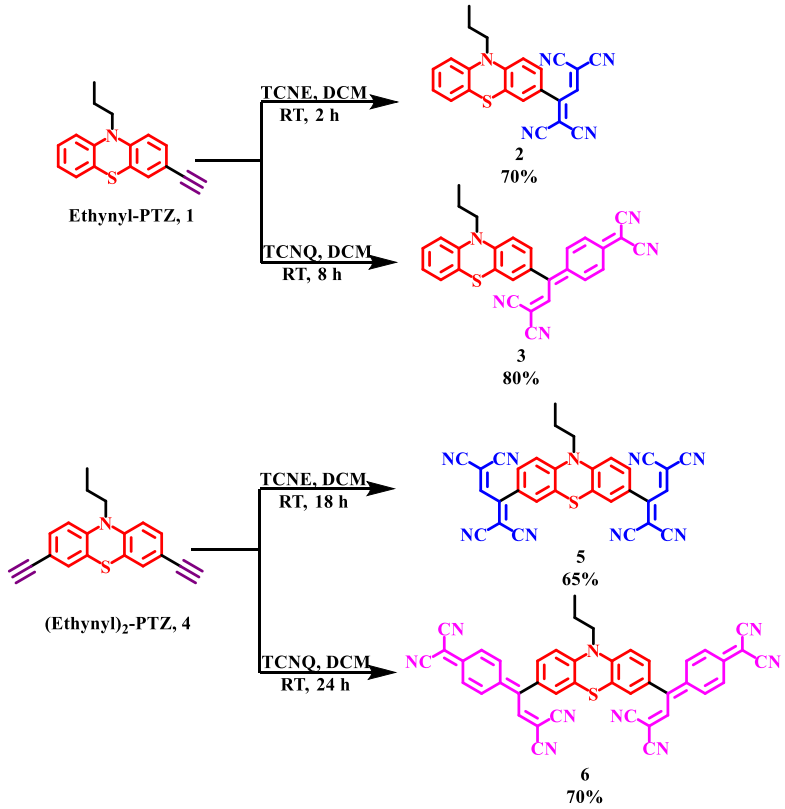

Scheme 3.2. Synthetic route of phenothiazine derivatives **2**, **3**, **5** and **6**.

The synthesis of phenothiazine derivatives **7–12** are shown in Scheme 3.3. The phenothiazine derivatives **7** and **10** were synthesized by the Pd-catalyzed Sonogashira cross-coupling reaction of ethynyl-phenothiazine **1** and (ethynyl)$_2$-phenothiazine **4** with 2-bromothiophene **Br-Th** in the

presence of THF:TEA (1:1) under argon atmosphere, in 60% and 55% yield respectively.

The reaction of mono-thiophene substituted phenothiazine **7** with 1.1 equivalent of TCNE in dichloromethane at room temperature resulted in the formation of **8** in 80% yield, whereas the reaction of 1.1 equivalent of TCNQ with mono-thiophene substituted phenothiazine **7** at 60 °C resulted in the formation of **9** in 75% yield. The [2 + 2] cycloaddition−retroelectrocyclization reaction of di-thiophene substituted phenothiazine **10** with 2.5 equivalent of TCNE in dichloromethane at 40 °C resulted in the formation of **11** in 80% yield, whereas the reaction of 2.5 equivalent of TCNQ with di-thiophene substituted phenothiazine **10** at 80 °C resulted in the formation of **12** in 65% yield.

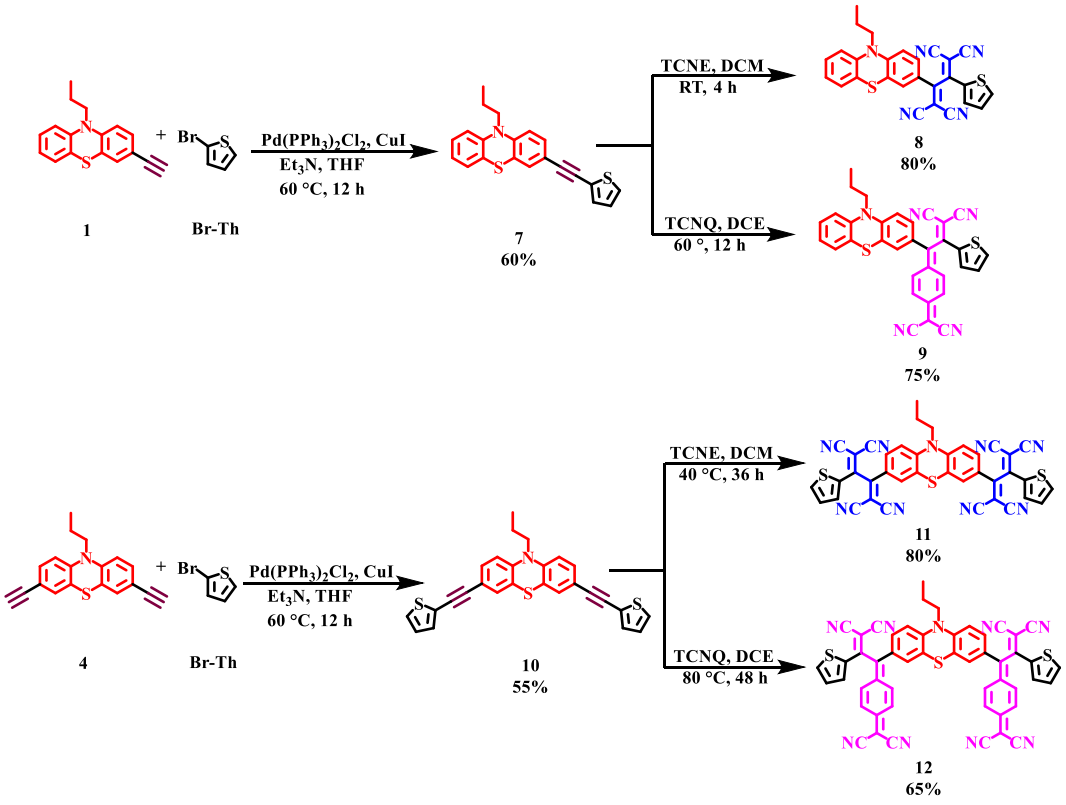

Scheme 3.3. Synthetic route of phenothiazine derivatives **7–12**.

The synthesis of phenothiazine derivatives **13–18** are shown in Scheme 3.4. The phenothiazine derivatives **13** and **16** were synthesized by the Pd-catalyzed Sonogashira cross-coupling reaction of ethynyl-phenothiazine **1** and (ethynyl)$_2$-phenothiazine **4** with 3-bromo-9-propyl-

9H-carbazole **Br-CBZ** in the presence of THF:TEA (1:1) under argon atmosphere, in 80% and 70% yield respectively.

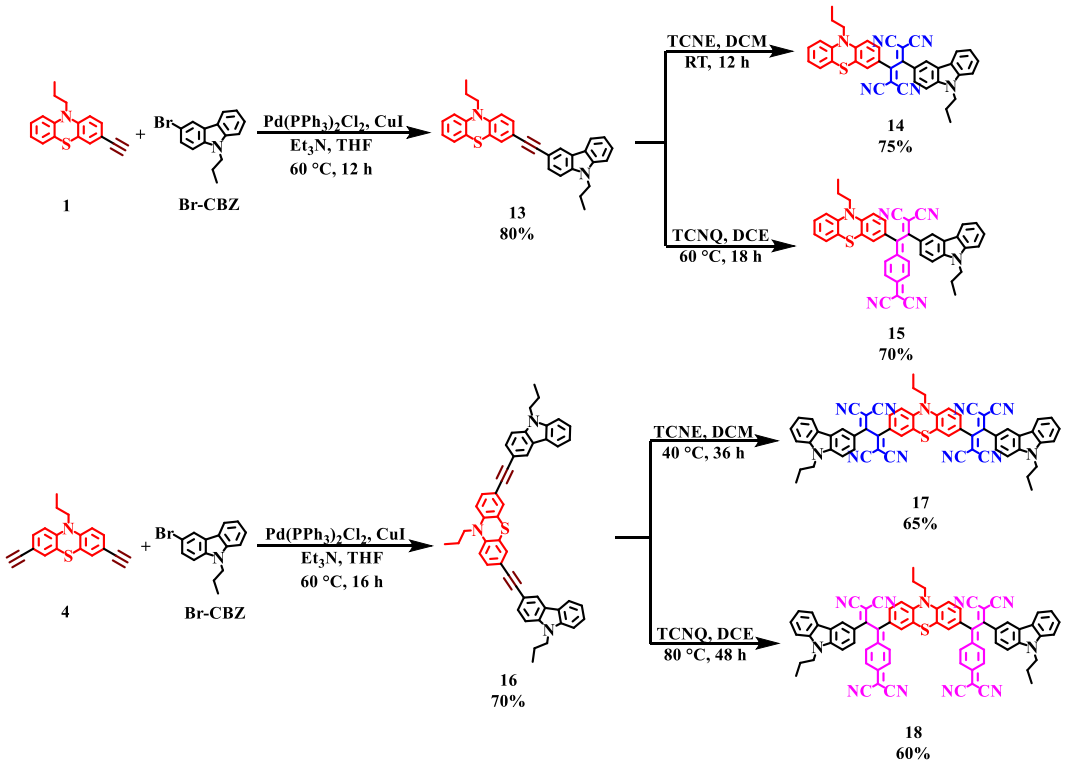

Scheme 3.4. Synthetic route of phenothiazine derivatives **13–18**.

The reaction of 1.1 equivalent of TCNE with mono-carbazole substituted phenothiazine **13** in dichloromethane at room temperature resulted in the formation of **14** in 75% yield, whereas the reaction of mono-carbazole phenothiazine **13** with 1.1 equivalent of TCNQ at 60 °C resulted in the formation of **15** in 70% yield. The [2 + 2] cycloaddition−retroelectrocyclization reaction of 2.5 equivalent of TCNE with di-carbazole phenothiazine **16** in dichloromethane at 40 °C resulted in the formation of **17** in 65% yield, whereas the reaction of di-carbazole phenothiazine **16** with 2.5 equivalent of TCNQ at 80 °C resulted in the formation of **18** in 60% yield.

The phenothiazines **1−18** were purified by column chromatography and were well-characterized by ^{1}H NMR, ^{13}C{H} NMR spectroscopy, and HRMS techniques.

3.3. Photophysical Properties

The photonic properties of the phenothiazine derivatives **1–18** were recorded in the dichloromethane solutions (1 × 10^{-5} M) at room

temperature depicted in Figures 3.1 and 3.2, and the corresponding data are summarized in Table 3.1.

The TCBD and DCNQ functionalized phenothiazine derivatives **2**, **3**, **5**, **6**, **8**, **9**, **11**, **12**, **14**, **15**, **17**, and **18** exhibit absorption bands in the high energy region (235–450 nm) corresponding to $\pi \rightarrow \pi^*$ transitions and in the low energy region (500–900 nm) corresponding to the intramolecular charge transfer (ICT) transition due to strong donor-acceptor interaction. The mono-substituted phenothiazine derivatives **1**, **7** and **13** exhibit π-π* transition at 324 nm, 357 nm and 356 nm respectively, whereas, the di-substituted phenothiazine derivatives **4**, **10** and **16** exhibit π-π* transition at 340 nm, 393 nm and 358 nm respectively (Figure 3.1). According to these observations, changing the terminal substituents from –H to donor thiophene and carbazole units resulted in red shifted absorption due to stronger communication between terminal thiophene and carbazole units of phenothiazine derivatives.

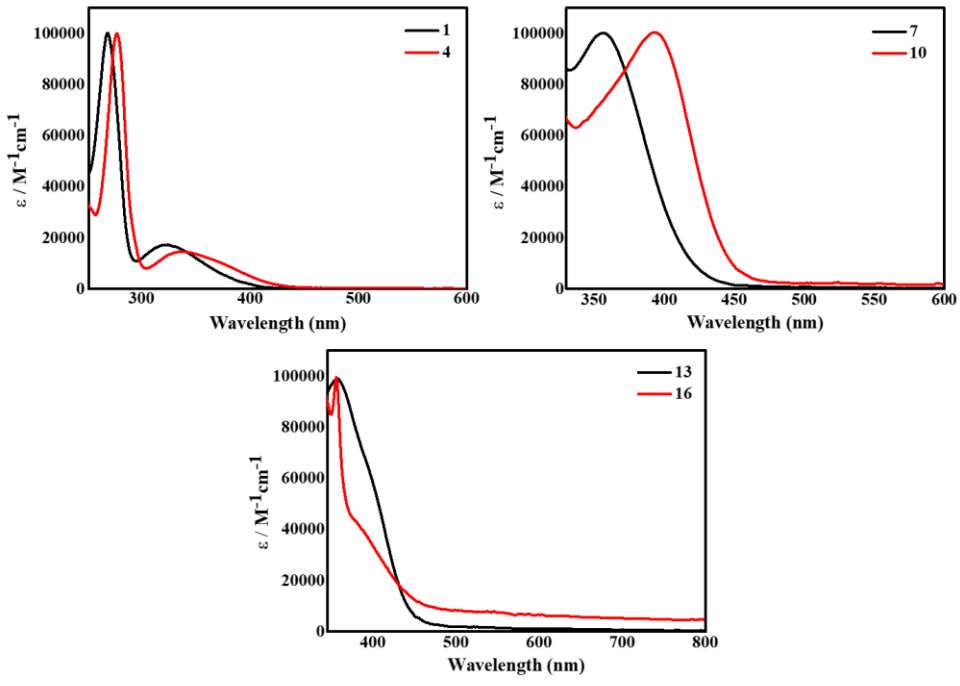

Figure 3.1. Normalized electronic absorption spectra of phenothiazine derivatives (a) **1**, **4**; (b) **7**, **10**; and (c) **13**, **16** recorded in dichloromethane (1×10^{-5} M) at room temperature.

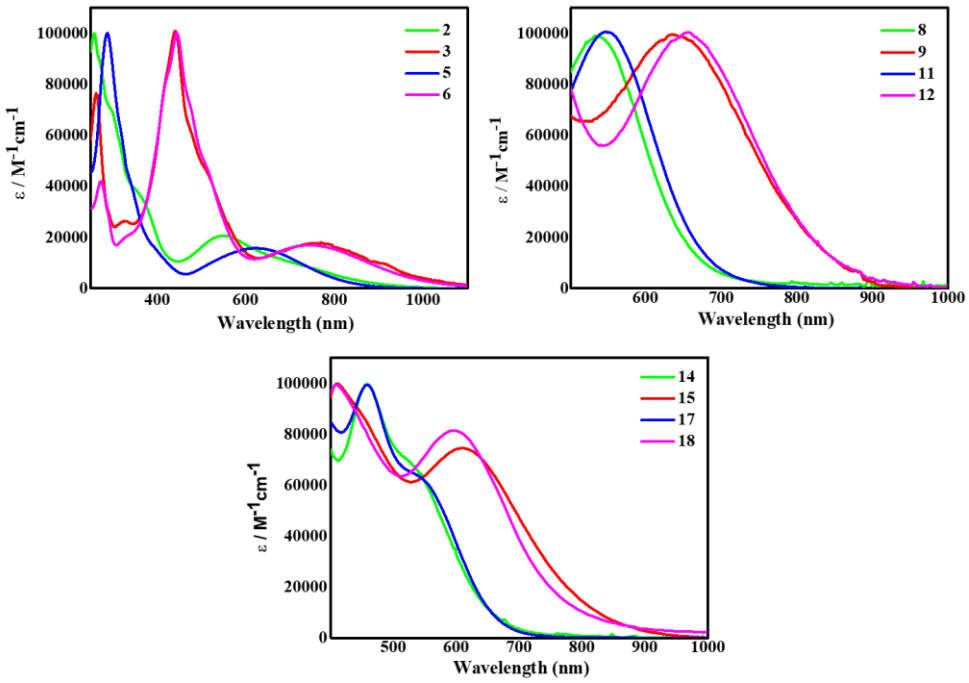

Figure 3.2. Normalized electronic absorption spectra of phenothiazine derivatives (a) **2**, **3**, **5**, **6**; (b) **8**, **9**, **11**, **12**; and (c) **14**, **15**, **17**, **18** recorded in dichloromethane (1×10^{-5} M) at room temperature.

The mono-TCBD substituted phenothiazine derivative **2** shows an absorption maxima at 545 nm, **8** shows an absorption maxima at 370 nm and 538 nm, and **14** shows an absorption maxima at 458 nm and 542 nm, the longer wavelength transitions in phenothiazine derivatives **2**, **8** and **14** are due to the intramolecular charge transfer (ICT) transition which is attributed to the strong donor and acceptor interactions. Similarly, the di-TCBD substituted derivative **5** shows an absorption maxima at 620 nm, **11** shows an absorption maxima at 367 nm and 548 nm, and **17** shows an absorption maxima at 459 nm and 552 nm. The di-TCBD functionalized derivatives **5**, **11** and **17** exhibit red shifted absorption with ~10–75 nm in comparison to mono-TCBD substituted phenothiazine derivatives **2**, **8** and **14** due to the incorporation of another TCBD moiety. On the other hand, the mono-DCNQ functionalized phenothiazine derivatives **3**, **9** and **15** exhibit two absorption bands at 439 nm, 760 nm; 402 nm, 640 nm; and 411 nm, 613 nm respectively, the higher energy transition bands are attributed to π-π* and lower energy transitions attributed to the intramolecular charge transfer (ICT) transition from the donor (thiophene, carbazole and phenothiazine) to

acceptor (TCNE/TCNQ) moieties. Similarly, the di-DCNQ functionalized derivatives **6**, **12** and **18** exhibit two absorption bands at 443 nm, 745 nm; 402 nm, 665 nm; and 409 nm, 597 nm respectively. The DCNQ derivatives **3**, **6**, **9**, **12**, **15** and **18** show bathochromically shifted absorption (~125–200 nm) as compared to the TCBD derivatives **2**, **5**, **8**, **11**, **14** and **17**, due to the strong electron-accepting nature of DCNQ moiety. The DCNQ functionalized unsubstituted phenothiazine derivatives **3** and **6** exhibit comparatively red-shifted absorption spectra than its donor substituted analogous of thiophene and carbazole.

The optical band gap for phenothiazine derivatives **1–18** were evaluated from the onset edge of the absorption band in dichloromethane, which was found to be 2.98, 1.39, 1.22, 2.84, 1.45, 1.20, 2.81, 1.70, 1.35, 2.59, 1.63, 1.49, 2.68, 1.78, 1.38, 2.64, 1.73, and 1.31 eV, respectively. The phenothiazine derivatives **2**, **3**, **5** and **6** exhibit low optical band gap after the incorporation of TCBD and DCNQ moiety as compared to the terminal substituents of phenothiazine derivatives of donor-substituted thiophene (**8**, **9**, **11** and **12**) and carbazole (**14**, **15**, **17** and **18**) units. It was observed that the optical band gap increases when the terminal substituents were varied from –H to donor-substituted (thiophene and carbazole) units. All transitions are explained by computational calculations, and their relevant data are included in Table 3.4.

Table 3.1. Photophysical data of phenothiazine derivatives **1–18**.

Phenothiazine derivatives	λ_{max} **(nm)**	**ε** **(M^{-1} cm^{-1})**	E_g^{opt} **(eV)**
1	324	66795	2.98
2	545	19625	1.39
3	439, 760	12920, 17735	1.22
4	340	19015	2.84
5	620	21875	1.45
6	443, 745	210850, 36145	1.20
7	357	44700	2.81
8	370, 538	19760, 9160	1.70

9	402, 640	15210, 4350	1.35
10	393	36160	2.59
11	367, 548	31520, 11300	1.63
12	402, 665	218400, 7060	1.49
13	356	37540	2.68
14	458, 542	11740, 7640	1.78
15	411, 613	31290, 23310	1.38
16	358	123750	2.64
17	459, 552	32160, 19810	1.73
18	409, 597	24270, 19890	1.31

Absorbance measured in dichloromethane at (1×10^{-5} M); λ_{max} = absorption wavelength; ε = extinction coefficient; E_g^{opt} = optical bandgap.

3.4. Electrochemical Properties

The redox potentials of the phenothiazines **1–18** were evaluated by cyclic voltammetry (CV) and differential pulse voltammetry (DPV) using 0.1 M tetrabutylammonium hexafluorophosphate ($TBAPF_6$) as a supporting electrolyte. The representative cyclic voltammograms and differential pulse voltammograms are shown in Figures 3.3–3.8 and the corresponding data are tabulated in Table 3.2.

Table 3.2. Electrochemical and thermal stability data of phenothiazine derivatives **1–18**.

Phenothiazine derivatives	E_{red} **(V)**[a]	E_{ox} **(V)**[a]	E_{HOMO} **(eV)**[a]	E_{LUMO} **(eV)**[a]	E_g **(eV)**[a]	**Thermal Stability**[b] T_d **(°C)**
1	–	0.86	–5.26	–	–	–
2	–0.05 –0.69	1.01	–5.41	–4.35	1.06	366
3	–0.07 –0.23	0.94	–5.33	–4.33	1.00	274
4	–	0.97	–5.36	–	–	–
5	–0.21	1.02	–5.42	–4.18	1.23	211

	–0.86					
6	–0.10 –0.36	0.85	–5.25	–4.30	0.95	312
7	–	0.71 1.34	–	–	–	264
8	–0.45 –0.75	0.91 1.65	–6.05	–3.95	2.10	241
9	–0.26 –0.85	0.24 1.01	–5.41	–4.14	1.27	228
10	–	0.77 1.45	–	–	–	266
11	–0.47 –0.75	0.91 1.46	–5.86	–3.93	1.93	303
12	–0.28 –0.45	0.11 0.76	–5.16	–4.12	1.04	236
13	–	0.66 1.13	–	–	–	277
14	–0.52– 0.89	0.82	–5.22	–3.88	1.34	247
15	–0.38 –0.95	0.83	–5.23	–4.02	1.21	318
16	–	0.58 1.23	–	–	–	–
17	–0.48 –0.84	1.11	–5.50	–3.92	1.58	210
18	–0.44 –0.86	1.38	–5.78	–3.96	1.82	199

[a]Electrochemical analysis was estimated by differential pulse voltammetry, in 0.1 M solution of $TBAPF_6$ in DCM at 100 mV s^{-1} scan rate *versus* saturated Ag/AgCl electrode at 25 °C. E_{ox} and E_{red} values are based on DPV analysis. [b]Decomposition temperatures for 5% weight loss at a heating rate of 10 °C min^{-1}, under a nitrogen atmosphere.

The phenothiazine derivatives **1**–**6** show one reversible oxidation wave in the range of 0.85 – 1.02 V corresponding to the phenothiazine donor unit on the anodic side. The ethynyl phenothiazines **1** and **4** show one oxidation wave at 0.86 V and 0.97 V, whereas the TCBD derivatives **2** and **5** show one oxidation wave at ~1.0 V corresponding to the phenothiazine moiety. The DCNQ derivatives **3** and **6** show one oxidation wave at 0.94 V and 0.85 V respectively, corresponding to the phenothiazine moiety. The ethynyl phenothiazines **1** and **4** do not show any reduction waves in their voltammogram (Figure 3.3). However, after the incorporation of the TCBD unit, **2** and **5** exhibit two reduction waves at –0.05 V and –0.69 V and, at –0.21 V and –0.86 V respectively, which are due to the TCBD moiety on the cathodic side. The DCNQ substituted derivatives **3** and **6** exhibit two reduction waves at –0.07 V and –0.23 V (for **3**) and, at –0.10 V and –0.36 V (for **6**) which are due to the DCNQ moiety on the cathodic side. The calculated electrochemical energy gap (E_{gap}) of **2**, **3**, **5**, and **6** were 1.06 eV, 1.00 eV, 1.23 eV, and 0.95 eV respectively. The E_{gap} values follow the order **5** > **2** > **3** > **6** which is in accordance with the optical HOMO–LUMO gap. The resulted HOMO–LUMO gap values of mono and di-DCNQ incorporated **3** and **6** suggest that the incorporation of di-DNCQ provides the better tuned HOMO and LUMO energy levels as compared to the mono derivative.

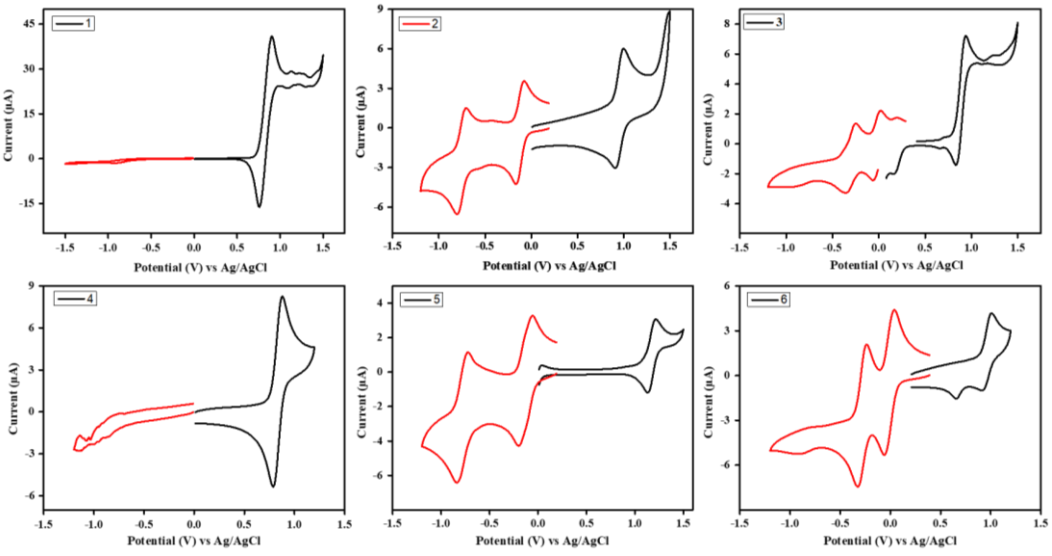

Figure 3.3. Cyclic voltammograms of phenothiazine derivatives **2** and **5** in 0.1 M solution of Bu_4NPF_6 in dichloromethane were recorded at a scan rate of 100 mV s^{-1} *versus* saturated Ag/AgCl electrode at 25 °C.

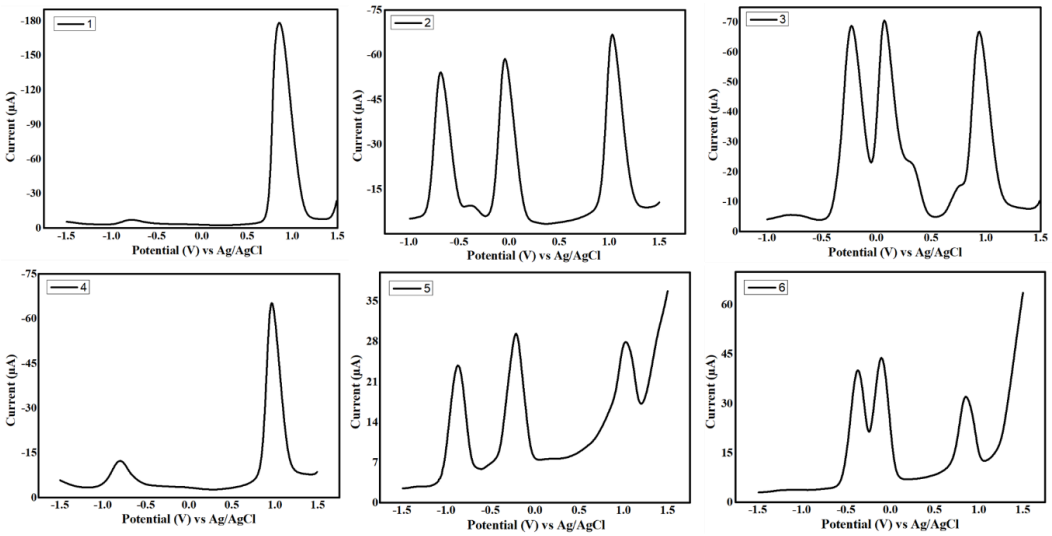

Figure 3.4. Differential pulse voltammograms of phenothiazine derivatives **1–6** in 0.1 M solutions of Bu_4NPF_6 in dichloromethane at 100 mV s^{-1} scan rate versus saturated Ag/AgCl electrode at 25 °C.

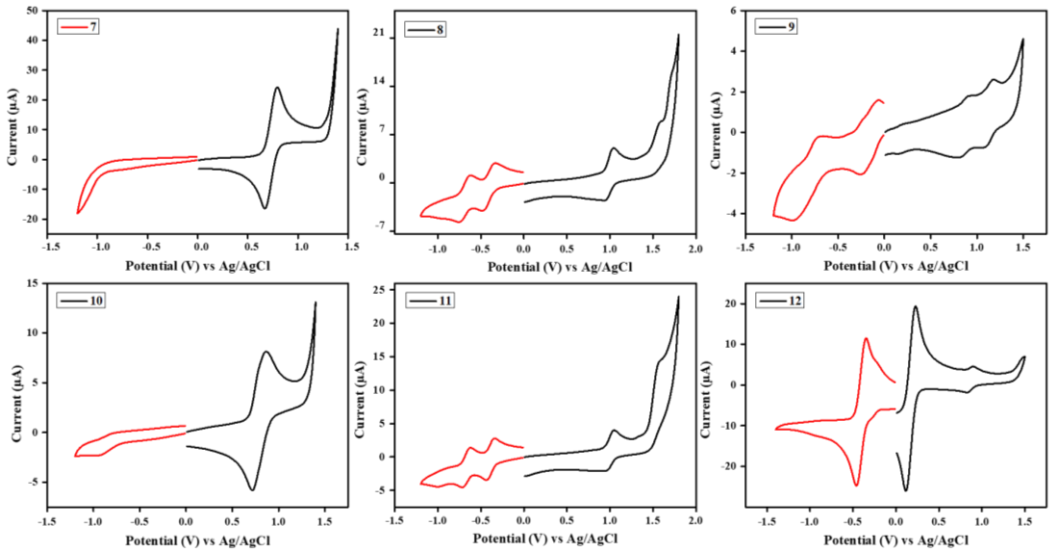

Figure 3.5. Cyclic voltammograms of phenothiazine derivatives **8** and **11** in 0.1 M solution of Bu_4NPF_6 in dichloromethane were recorded at a scan rate of 100 mV s^{-1} *versus* saturated Ag/AgCl electrode at 25 °C.

The phenothiazine derivatives **7–12** show two reversible oxidation waves in the range of 1.70 – 0.10 V. The thiophene substituted phenothiazine **7** and **10** show two oxidation waves at 0.71, 1.34 V and 0.77, 1.45 V, respectively. The first oxidation potential was observed

due to the presence of the phenothiazine unit and the second oxidation potential corresponds to the thiophene unit. The phenothiazine derivatives **7** and **10** do not show any reduction waves in their voltammogram (Figure 3.5). However, the TCBD and DCNQ incorporated phenothiazines **8**, **9**, **11** and **12** exhibit two reversible oxidation waves at 0.91, 1.65 V; 0.24, 1.01 V; 0.91, 1.46 V and 0.11, 0.76 V, as well as two reversible reduction waves at –0.45, –0.75 V; –0.26, –0.85 V; –0.47, –0.75 V and –0.28, –0.45 V respectively. These reduction values are due to the acceptor TCBD and DCNQ. The electrochemical band gap (E_{gap}) of **8**, **9**, **11**, and **12** are 2.10 eV, 1.27 eV, 1.93 eV, and 1.04 eV, respectively. The E_{gap} values follow the order **8** > **11** > **9** > **12**. The comparative study of the HOMO–LUMO energy gap of thiophene derivatives follow the similar trend and di-TCBD and DCNQ incorporated derivatives **9** and **12** exhibit low E_{gap} with respect to the mono-substituted analogues.

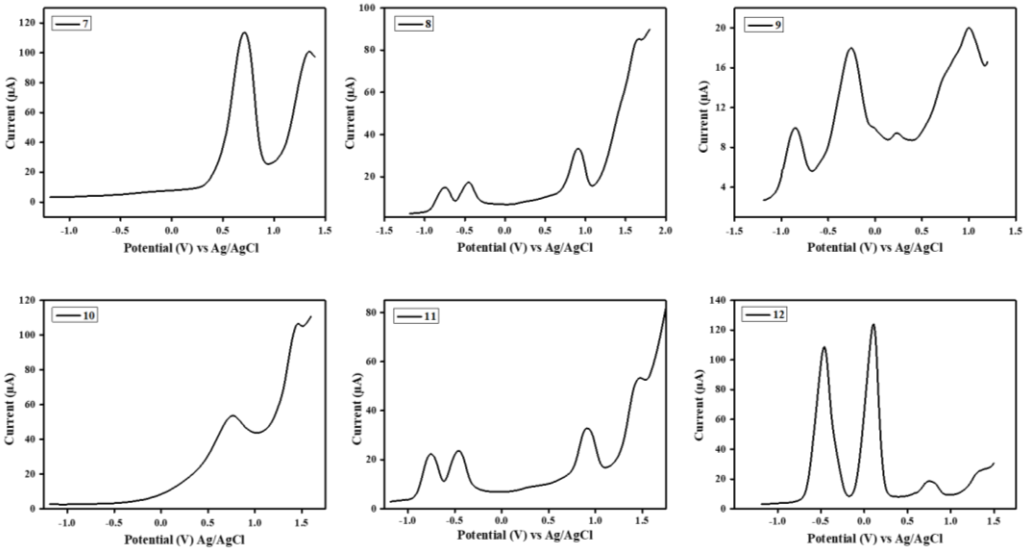

Figure 3.6. Differential pulse voltammograms of phenothiazine derivatives **7–12** in 0.1 M solutions of Bu_4NPF_6 in dichloromethane at 100 mV s^{-1} scan rate versus saturated Ag/AgCl electrode at 25 °C.

Similarly, the phenothiazine derivatives **13** and **16** show two reversible oxidation waves, and **14**, **15**, **17** and **18** show one reversible oxidation wave in the range of 1.40 – 0.55 V, and **14**, **15**, **17** and **18** show two reversible reduction waves in the range of –0.35 to –1.0 V. The carbazole substituted phenothiazine **13** and **16** exhibit two oxidation

potentials at 0.66, 1.13 V and 0.58, 1.23 V, respectively. The first oxidation potential was observed due to the presence of the phenothiazine unit and the second oxidation potential corresponds to the carbazole unit. The phenothiazine derivatives **13** and **16** do not show any reduction waves in their voltammogram (Figure 3.7). However, the TCBD and DCNQ linked phenothiazines **14**, **15**, **17** and **18** show one reversible oxidation wave at 0.82 V, 0.83 V, 1.11 V and 1.38 V, which are attributed to the simultaneous reversible oxidation of phenothiazine and carbazole units[36] and two reversible reduction waves at –0.52, –0.89 V; –0.38, –0.95 V; –0.48, –0.84 V and –0.44, –0.86 V respectively. This is caused by the acceptor TCNE and TCNQ moiety. The calculated electrochemical band gap (E_{gap}) of **14**, **15**, **17** and **18** are 1.34 eV, 1.21 eV, 1.58 eV, and 1.82 eV respectively. The E_{gap} values follow the order **18** > **17** > **14** > **15**. Interestingly in the case of carbazole substituted derivatives, the mono carbazole based derivatives exhibit low E_{gap} compared to the di-carbazole derivatives.

The electrochemical data reveals that the incorporation of cyano-based electron acceptor groups is able to perturb the redox properties of phenothiazines and the DCNQ unit and stabilizes the LUMO energy level to a greater extent as compared to the TCBD unit.

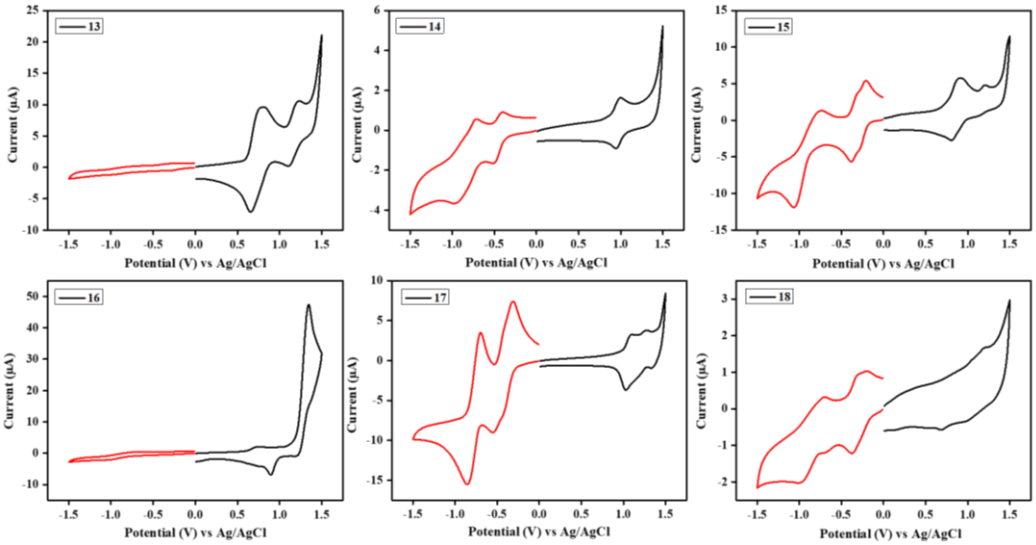

Figure 3.7. Cyclic voltammograms of phenothiazine derivatives **14** and **17** in 0.1 M solution of Bu_4NPF_6 in dichloromethane were recorded at a scan rate of 100 mV s^{-1} *versus* saturated Ag/AgCl electrode at 25 °C.

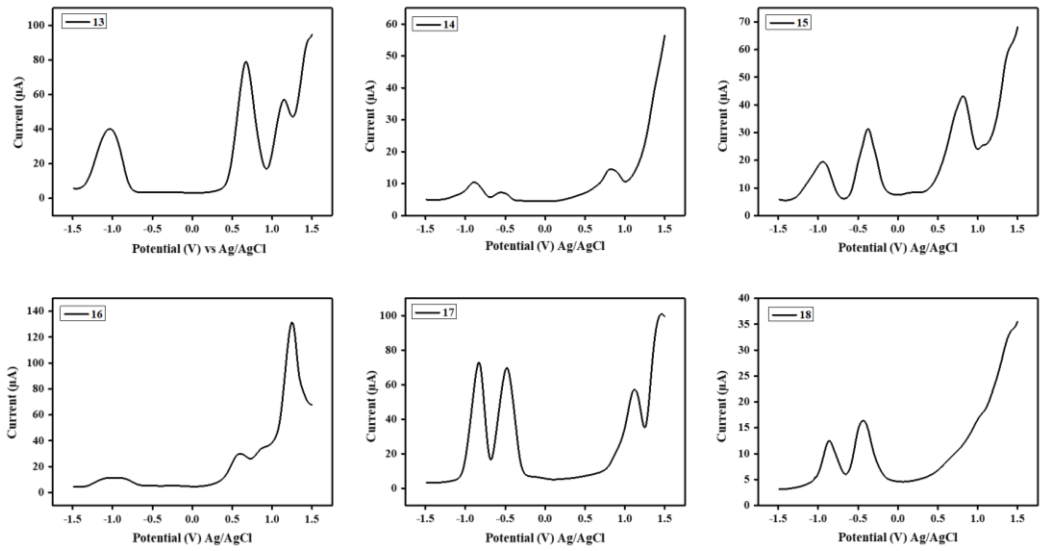

Figure 3.8. Differential pulse voltammograms of phenothiazine derivatives **13–18** in 0.1 M solutions of Bu_4NPF_6 in dichloromethane at 100 mV s^{-1} scan rate versus saturated Ag/AgCl electrode at 25 °C.

3.5. Thermogravimetric Analysis

The thermal properties of the phenothiazine derivatives **1–18** were investigated by the thermogravimetric analysis (TGA) at a heating rate of 10 °C min^{-1} under a nitrogen atmosphere, and their corresponding thermograms are shown in Figure 3.9. The π-conjugated phenothiazine derivatives **1–18** display good thermal stability.

The decomposition temperatures (T_{d5}) for phenothiazine derivatives **2**, **3**, **5**, **6**, **7–12**, **13**, **14**, **15**, **17**, and **18** at 5% weight loss were found to be at 366 °C, 274 °C, 211 °C, 312 °C, 264 °C, 241 °C, 228 °C, 266 °C, 303 °C, 236 °C, 277 °C, 247 °C, 318 °C, 210 °C and 199 °C, respectively (Table 3.2). These results indicate that phenothiazine derivative **2** is thermally more stable than the other phenothiazine derivatives. The mono TCBD incorporated phenothiazine derivative **2** shows better decomposition temperature than the mono TCBD substituted thiophene and carbazole derivatives **8** and **14**. A similar pattern was observed for the di DCNQ incorporated phenothiazine derivatives **6**, **12**, and **18**. On the other hand, a different pattern was observed for the mono DCNQ incorporated phenothiazine derivatives among **3**, **9**, and **15**. In this case, carbazole substituted phenothiazine derivative **15** shows good decomposition temperature as compared to

the mono DCNQ functionalized phenothiazine derivative **3** and thiophene substituted phenothiazine derivative **9**.

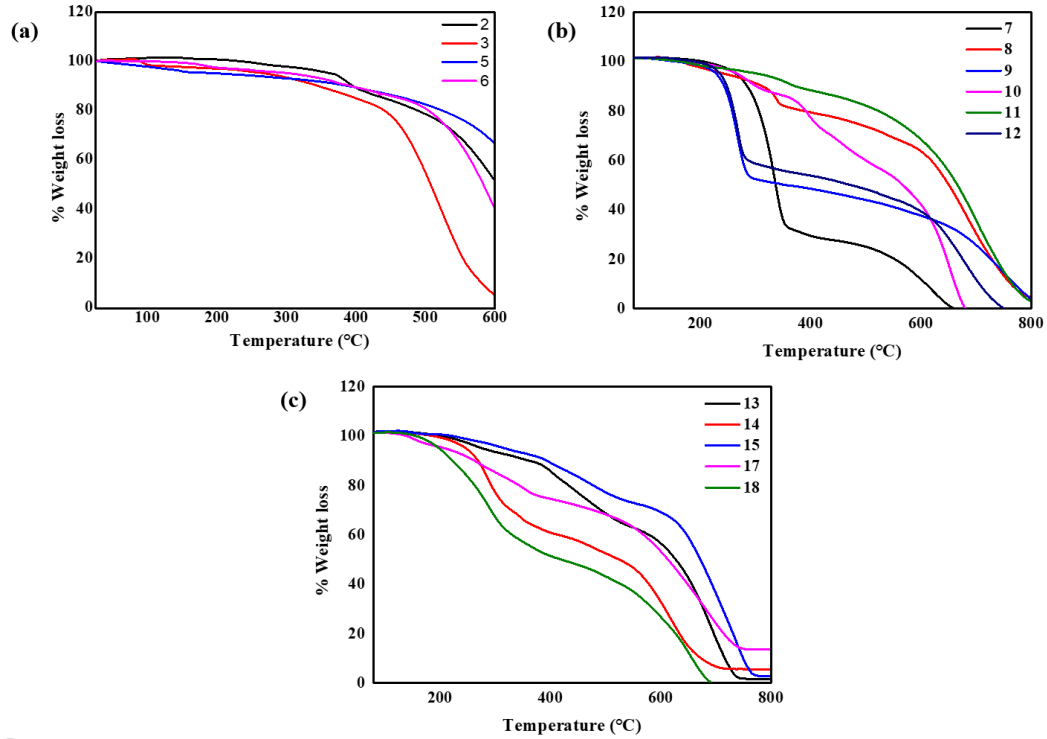

Figure 3.9. Thermogravimetric analysis of phenothiazine derivatives **(a) 2**, **3**, **5** and **6**; **(b) 7–12** and **(c) 13**, **14**, **15**, **17** and **18** measured at a heating rate of 10 °C min^{-1} under a nitrogen atmosphere.

3.6. Computational Calculations

In order to understand the molecular conformations and ground-state geometries of the phenothiazines **1–18**, density functional theory (DFT) calculation were performed at the B3LYP/6-31G (d,p) level in the Gaussian 09W program.[37] The frontier molecular orbitals of phenothiazine derivatives **1–18** are shown in Figures 3.10–3.12 and the corresponding data are listed in Table 3.3. The optimized structures of phenothiazine derivatives **1–18** are nonplanar with a twisted backbone due to the incorporation of the TCBD and DCNQ units. The HOMOs are mainly concentrated on the phenothiazine, thiophene, and carbazole units, whereas LUMOs are located on the TCBD and DCNQ units resulting in a strong charge transfer from the donor units (phenothiazine, thiophene, and carbazole) to the acceptor units (TCBD/DCNQ).

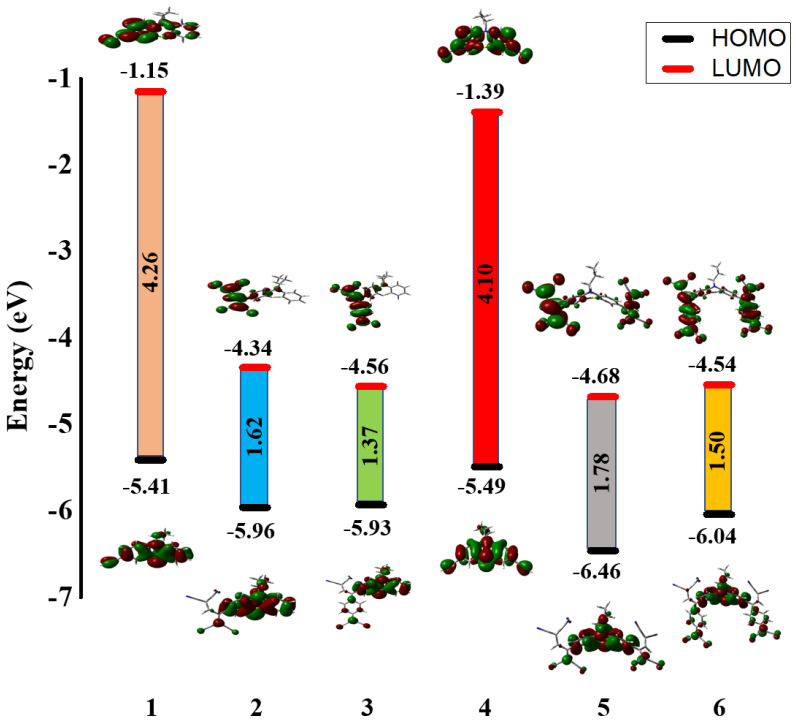

Figure 3.10. Energy level diagram of the HOMO–LUMO frontier orbitals of phenothiazine derivatives **1–6** calculated by DFT calculations at the B3LYP/6-31G (d,p) level.

The energy level diagrams of phenothiazine derivatives **1–6** are displayed in Figure 3.10. The theoretically calculated HOMO/LUMO levels of the phenothiazine derivatives **1−6** are –5.42/–1.15, –5.96/–4.34, –5.93/–4.56, –5.49/–1.39, –6.46/–4.68, and –6.05/–4.54 eV respectively. The incorporation of the strong acceptors TCBD and DCNQ units lowers the LUMO energy level. The theoretical HOMO–LUMO gap values for phenothiazine derivatives **1–6** are 4.26, 1.62, 1.37, 4.10, 1.78 and 1.50 eV respectively, and follow the order **1** > **4** > **5** > **2** > **6** > **3**.

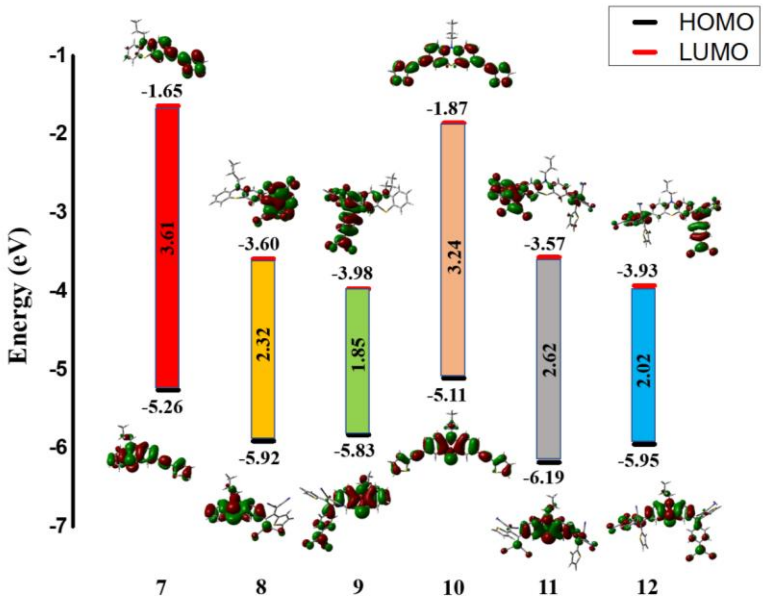

Figure 3.11. Energy level diagram of the HOMO–LUMO frontier orbitals of phenothiazine derivatives **7–12** calculated by DFT calculations at the B3LYP/6-31G (d,p) level.

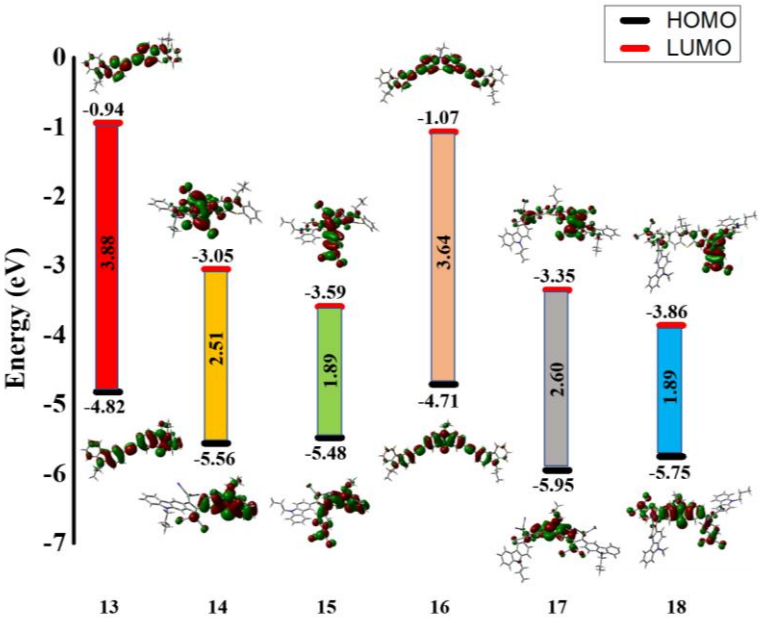

Figure 3.12. Energy level diagram of the HOMO–LUMO frontier orbitals of phenothiazine derivatives **13–18** calculated by DFT calculations at the B3LYP/6-31G (d,p) level.

The energy level diagrams of phenothiazine derivatives **7–12** are shown in Figure 3.11. The theoretically calculated HOMO/LUMO levels for the phenothiazine derivatives **7–12** are –5.26/–1.65, –5.92/–

3.60, –5.83/–3.98, –5.11/–1.87, –6.19/–3.57, and –5.95/–3.93 eV respectively. The incorporation of the strong acceptors TCBD and DCNQ units lower the LUMO energy level. The theoretical HOMO–LUMO gap values for phenothiazine derivatives **7–12** are 3.61, 2.32, 1.85, 3.24, 2.62 and 2.02 eV respectively, and follow the order **7** > **10** > **11** > **8** > **12** > **9**. Similarly, the energy level diagrams of phenothiazine derivatives **13–18** are shown in Figure 3.12. The theoretically calculated HOMO/LUMO levels of the phenothiazine derivatives **13–18** are –4.82/–0.94, –5.56/–3.05, –5.48/–3.59, –4.71/–1.07, –5.95/–3.35, and –5.75/–3.86 eV respectively. The incorporation of the strong acceptors TCBD and DCNQ units lower the LUMO energy level. The theoretical HOMO–LUMO gap values for phenothiazine derivatives **13–18** are 3.88, 2.51, 1.89, 3.64, 2.60 and 1.89 eV respectively, and follow the order **13** > **16** > **17** > **14** > **18** = **15**. The theoretical HOMO–LUMO gap of phenothiazines **1–18** were found to be in good agreement with the experimentally calculated optical band gap values estimated from the UV/Vis absorption spectra (Table 3.1 and 3.3). The DFT studies reveal that the effect of various donors at the terminal position influences the theoretically calculated HOMO and LUMO energy levels. The HOMO energy levels were more stable when the terminal substituents were changed from -H to donor thiophene and carbazole units. Nevertheless, the LUMOs were obtained relatively at high energy levels on changing the terminal -H with donor thiophene and carbazole units.

Table 3.3. Theoretical data of phenothiazine derivatives **1–18**:

Phenothiazine derivatives	**HOMO (eV)[a]**	**LUMO (eV)[a]**	**HOMO–LUMO gap (eV)[a]**
1	–5.42	–1.15	4.26
2	–5.96	–4.35	1.62
3	–5.93	–4.57	1.37
4	–5.49	–1.40	4.10
5	–6.46	–4.68	1.78

6	–6.05	–4.54	1.50
7	–5.26	–1.65	3.61
8	–5.92	–3.60	2.32
9	–5.83	–3.98	1.85
10	–5.11	–1.87	3.24
11	–6.19	–3.57	2.62
12	–5.95	–3.93	2.02
13	–4.82	–0.94	3.88
14	–5.56	–3.05	2.51
15	–5.48	–3.59	1.89
16	–4.71	–1.07	3.64
17	–5.95	–3.35	2.60
18	–5.75	–3.86	1.89

[a]Theoretical data was obtained from density functional theory (DFT) calculations performed at the B3LYP/6-31G (d,p) level.

The time-dependent DFT (TD-DFT) calculation was employed to study the nature of electronic transitions taking place in phenothiazine derivatives **1–18** by using the basis set B3LYP/6-31G (d,p) in dichloromethane and the computational data regarding frontier molecular orbitals involved in a transition with oscillator strength are demonstrated in Table 3.4.

The mono and di-ethynyl substituted phenothiazines **1** and **4** show the distribution of electron density of HOMO and LUMO energy levels over the entire molecular framework. However, the TCBD and DCNQ-based phenothiazine derivatives **2**, **3**, **5**, and **6** show the well-separated distribution of electron density of HOMO and LUMO energy levels. In **2**, **3**, **5**, and **6**, the HOMO is mainly localized over the donor phenothiazine, whereas the LUMO is mainly localized over the TCBD/DCNQ acceptor moieties (Figure 3.10). The well-separated electron density of HOMO and LUMO energy levels of **2**, **3**, **5**, and **6** indicated the possibilities of intramolecular charge transfer transitions. The simulated absorption spectra of **2**, **3**, **5**, and **6** obtained from TD-DFT studies revealed absorption bands at 599, 714, 568, and 691 nm,

respectively. These absorption bands were originated due to the transition from HOMO to LUMO and were assigned as ICT transition from donor phenothiazine to the acceptor TCBD/DCNQ moieties.

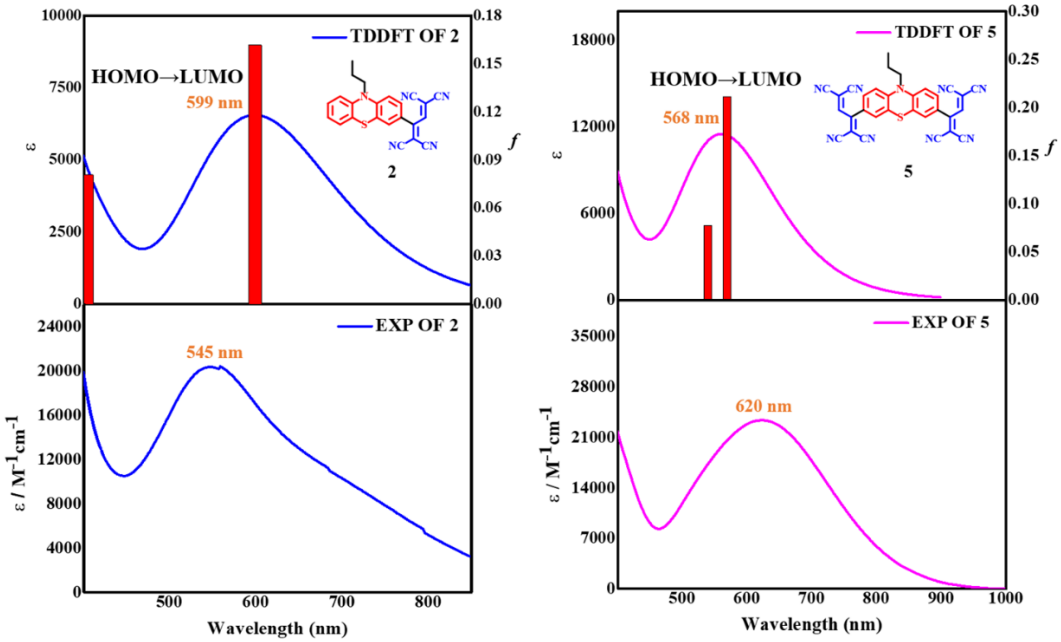

Figure 3.13. Theoretical (top) and experimental (bottom) absorption spectra of phenothiazine derivatives **2** and **5**.

The TD-DFT calculation reveals absorption maxima at 308 nm and 320 nm for the mono ethynyl and di ethynyl substituted phenothiazines **1** and **4** which was attributed to the π-π* transition localized on the phenothiazine moiety. A comparison of experimental absorption spectra and simulated absorption spectra of **2** and **5** are shown in Figure 3.13. The simulated absorption spectra of **2** revealed one absorption band at 599 nm which was originated due to the transition from HOMO→LUMO. The simulated absorption spectra of **5** revealed one absorption band at 568 nm which was originated due to the transition from HOMO→LUMO. The simulated absorption spectra of **3** revealed two absorption bands at 513 and 714 nm respectively which were originated due to the transition from HOMO-1→LUMO and HOMO→LUMO respectively. The simulated absorption spectra of **6** revealed two absorption bands at 493 and 691 nm respectively which were originated due to the transition from HOMO-2→LUMO+1 and HOMO→LUMO, respectively. A comparison of experimental

absorption spectra and simulated absorption spectra of **3** and **6** are shown in Figure 3.14.

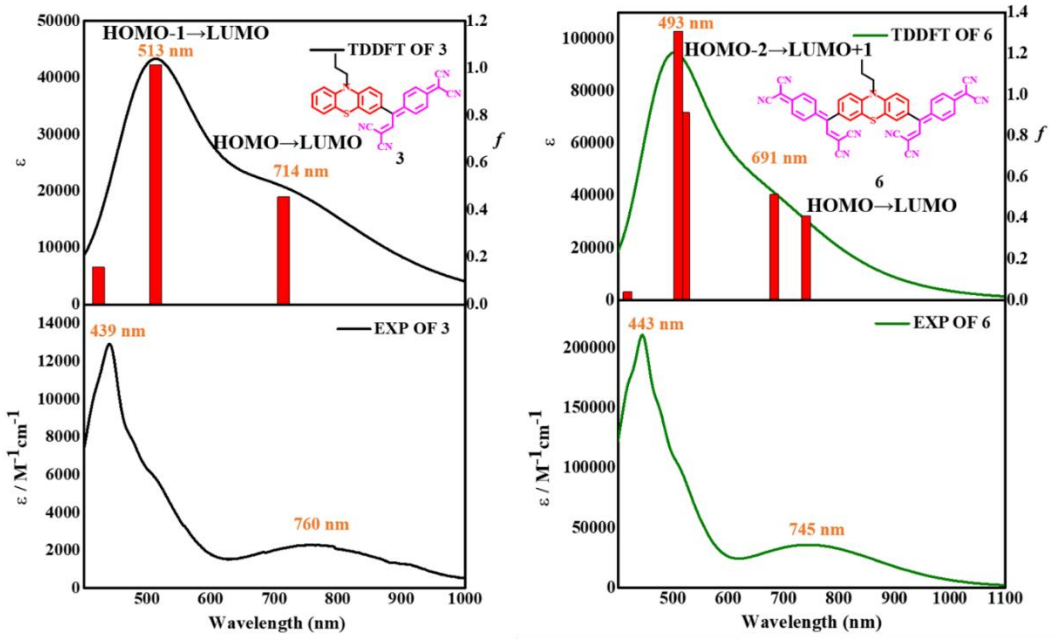

Figure 3.14. Theoretical (top) and experimental (bottom) absorption spectra of phenothiazine derivatives **3** and **6**.

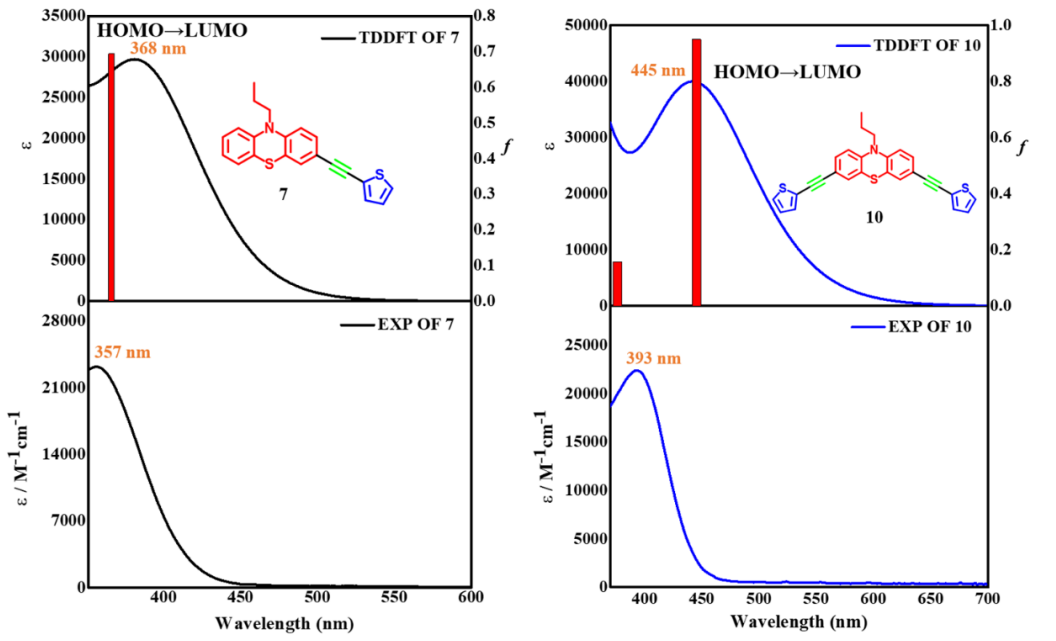

Figure 3.15. Theoretical (top) and experimental (bottom) absorption spectra of phenothiazine derivatives **7** and **10**.

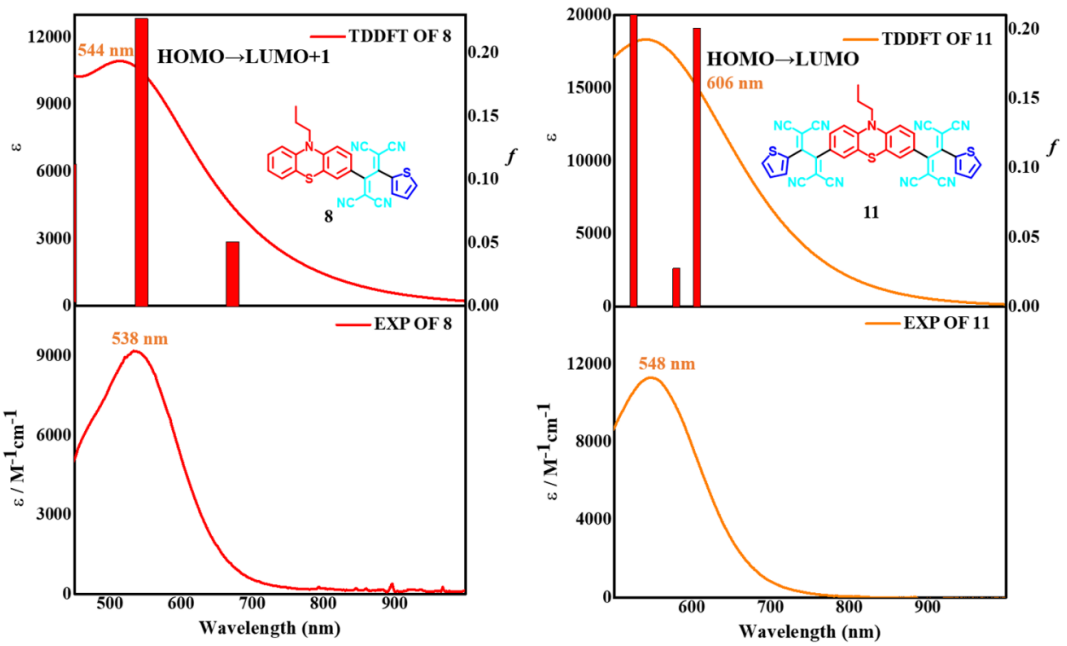

Figure 3.16. Theoretical (top) and experimental (bottom) absorption spectra of phenothiazine derivatives **8** and **11**.

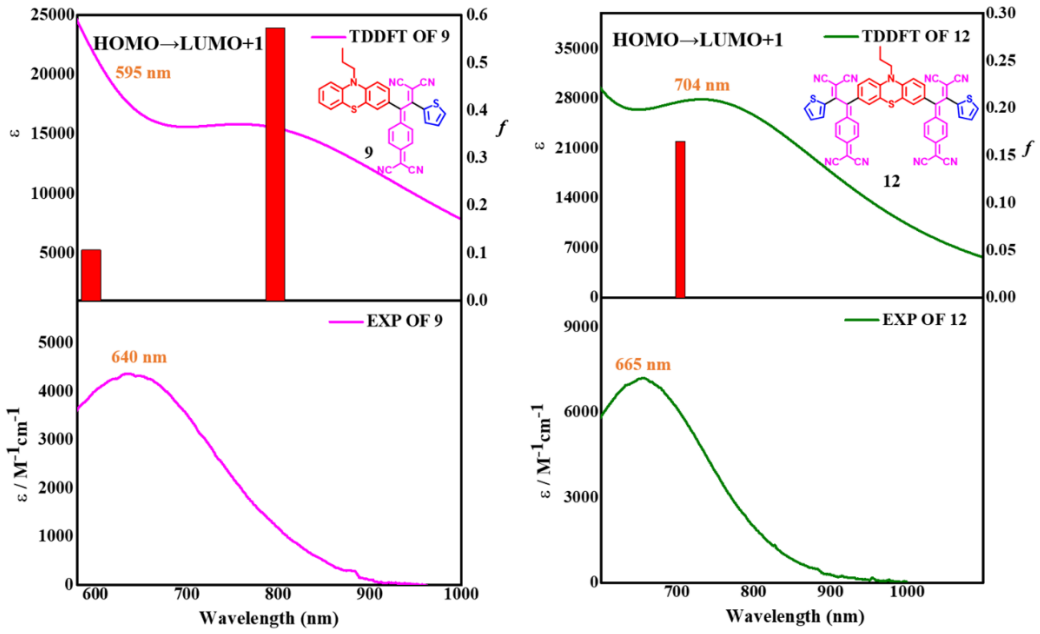

Figure 3.17. Theoretical (top) and experimental (bottom) absorption spectra of phenothiazine derivatives **9** and **12**.

The TD-DFT calculation of the phenothiazine derivatives **7** and **10** show absorption maxima at 368 and 445 nm respectively due to π–π* transition originating from HOMO→LUMO (Figure 3.15). The simulated absorption spectra of phenothiazine derivatives **8** and **11**

exhibit strong absorption bands at 544 and 606 nm respectively which are due to intramolecular charge transfer (ICT) transitions originating from HOMO→LUMO+1 and HOMO→LUMO, respectively (Figure 3.16). The simulated absorption spectra of the phenothiazine derivatives **9** and **12** show strong absorption bands at 595 and 704 nm, respectively. These absorption bands are attributed to intramolecular charge transfer (ICT) transitions which originate from HOMO→LUMO+1 (Figure 3.17). The donor-acceptor based phenothiazine derivatives **7–12** exhibit good agreement between the theoretically calculated ICT band and the experimentally observed ICT band from the UV-vis spectra. The computational data shows that the symmetrical phenothiazine derivatives **10–12** are bathochromic shifted as compared to unsymmetrical phenothiazine derivatives **7–9**, respectively.

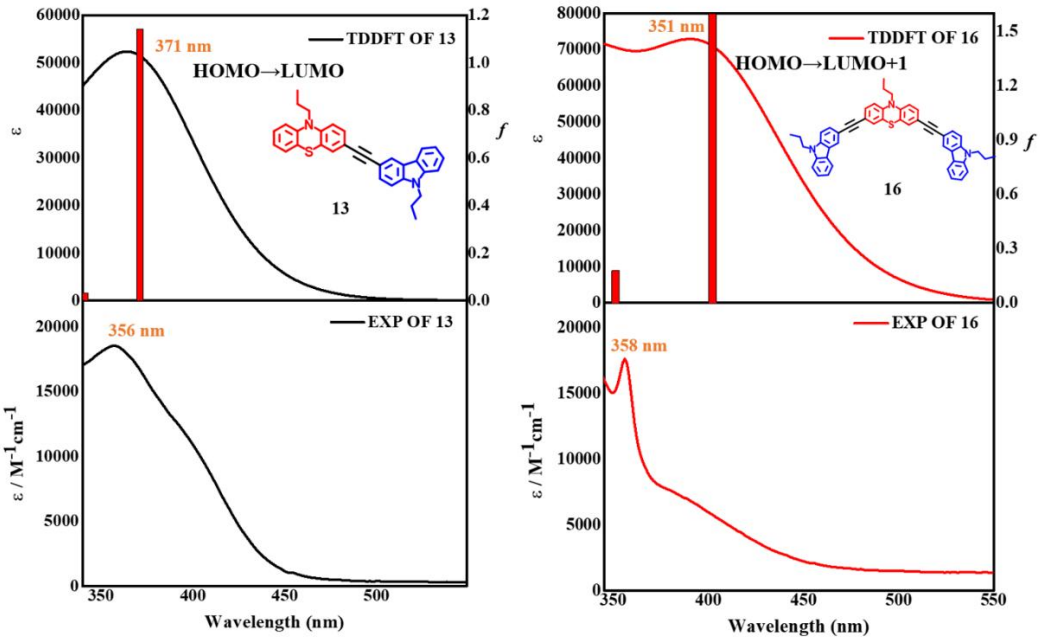

Figure 3.18. Theoretical (top) and experimental (bottom) absorption spectra of phenothiazine derivatives **13** and **16**.

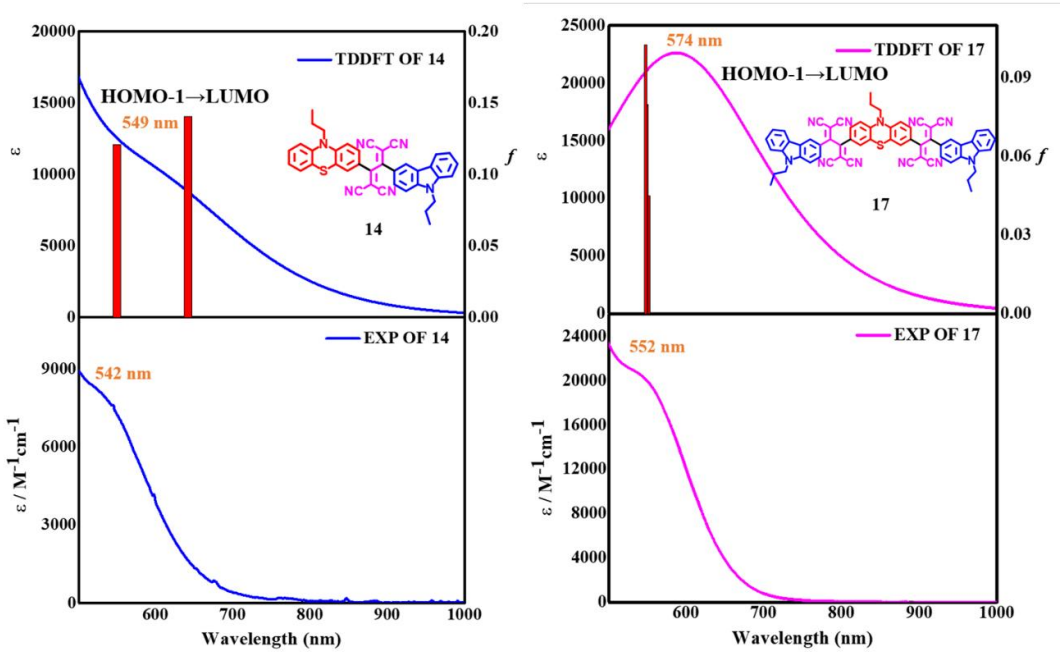

Figure 3.19. Theoretical (top) and experimental (bottom) absorption spectra of phenothiazine derivatives **14** and **17**.

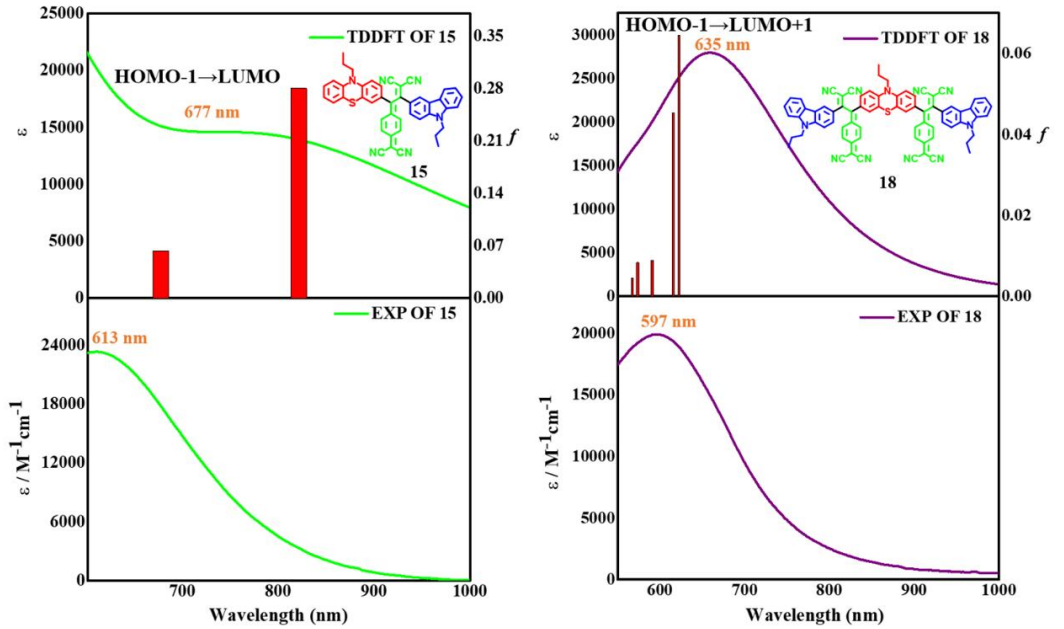

Figure 3.20. Theoretical (top) and experimental (bottom) absorption spectra of phenothiazine derivatives **15** and **18**.

Similarly, the phenothiazine derivatives **13** and **16** show absorption maxima at 371 and 351 nm respectively due to π–π* transition originating from HOMO→LUMO (Figure 3.18). The simulated absorption spectra of phenothiazine derivatives **14** and **17**

exhibit strong absorption bands at 549 and 574 nm, respectively, which are due to intramolecular charge transfer (ICT) transitions originating from HOMO-1→LUMO (Figure 3.19). The simulated absorption spectra of the phenothiazine derivatives **15** and **18** show strong absorption bands at 677 and 635 nm, respectively. These absorption bands are produced by intramolecular charge transfer (ICT) transitions that originate from HOMO-1→LUMO and HOMO-1→LUMO+1, respectively (Figure 3.20). The donor-acceptor based phenothiazine derivatives **13–18** exhibit a good agreement between the theoretically calculated ICT band and the experimentally observed ICT band from the UV-vis spectra. The computational data shows that the phenothiazine derivatives **13** and **15** are red shifted as compared to phenothiazine derivatives **16** and **18**, respectively.

The experimental values were found to be lower than the theoretical electronic absorption wavelengths, which may be caused by a number of factors, including the solvent effect, the dipole moment, and temperature.

Table 3.4. Calculated electronic transitions for phenothiazine derivatives **1–18** in dichloromethane:

Phenothiazine derivatives	**Wavelength (nm)**	**Composition and Molecular Contribution**	***f*[a]**	**Assignment**
1	308	HOMO→LUMO (0.63)	0.16	π–π*
2	599	HOMO→LUMO (0.68)	0.16	ICT
3	513 714	HOMO-1→LUMO (0.70) HOMO→LUMO (0.69)	1.01 0.45	ICT[1] ICT[2]
4	320	HOMO→LUMO (0.66)	0.28	π–π*
5	568	HOMO→LUMO (0.67)	0.21	ICT
6	493 691	HOMO-2→LUMO+1 (0.48) HOMO→LUMO (0.67)	1.31 0.41	ICT[1] ICT[2]
7	368	HOMO→LUMO (0.69)	0.69	π–π*

8	544	HOMO→LUMO+1 (0.69)	0.23	ICT
9	595	HOMO→LUMO+1 (0.65)	0.07	ICT
10	445	HOMO→LUMO (0.69)	0.95	π–π*
11	606	HOMO→LUMO (0.70)	0.20	ICT
12	704	HOMO→LUMO+1 (0.68)	0.16	ICT
13	371	HOMO→LUMO (0.69)	1.14	π–π*
14	549	HOMO-1→LUMO (0.70)	0.12	ICT
15	677	HOMO-1→LUMO (0.70)	0.07	ICT
16	351	HOMO→LUMO+1 (0.68)	0.18	π–π*
17	574	HOMO-1→LUMO (0.57)	0.10	ICT
18	635	HOMO-1→LUMO+1 (0.53)	0.009	ICT

[a]Oscillator strength.

3.7. Experimental Section

General Methods

The chemicals were used as received unless otherwise indicated. All oxygen or moisture-sensitive reactions were performed under a nitrogen/argon atmosphere. ^{1}H NMR (500 MHz) and $^{13}C\{^{1}H\}$ NMR (125 MHz) spectra were recorded on a Bruker 500 MHz FT-NMR spectrometer at room temperature. Structural assignments were made with additional information from the gCOSY, gHSQC, and gHMBC experiments. ^{1}H NMR chemical shifts are reported in parts per million (ppm) relative to the solvent residual peak ($CDCl_3$, 7.26 ppm). Multiplicities are given as s (singlet), d (doublet), t (triplet), and m (multiplet) and the coupling constants, *J*, are given in hertz. ^{13}C NMR chemical shifts are reported relative to the solvent residual peak ($CDCl_3$, 77.0 ppm). The UV-visible absorption spectra were recorded on a PerkinElmer LAMBDA 35 UV-visible Spectrophotometer in DCM solvent at room temperature. Thermogravimetric analysis was performed on a Mettler Toledo thermal analysis system. High-Resolution Mass Spectrometry (HRMS) was recorded on a Bruker-Daltonics micrOTOF-Q II mass spectrometer. The Cyclic

voltammograms (CVs) and differential pulse voltammograms (DPVs) were recorded on a PalmSence 4 electrochemical analyzer in dichloromethane (CH_2Cl_2) solvent and 0.1 M Tetrabutylammonium hexafluorophosphate (Bu_4NPF_6) was used as the supporting electrolyte. The electrodes used were glassy carbon as a working electrode, Pt wire as a counter electrode, and Ag/AgCl electrode was used as a reference electrode. The scan rate was 100 mV s^{-1} for cyclic voltammetry at 25 °C. The CVs and DPVs plotting convention is the IUPAC convention. The polishing material is a commercially available polishing pad and alumina (Al_2O_3).

Synthesis of 2-(10-propyl-10*H*-phenothiazin-3-yl) buta-1,3-diene-1,1,4,4-tetracarbonitrile (2)

In a 100 mL round bottomed flask TCNE (80 mg, 1 mmol) was added to a solution of compound 1 (160 mg, 1 mmol) in CH_2Cl_2 (20 mL). The mixture was stirred for 2 h at room temperature. The solvents were removed under vacuum, and the product was purified by silica gel column chromatography with DCM and hexane as the eluent to yield **2** as a dark-brown solid with 70% yield: mp 110−115 °C; **^{1}H NMR (500 MHz, $CDCl_3$) δ =** 7.96 (s, 1H), 7.34 (dd, *J* = 8.7, 2.4 Hz, 1H), 7.19 – 7.16 (m, 1H), 7.13 (d, *J* = 2.4 Hz, 1H), 7.07 (dd, *J* = 7.6, 1.6 Hz, 1H), 7.00 – 6.97 (m, 1H), 6.91 – 6.87 (m, 2H), 3.93 – 3.80 (m, 2H), 1.89 – 1.81 (m, 2H), 1.04 (t, *J* = 7.4 Hz, 3H); **^{13}C{^{1}H} NMR (125 MHz, $CDCl_3$) δ =** 159.4, 154.0, 150.8, 142.3, 129.8, 127.9, 127.6, 127.4, 126.1, 124.3, 123.6, 122.5, 116.2, 115.3, 112.2, 111.7, 111.5, 108.8, 97.7, 85.6, 50.0, 19.9, 11.1; **HRMS (ESI-TOF) m/z** calculated for $C_{23}H_{15}N_5S$ + Na 416.0940 $[M + Na]^+$, measured 416.0939 $[M + Na]^+$.

Synthesis of 2-(4-(3,3-dicyano-1-(10-propyl-10*H*-phenothiazin-3-yl)allylidene)cyclohexa-2,5-dien-1-ylidene)malononitrile (3)

In a 100 mL round bottomed flask TCNQ (96 mg, 1 mmol) was added to a solution of compound 1 (125 mg, 1 mmol) in dichloroethane (20 mL). The mixture was stirred for 8 h at room temperature. The solvents were removed under vacuum, and the product was purified by silica gel column chromatography with DCM and hexane as the eluent to yield **3** as a dark-green solid with 80% yield: mp 115−125 °C; **^{1}H NMR (500**

MHz, $CDCl_3$) δ = 8.12 (s, 1H), 7.39 (s, 2H), 7.29 (s, 1H), 7.19 – 7.15 (m, 1H), 7.09 (dd, *J* = 7.6, 1.5 Hz, 1H), 7.00 – 6.95 (m, 2H), 6.94 – 6.91 (m, 2H), 6.89 (d, *J* = 8.1 Hz, 2H), 3.87 (dd, *J* = 8.2, 6.3 Hz, 2H), 1.87 (q, *J* = 7.3 Hz, 2H), 1.04 (t, *J* = 7.4 Hz, 3H); **$^{13}C\{^1H\}$ NMR (125 MHz, $CDCl_3$) δ =** 153.5, 152.6, 148.5, 144.8, 143.5, 137.9, 131.2, 129.4, 127.8, 127.6, 127.5, 126.4, 123.6, 123.1, 121.4, 121.0, 116.0, 115.6, 113.9, 113.3, 112.8, 110.3, 110.2, 105.4, 91.8, 80.5, 49.8, 20.0, 11.2; **HRMS (ESI-TOF) m/z** calculated for $C_{29}H_{19}N_5S$ 469.1356 $[M]^+$, measured 469.1376 $[M]^+$.

Synthesis of 2,2'-(10-propyl-10*H*-phenothiazine-3,7-diyl)bis(buta-1,3-diene-1,1,4,4-tetracarbonitrile) (5)

In a 100 mL round bottomed flask, TCNE (74 mg, 0.5791 mmol) was added to a solution of compound phenothiazine 4 (80 mg, 0.2757 mmol) in CH_2Cl_2 (20 mL) under an argon atmosphere. The mixture was stirred for 18 h at room temperature. The solvent was removed in a vacuum, and the product was purified by SiO_2 column chromatography with DCM/hexane (2:1, v/v) as eluent to yield **5** as a dark brown solid with 65% yield: mp 135−145 °C; **^1H NMR (500 MHz, $CDCl_3$) δ =** 7.96 (s, 2H), 7.34 (dd, *J* = 8.6, 2.3 Hz, 2H), 7.09 (d, *J* = 2.3 Hz, 2H), 6.98 (d, *J* = 8.7 Hz, 2H), 3.90 (t, *J* = 7.5 Hz, 2H), 1.87 (q, *J* = 7.4 Hz, 2H), 1.06 (t, *J* = 7.3 Hz, 3H); **$^{13}C\{^1H\}$ NMR (125 MHz, $CDCl_3$) δ =** 159.6, 152.7, 148.2, 129.8, 127.5, 125.1, 116.5, 111.5, 111.0, 108.6, 104.3, 98.1, 89.2, 50.5, 31.9 14.1, 11.0; **HRMS (ESI-TOF) m/z** calculated for $C_{31}H_{15}N_9S$ + Na 568.1063 $[M + Na]^+$, measured 568.1083 $[M + Na]^+$.

Synthesis of 2,2'-((10-propyl-10*H*-phenothiazine-3,7-diyl)bis(2-(4-(dicyanomethylene)cyclohexa-2,5-dien-1-ylidene)ethan-2-yl-1-ylidene))dimalononitrile (6)

In a 100 mL round bottomed flask, TCNQ (100 mg, 0.4912 mmol) was added to a solution of compound 4 (57 mg, 0.1964 mmol) in DCE (25 mL). The mixture was heated at 80 °C in an oil bath for 24 h. After cooling to room temperature, the solvents were removed under vacuum, and the product was purified by silica gel column chromatography with DCM as the eluent to yield **6** as a dark-colored solid with 70% yield: mp 142−152 °C; **^1H NMR (500 MHz, $CDCl_3$) δ =** 8.16 (s, 2 H), 7.50 (br.

s., 2 H), 7.43 (br. s., 2 H), 7.31 (br. s., 2 H), 7.18 (br. s., 2 H), 7.06 - 7.01 (m, *J* = 7.9 Hz, 2 H), 6.99 - 6.95 (m, *J* = 8.4 Hz, 2 H), 6.91 (br. s., 2 H), 3.92 (t, *J* = 6.5 Hz, 2 H), 1.93 - 1.87 (m, 2 H), 1.07 (t, *J* = 7.0 Hz, 3 H); **$^{13}C\{^{1}H\}$ NMR (125 MHz, $CDCl_3$) δ** 169.6, 152.7, 152.4, 146.6, 144.1, 138.4, 131.3, 129.2, 128.5, 125.0, 116.2, 113.8, 113.0, 110.2, 91.5, 81.6, 50.3, 19.8, 11.0; **HRMS (ESI-TOF) m/z** calculated for $C_{43}H_{23}N_9S$ + Na 720.1689 $[M + Na]^+$, measured 720.1721 $[M + Na]^+$.

Synthesis of 10-propyl-3-(thiophen-2-ylethynyl)-10*H*-phenothiazine (7)

In a 100 mL round bottomed flask, 3-ethynyl-10-propyl-10*H*-phenothiazine **1** (400 mg, 1.5 mmol) and 2-bromothiophene (270 mg, 1.65 mmol) were purged under nitrogen and bis(triphenylphosphine)palladium (II)dichloride (40 mg) and copper(I) iodide (1 - 2 mg) were added in anhydrous triethylamine (20 mL) and tetrahydrofuran (20 mL), the reaction mixture was stirred and refluxed for 12 h at 60 °C in an oil bath. Then the solvent was evaporated under a vacuum. The residue was dissolved in dichloromethane, and this solution was washed with water for several times, dried with anhydrous Na_2SO_4, and filtered off. The crude was purified by column chromatography using dichloromethane-hexane (1/3 v/v) as eluent to give an oily yellowish of **7** with 60% yield: mp 72−80 °C; **^{1}H NMR (500 MHz, $CDCl_3$) δ** = 7.30 - 7.28 (m, 1 H), 7.27 (br. s., 2 H), 7.25 - 7.23 (m, 1 H), 7.17 - 7.10 (m, 2 H), 7.00 (dd, J = 3.7, 5.0 Hz, 1 H), 6.92 (t, J = 7.2 Hz, 1 H), 6.85 (d, J = 8.1 Hz, 1 H), 6.78 (d, J = 8.4 Hz, 1 H), 3.81 (br. s., 2 H), 1.86 - 1.80 (m, 2 H), 1.01 (t, J = 7.4 Hz, 3 H); **$^{13}C\{^{1}H\}$ NMR (125 MHz, $CDCl_3$) δ** = 145.5, 144.6, 131.5, 130.6, 130.0, 127.5, 127.3, 127.1, 127.0, 124.9, 124.2, 123.6, 122.8, 116.6, 115.6, 115.1, 92.6, 82.4, 49.3, 20.1, 11.3; **HRMS (ESI-TOF) m/z** calculated for $C_{21}H_{17}NS_2$ + Na 370.0695 $[M + Na]^+$, measured 370.0653 $[M + Na]^+$.

Synthesis of 2-(10-propyl-10*H*-phenothiazin-3-yl)-3-(thiophen-2-yl)buta-1,3-diene-1,1,4,4-tetracarbonitrile (8)

In a 100 mL round bottomed flask, TCNE (40 mg, 0.317 mmol) was added to a solution of compound **7** (100 mg, 0.288 mmol) in CH_2Cl_2 (20 mL) under an argon atmosphere. The mixture was stirred for 4 h at RT.

The solvent was removed in a vacuum, and the product was purified by column chromatography with DCM/hexane (2:1, v/v) as eluent to yield **8** as a dark brown solid with an 80% yield: mp 118−128 °C; **^{1}H NMR (500 MHz, $CDCl_3$) δ** = 7.97 (d, *J* = 4.6 Hz, 1 H), 7.87 (d, *J* = 3.5 Hz, 1 H), 7.70 (dd, *J* = 2.2, 8.9 Hz, 1 H), 7.37 (d, *J* = 2.3 Hz, 1 H), 7.30 (t, *J* = 4.5 Hz, 1 H), 7.21 - 7.15 (m, 1 H), 7.08 - 7.05 (m, 1 H), 7.02 - 6.97 (m, 1 H), 6.90 - 6.84 (m, 2 H), 3.86 (t, *J* = 7.3 Hz, 2 H), 1.85 (sxt, *J* = 7.3 Hz, 2 H), 1.04 (t, *J* = 7.3 Hz, 3 H); **^{13}C{^{1}H} NMR (125 MHz, $CDCl_3$) δ** = 162.7, 158.4, 151.4, 141.9, 138.3, 137.3, 134.9, 130.5, 130.0, 128.0, 127.7, 127.6, 125.5, 124.6, 124.0, 122.6, 116.3, 115.1, 112.8, 112.5, 112.0, 111.5, 80.8, 80.4, 50.0, 20.0, 11.1; **HRMS (ESI-TOF) m/z** calculated for $C_{27}H_{17}N_5S_2$ + K 514.0557 $[M + K]^+$, measured 514.0845 $[M + K]^+$.

Synthesis of 2-(4-(3,3-dicyano-1-(10-propyl-10*H*-phenothiazin-3-yl)-2-(thiophen-2-yl)allylidene)cyclohexa-2,5-dien-1-ylidene)malononitrile (9)

In a 100 mL round bottomed flask, TCNQ (58 mg, 0.285 mmol) was added to a solution of **7** (90 mg, 0.259 mmol) in DCE (20 mL). The mixture was heated at 60 °C for 12 h in an oil bath. After cooling to room temperature, the solvents were removed under vacuum, and the product was purified by column chromatography with DCM/hexane (3:1, v/v) as the eluent to yield **9** as a dark-colored solid with 75% yield: mp 220−225 °C; **^{1}H NMR (500 MHz, $CDCl_3$) δ** = 7.94 (d, J = 3.8 Hz, 1 H), 7.88 (d, J = 4.9 Hz, 1 H), 7.56 (br. s., 1 H), 7.51 (d, J = 9.8 Hz, 1 H), 7.31 (d, J = 9.6 Hz, 1 H), 7.23 - 7.15 (m, 3 H), 7.09 (d, J = 7.6 Hz, 1 H), 7.04 (s, 1 H), 7.00 - 6.94 (m, 2 H), 6.88 (dd, J = 4.4, 8.2 Hz, 2 H), 3.85 (t, J = 7.2 Hz, 2 H), 1.86 (sxt, J = 7.2 Hz, 2 H), 1.04 (t, J = 7.3 Hz, 3 H); **^{13}C{^{1}H} NMR (125 MHz, $CDCl_3$) δ** = 161.8, 153.9, 148.8, 148.2, 142.8, 137.7, 136.5, 134.5, 133.9, 132.4, 131.9, 129.9, 129.0, 128.8, 128.3, 128.2, 127.8, 127.6, 126.4, 126.0, 125.7, 123.9, 122.9, 122.0, 116.0, 115.3, 113.1, 112.4, 111.1, 110.9, 110.1, 49.7, 29.7, 27.7, 20.0, 11.2; **HRMS (ESI-TOF) m/z** calculated for $C_{33}H_{21}N_5S_2$ + K 590.0870 $[M + K]^+$, measured 590.0885 $[M + K]^+$.

Synthesis of 10-propyl-3,7-bis(thiophen-2-ylethynyl)-10*H*-phenothiazine (10)

In a 100 mL round-bottomed flask, 3,7-diethynyl-10-propyl-10*H*-phenothiazine **4** (479 mg, 1.65 mmol) and 2-bromothiophene (807.6 mg, 4.95 mmol) were purged under nitrogen and bis(triphenylphosphine)palladium (II)dichloride (100 mg) and copper(I) iodide (2 - 3 mg) were added in anhydrous triethylamine (25 mL) and tetrahydrofuran (25 mL), the reaction mixture was stirred and refluxed for 12 h at 60 °C in an oil bath. Then the solvent was evaporated under a vacuum. The residue was dissolved in dichloromethane, and this solution was washed with water for several times, dried with anhydrous Na_2SO_4, and filtered off. The crude was purified by column chromatography using dichloromethane-hexane (2/3 v/v) as eluent to give an oily yellowish of **10** with 55% yield: mp 128−135 °C; **^{1}H NMR (500 MHz, $CDCl_3$) δ** = 7.29 (d, *J* = 1.8 Hz, 1 H), 7.27 (d, *J* = 1.8 Hz, 1 H), 7.25 - 7.21 (m, 2 H), 7.16 - 7.13 (m, 1 H), 7.13 - 7.10 (m, 1 H), 7.10 - 7.08 (m, 1 H), 6.92 (t, *J* = 7.5 Hz, 2 H), 6.84 (d, *J* = 8.1 Hz, 1 H), 6.75 (d, *J* = 8.5 Hz, 2 H), 3.80 (t, *J* = 7.2 Hz, 2 H), 1.86 - 1.77 (m, 2 H), 1.00 (t, *J* = 7.4 Hz, 3 H); **^{13}C{^{1}H} NMR (125 MHz, $CDCl_3$) δ** = 144.7, 131.7, 130.7, 130.0, 127.1, 127.1, 124.1, 123.5, 117.1, 115.2, 92.4, 82.7, 49.5, 20.0, 11.2; **HRMS (ESI-TOF) m/z** calculated for $C_{27}H_{19}NS_3$ 453.0674 $[M]^+$, measured 453.0967 $[M]^+$.

Synthesis of 3,3'-(10-propyl-10*H*-phenothiazine-3,7-diyl)bis(2-(thiophen-2-yl)buta-1,3-diene-1,1,4,4-tetracarbonitrile) (11)

In a 100 mL round-bottomed flask, TCNE (70 mg, 0.551 mmol)) was added to a solution of **10** (100 mg, 0.221 mmol) in CH_2Cl_2 (25 mL) under an argon atmosphere. The mixture was heated at 40 °C in an oil bath for 36 h. After cooling to room temperature, the solvent was removed under vacuum, and the product was purified by column chromatography with DCM/hexane (3:1, v/v) as eluent to yield **11** as a dark brown solid with 80% yield: mp 148−160 °C; **^{1}H NMR (500 MHz, $CDCl_3$) δ** = 7.98 (dd, *J* = 5.1, 1.1 Hz, 1H), 7.88 (dd, *J* = 4.2, 1.1 Hz, 1H), 7.71 (dd, *J* = 8.9, 2.4 Hz, 1H), 7.39 – 7.27 (m, 4H), 7.19 (d, *J* = 1.9 Hz,

1H), 7.01 (dd, *J* = 5.2, 3.6 Hz, 1H), 6.87 (d, *J* = 8.9 Hz, 1H), 6.82 (d, *J* = 8.5 Hz, 1H), 3.85 (t, *J* = 8.5, 2H), 1.85 (q, *J* = 7.4 Hz, 2H), 1.05 (t, *J* = 7.4 Hz, 3H); **$^{13}C\{^{1}H\}$ NMR (125 MHz, $CDCl_3$) δ** = 162.6, 158.1, 150.5, 141.8, 138.4, 137.2, 134.8, 132.0, 131.1, 130.5, 130.0, 130.0, 127.5, 127.5, 127.1, 125.0, 124.4, 122.9, 122.7, 119.2, 116.2, 115.9, 115.2, 112.6, 112.4, 111.8, 111.5, 91.5, 83.8, 81.5, 50.1, 26.9, 19.9, 11.1; **HRMS (ESI-TOF) m/z** calculated for $C_{39}H_{19}N_9S_3$ + Na 732.0818 $[M + Na]^+$, measured 732.1099 $[M + Na]^+$.

Synthesis of 2,2'-((10-propyl-10*H*-phenothiazine-3,7-diyl)bis(2-(4-(dicyanomethylene)cyclohexa-2,5-dien-1-ylidene)-1-(thiophen-2-yl)ethan-2-yl-1-ylidene))dimalononitrile (12)

In a 100 mL round bottomed flask, TCNQ (191 mg, 0.938 mmol) was added to a solution of **10** (170 mg, 0.375 mmol) in DCE (25 mL). The mixture was heated at 80 °C in an oil bath for 48 h. After cooling to room temperature, the solvents were removed under vacuum, and the product was purified by column chromatography with DCM as the eluent to yield **12** as a dark-colored solid with 65% yield: mp 233−240 °C; **^{1}H NMR (500 MHz, $CDCl_3$) δ** = 7.96 (dd, *J* = 4.2, 1.1 Hz, 1H), 7.89 (dd, *J* = 5.0, 1.1 Hz, 1H), 7.56 (s, 6H), 7.50 (dd, *J* = 9.8, 2.0 Hz, 1H), 7.34 – 7.28 (m, 3H), 7.22 – 7.18 (m, 3H), 7.04 – 6.99 (m, 2H), 6.96 (dd, *J* = 9.6, 2.0 Hz, 1H), 6.87 (d, *J* = 8.7 Hz, 1H), 6.82 (d, *J* = 8.5 Hz, 1H), 3.84 (t, *J* = 7.4 Hz, 2H), 1.85 (p, *J* = 7.4 Hz, 2H), 1.05 (t, *J* = 7.3 Hz, 3H); **$^{13}C\{^{1}H\}$ NMR (125 MHz, $CDCl_3$) δ** = 161.7, 153.9, 150.7, 148.0, 147.8, 142.7, 137.8, 137.4, 136.5, 134.3, 133.8, 132.6, 131.9, 131.8, 131.2, 131.0, 130.0, 129.1, 129.0, 128.9, 127.4, 127.1, 126.5, 126.1, 125.1, 123.0, 123.0, 118.4, 115.7, 115.4, 113.5, 113.5, 112.4, 111.5, 94.9, 91.7, 84.1, 89.7, 65.9, 64.8, 49.9, 20.0, 11.1; **HRMS (ESI-TOF) m/z** calculated for $C_{51}H_{27}N_9S_3$ + Na + K - H 922.1003 $[M + Na + K - H]^+$, measured 922.1828 $[M + Na + K - H]^+$.

Synthesis of 10-propyl-3-((9-propyl-9*H*-carbazol-3-yl)ethynyl)-10*H*-phenothiazine (13)

In a 100 mL round-bottomed flask, 3-ethynyl-10-propyl-10*H*-phenothiazine **1** (300 mg, 1.130 mmol) and 3-bromo-9-propyl-9*H*-carbazole (357 mg, 1.243 mmol) were purged under nitrogen and

bis(triphenylphosphine)palladium (II)dichloride (60 mg) and copper(I) iodide (1 - 2 mg) were added in anhydrous triethylamine (20 mL) and tetrahydrofuran (20 mL), the reaction mixture was stirred and refluxed for 12 h at 60 °C in an oil bath. Then the solvent was evaporated under a vacuum. The residue was dissolved in dichloromethane, and this solution was washed with water several times, dried with anhydrous Na_2SO_4, and filtered off. The crude was purified by column chromatography using dichloromethane-hexane (1/3 v/v) as an eluent to give an oily yellowish **13** with an 80% yield: mp 85−95 °C; **^{1}H NMR (500 MHz, $CDCl_3$)** δ = 8.13 - 8.21 (m, 2 H), 8.05 (d, *J*=7.78 Hz, 2 H), 7.52 - 7.57 (m, 2 H), 7.46 - 7.51 (m, 2 H), 7.39 - 7.43 (m, 2 H), 7.31 - 7.38 (m, 1 H), 7.28 (d, *J*=8.55 Hz, 2 H), 7.22 - 7.25 (m, 1 H), 4.19 - 4.29 (m, 4 H), 1.85 - 1.96 (m, 4 H), 0.92 - 1.00 (m, 6 H); **^{13}C{^{1}H} NMR (125 MHz, $CDCl_3$)** δ = 140.8, 139.4, 139.2, 129.2, 129.0, 128.2, 126.3, 124.5, 123.4, 123.3, 123.1, 121.8, 120.5, 119.2, 112.0, 111.5, 110.5, 110.2, 109.0, 44.9, 44.7, 22.3, 22.3, 22.2, 11.8, 11.7; **HRMS (ESI-TOF) m/z** calculated for $C_{32}H_{28}N_2S$ 472.1968 [M], measured 472.1927 [M].

Synthesis of 2-(10-propyl-10*H*-phenothiazin-3-yl)-3-(9-propyl-9*H*-carbazol-3-yl)buta-1,3-diene-1,1,4,4-tetracarbonitrile (14)

In a 100 mL round-bottomed flask, TCNE (40 mg, 0.3028 mmol) was added to a solution of compound **13** (130 mg, 0.2753 mmol) in CH_2Cl_2 (20 mL) under an argon atmosphere. The mixture was stirred for 12 h at RT. The solvent was removed in a vacuum, and the product was purified by column chromatography with DCM/hexane (2:1, v/v) as eluent to yield **14** as a dark color solid with 75% yield: mp 144−155 °C; **^{1}H NMR (500 MHz, $CDCl_3$)** δ = 8.54 (d, *J*=1.83 Hz, 1 H), 8.13 (d, *J*=7.78 Hz, 1 H), 7.92 (dd, *J*=8.85, 1.83 Hz, 1 H), 7.77 (dd, *J*=8.85, 2.29 Hz, 1 H), 7.54 - 7.59 (m, 1 H), 7.48 (d, *J*=1.98 Hz, 1 H), 7.33 - 7.37 (m, 2 H), 7.14 - 7.19 (m, 1 H), 7.03 - 7.10 (m, 2 H), 6.96 - 7.00 (m, 1 H), 6.86 - 6.90 (m, 2 H), 4.28 - 4.34 (m, 2 H), 3.83 - 3.89 (m, 2 H), 1.92 - 1.99 (m, 2 H), 1.83 - 1.89 (m, 2 H), 1.03 - 1.07 (m, 3 H), 0.97 - 1.01 (m, 3 H); **^{13}C{^{1}H} NMR (125 MHz, $CDCl_3$)** δ = 166.9, 165.1, 151.1, 149.1, 145.4, 144.0, 142.0, 141.4, 138.9, 130.6, 130.4, 127.9, 127.7, 127.6,

127.5, 125.4, 125.1, 124.4, 124.3, 124.1, 123.9, 123.5, 123.4, 123.3, 122.7, 122.4, 121.8, 121.3, 121.2, 119.0, 118.8, 116.1, 115.0, 113.6, 113.1, 112.5, 111.2, 112.2, 110.5, 110.2, 109.8, 80.9, 80.4, 49.9, 45.1, 34.9, 34.5, 34.4, 31.9, 31.5, 31.4, 30.2, 30.1, 29.7, 29.3, 22.7, 22.3, 20.0, 14.1, 11.7, 11.7, 11.1; **HRMS (ESI-TOF) m/z** calculated for $C_{38}H_{28}N_6S$ + Na 623.1988 $[M + Na]^+$, measured 623.2057 $[M + Na]^+$.

Synthesis of 2-(4-(3,3-dicyano-1-(10-propyl-10*H*-phenothiazin-3-yl)-2-(9-propyl-9*H*-carbazol-3-yl)allylidene)cyclohexa-2,5-dien-1-ylidene)malononitrile (15)

In a 100 mL round-bottomed flask, TCNQ (48 mg, 0.2329 mmol) was added to a solution of compound **13** (100 mg, 0.2117 mmol) in DCE (20 mL). The mixture was heated at 60 °C in an oil bath for 18 h. After cooling to room temperature, the solvents were removed under vacuum, and the product was purified by column chromatography with DCM/hexane (3:1, v/v) as the eluent to yield **15** as a dark-colored solid with 70%yield: mp 162−175 °C; **^{1}H NMR (500 MHz, $CDCl_3$) δ** = 8.48 (d, *J*=1.68 Hz, 1 H), 8.04 - 8.13 (m, 1 H), 7.78 - 7.90 (m, 1 H), 7.59 - 7.68 (m, 1 H), 7.52 - 7.58 (m, 2 H), 7.42 - 7.47 (m, 2 H), 7.30 - 7.34 (m, 2 H), 7.21 - 7.24 (m, 1 H), 7.12 - 7.17 (m, 1 H), 7.02 - 7.10 (m, 3 H), 6.78 - 6.88 (m, 3 H), 4.29 (q, *J*=6.87 Hz, 2 H), 3.81 (q, *J*=7.68 Hz, 2 H), 1.90 - 1.96 (m, 2 H), 1.80 - 1.86 (m, 2 H), 0.97 - 1.03 (m, 6 H); **^{13}C{^{1}H} NMR (125 MHz, CDCl3) δ** = 171.0, 154.2, 152.8, 150.4, 148.6, 143.5, 142.9, 142.4, 142.3, 141.4, 141.3, 136.2, 134.9, 134.6, 134.5, 133.4, 133.3, 132.0, 130.5, 129.5, 129.4, 128.3, 127.9, 127.8, 127.6, 127.3, 126.2, 125.9, 125.8, 125.6, 124.7, 124.3, 124.2, 123.9, 123.8, 123.4, 123.0, 122.8, 122.5, 122.4, 121.0, 120.6, 116.1, 116.0, 115.3, 114.9, 113.9, 113.8, 113.4, 109.9, 109.8, 109.7, 81.6, 75.5, 49.8, 49.7, 45.1, 45.1, 29.7, 22.4, 22.3, 20.1, 20.0, 14.1, 11.8, 11.8, 11.2, 11.1; **HRMS (ESI-TOF) m/z** calculated for $C_{44}H_{32}N_6S$ + H 677.2482 $[M + H]^+$, measured 677.2276 $[M + H]^+$.

Synthesis of 10-propyl-3,7-bis((9-propyl-9*H*-carbazol-3-yl)ethynyl)-10*H*-phenothiazine (16)

In a 100 mL round-bottomed flask, 3,7-diethynyl-10-propyl-10*H*-phenothiazine **4** (500 mg, 1.727 mmol) and 3-bromo-9-propyl-9*H*-carbazole (1.244 g, 4.319 mmol) were purged under nitrogen and bis(triphenylphosphine)palladium (II)dichloride (80 mg) and copper(I) iodide (2 - 5 mg) were added in anhydrous triethylamine (20 mL) and tetrahydrofuran (20 mL), the reaction mixture was stirred and refluxed for 16 h at 60 °C in an oil bath. Then the solvent was evaporated under a vacuum. The residue was dissolved in dichloromethane, and this solution was washed with water for several times, dried with anhydrous Na_2SO_4, and filtered off. The crude was purified by column chromatography using dichloromethane-hexane (1/3 v/v) as eluent to give an oily yellowish of **16** with 70% yield: mp 105−110 °C; **^{1}H NMR (500 MHz, $CDCl_3$)** δ = 8.27 (s, 2 H), 8.09 (d, *J* = 7.8 Hz, 2 H), 7.63 - 7.58 (m, *J* = 8.4 Hz, 2 H), 7.47 (d, *J* = 7.6 Hz, 2 H), 7.43 - 7.39 (m, 2 H), 7.38 (s, 1 H), 7.36 - 7.34 (m, 2 H), 7.34 - 7.31 (m, 3 H), 7.27 (br. s., 1 H), 7.24 (s, 1 H), 6.83 - 6.79 (m, *J* = 8.2 Hz, 2 H), 4.28 (t, *J* = 7.2 Hz, 4 H), 3.83 (t, *J* = 7.1 Hz, 2 H), 1.96 - 1.89 (m, 4 H), 1.88 - 1.82 (m, 2 H), 1.04 (t, *J* = 7.3 Hz, 3 H), 0.98 (t, *J* = 7.3 Hz, 6 H); **^{13}C{^{1}H} NMR (125 MHz, $CDCl_3$)** δ = 146.1, 144.9, 144.8, 140.9, 140.1, 131.8, 130.9, 130.6, 130.0, 129.2, 128.2, 127.5, 127.4, 127.3, 126.3, 126.0, 124.8, 124.8, 124.3, 124.2, 124.0, 123.8, 123.3, 123.1, 122.9, 122.8, 122.6, 122.5, 121.8, 120.5, 119.3, 117.7, 115.6, 115.5, 115.4, 115.1, 115.1, 115.0, 113.4, 109.0, 108.8, 90.6, 86.9, 49.3, 49.3, 44.9, 44.8, 22.3, 22.3, 20.1, 20.1, 11.8, 11.8, 11.3, 11.3; **HRMS (ESI-TOF) m/z** calculated for $C_{49}H_{41}N_3S$ 703.3016 [M], measured 703.3035 [M].

Synthesis of 3,3'-(10-propyl-10*H*-phenothiazine-3,7-diyl)bis(2-(9-propyl-9*H*-carbazol-3-yl)buta-1,3-diene-1,1,4,4-tetracarbonitrile) (17)

In a 100 mL round-bottomed flask, TCNE (48 mg, 0.3728 mmol)) was added to a solution of **16** (105 mg, 0.1491 mmol) in CH_2Cl_2 (20 mL) under an argon atmosphere. The mixture was stirred for 36 h at 40 °C in an oil bath. The solvent was removed in a vacuum, and the product was purified by column chromatography with DCM/hexane (2:1, v/v) as

eluent to yield **17** as a dark color solid with 65% yield: mp 195−205 °C; **^{1}H NMR (500 MHz, CHLOROFORM-d) δ** = 8.54 (d, *J* = 1.7 Hz, 1 H), 8.41 (d, *J* = 1.8 Hz, 1 H), 8.22 (d, *J* = 1.8 Hz, 1 H), 8.12 (d, *J* = 7.8 Hz, 1 H), 7.95 (dd, *J* = 1.9, 8.9 Hz, 1 H), 7.89 (dd, *J* = 1.9, 8.9 Hz, 1 H), 7.81 - 7.74 (m, 2 H), 7.65 (dd, *J* = 1.8, 8.7 Hz, 1 H), 7.60 - 7.55 (m, 1 H), 7.55 - 7.45 (m, 4 H), 7.39 - 7.32 (m, 4 H), 6.99 - 6.90 (m, 2 H), 4.30 (td, *J* = 7.2, 10.7 Hz, 4 H), 3.87 (t, *J* = 9.4 Hz, 2 H), 1.94 (td, *J* = 7.7, 15.1 Hz, 4 H), 1.89 - 1.83 (m, 2 H), 1.06 (dt, *J* = 3.5, 7.2 Hz, 3 H), 1.02 - 0.96 (m, 6 H); **^{13}C{^{1}H} NMR (125 MHz, CHLOROFORM-d) δ** = 166.2, 165.4, 144.1, 141.5, 130.6, 128.0, 127.8, 127.4, 124.5, 124.0, 123.5, 123.2, 123.1, 121.4, 121.2, 116.1, 116.1, 113.4, 112.5, 111.6, 111.4, 110.7, 110.4, 110.0, 83.9, 80.2, 45.2, 31.4, 30.2, 22.3, 11.8, 11.1; **HRMS (ESI-TOF) m/z** calculated for $C_{61}H_{41}N_{11}S$ + Na 982.3159 $[M + Na]^+$, measured 982.2119 $[M + Na]^+$.

Synthesis of 2,2'-((10-propyl-10*H*-phenothiazine-3,7-diyl)bis(2-(4-(dicyanomethylene)cyclohexa-2,5-dien-1-ylidene)-1-(9-propyl-9*H*-carbazol-3-yl)ethan-2-yl-1-ylidene))dimalononitrile (18)

In a 100 mL round-bottomed flask, TCNQ (76 mg, 0.3728 mmol) was added to a solution of compound **16** (105 mg, 0.1491 mmol) in DCE (20 mL). The mixture was heated at 80 °C in an oil bath for 48 h. After cooling to room temperature, the solvents were removed under vacuum, and the product was purified by column chromatography with DCM as the eluent to yield **18** as a dark-colored solid with 60% yield: mp 280−290 °C; **^{1}H NMR (500 MHz, CHLOROFORM-d) δ** = 8.45 (s, 1 H), 8.12 - 8.04 (m, 2 H), 8.03 - 8.00 (m, 1 H), 7.81 (d, *J* = 8.9 Hz, 1 H), 7.57 - 7.52 (m, 4 H), 7.48 - 7.44 (m, 4 H), 7.38 (br. s., 2 H), 7.33 (d, *J* = 4.7 Hz, 3 H), 7.31 (br. s., 2 H), 7.24 - 7.16 (m, 3 H), 7.06 (d, *J* = 11.0 Hz, 1 H), 7.02 (d, *J* = 9.5 Hz, 1 H), 6.96 (s, 1 H), 6.84 (d, *J* = 8.7 Hz, 1 H), 6.81 - 6.78 (m, 1 H), 4.29 (t, *J* = 7.0 Hz, 4 H), 3.76 (td, *J* = 8.0, 15.7 Hz, 2 H), 1.97 - 1.90 (m, 4 H), 1.78 (td, *J* = 7.9, 15.6 Hz, 2 H), 0.99 (q, *J* = 6.9 Hz, 9 H); **^{13}C{^{1}H} NMR (125 MHz, CHLOROFORM-d) δ** = 168.8, 151.9, 147.3, 142.5, 141.3, 136.1, 134.2, 133.5, 131.1, 130.6, 129.3, 129.2, 128.1, 127.5, 126.4, 126.0, 125.9, 124.6, 124.1, 123.4,

122.3, 121.2, 120.9, 120.7, 115.8, 114.1, 113.9, 113.3, 110.1, 109.8, 84.2, 81.4, 50.2, 45.1, 22.7, 22.4, 11.8, 11.0; **HRMS (ESI-TOF) m/z** calculated for $C_{73}H_{49}N_{11}S$ + Na 1134.3785 $[M + Na]^+$, measured 1134.3519 $[M + Na]^+$.

3.8. Conclusion

In conclusion, a series of donor-acceptor functionalized symmetrical and unsymmetrical phenothiazine derivatives **1–18** were synthesized by the Pd-catalyzed Sonogashira cross-coupling followed by [2+2] cycloaddition electrocyclic ring-opening reaction with TCNE and TCNQ acceptors. The di-DCNQ substituted phenothiazine derivatives **6**, **12**, and **18** show a strong intramolecular charge transfer (ICT) band at a low energy region as compared to mono-DCNQ substituted phenothiazine derivatives **3**, **9**, and **15** due to strong donor-acceptor interaction. The electrochemical analysis reveals reduction waves at low potential due to the TCBD and DCNQ acceptors, whereas oxidation waves at high potential are due to the donor (phenothiazine, thiophene, and carbazole). In comparison to TCBD, the incorporation of DCNQ stabilizes the LUMO energy level considerably. The photophysical and electrochemical data show that the incorporation of TCBD and the DCNQ acceptor into ethynyl phenothiazine derivatives resulted in stronger D–A interactions that led to a lower HOMO–LUMO energy gap. The thermogravimetric analysis (TGA) of phenothiazine derivatives **1–18** shows that the TCBD substituted phenothiazine derivative **2** exhibits the highest thermal stability as compared to other phenothiazine derivatives. The computational studies show that the electron density on HOMO energy level is mainly localized over the donor phenothiazine, thiophene, and carbazole units, whereas the electron density on LUMO energy level is concentrated over the acceptor TCBD and DCNQ units. The proposed symmetrical and unsymmetrical phenothiazine derivatives **1–18** provide a new approach for the development of donor-acceptor chromophores, which are useful for a variety of optoelectronic applications.

3.9. References

[1] (a) Poddar, M., Gautam, P., Rout, Y., Misra, R. (2017). Donor–acceptor phenothiazine functionalized BODIPYs. *Dyes and Pigments*, *146*, 368–373. (DOI: 10.1016/j.dyepig.2017.07.017); (b) Chu, T. Y., Lu, J., Beaupre, S., Zhang, Y., Pouliot, J. R., Wakim, S., Zhou, J., Leclerc, M., Li, Z., Ding, J., Tao, Y. (2011). Synthesis, Characterization, and Transistor and Solar Cell Applications of a Naphthobisthiadiazole-Based Semiconducting Polymer. *Journal of the American Chemical Society*, *133*, 4250–4253. (DOI: 10.1021/ja200314m).

[2] (a) Sonar, P., Singh, S. P., Li, Y., Soh, M. S., Dodabalapur, A. (2010). A low-bandgap diketopyrrolopyrrole-benzothiadiazole-based copolymer for high-mobility ambipolar organic thin-film transistors. *Advanced Materials*, *22*, 5409–5413. (DOI: 10.1002/adma.201002973); (b) Kato, S., Furuya, T., Kobayashi, A., Nitani, M., Ie, Y., Aso, Y., Yoshihara, T., Tobita, S., Nakamura, Y. (2012). π-Extended thiadiazoles fused with thienopyrrole or indole moieties: synthesis, structures, and properties. *The Journal of Organic Chemistry*, *77*, 7595–7606. (DOI: 10.1021/jo301458m).

[3] (a) Lin, Y., Fan, H., Li, Y., Zhan, X. (2012). Thiazole-based organic semiconductors for organic electronics. *Advanced Materials, 24*, 3087–3106. (DOI: 10.1002/adma.201200721); (b) Meyer, T., Ogermann, D., Pankrath, A., Kleinermanns, K., Müller, T. J. J. (2012). Phenothiazinyl Rhodanylidene Merocyanines for Dye-Sensitized Solar Cells. *The Journal of Organic Chemistry*, *77*, 3704–3715. (DOI: 10.1021/jo202608w); (c) Parker, T. C., Patel, D. G., Moudgil, K., Barlow, S., Risko, C., Brédas, J. L., Reynolds, J. R., Marder, S. R. (2015). Thia- and Selena-diazole containing polymers for near-infrared light-emitting diodes. *Materials Horizons*, *2*, 22. (DOI: 10.1039/C4MH00102H).

[4] (a) Roncali, J. (2009). Molecular Bulk Heterojunctions: An Emerging Approach to Organic Solar Cells. *Accounts of*

Chemical Research, *42*, 1719–1730. (DOI: 10.1021/ar900041b); (b) Bureš, F., Pytela, O., Kivala, M., Diederich, F. (2011). Solvatochromism as an efficient tool to study N,N-dimethylamino- and cyano-substituted π-conjugated molecules with an intramolecular charge-transfer absorption. *The Journal of Physical Organic Chemistry*, *24*, 274–281. (DOI: 10.1002/poc.1744); (c) Sheokand, M., Tiwari, N. J., Misra, R. (2023). Near-IR absorbing 1,1,4,4-tetracyanobutadiene functionalized phenothiazine sulfones. *Organic & Biomolecular Chemistry*, *21*, 3896–3905. (DOI: 10.1039/D3OB00361B).

[5] (a) Khan, F., Mahmoudi, M., Gupta, P. K., Volyniuk, D., Grazulevicius, J. V., Misra, R. (2023). Mechanochromic Materials Based on Tetraphenylethylene-Substituted Phenothiazines: Substituent-Dependent Hypsochromic and Bathochromic Switching of Emission. *The Journal of Physical Chemistry*, *C*, *127*, 1643–1654. (DOI: 10.1021/acs.jpcc.2c07010); (b) Michinobu, T., Satoh, N., Cai, J., Li, Y., Han, L. (2014). Novel design of organic donor–acceptor dyes without carboxylic acid anchoring groups for dye-sensitized solar cells. *Journal of Materials Chemistry C*, *2*, 3367–3372. (DOI: 10.1039/c3tc32165g).

[6] Wang, J. L., Xiao, Q., Pei, J. (2010). Benzothiadiazole-based D–π-A– π-D organic dyes with tunable band gap: Synthesis and photophysical properties. *Organic Letters*, *12*, 4164–4167. (DOI: 10.1021/ol101754q).

[7] Zhang, H., Wan, X., Xue, X., Li, Y., Yu, A., Chen, Y. (2010). Selective tuning of the HOMO–LUMO gap of carbazole-based donor–acceptor–donor compounds toward different emission colors. *European Journal of Organic Chemistry*, *2010*, 1681–1687. (DOI: 10.1002/ejoc.200901167).

[8] Khan, F., Misra, R. (2023). Recent advances in the development of phenothiazine and its fluorescent derivatives for

optoelectronic applications. *Journal of Materials Chemistry C, 11*, 2786–2825. (DOI: 10.1039/D2TC04326B).

[9] Hauck, M., Schonhaber, J., Zucchero, A. J., Hardcastle, K. I., Muller, T. J. J., Bunz, U. H. F. (2007). Phenothiazine cruciforms synthesis and metallochromic properties. *The Journal of Organic Chemistry*, *72*, 6714–6725. (DOI: 10.1021/jo070922l).

[10] Gupta, R. R., Ojha, K. G. (1988). Phenothiazines and 1, 4-benzothiazines: chemical and biomedical aspects. *Elsevier Amsterdam, p*. 163-269.

[11] (a) Hauck, M., Stolte, M., Schönhaber, J., Kuball, H. G., Muller, T. J. J. (2011). Synthesis, Electronic, and Electro-Optical Properties of Emissive Solvatochromic Phenothiazinyl Merocyanine Dyes. *Chemistry a European Journal, 17*, 9984–9998. (DOI: 10.1002/chem.201100592); (b) Sailer, M., Gropeanu, R. A., Müller, T. J. J. (2003). Practical Synthesis of Iodo Phenothiazines: A Facile Access to Electrophore Building Blocks. *The Journal of Organic Chemistry*, *68*, 7509–7512. (DOI: 10.1021/jo034555z).

[12] (a) Müller, T. J. J. (1999). First synthesis and electronic properties of ring-alkynylated phenothiazines. *Tetrahedron Letters*, *40*, 6563– 6566. (DOI: 10.1016/S0040-4039(99)01402-1); (b) Krämer, C. S., Zeitler, K.; Müller, T. J. J. (2000). Synthesis of functionalized ethynylphenothiazine fluorophores. *Organic Letters.*, *2*, 3723– 3726. (DOI: 10.1021/ol0066328); (c) Krämer, C. S., Müller, T. J. J. (2003). Synthesis and electronic properties of alkynylated phenothiazines. *European Journal of Organic Chemistry, 2003*, 3534– 3548. (DOI: 10.1002/ejoc.200300250).

[13] Srinivas, K., Kumar, C. R., Reddy, M. A., Bhanuprakash, K., Rao, V. J., Giribabu, L. (2011). D−π–A organic dyes with carbazole as donor for dye sensitized solar cells. *Synthetic Metals, 161*, 96–105. (DOI: 10.1016/j.synthmet.2010.11.004).

[14] Wu, C., Decker, E. R., Blok, N., Bui, H., You, T. J., Wang, J., Bourgoyne, A. R., Knowles, V., Berens, K. L., Holland, G. W., Brock, T. A., Dixon, R. A. F. (2004). Discovery, Modeling, and Human Pharmacokinetics of N-(2-Acetyl-4,6-dimethylphenyl)-3-(3,4-dimethylisoxazol-5-ylsulfamoyl)-thiophene-2-carboxamide (TBC3711), a Second Generation, ETA Selective, and Orally Bioavailable Endothelin Antagonist. *The Journal of Medicinal Chemistry*, *47*, 1969–1986. (DOI: 10.1021/jm030528p).

[15] Zhang, F., Wu, D., Xu, Y., Feng, X. (2011). Thiophene-based conjugated oligomers for organic solar cells. *Journal of Materials Chemistry C*, *21*, 17590–17600. (DOI: 10.1039/c1jm12801a).

[16] (a) Halik, M., Klauk, H., Zschieschang, U., Schmid, G., Ponomarenko, S., Kirchmeyer, S., Weber, W. (2003). Relationship Between Molecular Structure and Electrical Performance of Oligothiophene Organic Thin Film Transistors. *Advanced Materials*, *15*, 917–922. (DOI: 10.1002/adma.200304654); (b) Rost, C., Karg, S., Riess, W., Loi, M. A., Murgia, M., Muccini, M. (2004). Ambipolar light-emitting organic field-effect transistor. *Applied Physics Letters*, *85*, 1613–1615. (DOI: 10.1063/1.1785290).

[17] Vaitkeviciene, V., Grigalevicius, S., Grazulevicius, J. V., Jankauskas, V., Syromyatnikov, V. G. (2006). Hole-transporting [3,3′]bicarbazolyl-based polymers and well-defined model compounds. *European Polymer Journal*, *42*, 2254–2260. (DOI: 10.1016/j.eurpolymj.2006.06.023).

[18] (a) Segura, J. L. (1998). The chemistry of electroluminescent organic materials. *Acta Polymerica*, *49*, 319–344. (DOI: 10.1002/(SICI)1521-4044(199807)49:7<319::AID-APOL319>3.0.CO;2-Q); (b) Kraft, A., Grimsdale, A. C., Holmes, A. B. (1998). Electroluminescent Conjugated Polymers-Seeing Polymers in a New Light. *Angewandte Chemie*

International Edition,*37*, 402–428. (DOI: 10.1002/(SICI)1521-3773(19980302)37:4<402::AID-ANIE402>3.0.CO;2-9).

[19] (a) Zatsikha, Y. V., Maligaspe, E., Purchel, A. A., Didukh, N. O., Wang, Y., Kovtun, Y. P., Blank, D. A., Nemykin, V. N. (2015). Tuning Electronic Structure, Redox, and Photophysical Properties in Asymmetric NIR-Absorbing Organometallic BODIPYs. *Inorganic chemistry*, *54*, 7915–7928. (DOI: 10.1021/acs.inorgchem.5b00992); (b) Jordan, M., Kivala, M., Boudon, C., Gisselbrecht, J. P., Schweizer, W. B., Seiler, P., Diederich, F. (2011). Switching the regioselectivity in cycloaddition-retro-electrocyclizations between donor-activated alkynes and the electron-accepting olefins TCNE and TCNQ. *Chemistry – An Asian Journal*, *6*, 396–401. (DOI: 10.1002/asia.201000539); (c) Patil, Y., Butenschön, H.; Misra, R. (2023). Tetracyanobutadiene Bridged Push-Pull Chromophores: Development of New Generation Optoelectronic Materials. *The Chemical Record*, *23* (1), e202200208. (DOI: 10.1002/tcr.202200208); (d) Michinobu, T., Boudon, C., Gisselbrecht, J. P., Seiler, P., Frank, B., Moonen, N. N. P., Gross, M., Diederich, F. (2006). Donor-substituted 1,1,4,4-tetracyanobutadienes (TCBDS): new chromophores with efficient intramolecular charge-transfer interactions by atom-economic synthesis. *Chemistry – A European Journal*, *12*, 1889– 1905. (DOI: 10.1002/chem.200501113).

[20] (a) Philippe, C., Bui, A. T., Beau, M., Bloux, H., Riobé, F., Mongin, O., Roisnel, T., Cordier, M., Paul, F., Lemiègre, L., Trolez, Y. (2022). Synthesis and Photophysical Properties of 1,1,4,4- Tetracyanobutadienes Derived from Ynamides Bearing Fluorophores. *Chemistry – A European Journal*, *28*, e202200025. (DOI: 10.1002/chem.202200025); (b) Philippe, C., Bui, A. T., Batsongo-Boulingui, S., Pokladek, Z., Matczyszyn, K., Mongin, O., Lemiègre, L., Paul, F., Hamlin, T. A., Trolez, Y. (2021). 1,1,4,4-Tetracyanobutadiene-

Functionalized Anthracenes: Regioselectivity of Cycloadditions in the Synthesis of Small Near-IR Dyes. *Organic Letters*, *23*, 2007–2012. (DOI: 10.1021/acs.orglett.1c00136); (c) Philippe, C., Melan, J., Barsella, A., Vives, T., Leroux, Y. R., Robin-Le Guen, F., Lemiègre, L., Jacquemin, D., Gauthier, S., Trolez, Y. (2023). A comprehensive study of tetracyanobutadiene push-pull chromophores derived from γ-pyranylidene. *Tetrahedron Chem*, *5*, 100036. (DOI: 10.1016/j.tchem.2023.100036); (d) Dar, A. H., Gowri, V., Gopal, A., Muthukrishnan, A., Bajaj, A., Sartaliya, S., Selim, A., Ali, Md. E., Jayamurugan, G. (2019). Designing of Push–Pull Chromophores with Tunable Electronic and Luminescent Properties Using Urea as the Electron Donor. *The Journal of Organic Chemistry*, *84*, 8941–8947. (DOI: 10.1021/acs.joc.9b00841); (e) Neethu, K. M., Nag, K., Dar, A. H., Bajaj, A., Gopal, S. A., Gowri, V., Nagpure, M., Sartaliya, S., Sharma, R., Solanki, A. K., Ali, Md. E., Muthukrishnan, A., Jayamurugan, G. (2023). A study of [2 + 2] cycloaddition–retroelectrocyclization in water: observation of substrate-driven transient-nanoreactor-induced new reactivity. *Organic & Biomolecular Chemistry*, *21*, 2922. (DOI: 10.1039/D3OB00053B); (f) Erden, K., Dengiz, C. (2022). 3-Alkynylindoles as Building Blocks for the Synthesis of Electronically Tunable Indole-Based Push–Pull Chromophores. *The Journal of Organic Chemistry*, *87*, 4385–4399. (DOI: 10.1021/acs.joc.2c00067); (g) Zhang, Z., Gou, G., Wan, J., Li, H., Wang, M., Li, L. (2022). Synthesis, Structure, and Significant Energy Gap Modulation of Symmetrical Silafluorene-Cored Tetracyanobutadiene and Tetracyanoquinodimethane Derivatives. *The Journal of Organic Chemistry*, *87*, 2470–2479. (DOI: 10.1021/acs.joc.1c02382); (h) Mammadova, F., Inyurt, F. C., Barsella, A., Dengiz, C. (2023). Cyano-rich donor-acceptor-donor-type NLOphores

containing dialkylated triazene and aniline groups. *Dyes and Pigments*, *209*, 110894. (DOI: 10.1016/j.dyepig.2022.110894).

[21] (a) Sekita, M., Ballesteros, B., Diederich, F., Guldi, D. M., Bottari, G., Torres, T. (2016). Intense Ground-State Charge-Transfer Interactions in Low-Bandgap, Panchromatic Phthalocyanine-Tetracyanobuta-1,3-diene Conjugates. *Angewandte Chemie International Edition*, *55*, 5560–5564. (DOI: 10.1002/anie.201601258); (b) Winterfeld, K. A., Lavarda, G., Guilleme, J., Sekita, M., Guldi, D. M., Torres, T., Bottari, G. (2017). Subphthalocyanines Axially Substituted with a Tetracyanobuta-1,3-diene-Aniline Moiety: Synthesis, Structure, and Physicochemical Properties. *Journal of the American Chemical Society*, *139*, 5520–5529. (DOI: 10.1021/jacs.7b01460).

[22] Leliège, A., Blanchard, P., Rousseau, T., Roncali, J. (2011). Triphenylamine /Tetracyanobutadiene -Based D-A-D π-Conjugated Systems as Molecular Donors for Organic Solar Cells. *Organic Letters, 13*, 3098–3101. (DOI: 10.1021/ol201002j).

[23] Bures, F., Schweizer, W. B., May, J. C., Boudon, C., Gisselbrecht, J. P., Gross, M., Biaggio, I., Diederich, F. (2007). Property Tuning in Charge-Transfer Chromophores by Systematic Modulation of the Spacer between Donor and Acceptor. *Chemistry – A European Journal*, *13*, 5378–5387. (DOI: 10.1002/chem.200601735).

[24] Wang, J. L., Xiao, Q., Pei, J. (2010). Benzothiadiazole-based D–π-A– π-D organic dyes with tunable band gap: Synthesis and photophysical properties. *Organic Letters, 12*, 4164–4167. (DOI: 10.1021/ol101754q).

[25] Zhang, W. W., Mao, W. L., Hu, Y. X., Tian, Z. Q., Wang, Z. L., Meng, Q. J. (2009). Phenothiazine–Anthraquinone Donor–Acceptor Molecules: Synthesis, Electronic Properties, and DFT-TDDFT Computational Study. *The Journal of Physical Chemistry A*, *113*, 9997–10004. (DOI: 10.1021/jp903390v).

[26] (a) Michinobu, T., May, J. C., Lim, J. H., Boudon, C., Gisselbrecht, J. P., Seiler, P., Gross, M., Biaggio, I., Diederich, F. (2005). A new class of organic donor–acceptor molecules with large third-order optical nonlinearities. *Chemical Communications*, 737–739. (DOI: 10.1039/B417393G); (b) Michinobu, T., Boudon, I., Gisselbrecht, J. P., Seiler, P., Frank, B., Moonen, N. N. P., Gross, M., Diederich, F. (2006). Donor-substituted 1,1,4,4-tetracyanobutadienes (TCBDS): new chromophores with efficient intramolecular charge-transfer interactions by atom-economic synthesis. *Chemistry – A European Journal*, *12*, 1889–1905. (DOI: 10.1002/chem.200501113).

[27] (a) Yamada, M., Schweizer, W. B., Schoenebeck, F., Diederich, F. (2010). Unprecedented thermal rearrangement of push–pull-chromophore–[60] fullerene conjugates: formation of chiral 1,2,9,12-tetrakis-adducts. *Chemical Communications*, *46*, 5334–5336. (DOI: 10.1039/c0cc00881h); (b) Kivala, M., Boudon, C., Gisselbrecht, J. P., Seiler, P., Gross, M., Diederich, F. (2007). A novel reaction of 7, 7, 8, 8-tetracyanoquinodimethane (TCNQ): charge-transfer chromophores by [2+ 2] cycloaddition with alkynes. *Chemical Communications*, 4731–4733. (DOI: 10.1039/b713683h).

[28] (a) Michinobu, T. (2008). Click-type reaction of aromatic polyamines for improvement of thermal and optoelectronic properties *Journal of the American Chemical Society*, *130*, 14074–14075. (DOI: 10.1021/ja8061612); (b) Li, Y., Tsuboi, K., Michinobu, T. (2010). Double Click Synthesis and Second-Order Nonlinearities of Polystyrenes Bearing Donor-Acceptor Chromophores. *Macromolecules*, *43*, 5277–5286. (DOI: 10.1021/ma100869m); (c) Michinobu, T. (2011). Adapting semiconducting polymer doping techniques to create new types of click post functionalization. *Chemical Society Reviews*, *40*, 2306–2316. (DOI: 10.1039/c0cs00205d); (d) Fujita, T.; Tsuboi, K.; Michinobu, T. (2011). High-Yielding

Alkyne-Tetracyanoethylene Addition Reactions: A Powerful Tool for Analyzing Alkyne-Linked Conjugated Polymer Structures. *Macromolecular Chemistry and Physics, 212*, 1758–1766. (DOI: 10.1002/macp.201100198).

[29] (a) Shoji, T., Ito, S., Toyota, K., Yasunami, M., Morita, N. (2008). Synthesis, Properties, and Redox Behavior of Mono-, Bis-, and Tris[1,1,4,4,-tetracyano-2-(1-azulenyl)-3-butadienyl] Chromophores Binding with Benzene and Thiophene Cores. *Chemistry – A European Journal, 14*, 8398–8408. (DOI: 10.1002/chem.200701981); (b) Shoji, T., Ito, S., Toyota, K., Iwamoto, T., Yasunami, M., Morita, N. (2009). Reactions between 1-Ethynylazulenes and 7,7,8,8-Tetracyanoquinodimethane (TCNQ): Preparation, Properties, and Redox Behavior of Novel Azulene-Substituted Redox-Active Chromophores. *European Journal of Organic Chemistry, 2009*, 4316–4324. (DOI: 10.1002/ejoc.200900539).

[30] Bui, A. T., Philippe, C., Beau, M., Richy, N., Cordier, M., Roisnel, T., Lemiègre, L., Mongin, O., Paul, F., Trolez, Y. (2020). Synthesis, characterization, and unusual near-infrared luminescence of 1,1,4,4-tetracyanobutadiene derivatives. *Chemical Communications*, *56*, 3571–3574. (DOI: 10.1039/C9CC09560H).

[31] Kato, S., Noguchi, H., Jin, S., Nakamura, Y. (2016). Synthesis and Electronic, Optical, and Electrochemical Properties of a Series of Tetracyanobutadiene-Substituted Carbazoles. *Asian Journal of Organic Chemistry, 5*, 246–256. (DOI: 10.1002/ajoc.201500431).

[32] Kraußе, N., Kielmann, M., Ma, J., Butenschön, H. (2015). Reactions of Alkynyl- and 1,1-Dialkynylferrocenes with Tetracyanoethylene–Unanticipated Addition at the Less Electron-Rich of Two Triple Bonds. *European Journal of Organic Chemistry, 2015*, 2622–2631. (DOI: 10.1002/ejoc.201500105).

[33] Poddar, M., Misra, R. (2017). NIR Absorbing Donor–Acceptor Based 1,1,4,4–Tetracyanobuta–1,3–Diene (TCBD) and Cyclohexa–2,5–Diene–1,4–Ylidene–Expanded TCBD Substituted Ferrocenyl Phenothiazines. *Chemistry – An Asian Journal*, *12*, 2908–2915. (DOI: 10.1002/asia.201700879).

[34] Rout, Y., Gautam, P., Misra, R. (2017). Unsymmetrical and Symmetrical Push–Pull Phenothiazines. *The Journal of Organic Chemistry*, *82*, 6840–6845. (DOI: 10.1021/acs.joc.7b00991).

[35] (a) Yadav, I. S., Misra, R. (2022). Phenothiazine and phenothiazine-5,5-dioxidebased push–pull derivatives: synthesis, photophysical, electrochemical and computational studies. *New Journal of Chemistry*, *46*, 15999–16006. (DOI: 10.1039/D2NJ03089F); (b) Erden, K., Dengiz, C. (2022). 3-Alkynylindoles as Building Blocks for the Synthesis of Electronically Tunable Indole-Based Push–Pull Chromophores. *The Journal of Organic Chemistry*, *87*, 4385–4399. (DOI: 10.1021/acs.joc.2c00067); (c) Fesser, P., Iacovita, C., Wäckerlin, C., Vijayaraghavan, S., Ballav, N., Howes, K., Gisselbrecht, J. P., Crobu, M., Boudon, C., Stöhr, M., Jung, T. A., Diederich, F. (2011). Visualizing the Product of a Formal Cycloaddition of 7,7,8,8-Tetracyano-p- Quinodimethane (TCNQ) to an Acetylene-Appended Porphyrin by Scanning Tunneling Microscopy on Au(111). *Chemistry – A European Journal*, *17*, 5246–5250. (DOI: 10.1002/chem.201100733).

[36] Misra, R., Gautam, P. (2014). Tuning of the HOMO–LUMO gap of donor-substituted symmetrical and unsymmetrical benzothiadiazoles. *Organic & Biomolecular Chemistry*, *12*, 5448–5457. (DOI: 10.1039/c4ob00629a).

[37] Frisch, M. J., Trucks, G. W., Schlegel, G. W., Scuseria, G. E., Robb, M. A., Cheeseman, J. R., Scalmani, G., Barone, V., Petersson, G. A., Li, Nakatsuji, X., Caricato, M., Marenich, A., Bloino, J., Janesko, B. G., Gomperts, R., Mennucci, B., Hratchian, H. P., Ortiz, J. V., Izmaylov, A. F., Sonnenberg, J. L., Williams-Young, D., Ding, F., Lipparini, F., Egidi, F., Goings,

J., Peng, B., Petrone, A., Henderson, T., Ranasinghe, D., Zakrzewski, V. G., Gao, J., Rega, N., Zheng, G., Liang, W., Hada, M., Ehara, M., Toyota, K., Fukuda, R., Hasegawa, J., Ishida, M., Nakajima, T., Honda, Y., Kitao, O., Nakai, H., Vreven, T., Throssell, K., Montgomery, J. A., Peralta, Jr., J. E., Ogliaro, F., Bearpark, M., Heyd, J. J., Brothers, E., Kudin, K. N., Staroverov, V. N., Keith, T., Kobayashi, R., Normand, J., Raghavachari, K., Rendell, A., Burant, J. C., Iyengar, S. S., Tomasi, J., Cossi, M., Millam, J. M., Klene, M., Adamo, C., Cammi, R., Ochterski, J. W., Martin, R. L., Morokuma, K., Farkas, O., Foresman, J. B. and Fox, D. J. (2016). Gaussian 09, revision A.02; Gaussian, Inc.: Wallingford, CT.

Chapter 4

Near-Infrared Absorbing Donor-Acceptor Based *N*,4-dimethylbenzenesulfonamide Substituted Phenothiazine Derivatives

4.1. Introduction

In recent years, π-conjugated systems are widely used in electronic and optical devices such as organic light-emitting diodes (OLEDs), organic photovoltaics (OPVs), organic field-effect transistors (OFETs), organic photodetectors, nonlinear optics and bioimaging.[1–8] π-conjugated donor-acceptor system is a type of chromophore or system that has both electron-donating group (donor) and an electron-withdrawing group (acceptor) within its π-conjugated system.[9–13] In these π-conjugated chromophores, the heteroatom-containing cyclic systems were used to tune the photophysical and redox properties of push–pull dyes.[14, 15] Many studies have been reported on developing novel push–pull organic materials for optoelectronic applications.[16–20] Heterocyclic derivatives such as thiazoles, benzothiazoles, benzothiadiazole, phenothiazine, and many more have been explored for non-linear optics (NLO), organic light-emitting diodes (OLEDs), organic photovoltaics (OPVs), and organic field-effect transistors (OFETs).[21–26]

Phenothiazine can be easily functionalized by the aromatic electrophilic substitution reactions at the 3- & 7- positions, and nucleophilic substitution reaction at the *N*-position.[27–29] The phenothiazine derivatives possesses low reversible oxidation potential making them suitable candidates to be used as electron donor in various optoelectronic applications.[30, 31] The 1,1,2,2-tetracyanoethylene (TCNE) and 7,7,8,8-tetracyanoquinodimethane (TCNQ) are strong electron acceptors because they contain four cyano groups,[32, 33] and are highly reactive towards electron-rich alkynes, undergo [2 + 2] cycloaddition reaction to form cyclobutene rings followed by retroelectrocyclization reaction to produce 1,1,4,4-tetracyanobutadiene

(TCBD) and cyclohexa-2,5-diene-1,4-diylidene-expanded TCBD or DCNQ (DCNQ = dicyanoquinodimethane) derivatives.[34] The donor-acceptor systems containing TCBD and DCNQ acceptors are promising candidates for organic photovoltaics applications.[35] Diederich, Michinobu, Shoji, Butenschön, Kato, Paul, Nakamura and Trolez *et al*. have explored the donor-acceptor based TCBD and DCNQ functionalized derivatives as redox-active ICT chromophores for various optoelectronic applications.[36–46] Recently, our group has reported a series of donor-acceptor TCBD and DCNQ functionalized phenothiazine derivatives for optoelectronic applications.[47, 48] The TCBD and DCNQ functionalized donor-acceptor small molecules and polymers have been investigated for organic photovoltaics and nonlinear optics (NLOs).[49, 50]

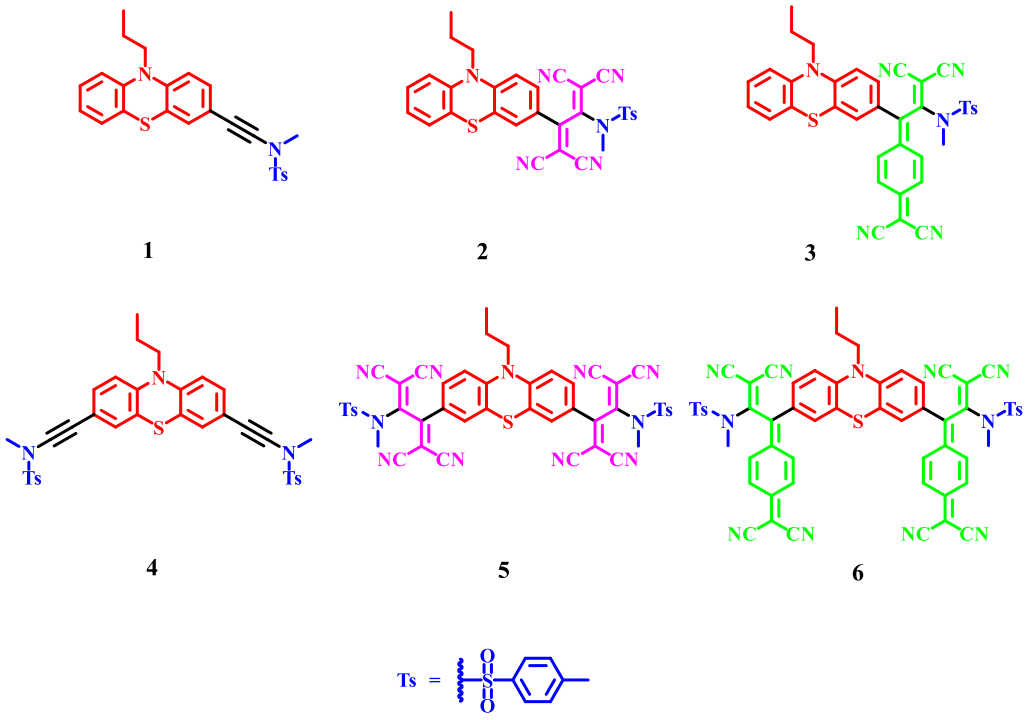

Figure 4.1. Chemical structures of donor-acceptor chromophores **1–6**.

In this manuscript, we have designed and synthesized donor-acceptor chromophores **1–6** by Corey-Fuchs reaction *via* Evano′s conditions followed by [2 + 2] cycloaddition retroelectrocyclic ring-opening reaction with strong electron acceptors TCNE and TCNQ in good yields (Figure 4.1 for structures; NTs = *N*,4-dimethylbenzenesulfonamide). Herein, our aim was to explore the

photophysical, thermal stability, and electrochemical characteristics of donor-acceptor chromophores **1–6** by introducing strong electron acceptors TCNE and TCNQ moieties. The photophysical results indicate that the DCNQ-functionalized **3** and **6** reveal a significant ICT band at the higher wavelength region in comparison to TCBD-functionalized **2** and **5** which corresponds to strong donor–acceptor (D–A) interactions.[47]

4.2. Result and Discussion

The synthesis of donor-acceptor chromophores **1–6** are shown in Scheme 4.1. The ynamides precursors **1** and **4** were synthesized by the Corey-Fuchs reaction followed by Evano′s procedure.[51] The reaction of aldehydes **PTZ-CHO** and **PTZ-(CHO)$_2$** with carbon tetrabromide and triphenylphosphine in dichloromethane at 0 °C resulted the geminal-dibromovinyl compounds **PTZ-CBr$_2$** and **PTZ-(CBr$_2$)$_2$** in 75% and 80% yield respectively, and after the Evano′s conditions using *N*-methyl-*p*-toluenesulfonamide, cesium carbonate, *N*,*N*-dimethylethylenediamine (DMEDA), and copper iodide as catalysts in 1,4-dioxane at 60 °C, **1** and **4** are formed in 60% and 65% yield, respectively. The reaction of **1** and **4** with 1.1 equivalent and 2.5 equivalent of TCNE in dichloromethane at room temperature resulted in **2** and **5** in 85% and 65%, respectively. Similarly, the reaction of **1** and **4** with 1.1 equivalent and 2.5 equivalent of TCNQ in dichloroethane (DCE) at 80 °C resulted in **3** and **6** in 70% and 60%, respectively.

All the reported donor-acceptor chromophores **1–6** were purified by column chromatography using hexane/DCM as the solvent and were well-characterized by ^{1}H-NMR, ^{13}C-NMR spectroscopy and HRMS techniques.

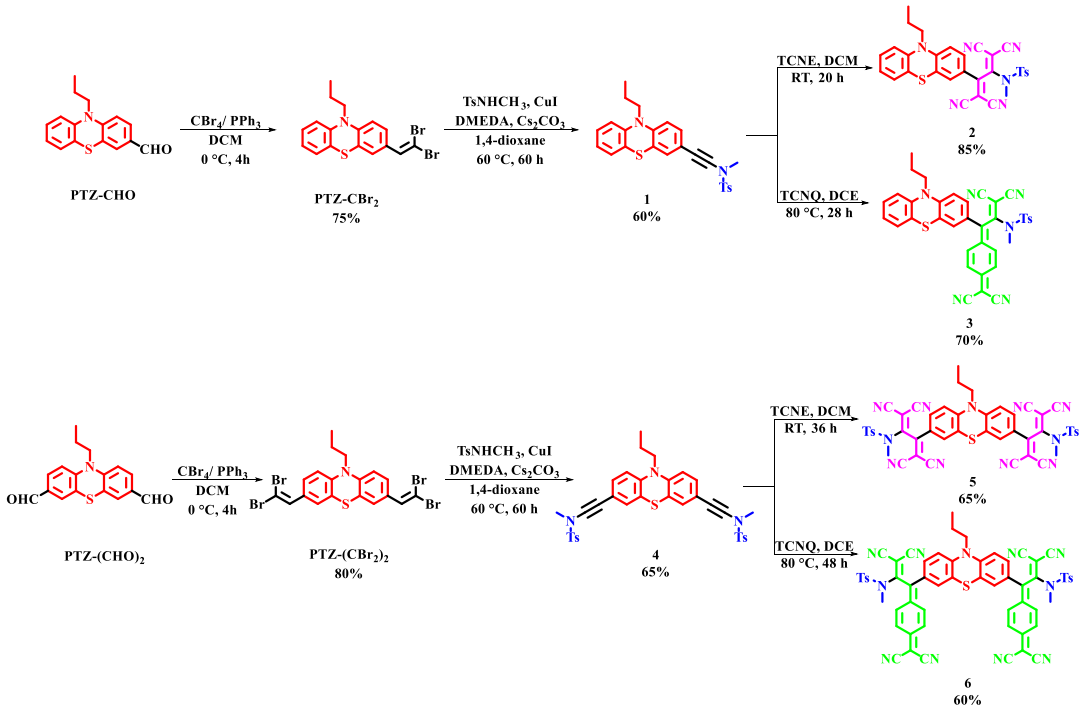

Scheme 4.1. Synthetic route of donor-acceptor chromophores **1–6**.

4.3. Photophysical Properties

The optical properties of the donor-acceptor chromophores **1–6** were recorded in dilute dichloromethane solutions (1×10^{-5} M) at room temperature (Figure 4.2), and the data including absorption maxima (λ_{max}), extinction coefficient, and optical bandgap are summarized in Table 4.1. The absorption maxima of mono- and di-ynamide derivatives **1** and **4** are at 325 nm and 342 nm, respectively, which is due to the π-π* transition at higher energy region. The mono- and di-TCBD substituted **2** and **5** exhibit absorption maxima at 591 nm and 599 nm respectively, indicating that the incorporation of the TCBD unit results in strong donor-acceptor interaction. The di TCBD substituted chromophore **5** shows an 8 nm red shift in compared to mono TCBD substituted chromophore **2**. While, the mono- and di-DCNQ functionalized chromophores **3** and **6** exhibit their absorption maxima at 686 nm and 702 nm, respectively, which is attributed to the intramolecular charge transfer (ICT) transitions at the longer wavelength. The strong absorption bands are due to the strong electron accepting nature of DCNQ. The di DCNQ substituted **6** exhibits a bathochromic shift of 16 nm as compared to mono DCNQ substituted **3**.

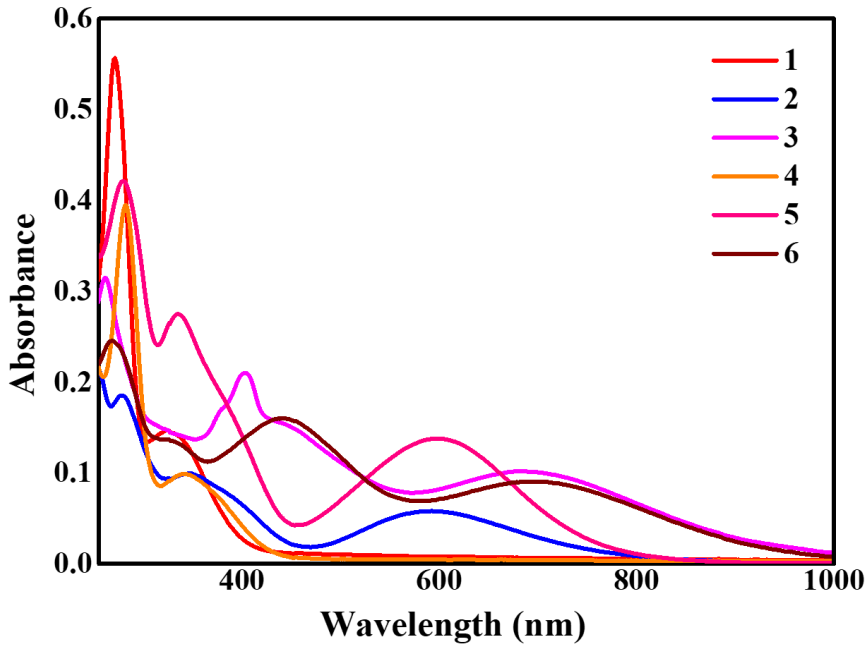

Figure 4.2. Electronic absorption spectra of donor-acceptor chromophores **1–6** in dichloromethane (1×10^{-5} M).

The DCNQ functionalized chromophores **3** and **6** exhibit a bathochromically shifted absorption (~100 nm) as compared to the TCBD substituted chromophores **2** and **5** which corresponds to the strong electron-accepting nature of the DCNQ moiety. The optical energy gaps of **1–6** were estimated from the onset edge of the absorption spectra in dichloromethane, which were found to be 2.98, 1.46, 1.18, 2.78, 1.48, and 1.20 eV, respectively. The optical band gaps of **1–6** are listed in the following order **1** > **4** > **5** > **2** > **6** > **3**. All transitions are explained by TD-DFT calculations, and relevant data are included in Table 4.3.

Table 4.1. Photophysical and Computational Data of Donor–Acceptor Chromophores **1–6**.

Compounds	λ_{max} (nm)[a]	ε (M^{-1} cm^{-1})[a]	E_g^{opt} (eV)[a]	HOMO (eV)[b]	LUMO (eV)[b]	band-gap (eV)[b]
1	325	14770	2.98	–5.05	–1.16	3.89
2	591	5815	1.46	–5.71	–3.29	2.42
3	686	10180	1.18	–5.58	–3.77	1.81
4	342	9890	2.78	–5.06	–1.27	3.79
5	599	13820	1.48	–6.04	–3.85	2.19

6	702	9020	1.20	–5.89	–4.11	1.78

[a]Absorbance measured in dichloromethane at (10^{-5} M); λmax = absorption wavelength; ε = extinction coefficient; E_g^{opt} = optical bandgap; [b]Theoretical data obtained from density functional theory (DFT) calculations performed at the B3LYP/6-31G (d,p) level.

4.4. Electrochemical Properties

The redox potentials of donor-acceptor chromophores **1–6** were evaluated by cyclic voltammetry (CV) and differential pulse voltammetry (DPV) using 0.1 M tetrabutylammonium hexafluorophosphate ($TBAPF_6$) as a supporting electrolyte. The electrochemical data are demonstrated in Table 4.2, and the representative cyclic voltammograms and differential pulse voltammograms for chromophores **1–6** are shown in Figures 4.3 and 4.4. At low potential, phenothiazine displays only one reversible oxidation wave.[52, 53] The donor-acceptor chromophores **1–6** exhibit two reversible oxidation waves in the range of 1.65 – 0.75 V corresponding to the phenothiazine and ynamide donor moieties on the anodic side. The mono- and di-ynamide derivatives **1** and **4** exhibit two oxidation waves at (0.79 V and 1.46 V) and (0.77 V and 1.33 V), respectively. The phenothiazine moiety is responsible for the first oxidation potential, while the ynamide moiety is responsible for the second oxidation potential. The mono- and di-TCBD incorporated chromophores **2** and **5** exhibit two oxidation waves at (1.02 V and 1.58 V) and (1.23 V and 1.65 V), respectively, while the DCNQ substituted chromophores **3** and **6** display two oxidation waves at (0.89 V and 1.47 V) and (1.01 V and 1.55 V), respectively. These results suggest that the incorporation of the TCBD/DCNQ acceptors unit enhances the oxidation potential of phenothiazine at the anodic side while reducing its electron density.

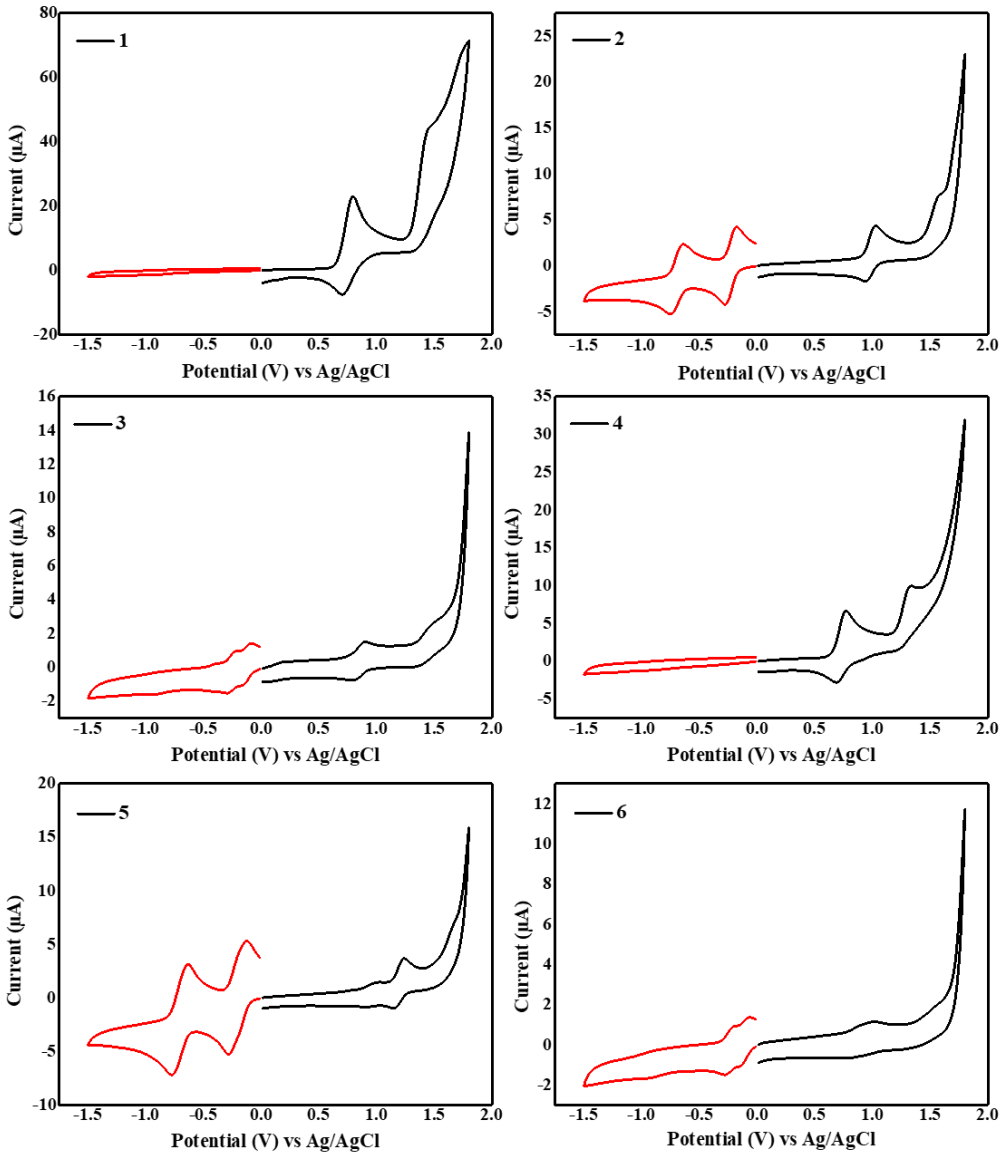

Figure 4.3. Cyclic voltammograms of **2** and **3** in 0.1 M solution of Bu_4NPF_6 in dichloromethane at 100 mV s^{-1} scan rate *versus* saturated Ag/AgCl at 25 °C.

The TCBD/DCNQ functionalized chromophores **2**, **3**, **5**, and **6** exhibit two reduction waves in the range of –0.10 V to –0.80 V on the cathodic side. The mono- and di-TCBD substituted chromophores **2** and **5** show two reduction waves at (–0.27 V and –0.75 V) and (–0.28 V and –0.78 V), respectively. While the mono- and di-DCNQ functionalized chromophores **3** and **6** exhibit two reduction waves at (–0.16 V and –0.29 V) and (–0.13 V and –0.27 V), respectively.

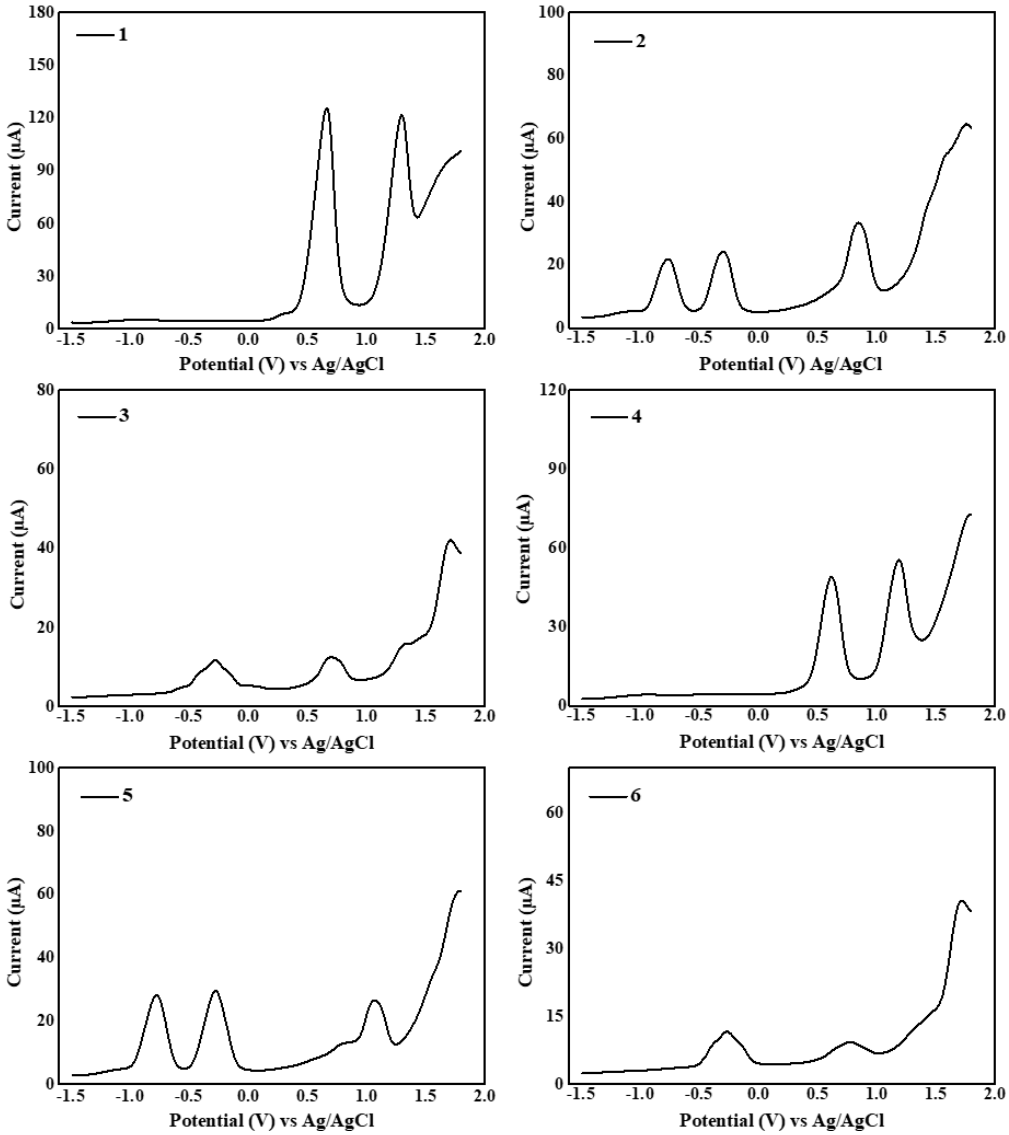

Figure 4.4. Differential pulse voltammograms of **1–6** in 0.1 M solutions of Bu_4NPF_6 in dichloromethane at 100 mV s^{-1} scan rate *versus* saturated Ag/AgCl electrode at 25 °C.

The reduction potential values of chromophores **3** and **6** exhibit a more pronounced anodic shift compared to chromophores **2** and **5** which indicates that the DCNQ unit has a greater influence on the electronic properties and contributes more to the stabilization of the LUMO energy levels than the TCBD unit. The electrochemically calculated HOMO energy levels of chromophores **2**, **3**, **5**, and **6** are –5.98, –5.87, –6.05, and –5.95 eV, respectively and LUMO energy levels are –4.13, –4.24, –4.12 and –4.27 eV, respectively. The calculated electrochemical band gaps (E_{gap}) of chromophores **2**, **3**, **5**, and **6** are 1.85

eV, 1.63 eV, 1.93 eV and 1.68 eV respectively. The E_{gap} values follow the order **5** > **2** > **6** > **3**. The calculated electrochemical band gap and the optical band gap for **2**, **3**, **5**, and **6** are in good agreement.

Table 4.2. Electrochemical data of donor–acceptor chromophores **1–6**.

Compounds	E_{red} **(V)**[a]	E_{ox} **(V)**[a]	E_{HOMO} **(eV)**[a]	E_{LUMO} **(eV)**[a]	E_g **(eV)**[a]
1	–	0.79 1.46	–	–	–
2	–0.27 –0.75	1.02 1.58	–5.98	–4.13	1.85
3	–0.16 –0.29	0.89 1.47	–5.87	–4.24	1.63
4	–	0.77 1.33	–	–	–
5	–0.28 –0.78	1.23 1.65	–6.05	–4.12	1.93
6	–0.13 –0.27	1.01 1.55	–5.95	–4.27	1.68

[a]Electrochemical analysis was estimated by differential pulse voltammetry, in 0.1 M solution of $TBAPF_6$ in DCM at 100 mV s^{-1} scan rate *versus* saturated Ag/AgCl electrode at 25 °C.

4.5. Computational Calculations

The density functional theory calculation was carried out on donor-acceptor chromophores **1–6** to investigate the molecular conformations and ground-state geometries at B3LYP/6-31G (d,p) level in the Gaussian 09W program.[54] The HOMO–LUMO frontier molecular orbitals and the energy level diagram of the optimized geometries of **1–6** with the HOMOs (highest occupied molecular orbitals), LUMOs (lowest unoccupied molecular orbitals), and energy gap are displayed in Figure 4.5, and the relevant data are displayed in Table 4.1. The ynamides substituted **1** and **4** exhibit a non-planar structure due to the presence of phenothiazine (butterfly shape) and ynamide moiety. However, the **2**, **3**, **5**, and **6** show a more twisted geometry due to the

presence of multiple nonplanar acceptor TCBD and DCNQ moieties. The HOMOs of **1** and **4** are concentrated on the phenothiazine unit and the LUMOs are mainly localized on the ynamide moiety. In the case of **2**, **3**, **5**, and **6** the HOMOs are mainly concentrated on the phenothiazine unit, whereas the LUMOs are centered on TCBD and DCNQ units. The TCBD (tetracyanobutadiene) and DCNQ (dicyanoquinodimethane) units are introduced as cyano-based strong electron acceptors and this lowers the LUMO energy levels, which leads to a red shift in the UV-vis spectra. The HOMO-LUMO energy gap in DCNQ functionalized **3** and **6** is lower than in TCBD functionalized derivatives **2** and **5**, because of their strong accepting character of the DCNQ unit. The theoretically calculated HOMO energy levels of **1–6** are –5.05 eV, –5.71 eV, –5.58 eV, –5.06 eV, –6.04 eV and –5.89 eV, respectively and the corresponding LUMO energy levels are –1.16 eV, –3.29 eV, –3.77 eV, –1.27 eV, –3.85 eV and –4.11 eV, respectively. The theoretically calculated HOMO–LUMO gap values for **1–6** are 3.89, 2.42, 1.81, 3.79, 2.19 and 1.78, respectively, and follows the order **1** > **4** > **2** > **5** > **3** > **6**.

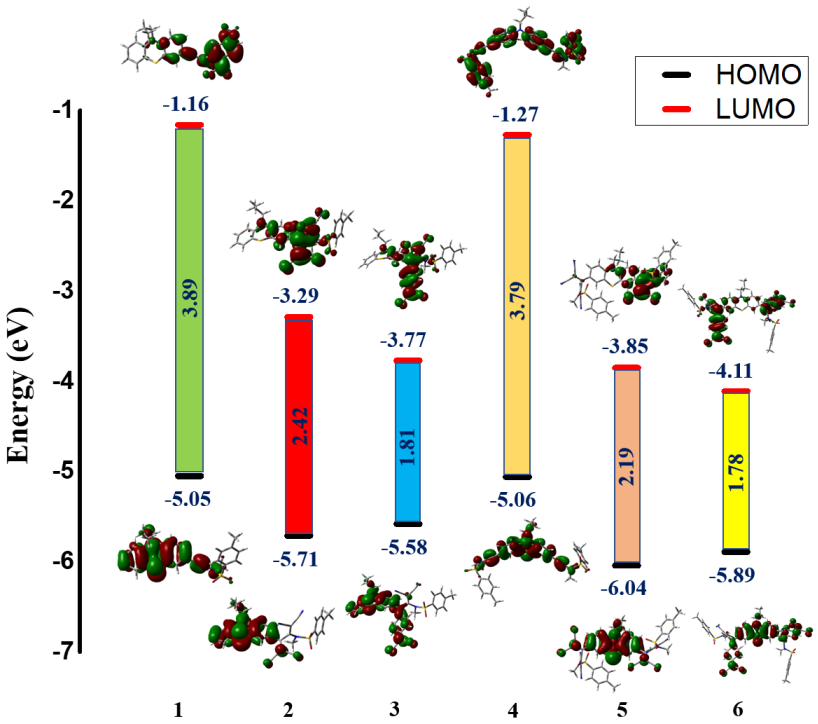

Figure 4.5. Energy level diagram and HOMO–LUMO frontier orbitals pictures of donor-acceptor chromophores **1–6** calculated by DFT calculations at the B3LYP/6-31G (d,p) level.

The time-dependent density functional theory (TD-DFT) calculation was carried out at the B3LYP/6-31G (d,p) level on optimized **1–6** in dichloromethane to determine the transitions involved in the electronic absorption spectra. The experimentally and theoretically calculated absorption spectra are displayed in Figure 4.6 and the corresponding data including transitions with oscillator strengths, composition, and assignments are shown in Table 4.3.

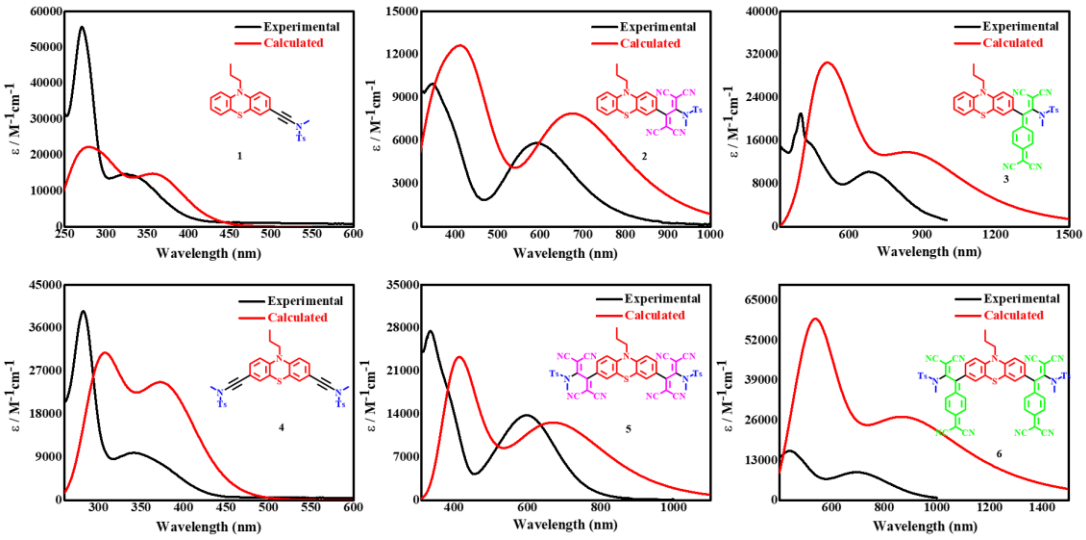

Figure 4.6. Calculated (red line) TD-DFT: B3LYP/6-31G (d,p) level in dichloromethane and experimental (black line) UV/vis spectrum of donor-acceptor chromophores **1–6** in dichloromethane.

The theoretically estimated electronic absorption spectra of ynamides substituted **1** and **4** exhibits an absorption band at 362 nm and 381 nm respectively, which are attributed to the transition from HOMO→LUMO. This absorption band was originated from the π–π* transition localized on the phenothiazine to ynamides moiety. For TCBD substituted **2** and **5** show the absorption band at 676 nm and 595 nm respectively, which are originated from HOMO→LUMO and HOMO→LUMO+1. On the other hand, the DCNQ functionalized **3** and **6** reveal the absorption band at 872 nm and 796 nm respectively, which are attributed to the transition from HOMO→LUMO and HOMO→LUMO+1. The DCNQ functionalized derivatives **3** and **6** display a stronger intramolecular charge transfer (ICT) band at the longer wavelength region as compared to TCBD substituted derivatives

2 and **5** because of the strong donor-acceptor nature of the DCNQ moiety.

Table 4.3. Calculated electronic transitions for donor-acceptor chromophores **1–6** in dichloromethane:

Compounds	Wavelength (nm)	Composition and Molecular Contribution	f^a	Assignment
1	362	HOMO→LUMO (0.65)	0.34	π–π*
2	676	HOMO→LUMO (0.70)	0.19	ICT
3	872	HOMO→LUMO (0.69)	0.32	ICT
4	381	HOMO→LUMO (0.67)	0.52	π–π*
5	595	HOMO→LUMO+1 (0.70)	0.12	ICT
6	796	HOMO→LUMO+1 (0.68)	0.11	ICT

[a]Oscillator strength.

The theoretical data were found to be higher than the experimentally calculated values for electronic absorption wavelengths, which might be related to a number of things namely the solvent effect, temperature, and dipole moment.

4.6. Experimental section

General methods

The chemicals were used as received unless otherwise indicated. All oxygen or moisture-sensitive reactions were performed under a nitrogen/argon atmosphere. ^{1}H NMR (500 MHz) and ^{13}C NMR (125 MHz) spectra were recorded on Bruker 500 MHz FT-NMR spectrometers at room temperature. ^{1}H NMR chemical shifts are reported in parts per million (ppm) relative to the solvent residual peak ($CDCl_3$, 7.26 ppm). Multiplicities are given as s (singlet), d (doublet), t (triplet) and m (multiplet) and the coupling constants, *J*, are given in hertz. ^{13}C NMR chemical shifts are reported relative to the solvent residual peak ($CDCl_3$, 77.0 ppm). UV-visible absorption spectra were recorded on a PerkinElmer Lambda 35 instrument. HRMS was recorded with an Agilent 6545A Q-TOF mass spectrometer and on a Bruker-Daltonics micrOTOF-Q II mass spectrometer used to measure the mass

of the compounds. The voltammograms were recorded on a PalmSens 4 electrochemical analyzer in dichloromethane solvent and 0.1 M $TBAPF_6$ as the supporting electrolyte. The electrodes used were glassy carbon as a working electrode, Pt wire as a counter electrode and Ag/AgCl as a reference electrode, the scan rate was 100 mV s^{-1} for cyclic voltammetry.

Synthesis of *N*,4-dimethyl-*N*-((10-propyl-10*H*-phenothiazin-3-yl)ethynyl)benzene sulfonamide (1)

In a 100 mL round bottomed flask, a solution of dibromoalkene **PTZ-CBr$_2$** (350 mg, 0.8231 mmol), TsNHMe (168 mg, 0.9054 mmol), CuI (17 mg, 0.0897 mmol), *N*,*N*'-dimethylethylenediamine (22 μL, 0.2057 mmol) and Cs_2CO_3 (992 mg, 3.0457 mmol) in dry 1,4-dioxane (10 mL) was heated to 60 °C under a nitrogen atmosphere over 60 h. Then the solvent was evaporated under vacuum. The residue was dissolved in dichloromethane, and this solution was washed with water for several times, dried with anhydrous Na_2SO_4, and filtered off. The crude was purified by column chromatography (cyclohexane:dichloromethane 1:0 to 4:6) to give **1** as a yellow/brown solid with 60% yield. ^{1}H NMR (500 MHz, CHLOROFORM-d) δ = 7.84 - 7.79 (m, *J* = 8.1 Hz, 2 H), 7.39 - 7.34 (m, *J* = 7.9 Hz, 2 H), 7.18 - 7.12 (m, 2 H), 7.12 - 7.07 (m, 2 H), 6.93 - 6.89 (m, 1 H), 6.84 (d, *J* = 8.1 Hz, 1 H), 6.73 (d, *J* = 8.4 Hz, 1 H), 3.79 (t, *J* = 7.1 Hz, 2 H), 3.12 (s, 3 H), 2.46 (s, 3 H), 1.81 (sxt, *J* = 7.3 Hz, 2 H), 1.00 (t, *J* = 7.3 Hz, 3 H); ^{13}C NMR (125 MHz, CHLOROFORM-d) δ = 145.2, 144.8, 144.7, 133.2, 131.0, 130.4, 129.8, 127.9, 127.4, 127.3, 124.8, 124.2, 122.7, 116.3, 115.5, 115.0, 83.6, 68.3, 49.3, 39.4, 21.7, 20.1, 11.3; HRMS (ESI-TOF) m/z calculated for $C_{25}H_{24}N_2O_2S_2$ 448.1279 $[M]^+$, measured 448.1296 $[M]^+$.

Synthesis of *N*,4-dimethyl-*N*-(1,1,4,4-tetracyano-3-(10-propyl-10*H*-phenothiazin-3-yl) buta-1,3-dien-2-yl)benzenesulfonamide (2)

In a 100 mL round bottomed flask, TCNE (47 mg, 0.3678 mmol) was added to a solution of **1** (150 mg, 0.3343 mmol) in CH_2Cl_2 (20 mL) under an argon atmosphere. The mixture was stirred for 20 h at RT. The solvent was removed in vacuum, and the product was purified by

column chromatography with DCM/hexane (2:1, v/v) as eluent to yield **2** as a dark color solid with 85% yield. ^{1}H NMR (500 MHz, CHLOROFORM-d) δ = 7.77 - 7.71 (m, *J* = 8.2 Hz, 2 H), 7.66 (dd, *J* = 2.3, 8.9 Hz, 1 H), 7.47 - 7.42 (m, *J* = 8.1 Hz, 2 H), 7.36 (d, *J* = 2.3 Hz, 1 H), 7.19 (t, *J* = 7.8 Hz, 1 H), 7.09 (d, *J* = 7.6 Hz, 1 H), 7.01 (t, *J* = 7.5 Hz, 1 H), 6.90 (d, *J* = 8.9 Hz, 2 H), 3.89 (t, *J* = 7.3 Hz, 2 H), 3.55 (s, 3 H), 2.49 (s, 3 H), 1.89 (sxt, *J* = 7.4 Hz, 2 H), 1.06 (t, *J* = 7.3 Hz, 3 H); ^{13}C NMR (125 MHz, CHLOROFORM-d) δ = 164.4, 161.5, 151.2, 147.4, 143.5, 142.0, 135.9, 132.4, 131.7, 130.8, 129.7, 128.5, 128.3, 127.9, 127.7, 127.3, 127.0, 125.2, 124.8, 124.5, 122.8, 116.3, 115.0, 112.9, 112.6, 110.8, 110.7, 82.4, 79.0, 50.1, 41.4, 21.9, 20.1, 11.2; HRMS (ESI-TOF) m/z calculated for $C_{31}H_{24}N_6O_2S_2$ + Na 599.1294 [M + Na]$^{+}$, measured 599.1325 [M + Na]$^{+}$.

Synthesis of *N*-(1,1-dicyano-3-(4-(dicyanomethylene)cyclohexa-2,5-dien-1-ylidene)-3-(10-propyl-10*H*-phenothiazin-3-yl)prop-1-en-2-yl)-*N*,4-dimethylbenzenesulfonamide (3)

In a 100 mL round bottomed flask, TCNQ (75 mg, 0.3678 mmol) was added to a solution of **1** (150 mg, 0.3343 mmol) in DCE (20 mL). The mixture was heated at 80 °C for 24 h. After cooling to room temperature, the solutions were removed under vacuum, and the product was purified by column chromatography with DCM/hexane (3:1, v/v) as the eluent to yield **3** as a dark color solid with 70% yield. ^{1}H NMR (500 MHz, CHLOROFORM-d) δ = 7.47 (d, *J* = 8.2 Hz, 2 H), 7.31 (s, 3 H), 7.22 (d, *J* = 7.5 Hz, 3 H), 7.16 - 7.10 (m, 3 H), 7.04 - 6.99 (m, 1 H), 6.98 - 6.95 (m, 1 H), 6.92 (d, *J* = 8.1 Hz, 1 H), 6.89 (d, *J* = 8.5 Hz, 1 H), 3.88 (t, *J* = 7.2 Hz, 2 H), 3.37 (s, 3 H), 2.38 (s, 3 H), 1.92 - 1.86 (m, 2 H), 1.07 (t, *J* = 7.3 Hz, 3 H); ^{13}C NMR (125 MHz, CHLOROFORM-d) δ = 166.1, 152.5, 147.9, 145.5, 145.2, 141.9, 135.9, 134.4, 132.9, 131.9, 131.6, 130.2, 129.3, 129.0, 128.7, 127.8, 127.0, 126.8, 126.7, 126.3, 125.9, 125.6, 124.6, 123.0, 122.1, 115.1, 114.3, 112.6, 111.0, 110.7, 79.3, 48.8, 39.4, 28.7, 20.7, 19.1, 10.2; HRMS (ESI-TOF) m/z calculated for $C_{37}H_{28}N_6O_2S_2$ + Na 675.1607 [M + Na]$^{+}$, measured 675.1617 [M + Na]$^{+}$.

Synthesis of *N*,*N*'-((10-propyl-10*H*-phenothiazine-3,7-diyl)bis(ethyne-2,1-diyl))bis(*N*,4-dimethylbenzenesulfonamide) (4)

In a 100 mL round bottomed flask, a solution of dibromoalkene **PTZ-(CBr$_2$)$_2$** (1 g, 1.642 mmol), TsNHMe (760 mg, 4.105 mmol), CuI (125 mg, 0.6568 mmol), *N*,*N*'-dimethylethylenediamine (107 μL, 0.9852 mmol) and Cs_2CO_3 (4 g, 12.315 mmol) in dry 1,4-dioxane (20 mL) was heated to 60 °C under a nitrogen atmosphere over 60 h. Then the solvent was evaporated under vacuum. The residue was dissolved in dichloromethane, and this solution was washed with water for several times, dried with anhydrous Na_2SO_4, and filtered off. The crude was purified by column chromatography (cyclohexane:dichloromethane 1:0 to 4:6) to give **4** as a yellow/brown solid with 65% yield. ^{1}H NMR (500 MHz, CHLOROFORM-d) δ = 7.82 (d, *J* = 8.1 Hz, 4 H), 7.37 (d, *J* = 8.1 Hz, 4 H), 7.17 - 7.11 (m, 2 H), 7.09 - 7.05 (m, 2 H), 6.72 (d, *J* = 8.4 Hz, 2 H), 3.77 (t, *J* = 7.1 Hz, 2 H), 3.12 (s, 6 H), 2.47 (s, 6 H), 1.82 - 1.75 (m, 2 H), 0.99 (t, *J* = 7.3 Hz, 3 H); ^{13}C NMR (125 MHz, CHLOROFORM-d) δ = 144.8, 144.5, 143.5, 135.8, 133.2, 131.1, 130.4, 130.0, 129.8, 129.7, 128.0, 127.8, 127.3, 124.0, 116.7, 115.1, 83.8, 68.1, 49.3, 39.4, 21.5, 20.0, 11.2; HRMS (ESI-TOF) m/z calculated for $C_{35}H_{33}N_3O_4S_3$ + Na 678.1525 $[M + Na]^+$, measured 678.1516 $[M + Na]^+$.

Synthesis of *N*,*N*'-((10-propyl-10*H*-phenothiazine-3,7-diyl)bis(1,1,4,4-tetracyanobuta-1,3-diene-3,2-diyl))bis(*N*,4-dimethylbenzenesulfonamide) (5)

In a 100 mL round bottomed flask, TCNE (73 mg, 0.5717 mmol)) was added to a solution of **4** (150 mg, 0.2287 mmol) in CH_2Cl_2 (20 mL) under an argon atmosphere. The mixture was stirred at RT for 36 h. The solvent was removed under vacuum, and the product was purified by column chromatography with DCM/hexane (3:1, v/v) as eluent to yield **5** as a dark color solid with 65% yield. ^{1}H NMR (500 MHz, CHLOROFORM-d) δ = 7.77 (d, *J* = 8.2 Hz, 4 H), 7.69 (dd, *J* = 2.3, 8.9 Hz, 2 H), 7.48 (d, *J* = 8.2 Hz, 4 H), 7.35 (d, *J* = 2.3 Hz, 2 H), 7.00 (d, *J* = 8.9 Hz, 2 H), 3.95 - 3.90 (m, 2 H), 3.53 (s, 6 H), 2.51 (s, 6 H), 1.96 -

1.90 (m, 2 H), 1.12 (t, *J* = 7.3 Hz, 3 H); ^{13}C NMR (125 MHz, CHLOROFORM-d) δ = 163.6, 162.1, 148.0, 147.6, 143.6, 135.8, 132.2, 131.7, 131.0, 129.8, 128.4, 128.3, 127.3, 126.7, 124.1, 116.1, 112.3, 112.1, 110.8, 110.5, 85.6, 79.4, 50.6, 41.3, 21.9, 21.5, 19.9, 11.1; HRMS (ESI-TOF) m/z calculated for $C_{47}H_{33}N_{11}O_4S_3$ + Na 934.1771 $[M + Na]^+$, measured 934.1772 $[M + Na]^+$.

Synthesis of *N*,*N*'-((10-propyl-10*H*-phenothiazine-3,7-diyl)bis(3,3-dicyano-1-(4-(dicyanomethylene)cyclohexa-2,5-dien-1-ylidene)prop-2-ene-1,2-diyl))bis(*N*,4-dimethylbenzenesulfonamide) (6)

In a 100 mL round bottomed flask, TCNQ (101 mg, 0.4955 mmol) was added to a solution of **4** (130 mg, 0.1982 mmol) in DCE (20 mL). The mixture was heated at 80 °C for 48 h. After cooling to room temperature, the solutions were removed under vacuum, and the product was purified by column chromatography with DCM as the eluent to yield **6** as a dark color solid with 60% yield. ^{1}H NMR (500 MHz, CHLOROFORM-d) δ = 7.70 (d, *J* = 8.2 Hz, 1 H), 7.60 (s, 1 H), 7.54 - 7.46 (m, 2 H), 7.39 - 7.34 (m, 2 H), 7.34 - 7.27 (m, 6 H), 7.25 - 7.18 (m, 2 H), 7.17 - 7.11 (m, 2 H), 7.11 - 7.07 (m, 1 H), 7.06 - 6.97 (m, 2 H), 6.97 - 6.90 (m, 2 H), 6.85 (dd, *J* = 8.5, 14.0 Hz, 1 H), 3.95 - 3.84 (m, 2 H), 3.44 - 3.25 (m, 6 H), 2.49 - 2.39 (m, 6 H), 1.97 - 1.85 (m, 2 H), 1.14 - 1.05 (m, 3 H); ^{13}C NMR (125 MHz, CHLOROFORM-d) δ = 167.3, 167.2, 167.0, 153.4, 148.8, 146.8, 146.5, 145.9, 141.1, 137.4, 136.8, 135.1, 133.8, 133.6, 133.0, 132.9, 132.8, 130.6, 130.4, 129.4, 129.2, 128.9, 128.2, 128.0, 127.9, 127.8, 127.5, 127.3, 126.9, 126.6, 125.1, 124.1, 123.3, 116.1, 115.9, 113.6, 113.4, 112.0, 111.6, 80.3, 80.2, 78.6, 73.5, 50.4, 49.9, 40.7, 40.6, 40.5, 33.4, 22.3, 21.8, 21.8, 21.7, 20.1, 20.0, 14.1, 11.3, 11.2; HRMS (ESI-TOF) m/z calculated for $C_{59}H_{41}N_{11}O_4S_3$ + Na 1086.2397 $[M + Na]^+$, measured 1086.2469 $[M + Na]^+$.

4.7. Conclusion

In summary, we have designed and synthesized phenothiazine- and ynamide-based chromophores **1–6** by the Corey-Fuchs reaction *via* Evano′s conditions followed by [2 + 2] cycloaddition retroelectrocyclic

ring-opening reaction with strong electron acceptors TCNE and TCNQ in good yields. The electronic absorption maxima of the DCNQ substituted **3** and **6** exhibit a significant bathochromic shift of around 100 nm, compared to those of TCBD substituted **2** and **5**, due to the strong electron-accepting nature of the DCNQ moiety. Based on the electrochemical properties, it can be observed that the reduction potential values of **3** and **6** are comparatively lower than those of **2** and **5**. This indicates that the DCNQ unit has a greater impact on the electronic properties and contributes more towards stabilizing the LUMO energy levels in comparison to the TCBD unit. In DFT calculation, the HOMO–LUMO energy gap in DCNQ functionalized **3** and **6** is lower than in TCBD functionalized derivatives **2** and **5**, because of their strong accepting character of the DCNQ unit. The TD-DFT calculations reveal significant donor-acceptor interactions and correspond well with the experimental data.

4.8. References

[1] Konidena, R. K., Thomas, K. R. J., & Park, J. W. (2022). Recent Advances in the Design of Multi-Substituted Carbazoles for Optoelectronics: Synthesis and Structure-Property Outlook. *ChemPhotoChem*, *6*(10). (DOI: 10.1002/CPTC.202200059).

[2] Zhang, J., Jin, J., Xu, H., Zhang, Q., & Huang, W. (2018). Recent progress on organic donor-acceptor complexes as active elements in organic field-effect transistors. *Journal of Materials Chemistry C*, *6*, 3485–3498. (DOI: 10.1039/c7tc04389a).

[3] Srinivasa Rao, P., Brixi, S., Shaikh, D. B., Al Kobaisi, M., Lessard, B. H., Bhosale, S. V., & Bhosale, S. V. (2021). The Effect of TCNE and TCNQ Acceptor Units on Triphenylamine-Naphthalenediimide Push-Pull Chromophore Properties. *European Journal of Organic Chemistry*, *2021*(18), 2615–2624. (DOI: 10.1002/EJOC.202100198).

[4] Revoju, S., Matuhina, A., Canil, L., Salonen, H., Hiltunen, A., Abate, A., & Vivo, P. (2020). Structure-induced optoelectronic properties of phenothiazine-based materials. *Journal of*

Materials Chemistry C, *8*, 15486–15506. (DOI: 10.1039/d0tc03421e).

[5] Erden, K., & Dengiz, C. (2022). 3-Alkynylindoles as Building Blocks for the Synthesis of Electronically Tunable Indole-Based Push−Pull Chromophores. *Journal of Organic Chemistry*, *87*, 4385–4399. (DOI: 10.1021/acs.joc.2c00067).

[6] Kobayashi, N., Inagaki, S., Nemykin, V. N., & Nonomura, T. (2001). A Novel Hemiporphyrazine Comprising Three Isoindolediimine and Three Thiadiazole Units. *Angewandte Chemie International Edition*, *40*(14), 2710–2712. (DOI: 10.1002/1521-3773(20010716)40:14<2710::AID-ANIE2710>3.0.CO;2-A).

[7] Ji, C., Yin, L., Li, K., Wang, L., Jiang, X., Sun, Y., & Li, Y. (2015). D–π–A–π–D-type low band gap diketopyrrolopyrrole based small molecules containing an ethynyl-linkage: synthesis and photovoltaic properties. *RSC Advances*, *5*(40), 31606–31614. (DOI: 10.1039/C5RA01946J).

[8] Poddar, M., Jang, Y., Misra, R., & D'Souza, F. (2020). Excited-State Electron Transfer in 1,1,4,4-Tetracyanobuta-1,3-diene (TCBD)- and Cyclohexa-2,5-diene-1,4-diylidene-Expanded TCBD-Substituted BODIPY-Phenothiazine Donor–Acceptor Conjugates. *Chemistry – A European Journal*, *26*(30), 6869–6878. (DOI: 10.1002/chem.202000346).

[9] Gautam, P., Sharma, R., Misra, R., Keshtov, M. L., Kuklin, S. A., & Sharma, G. D. (2017). Donor-acceptor-acceptor (D-A-A) type 1,8-naphthalimides as non-fullerene small molecule acceptors for bulk heterojunction solar cells. *Chemical Science*, *8*(3), 2017–2024. (DOI: 10.1039/c6sc04461a).

[10] Misra, R., Gautam, P., Jadhav, T., & Mobin, S. M. (2013). Donor-acceptor ferrocenyl-substituted benzothiadiazoles: Synthesis, structure, and properties. *Journal of Organic Chemistry*, *78*(10), 4940–4948. (DOI: 10.1021/JO4005734).

[11] Abraham, J. P., Sajan, D., Shettigar, V., Dharmaprakash, S. M., Němec, I., Joe, I. H., & Jayakumar, V. S. (2009). Efficient π-

electron conjugated push-pull nonlinear optical chromophore 1-(4-methoxyphenyl)-3-(3,4-dimethoxyphenyl)-2-propen-1-one: A vibrational spectral study. *Journal of Molecular Structure*, *917*, 27–36. (DOI: 10.1016/j.molstruc.2008.06.031).

[12] Jadhav, T., Maragani, R., Misra, R., Sreeramulu, V., Rao, D. N., & Mobin, S. M. (2013). Design and synthesis of donor–acceptor pyrazabole derivatives for multiphoton absorption. *Dalton Transactions*, *42*(13), 4340–4342. (DOI: 10.1039/c3dt33065f).

[13] Hacıefendioğlu, T., & Yildirim, E. (2022). Design Principles for the Acceptor Units in Donor–Acceptor Conjugated Polymers. *ACS Omega*, *7*(43), 38969–38978. (DOI: 10.1021/acsomega.2c04713).

[14] Rout, Y., Gautam, P., & Misra, R. (2017). Unsymmetrical and Symmetrical Push-Pull Phenothiazines. *Journal of Organic Chemistry*, *82*(13), 6840–6845. (DOI: 10.1021/ACS.JOC.7B00991).

[15] Poddar, M., Cesaretti, A., Ferraguzzi, E., Carlotti, B., & Misra, R. (2020). Singlet and Triplet Excited-State Dynamics of 3,7-Bis(arylethynyl)phenothiazines: Intramolecular Charge Transfer and Reverse Intersystem Crossing. *Journal of Physical Chemistry C*, *124*(33), 17864–17878. (DOI: 10.1021/ACS.JPCC.0C01786).

[16] Jang, Y., Rout, Y., Misra, R., & D'Souza, F. (2021). Symmetric and Asymmetric Push-Pull Conjugates: Significance of Pull Group Strength on Charge Transfer and Separation. *Journal of Physical Chemistry B*, *125*(16), 4067–4075. (DOI: 10.1021/ACS.JPCB.0C09996).

[17] Sharma, R., Thomas, M. B., Misra, R., & D'Souza, F. (2019). Strong Ground- and Excited-State Charge Transfer in C 3 -Symmetric Truxene-Derived Phenothiazine-Tetracyanobutadine and Expanded Conjugates . *Angewandte Chemie International Edition*, *131*(13), 4394–4399. (DOI: 10.1002/ANGE.201814388).

[18] Rout, Y., Montanari, C., Pasciucco, E., Misra, R., & Carlotti, B. (2021). Tuning the Fluorescence and the Intramolecular Charge Transfer of Phenothiazine Dipolar and Quadrupolar Derivatives by Oxygen Functionalization. *Journal of the American Chemical Society*, *143*(26), 9933–9943. (DOI: 10.1021/JACS.1C04173).

[19] Bureš, F. (2014). Fundamental aspects of property tuning in push-pull molecules. *RSC Advances*, *4*, 58826–58851. (DOI: 10.1039/c4ra11264d).

[20] Dengiz, C., Breiten, B., Gisselbrecht, J. P., Boudon, C., Trapp, N., Schweizer, W. B., & Diederich, F. (2015). Synthesis and optoelectronic properties of janus -dendrimer-type multivalent donor-acceptor systems. *Journal of Organic Chemistry*, *80*(2), 882–896. (DOI: 10.1021/JO502367H).

[21] Poddar, M., & Misra, R. (2017). NIR-Absorbing Donor–Acceptor Based 1,1,4,4-Tetracyanobuta-1,3-Diene (TCBD)- and Cyclohexa-2,5-Diene-1,4-Ylidene-Expanded TCBD-Substituted Ferrocenyl Phenothiazines. *Chemistry - An Asian Journal*, *12*(22), 2908–2915. (DOI: 10.1002/ASIA.201700879).

[22] Siva Gangadhar, P., Reddy, G., Prasanthkumar, S., & Giribabu, L. (2021). Phenothiazine functional materials for organic optoelectronic applications. *Physical Chemistry Chemical Physics*, *23*, 14969–14996. (DOI: 10.1039/d1cp01185e).

[23] Al-Busaidi, I. J., Haque, A., Al Rasbi, N. K., & Khan, M. S. (2019). Phenothiazine-based derivatives for optoelectronic applications: A review. *Synthetic Metals*, *257*, 116189. (DOI: 10.1016/j.synthmet.2019.116189).

[24] Mahadik, S. S., Garud, D. R., Ware, A. P., Pingale, S. S., & Kamble, R. M. (2021). Design, Synthesis and Opto-electrochemical Properties of Novel Donor–Acceptor Based 2,3-di(hetero-2-yl)pyrido[2,3-b]pyrazine amine derivatives as Blue-Orange Fluorescent Materials. *Dyes and Pigments*, *184*, 108742. (DOI: 10.1016/j.dyepig.2020.108742).

[25] Kc, C. B., & Souza, F. D'. (2016). Design and photochemical study of supramolecular donor-acceptor systems assembled via

metal-ligand axial coordination. *Coordination Chemistry Reviews*, *322*, 104–141. (DOI: 10.1016/j.ccr.2016.05.012).

[26] El-Khouly, M. E., Fukuzumi, S., & D'Souza, F. (2014). Photosynthetic antenna-reaction center mimicry by using boron dipyrromethene sensitizers. *ChemPhysChem*, *15*(1), 30–47. (DOI: 10.1002/CPHC.201300715).

[27] Hauck, M., Schönhaber, J., Zucchero, A. J., Hardcastle, K. I., Müller, T. J. J., & Bunz, U. H. F. (2007). Phenothiazine cruciforms: Synthesis and metallochromic properties. *Journal of Organic Chemistry*, *72*(18), 6714–6725. (DOI: 10.1021/JO070922L).

[28] Gupta, R. R.; Ojha, K. G. (1988). Phenothiazines and 1, 4-benzothiazines: chemical and biomedical aspects. *Elsevier Amsterdam*, *p*. 163-269.

[29] Khan, F., Mahmoudi, M., Gupta, P. K., Volyniuk, D., Grazulevicius, J. V., & Misra, R. (2023). Mechanochromic Materials Based on Tetraphenylethylene-Substituted Phenothiazines: Substituent-Dependent Hypsochromic and Bathochromic Switching of Emission. *Journal of Physical Chemistry C*, *127*(3), 1643–1654. (DOI: 10.1021/ACS.JPCC.2C07010).

[30] Hauck, M., Stolte, M., Schönhaber, J., Kuball, H. G., & Müller, T. J. J. (2011). Synthesis, electronic, and electro-optical properties of emissive solvatochromic phenothiazinyl merocyanine dyes. *Chemistry - A European Journal*, *17*(36), 9984–9998. (DOI: 10.1002/CHEM.201100592).

[31] Krämer, C. S., & Müller, T. J. J. (2003). Synthesis and electronic properties of alkynylated phenothiazines. *European Journal of Organic Chemistry*, (18), 3534–3548. (DOI: 10.1002/EJOC.200300250).

[32] Breiten, B., Jordan, M., Taura, D., Zalibera, M., Griesser, M., Confortin, D., … Diederich, F. (2013). Donor-substituted octacyano[4]dendralenes: Investigation of π-electron

delocalization in their radical ions. *Journal of Organic Chemistry*, *78*(5), 1760–1767. (DOI: 10.1021/JO301194Y).

[33] Michinobu, T., Boudon, C., Gisselbrecht, J. P., Seiler, P., Frank, B., Moonen, N. N. P., … Diederich, F. (2006). Donor-substituted 1,1,4,4-tetracyanobutadienes (TCBDs): New chromophores with efficient intramolecular charge-transfer interactions by atom-economic synthesis. *Chemistry - A European Journal*, *12*(7), 1889–1905. (DOI: 10.1002/CHEM.200501113).

[34] Sekita, M., Ballesteros, B., Diederich, F., Guldi, D. M., Bottari, G., & Torres, T. (2016). Intense Ground-State Charge-Transfer Interactions in Low-Bandgap, Panchromatic Phthalocyanine–Tetracyanobuta-1,3-diene Conjugates. *Angewandte Chemie*, *128*(18), 5650–5654. (DOI: 10.1002/ANGE.201601258).

[35] Zhang, H., Wan, X., Xue, X., Li, Y., Yu, A., & Chen, Y. (2010). Selective tuning of the HOMO-LUMO gap of carbazole-based donor-acceptor-donor compounds toward different emission colors. *European Journal of Organic Chemistry*, (9), 1681–1687. (DOI: 10.1002/EJOC.200901167).

[36] Misra, R., & Gautam, P. (2014). Organic & Biomolecular Chemistry Tuning of the HOMO-LUMO gap of donor-substituted symmetrical and unsymmetrical benzothiadiazoles. *Organic & Biomolecular Chemistry*, *12*, 5448–5457. (DOI: 10.1039/c4ob00629a).

[37] Yamada, M., Schweizer, W. B., Schoenebeck, F., & Diederich, F. (2010). Unprecedented thermal rearrangement of push-pull-chromophore-[60]fullerene conjugates: formation of chiral 1,2,9,12-tetrakis-adducts. *Chemical Communications*, *46*, 5334–5336. (DOI: 10.1039/c0cc00881h).

[38] Kato, S. I., & Diederich, F. (2010). Non-planar push-pull chromophores. *Chemical Communications*, 46, 1994–2006. (DOI: 10.1039/b926601a).

[39] Jayamurugan, G., Gisselbrecht, J. P., Boudon, C., Schoenebeck, F., Schweizer, W. B., Bernet, B., & Diederich, F. (2011). Expanding the chemical space for push-pull chromophores by

non-concerted [2+2] and [4+2] cycloadditions: access to a highly functionalised 6,6-dicyanopentafulvene with an intense, low-energy charge-transfer band. *Chemical Communications*, *47*, 4520–4522. (DOI: 10.1039/c1cc10247h).

[40] Michinobu, T.; May, J. C.; Lim, J. H.; Boudon, C.; Gisselbrecht, J. P.; Seiler, P.; Gross, M.; Biaggio, I.; Diederich, F. (2005). A new class of organic donor–acceptor molecules with large third-order optical nonlinearities. *Chemical Communications*, 737–739. (DOI: 10.1039/b417393g).

[41] Michinobu, T. (2008). Click-type reaction of aromatic polyamines for improvement of thermal and optoelectronic properties. *Journal of the American Chemical Society*, *130*(43), 14074–14075. (DOI: 10.1021/JA8061612).

[42] Shoji, T., Ito, S., Toyota, K., Iwamoto, T., Yasunami, M., & Morita, N. (2009). Reactions between 1-ethynylazulenes and 7,7,8,8-tetracyanoquinodimethane (TCNQ): Preparation, properties, and redox behavior of novel azulene-substituted redox-active chromophores. *European Journal of Organic Chemistry*, (25), 4316–4324. (DOI: 10.1002/EJOC.200900539).

[43] Kraußе, N., Kielmann, M., Ma, J., & Butenschön, H. (2015). Reactions of Alkynyl- and 1,1′-Dialkynylferrocenes with Tetracyanoethylene – Unanticipated Addition at the Less Electron-Rich of Two Triple Bonds. *European Journal of Organic Chemistry*, *2015*(12), 2622–2631. (DOI: 10.1002/EJOC.201500105).

[44] Kato, S., Kijima, T., Shiota, Y., Abe, T., Kuwako, S., Miyauchi, H., … Nakamura, Y. (2020). Chemical transformations of push–pull fluorenones: push–pull dibenzodicyanofulvenes as well as fluorenone– and dibenzodicyanofulvene–tetracyanobutadiene conjugates. *Organic & Biomolecular Chemistry*, *18*(22), 4198–4209. (DOI: 10.1039/C9OB02706H).

[45] Kato, S., Noguchi, H., Jin, S., & Nakamura, Y. (2016). Synthesis and Electronic, Optical, and Electrochemical Properties of a Series of Tetracyanobutadiene-Substituted Carbazoles. *Asian*

Journal of Organic Chemistry, *5*(2), 246–256. (DOI: 10.1002/AJOC.201500431).

[46] Bui, A. T., Philippe, C., Beau, M., Richy, N., Cordier, M., & Roisnel, T. (2020). Synthesis, characterization and unusual near-infrared luminescence of 1,1,4,4-tetracyanobutadiene derivatives. *Chemical Communications*, *56*, 3571–3574. (DOI: 10.1039/c9cc09560h).

[47] Sheokand, M., Tiwari, N. J., & Misra, R. (2023). Near-IR absorbing 1,1,4,4-tetracyanobutadiene-functionalized phenothiazine sulfones. *Organic & Biomolecular Chemistry*, *21*, 3896–3905. (DOI: 10.1039/d3ob00361b).

[48] Yadav, I. S., & Misra, R. (2022). Phenothiazine and phenothiazine-5,5-dioxide-based push–pull derivatives: synthesis, photophysical, electrochemical and computational studies. *New Journal of Chemistry*, *46*(33), 15999–16006. (DOI: 10.1039/D2NJ03089F).

[49] Zhang, H., Wan, X., Xue, X., Li, Y., Yu, A., & Chen, Y. (2010). Selective tuning of the HOMO-LUMO gap of carbazole-based donor-acceptor-donor compounds toward different emission colors. *European Journal of Organic Chemistry*, (9), 1681–1687. (DOI: 10.1002/EJOC.200901167).

[50] Leliège, A., Blanchard, P., Rousseau, T., & Roncali, J. (2011). Triphenylamine/tetracyanobutadiene-based1 D-A-D π-conjugated systems as molecular donors for organic solar cells. *Organic Letters*, *13*(12), 3098–3101. (DOI: 10.1021/OL201002J).

[51] Coste, A., Karthikeyan, G., Couty, F., & Evano, G. (2009). Copper-Mediated Coupling of 1,1-Dibromo-1-alkenes with Nitrogen Nucleophiles: A General Method for the Synthesis of Ynamides. *Angewandte Chemie International Edition*, *121*(24), 4445–4449. (DOI: 10.1002/ANGE.200901099).

[52] Lai, R. Y., Fabrizio, E. F., Lu, L., Jenekhe, S. A., & Bard, A. J. (2001). Synthesis, cyclic voltammetric studies, and electrogenerated chemiluminescence of a new donor - Acceptor

molecule: 3,7-[bis[4-phenyl-2-quinolyl]]-10-methylphenothiazine. *Journal of the American Chemical Society*, *123*(37), 9112–9118. (DOI: 10.1021/JA0102235).

[53] Kulkarni, A. P., Wu, P. T., Kwon, T. W., & Jenekhe, S. A. (2005). Phenothiazine-phenylquinoline donor-acceptor molecules: Effects of structural isomerism on charge transfer photophysics and electroluminescence. *Journal of Physical Chemistry B*, *109*(42), 19584–19594. (DOI: 10.1021/JP0529772).

[54] Frisch, M. J.; Trucks, G. W.; Schlegel, G. W.; Scuseria, G. E.; Robb, M. A.; Cheeseman, J. R.; Scalmani, G.; Barone, V.; Mennucci, B.; Petersson, G. A.; et al. (2009). Gaussian 09, revision A.02; Gaussian, Inc.: Wallingford, CT.

Chapter 5

NIR Absorbing TCBD and DCNQ Functionalized Donor-Acceptor Based Symmetrical and Unsymmetrical *N*-Methyl-*p*-toluenesulfonamide-Phenothiazine Derivatives

5.1. Introduction

Over the past few years, the design and synthesis of π-conjugated systems with specific electronic and optical properties have been an active area of research in the field of materials sciences.[1–6] The exploration of new π-conjugated materials that exhibit enhanced properties possesses the potential for advancing the development of optoelectronic devices with better efficiency and cost-effectiveness.[7–12] The π-conjugated systems are widely used as prominent materials in electronic and optical devices, comprising an important area of research owing to their numerous applications in organic photovoltaic cells (OPVs), organic field-effect transistors (OFETs), organic photodetectors, organic light-emitting diodes (OLEDs), nonlinear optics, and bioimaging.[13–20]

The phenothiazine (PTZ) moiety is an important class of heterocyclic compound with a non-planar butterfly structure because it contains electron-rich nitrogen (*N*) and sulfur (*S*) heteroatoms. Phenothiazine has a dihedral angle of 158.51° between the planes of its two benzene rings.[21–23] Phenothiazine derivatives have unique electrical and optical properties that make them useful in optoelectronic devices including organic field effect transistors (OFETs), dye-sensitized solar cells (DSSCs), organic light-emitting diodes (OLEDs), and organic solar cells.[24–26] *N*-Methyl-*p*-toluenesulfonamide (NTs) can be used as a mild dehydrating agent in reactions that involve the formation of amides and other nitrogen-containing compounds.[27] It can also be used as a protecting group for amines and as a catalyst in various chemical reactions.[28] The ability of *N*-Methyl-*p*-toluenesulfonamide to act as a donor molecule is due to the presence of a lone pair of electrons on the nitrogen atom in its molecular

structure.[29] The use of *N*-Methyl-*p*-toluenesulfonamide as a donor-acceptor system in organic electronics has been studied for its potential applications in organic solar cells, organic light-emitting diodes (OLEDs), organic field-effect transistors (OFETs) and other electronic devices.[30, 31] The 1,1,2,2-tetracyanoethylene (TCNE) and 7,7,8,8-tetracyanoquinodimethane (TCNQ) are π-conjugated molecules that possess strong electron-accepting properties. This is attributed to the electron-withdrawing nature of the four cyano groups present in both compounds. They undergo a [2 + 2] cycloaddition-retroelectrocyclization (CA-RE) reaction with π-conjugated electron-rich alkynes to produce donor-acceptor (D-A) based compounds in a good yield.[32–35] TCNE and TCNQ are utilized in a variety of applications such as organic field-effect transistors, organic solar cells, and nonlinear optical materials.[36, 37] Diederich, Michinobu, Shoji, Trolez, Nakamura and Kato *et al*. investigated the potential of donor-acceptor-based TCBD and DCNQ functionalized derivatives as redox-active ICT chromophores for a variety of optoelectronic applications.[38–46] Our group has recently reported a set of donor-acceptor TCBD and DCNQ functionalized phenothiazine derivatives with *N*,4-dimethylbenzenesulfonamide, hydrogen, thiophene, carbazole, and triphenylamine donors at the terminal position.[47, 48] The DCNQ moiety exhibits a robust ICT band in the NIR region and a facile reduction wave compared to the TCBD moiety.[47, 49] Herein, we have investigated the optoelectronic, thermal, and computational studies by introducing *N*,4-dimethylbenzenesulfonamide at the terminal position and incorporation of TCBD and DCNQ in phenothiazine derivatives **1**–**5** (Figure 5.1).

In this contribution, the symmetrical phenothiazine derivative (**PTZ-NTs)$_2$**, **1** was designed and synthesized *via* the Corey-Fuchs reaction followed by Evano′s condition. Further, the TCBD/DCNQ-functionalized symmetrical and unsymmetrical phenothiazine derivatives (**PTZ-NTs)$_2$-TCBD**, **2**; (**PTZ-NTs)$_2$-(TCBD)$_2$**, **3**; (**PTZ-NTs)$_2$-DCNQ**, **4**; and (**PTZ-NTs)$_2$-(DCNQ)$_2$**, **5** were synthesized by [2 + 2] cycloaddition retroelectrocyclization [CA-RE] reaction with strong

electron acceptors TCNE and TCNQ in good yields (see Figure 5.1 for structures; PTZ = 10-propyl-10*H*-phenothiazine, NTs = *N*,4-dimethylbenzenesulfonamide or *N*-Methyl-*p*-toluenesulfonamide, TCBD = 1,1,4,4-tetracyanobutadiene and DCNQ = dicyanoquinodimethane). Our objective was to investigate the effects of incorporating strong acceptor TCBD and DCNQ moieties on the electrochemical, photophysical, thermal stability, and computational studies of phenothiazine derivatives (**PTZ-NTs)$_2$-TCBD**, **2**; (**PTZ-NTs)$_2$-(TCBD)$_2$**, **3**; (**PTZ-NTs)$_2$-DCNQ**, **4**; and (**PTZ-NTs)$_2$-(DCNQ)$_2$**, **5**. The photophysical results indicate that the phenothiazine derivatives **4** and **5** functionalized with DCNQ exhibit an intramolecular charge transfer (ICT) band at longer wavelengths as compared to phenothiazine derivatives **2** and **3** which are substituted with TCBD. This difference can be explained by the existence of strong donor–acceptor (D–A) interactions.[47–49]

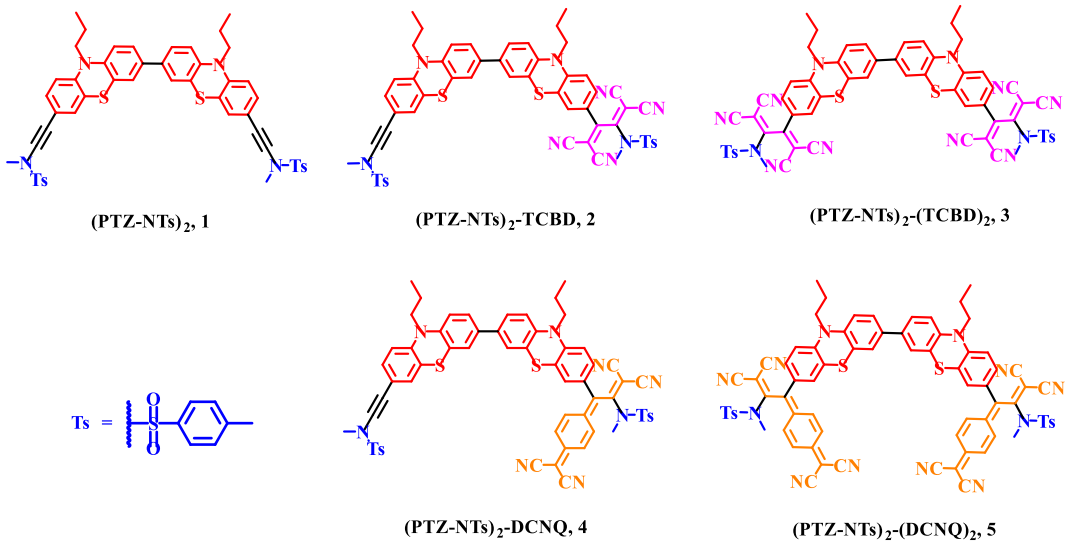

Figure 5.1. Chemical structures of unsymmetrical and symmetrical phenothiazine derivatives **1–5**.

5.2. Results and Discussion

The synthesis of unsymmetrical and symmetrical donor-acceptor-based phenothiazine derivatives **1–5** are shown in Schemes 5.1 and 5.2. The ynamides precursor **1** was synthesized by the Corey-Fuchs reaction followed by Evano′s procedure.[50] The reaction of aldehydes **6** with carbon tetrabromide and triphenylphosphine in dichloromethane at 0 °C

resulted geminal-dibromovinyl compounds **7** in 85% yield, after the Evano′s conditions using *N*-methyl-*p*-toluenesulfonamide, cesium carbonate, *N*,*N*-dimethylethylenediamine (DMEDA), and copper iodide as catalysts in 1,4-dioxane at 60 °C, symmetrical phenothiazine derivative **1** was formed in 60% yield (Scheme 5.1).

The [2 + 2] cycloaddition-retroelectrocyclization (CA-RE) reaction of symmetrical phenothiazine **1** with 1.1 equivalents of TCNE in dichloromethane (DCM) for 4 h at room temperature resulted in an unsymmetrical phenothiazine **2** in 55% yield, whereas the reaction of **1** with 2.5 equivalents of TCNE in DCM for 24 h at 40 °C resulted in a symmetrical phenothiazine **3** in 65% yield. The DCNQ functionalized symmetrical and unsymmetrical phenothiazines **4** and **5** were synthesized by [2 + 2] cycloaddition-retroelectrocyclization reaction. The reaction of symmetrical phenothiazine **1** with 1.1 equivalents of TCNQ in dichloroethane (DCE) for 10 h at 80 °C resulted in an unsymmetrical phenothiazine **4** in 50% yield, whereas the reaction of **1** with 2.5 equivalents of TCNQ in dichloroethane for 24 h at 100 °C resulted in the DCNQ substituted symmetrical phenothiazine **5** in 60% yield (Scheme 5.2).

The unsymmetrical and symmetrical phenothiazine derivatives **1–5** were purified by column chromatography using hexane:DCM as the solvent and characterized by ^{1}H NMR spectroscopy, ^{13}C{H} NMR spectroscopy, and HRMS techniques.

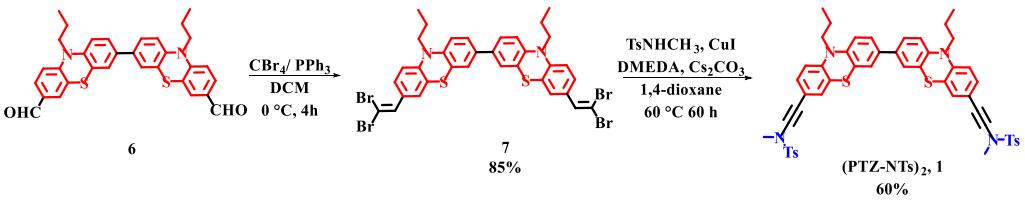

Scheme 5.1. Synthetic route for symmetrical phenothiazine (**PTZ-NTs)$_2$**, **1**.

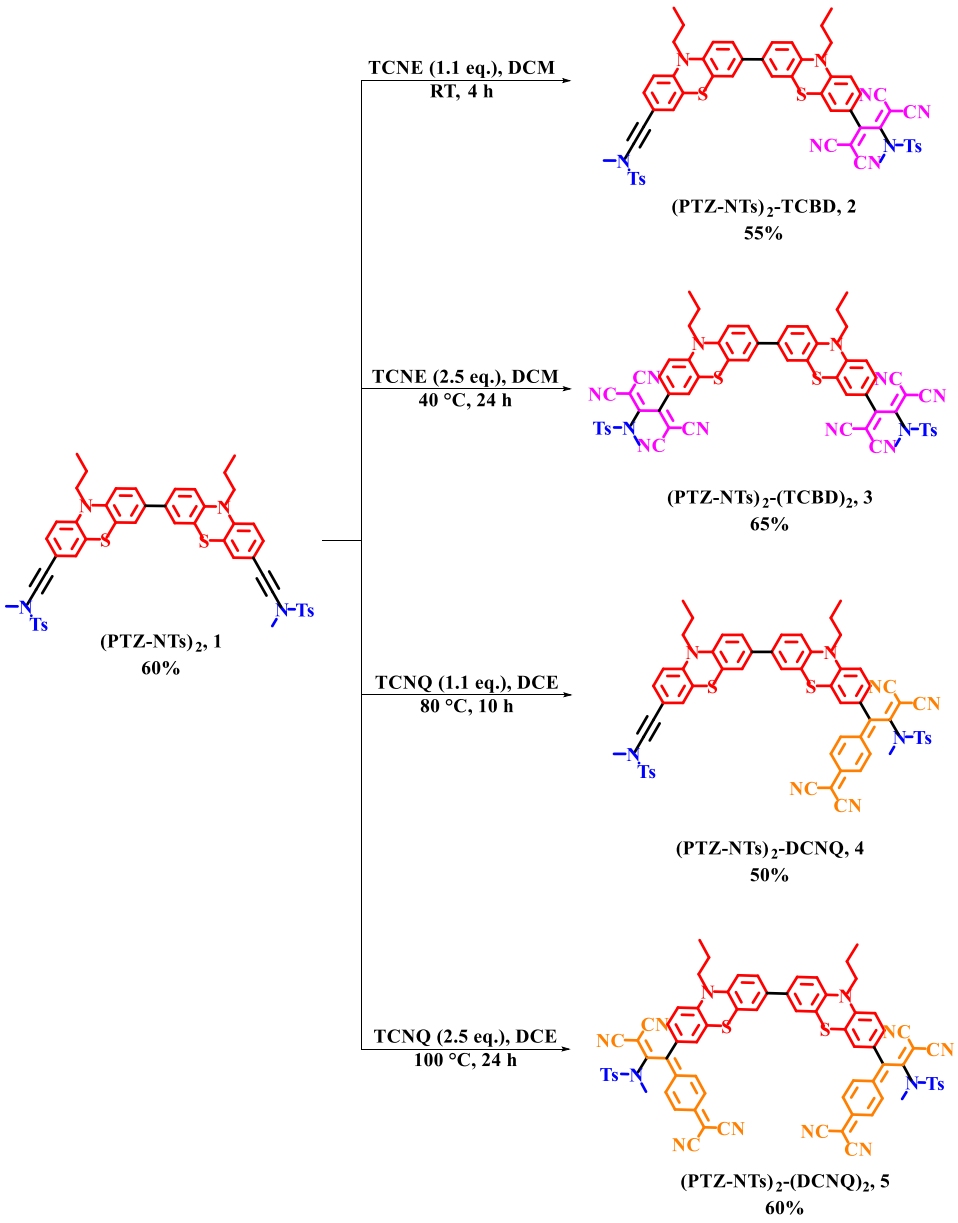

Scheme 5.2. Synthetic route for unsymmetrical and symmetrical phenothiazine derivatives (**PTZ-NTs)2-TCBD**, **2**; (**PTZ-NTs)2-(TCBD)2**, **3**; (**PTZ-NTs)2-DCNQ**, **4**; and (**PTZ-NTs)2-(DCNQ)2**, **5**.

5.3. Photophysical Properties

The optical characteristics of the unsymmetrical and symmetrical donor-acceptor-based phenothiazine derivatives **1–5** were recorded at room temperature in dilute DCM solutions (1×10^{-5} M) as shown in Figure 5.2. The relevant information such as the optical bandgap, extinction coefficient, and absorption maxima (λ_{max}) are listed in Table 5.1.

The absorption maxima of the ynamide functionalized symmetrical phenothiazine derivative **1** exhibit an absorption band at 377 nm corresponding to the π–π* transition. The absorption spectra of the mono- and di-TCBD/DCNQ substituted unsymmetrical and symmetrical phenothiazine derivatives **2–5** exhibit three absorption bands at higher energy region in the range of 280–500 nm, corresponding to π→π* transition and broad absorption band at lower energy region in the range of 500–1000 nm attributed to intramolecular charge transfer (ICT) transition. The absorption maxima of the mono- and di-TCBD incorporated unsymmetrical and symmetrical phenothiazine derivatives **2** and **3** reveal an absorption band in the lower energy region at 629 nm and 625 nm, respectively which corresponds to intramolecular charge transfer (ICT) transitions from the donor PTZ to acceptor TCBD moiety.[47,48] At the same time, the phenothiazine derivatives **4** and **5** functionalized with mono- and di-DCNQ show absorption maxima in the lower energy region at 734 nm and 728 nm, respectively attributed to the ICT transitions because of the strong donor-acceptor interactions between donor phenothiazine to strong acceptor DCNQ moiety. The ICT bands of phenothiazine derivatives **4** and **5** are bathochromically shifted by ~105 nm corresponding to the incorporation of DCNQ acceptor moieties as compared to TCBD functionalized derivatives **2** and **3**.

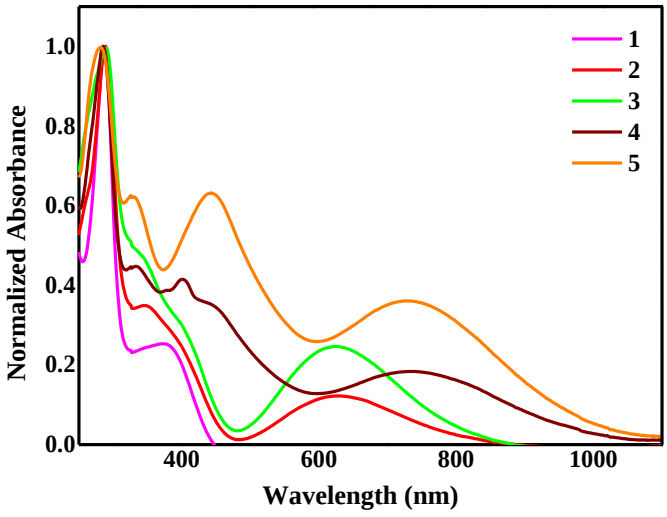

Figure 5.2. Normalized electronic absorption spectra of symmetrical and unsymmetrical phenothiazine derivatives **1–5** in dichloromethane (1×10^{-5} M) were recorded at 25 °C.

The optical band gap values of the TCBD and DCNQ incorporated phenothiazine derivatives **2**, **3**, **4**, and **5** are 1.45, 1.49, 1.15, and 1.17, respectively, and follow the order **3** > **2** > **5** > **4**. The trend clearly shows that the strong electron acceptor DCNQ unit functionalized donor–acceptor phenothiazines **4** and **5** resulted in an ICT band at a longer wavelength region with a low optical bandgap in comparison with TCBD substituted phenothiazines **2** and **3** which corresponds to a strong donor–acceptor interaction. The transitions can be explained through theoretical studies using TD-DFT calculations.

Table 5.1. Photophysical and Computational data of symmetrical and unsymmetrical phenothiazine **1–5**.

Compounds	λ_{max} **(nm)**[a]	**ε** **(M^{-1} cm^{-1})**[a]	E_g^{opt} **(eV)**[a]	**HOMO (eV)**[b]	**LUMO (eV)**[b]	**band-gap (eV)**[b]
1	377	15900	2.74	–4.89	–1.17	3.72
2	629	7100	1.45	–5.11	–3.24	1.87
3	625	8700	1.49	–5.61	–3.36	2.25
4	734	9200	1.15	–5.09	–3.74	1.35
5	728	14800	1.17	–5.53	–3.83	1.70

[a]Absorbance measured in dichloromethane at (1×10^{-5} M); λ_{max} = absorption wavelength; ε = extinction coefficient; E_g^{opt} = optical bandgap; [b]Theoretical data obtained from density functional theory (DFT) calculations performed at the B3LYP/6-31G (d,p) level.

5.4. Electrochemical Properties

The electrochemical potentials of unsymmetrical and symmetrical phenothiazine derivatives **1–5** were determined using differential pulse voltammetry (DPV) and cyclic voltammetry (CV) with 0.1 M tetrabutylammonium hexafluorophosphate ($TBAPF_6$) working as a supporting electrolyte. The electrochemical data are demonstrated in

Table 5.2, and the representative cyclic voltammograms and differential pulse voltammograms for phenothiazine derivatives **1–5** are shown in Figures 5.3 and 5.4.

The unsymmetrical and symmetrical phenothiazine derivatives **1–5** exhibit two oxidation waves corresponding to the phenothiazine unit and one oxidation wave corresponding to the NTs moiety. The first and second oxidation waves for **1–5** at 0.70 V, 0.86 V; 0.75 V, 1.04 V; 0.93 V, 1.08 V; 0.71 V, 0.93 V; and 0.84 V, 0.97 V, respectively, which are attributed to the PTZ unit, whereas the third oxidation wave at 1.58 V, 1.57 V, 1.64 V, 1.63 V, and 1.65 V, respectively corresponding to the terminal NTs moiety. The phenothiazine derivatives **2–5** functionalized with TCBD and DCNQ show two reduction waves at –0.27 V, –0.74 V; –0.28 V, –0.77 V; –0.15 V, –0.29 V; and –0.15 V, –0.28 V, respectively, corresponding to the acceptors TCBD/DCNQ moiety. The HOMO and LUMO values were determined using the formula HOMO/LUMO = –(E_{onset} + 4.4) eV from the onset value of the oxidation or reduction wave (E_{onset}).[51, 52] The values for HOMO energy levels of unsymmetrical and symmetrical phenothiazine derivatives **1–5** are –5.98 eV, –5.97 eV, –6.04 eV, –6.03 eV and –6.05 eV, respectively, and the LUMO energy levels are –4.13 eV, –4.12 eV, –4.25 eV and –4.25 eV, respectively. The electrochemical HOMO–LUMO gaps for unsymmetrical and symmetrical phenothiazine derivatives **2–5** are 1.84 eV, 1.93 eV, 1.78 eV and 1.80 eV, respectively. The energy gap of phenothiazine derivatives **2–5** follows the order **3** > **2** > **5** > **4** which is consistent with the optical and theoretical HOMO-LUMO gap. The electrochemical studies indicate that the mono and di-DCNQ functionalized phenothiazine chromophores **4** and **5** have a low HOMO–LUMO gap and a substantial role in stabilizing the LUMO energy levels as compared to the TCBD substituted chromophores **2** and **3**.

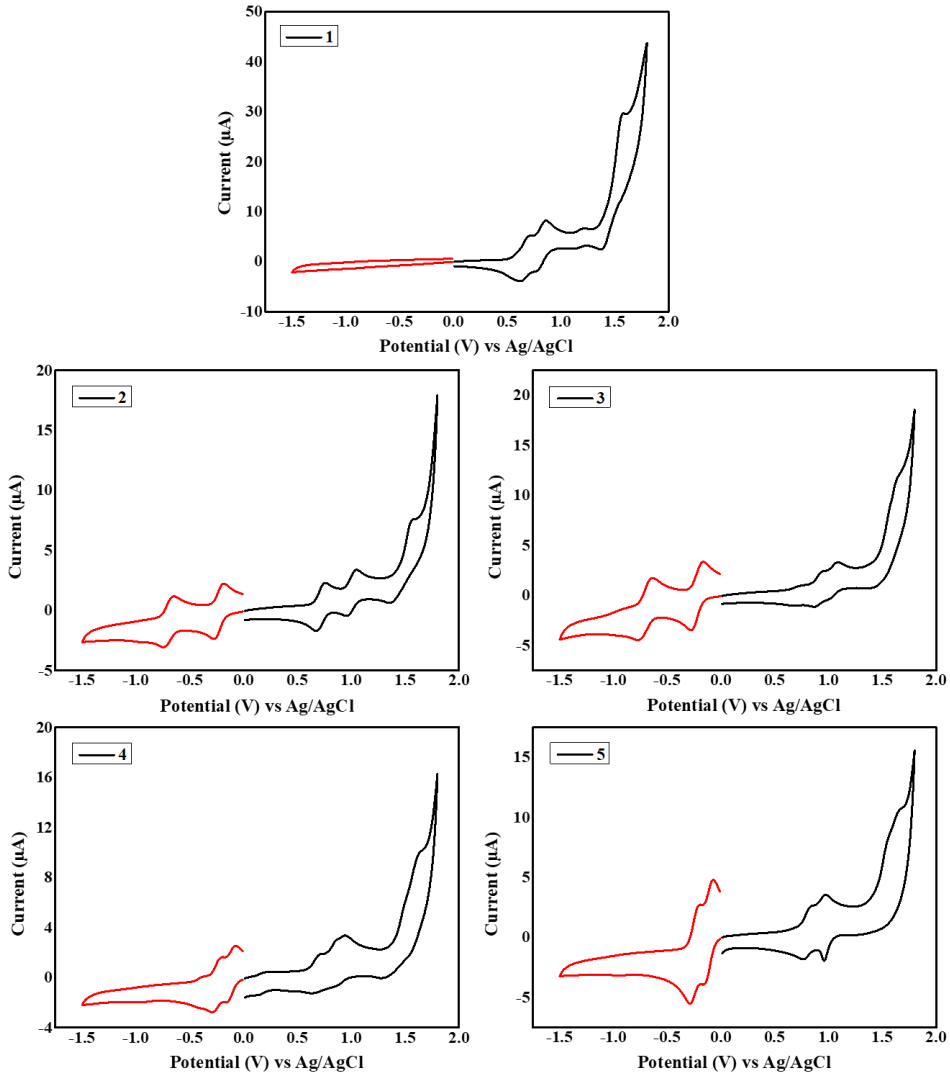

Figure 5.3. Cyclic voltammograms of phenothiazine derivatives **1–5** in 0.1 M solution of Bu_4NPF_6 in dichloromethane at 100 mV s^{-1} scan rate *versus* saturated Ag/AgCl electrode at 25 °C.

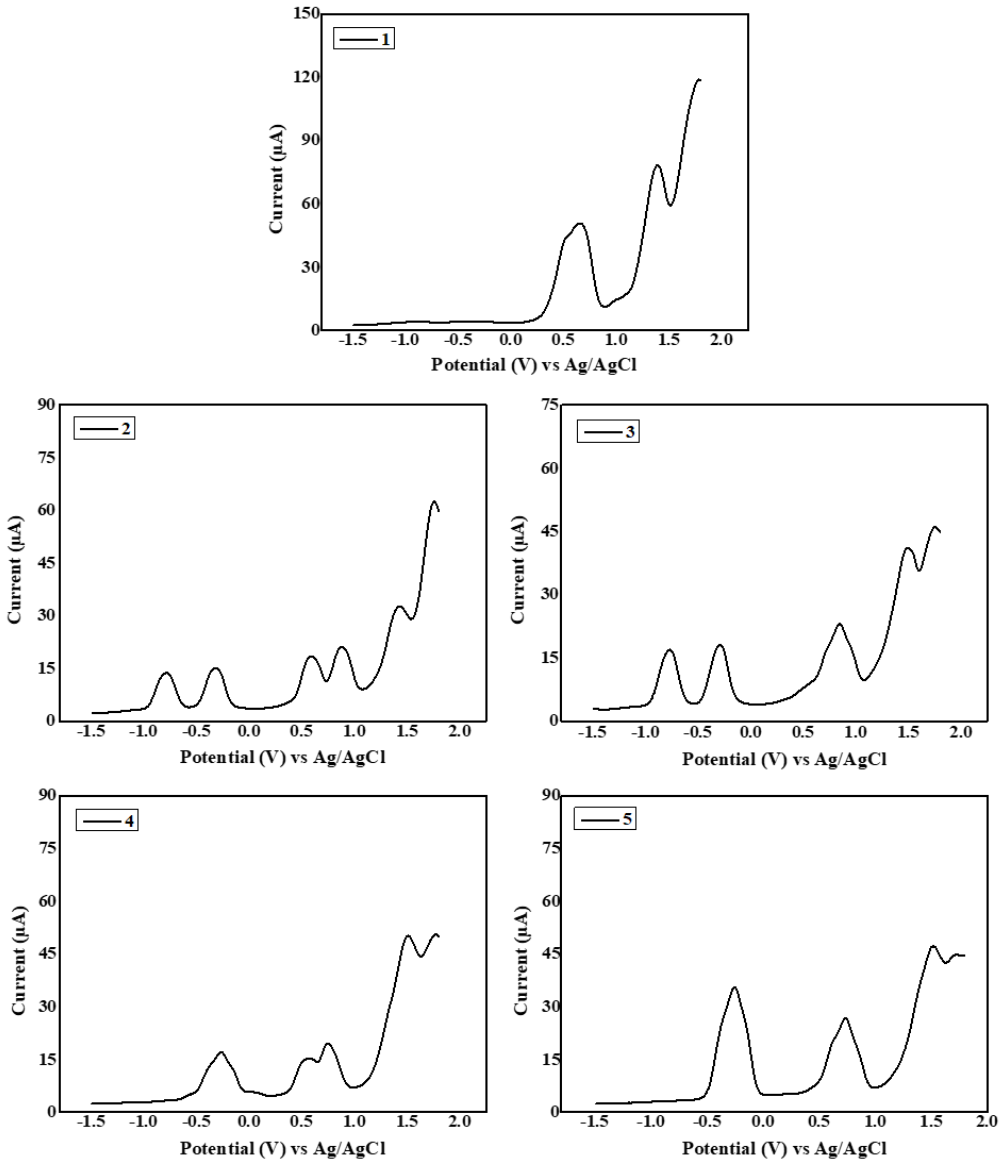

Figure 5.4. Differential pulse voltammograms of phenothiazine derivatives **1–5** in 0.1 M solutions of Bu_4NPF_6 in dichloromethane at 100 mV s^{-1} scan rate *versus* saturated Ag/AgCl electrode at 25 °C.

Table 5.2. Electrochemical data and Thermal Stability of symmetrical and unsymmetrical phenothiazine **1–5**.

Compounds	E_{red} **(V)**[a]	E_{ox} **(V)**[a]	E_{HOMO} **(eV)**[a]	E_{LUMO} **(eV)**[a]	E_g **(eV)**[a]	**Thermal Stability**[b] T_d **(°C)**
1	-	0.70 0.86 1.58	-5.98	-	-	224

2	-0.27 -0.74	0.75 1.04 1.57	-5.97	-4.13	1.84	209
3	-0.28 -0.77	0.93 1.08 1.64	-6.04	-4.12	1.93	214
4	-0.15 -0.29	0.71 0.93 1.63	-6.03	-4.25	1.78	251
5	-0.15 -0.28	0.84 0.97 1.65	-6.05	-4.25	1.80	249

[a]Electrochemical analysis was estimated by differential pulse voltammetry, in 0.1 M solution of $TBAPF_6$ in DCM at 100 mV s^{-1} scan rate *versus* saturated Ag/AgCl electrode at 25 °C. [b]Decomposition temperatures for 5% weight loss at a heating rate of 10 °C min^{-1}, under a nitrogen atmosphere.

5.5. Thermogravimetric Analysis

The thermal characteristics of the symmetrical and unsymmetrical phenothiazines **1–5** were examined using a thermogravimetric analysis (TGA) in a nitrogen atmosphere at a heating rate of 10 °C min^{-1}. The relevant thermograms are represented in Figure 5.5 and the data are listed in Table 5.2. The decomposition temperatures (T_d) for ynamide functionalized symmetrical phenothiazine derivative **1** at 5% weight loss was found to be at 224 °C, whereas for mono- and di-TCBD/DCNQ functionalized unsymmetrical and symmetrical phenothiazine derivatives **2–5** show decomposition temperatures (T_d) were found to be at 209 °C, 214 °C, 251 °C, 249 °C, respectively. The thermal stability of the phenothiazine derivatives **1–5** follows the order **4** > **5** > **1** > **3** > **2**. The thermogram of phenothiazine derivatives **1–5** exhibited three weight loss stages between 180–800 °C, with a residual mass of 40% at 600 °C. These decomposition temperatures reveal that the phenothiazine derivatives **4** and **5** functionalized with DCNQ are thermally more stable than the phenothiazine derivatives **2** and **3** substituted with TCBD.

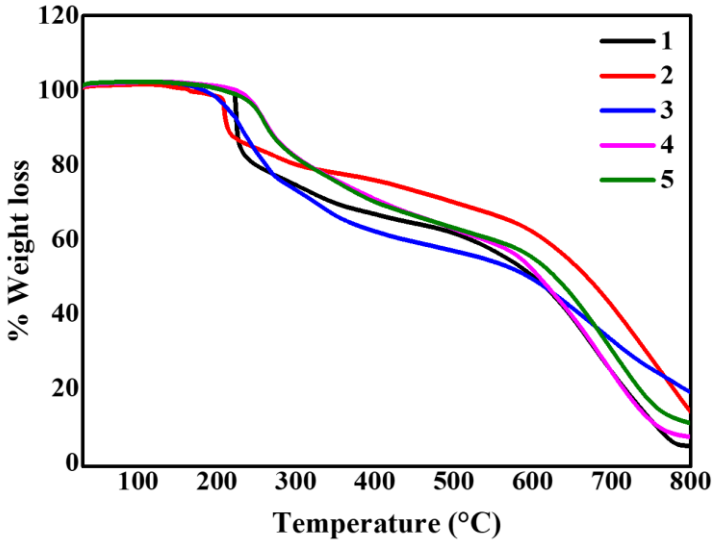

Figure 5.5. Thermogravimetric analysis of symmetrical and unsymmetrical phenothiazine derivatives **1–5** measured at a heating rate of 10 °C min^{-1} under a nitrogen atmosphere.

5.6. Computational Calculations

The density functional theory calculation was carried out on unsymmetrical and symmetrical donor-acceptor-based phenothiazine derivatives **1–5** to investigate ground-state geometries and molecular conformations at B3LYP/6-31G(d,p) basis set level for C, H, N, O, and S in the Gaussian 09W program.[53] Figure 5.6b shows the frontier molecular orbitals and the energy level diagram for the optimized symmetrical and unsymmetrical phenothiazine **1–5** geometries with the HOMOs (highest occupied molecular orbitals), LUMOs (lowest unoccupied molecular orbitals), energy gap and the relevant data are demonstrated in Table 5.1. The optimized geometry showed that the entire molecule framework had a twisted backbone, enabling effective π-delocalization (Figure 5.6a). The ynamides functionalized symmetrical phenothiazine **1** exhibit a non-planar structure due to the presence of phenothiazine (butterfly shape) and ynamide moiety. However, the symmetrical and unsymmetrical phenothiazine **2–5** exhibit a twisted geometry due to the presence of multiple nonplanar acceptor units TCBD and DCNQ moieties. The HOMOs of the symmetrical and unsymmetrical phenothiazines **1–5** are mainly concentrated on both phenothiazine units and the LUMO of symmetrical

phenothiazine **1** is mainly localized on the ynamide moiety with some contributions of centered phenothiazine units. On the other hand, in the case of symmetrical and unsymmetrical phenothiazines **2–5** the lowest unoccupied molecular orbitals are centered on the TCBD and DCNQ moieties.

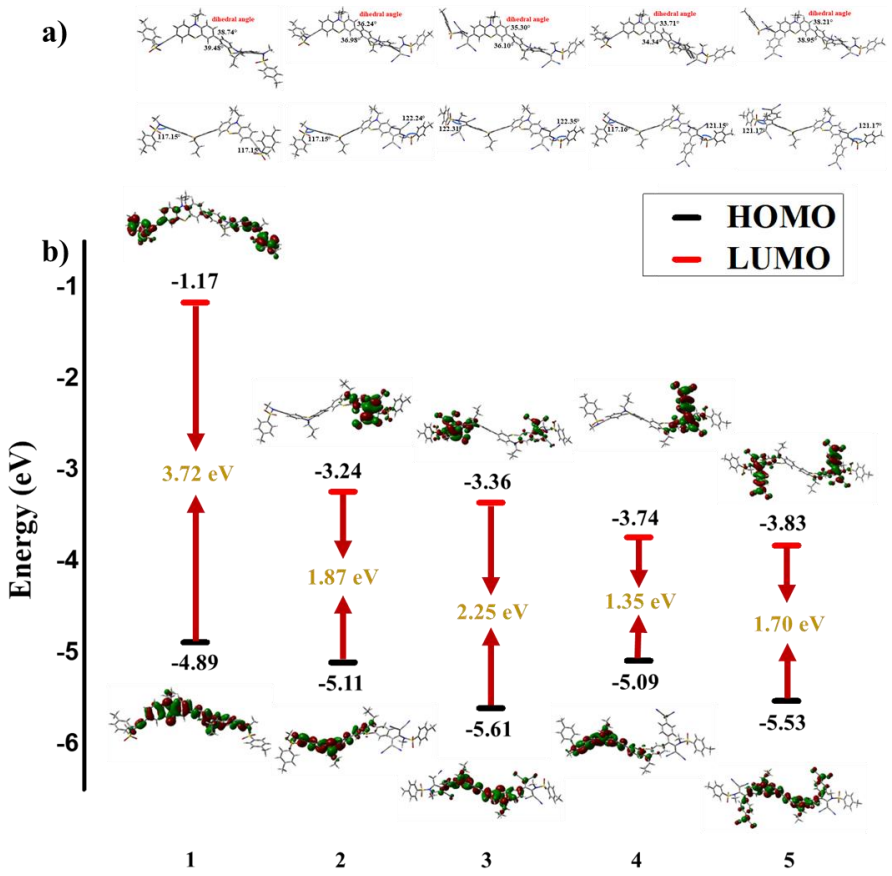

Figure 5.6. (a) The geometry-optimized structures (front view and side view) and (b) Energy level diagram and HOMO–LUMO frontier molecular orbitals pictures of phenothiazine derivatives **1–5** calculated by DFT calculations at the B3LYP/6-31G (d,p) level.

The theoretically calculated HOMO energy levels of the symmetrical and unsymmetrical phenothiazine derivatives **1–5** are –4.89 eV, –5.11 eV, –5.61 eV, –5.09 eV and –5.53 eV and the corresponding LUMO energy levels are –1.17 eV, –3.24 eV, –3.36 eV, –3.74 eV and –3.83 eV, respectively. The theoretically calculated HOMO–LUMO energy gaps for **1–5** are 3.72, 1.87, 2.25, 1.35 and 1.70 eV, respectively, and the order of the gaps follows the pattern **1** > **3** > **2** > **5** > **4**. The symmetrical phenothiazine **1** with the highest HOMO–

LUMO energy gap exhibits a lower wavelength region in the absorption spectra, while the TCBD/DCNQ substituted phenothiazine **2−5** exhibited bathochromically shifted absorption in the NIR region because of the tunable HOMO–LUMO gap. The DCNQ functionalized phenothiazine **4** and **5** reveal a lower HOMO–LUMO energy gap as compared to TCBD functionalized phenothiazine **2** and **3** due to the strong accepting character of the DCNQ moiety.

The TD-DFT (Time-dependent density functional theory) calculation was performed at the B3LYP/6-31G(d,p) level on the optimized unsymmetrical and symmetrical phenothiazine derivatives **1–5** in DCM to calculate the transitions involved in the electronic absorption spectra. All the transitions with compositions, assignments, and oscillator strengths are tabulated in Table 5.3.

The TD-DFT results show that the absorption band originating from HOMO→LUMO at 382 nm for ynamides functionalized phenothiazine derivative **1** corresponds to π-π* transition (Figure 5.7). A comparison of experimental and theoretically calculated absorption spectra of the mono- and di-TCBD incorporated unsymmetrical and symmetrical phenothiazine derivatives **2** and **3** are shown in Figure 5.8. The simulated absorption spectra of derivatives **2** and **3** of phenothiazine showed absorption maxima at 654 nm and 737 nm, respectively. These absorption maxima arises due to the transition from HOMO-1→LUMO to HOMO→LUMO, respectively. The symmetrical and unsymmetrical phenothiazine derivatives **4** and **5** that are incorporated with mono- and di-DCNQ exhibit absorption maxima at 857 nm and 794 nm, respectively, originating from HOMO-1→LUMO. These absorption maxima correspond to ICT transition because of the strong donor–acceptor interaction (Figure 5.9). The theoretically calculated electronic transitions and simulated spectra of symmetrical and unsymmetrical phenothiazine **2–5** demonstrate the role of the intramolecular charge transfer (ICT) effect.[54, 55] The experimentally predicted electronic absorption wavelength was found to be lower than the theoretically calculated values, which may be due to various factors such as temperature, solvent effect, and dipole moment.

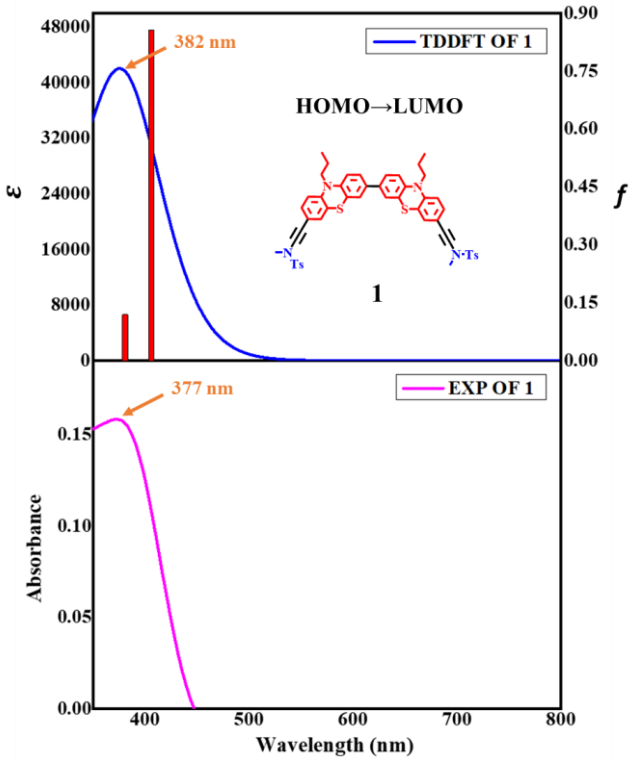

Figure 5.7. Theoretical (top) and experimental (bottom) absorption spectra of phenothiazine derivative **1**.

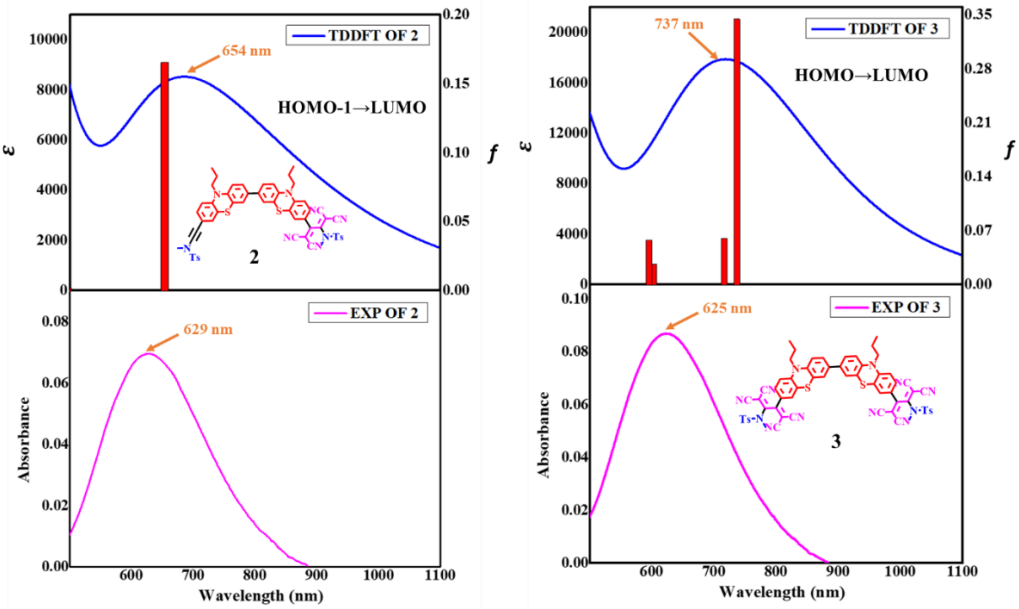

Figure 5.8. Theoretical (top) and experimental (bottom) absorption spectra of phenothiazine derivatives **2** and **3**.

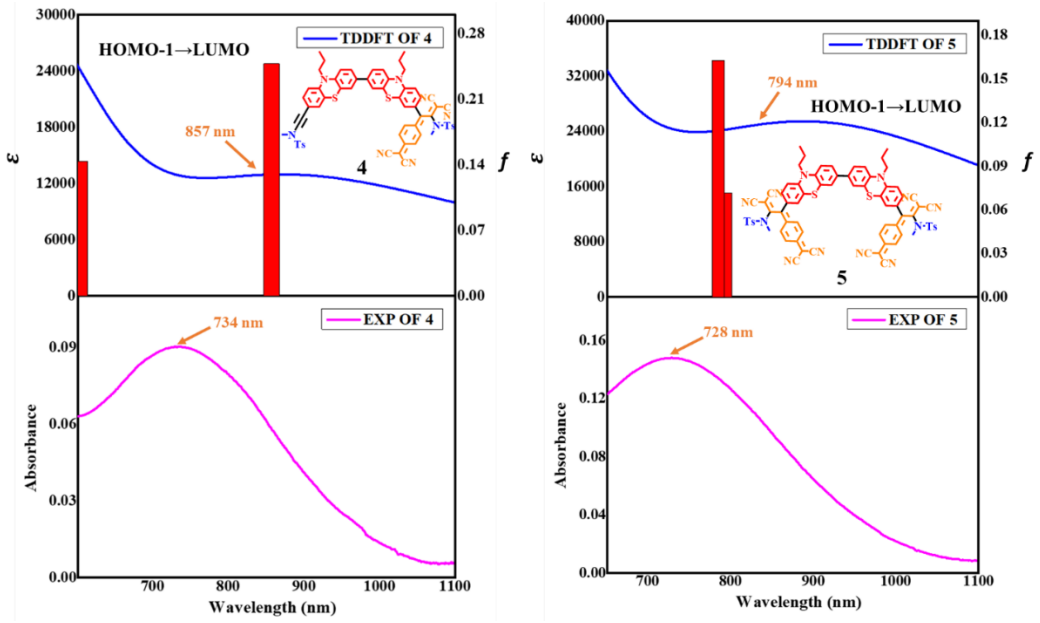

Figure 5.9. Theoretical (top) and experimental (bottom) absorption spectra of phenothiazine derivatives **4** and **5**.

Table 5.3. Calculated electronic transitions for symmetrical and unsymmetrical phenothiazine **1–5** in dichloromethane.

Compounds	Wavelength (nm)	Composition and Molecular Contribution	f^a	Assignment
1	382	HOMO→LUMO (0.59)	0.85	π–π*
2	654	HOMO-1→LUMO (0.69)	0.16	ICT
3	737	HOMO→LUMO (0.68)	0.34	ICT
4	857	HOMO-1→LUMO (0.69)	0.25	ICT
5	794	HOMO-1→LUMO (0.69)	0.17	ICT

[a]Oscillator strength.

5.7. Molecular Electrostatic Potentials

The molecular electrostatic potentials (MEPs) analysis of the unsymmetrical and symmetrical phenothiazine derivatives **1–5** was used to analyze the distribution of electrostatic charge on various components of the compounds using the B3LYP/6-31G(d,p) basis set level by the Gaussian 09W program. The molecular electrostatic potential (ESP) plots were investigated for a qualitative assessment of the charge transfer from the donor PTZ to the acceptor TCBD/DCNQ moieties. The

examined molecular ESP surfaces of the unsymmetrical and symmetrical phenothiazine derivatives **1–5** have been demonstrated in Figure 5.10. The complete self-consistent field (SCF) density surface from -5.684e-2 to +5.684e-2 has been used to analyze the ESP plots for the various compounds. The area with low electron density is represented by the blue colour (positive region), whereas the area with high electron density is represented by the red colour (negative region).[56] These compounds produced high electron density red colors in the sulfonyl and cyano regions, as well as low electron density blue colors in the phenothiazine and phenyl ring regions. The molecular ESP surfaces of the symmetrical and unsymmetrical phenothiazine derivatives **1–5** containing *N*,4-dimethylbenzenesulfonamide (NTs), TCBD, and DCNQ moieties have a larger region of negative potential (red regions) because of the more electronegative sulfonyl and cyano units than the corresponding phenothiazine and phenyl rings. Moreover, it can be concluded that in the charge transfer phenomena, the electron density of the donor phenothiazine is distributed over the acceptor TCBD and DCNQ moieties, resulting in considerable delocalization of the charge from the donor unit to the acceptor unit.

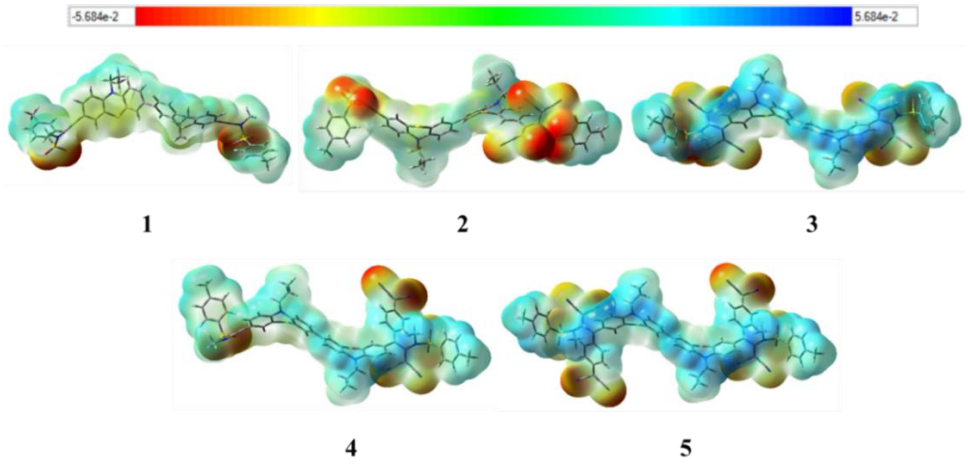

Figure 5.10. Molecular electrostatic potentials (MEPs) of phenothiazine derivatives **1–5** calculated by B3LYP/6-31G (d,p) basis set level using Gaussian 09W program.

5.8. Experimental Section

General methods

The chemicals were used as received unless otherwise indicated. All oxygen or moisture-sensitive reactions were performed under a nitrogen/argon atmosphere. ^{1}H NMR (500 MHz) and ^{13}C{H} NMR (125 MHz) spectra were recorded on Bruker 500 MHz FT-NMR spectrometers at room temperature. ^{1}H NMR chemical shifts are reported in parts per million (ppm) relative to the solvent residual peak ($CDCl_3$, 7.26 ppm). Multiplicities are given as s (singlet), d (doublet), t (triplet) and m (multiplet) and the coupling constants, *J*, are given in hertz. ^{13}C{H} NMR chemical shifts are reported relative to the solvent residual peak ($CDCl_3$, 77.0 ppm). The UV-visible absorption spectra were recorded on a PerkinElmer Lambda 35 UV−visible spectrophotometer in DCM solvent at room temperature. Thermogravimetric analysis was performed on a Mettler Toledo thermal analysis system. High-resolution mass spectrometry (HRMS) was recorded with an Agilent 6545A Q-TOF mass spectrometer and on a Bruker-Daltonics micrOTOF-Q II mass spectrometer used to measure the mass of the compounds. The cyclic voltammograms (CVs) and differential pulse voltammograms (DPVs) were recorded on a PalmSence 4 electrochemical analyzer in dichloromethane (CH_2Cl_2) solvent, and 0.1 M tetrabutylammonium hexafluorophosphate (Bu_4NPF_6) was used as the supporting electrolyte. The electrodes used were glassy carbon as a working electrode, Pt wire as a counter electrode, and Ag/AgCl electrode as a reference electrode. The scan rate was 100 mV s^{-1} for cyclic voltammetry at 25 °C. The CV and DPV plotting convention is the IUPAC convention. The polishing material is a commercially available polishing pad and alumina (Al_2O_3).

Synthesis of *N*,*N*'-((10,10'-dipropyl-10*H*,10'*H*-[3,3'-biphenothiazine]-7,7'-diyl)-bis(ethyne-2,1-diyl))bis(*N*,4-dimethylbenzenesulfonamide) [(PTZ-NTs)$_2$, 1]

In a 100 mL round-bottomed flask, a solution of dibromoalkene **7** (500 mg, 0.5925 mmol), TsNHMe (274 mg, 1.48 mmol), CuI (45 mg, 0.2370 mmol), *N*,*N*'-dimethylethylenediamine (52 μL, 0.4740 mmol) and Cs_2CO_3 (1.45 g, 4.44 mmol) in dry 1,4-dioxane (20 mL) was heated to 60 °C under a nitrogen atmosphere over 60 h. Then the solvent was

evaporated under a vacuum. The residue was dissolved in dichloromethane, and this solution was washed with water for several times, dried with anhydrous Na_2SO_4, and filtered off. The crude was purified by column chromatography (cyclohexane:dichloromethane 1:0 to 4:6) to give **phenothiazine 1** as a yellow solid with a 60% yield: m.p. 106–107 °C; ^{1}H NMR (500 MHz, CHLOROFORM-d) δ = 7.84 (d, *J* = 8.1 Hz, 4 H), 7.39 (d, *J* = 7.9 Hz, 4 H), 7.17 (d, *J* = 8.4 Hz, 3 H), 7.14 - 7.11 (m, 3 H), 6.97 - 6.91 (m, 2 H), 6.86 (d, *J* = 8.1 Hz, 2 H), 6.76 (d, *J* = 8.4 Hz, 2 H), 3.81 (t, *J* = 7.1 Hz, 4 H), 3.15 (s, 6 H), 2.49 (s, 6 H), 1.89 - 1.75 (m, 4 H), 1.02 (t, *J* = 7.3 Hz, 6 H); ^{13}C{H} NMR (125 MHz, CHLOROFORM-d) δ = 144.9, 144.7, 143.6, 134.5, 133.2, 131.0, 130.5, 130.3, 129.9, 129.8, 129.7, 128.0, 127.9, 127.5, 125.3, 125.1, 124.6, 124.2, 116.3, 115.6, 114.9, 83.6, 68.2, 67.1, 49.3, 39.4, 29.4, 21.7, 20.1, 14.1, 11.3; HRMS (ESI-TOF) m/z calculated for $C_{50}H_{46}N_4O_4S_4$ + K 933.2033 $[M + K]^+$, measured 933.2288 $[M + K]^+$.

Synthesis of *N*-((10,10'-dipropyl-7'-(1,1,4,4-tetracyano-3-((*N*,4-dimethylphenyl) sulfonamido)buta-1,3-dien-2-yl)-10*H*,10'*H*-[3,3'-biphenothiazin]-7-yl)ethynyl)-*N*,4-dimethylbenzenesulfonamide [(PTZ-NTs)$_2$-TCBD, 2]

In a 100 mL round-bottomed flask, TCNE (18 mg, 0.134 mmol) was added to a solution of **phenothiazine 1** (150 mg, 0.1675 mmol) in CH_2Cl_2 (20 mL) under an argon atmosphere. The mixture was stirred for 4 h at RT. The solvent was removed in a vacuum, and the product was purified by column chromatography with DCM/hexane (2:1, v/v) as eluent to **phenothiazine 2** as a dark blue color solid with 55% yield: m.p. 115–118 °C; ^{1}H NMR (500 MHz, CHLOROFORM-d) δ = 7.75 (d, *J* = 8.4 Hz, 2 H), 7.66 (dd, *J* = 2.3, 8.9 Hz, 1 H), 7.47 - 7.43 (m, 2 H), 7.38 (d, *J* = 2.4 Hz, 1 H), 7.36 (s, 1 H), 7.35 - 7.32 (m, 2 H), 7.32 - 7.28 (m, 2 H), 7.27 (br. s., 4 H), 7.23 (d, *J* = 2.0 Hz, 1 H), 6.94 - 6.86 (m, 3 H), 6.82 (d, *J* = 8.4 Hz, 1 H), 3.90 (t, *J* = 7.2 Hz, 2 H), 3.83 (t, *J* = 7.2 Hz, 2 H), 3.55 (s, 3 H), 2.49 (s, 3 H), 1.94 - 1.88 (m, 2 H), 1.88 - 1.82 (m, 2 H), 1.56 (s, 6 H), 1.08 (t, *J* = 7.3 Hz, 3 H), 1.03 (t, *J* = 7.3 Hz, 3 H); ^{13}C{H} NMR (125 MHz, CHLOROFORM-d) δ = 164.5, 161.3,

150.8, 147.4, 145.0, 143.9, 140.7, 136.3, 135.5, 133.8, 132.3, 131.8, 130.8, 129.5, 128.5, 128.3, 127.9, 127.0, 125.7, 125.4, 125.2, 125.2, 124.9, 124.7, 124.6, 124.0, 123.1, 116.4, 115.6, 114.9, 114.8, 113.0, 112.6, 110.7, 110.7, 87.9, 82.1, 79.0, 50.1, 49.3, 41.4, 21.9, 20.0, 11.3, 11.2; HRMS (ESI-TOF) m/z calculated for $C_{56}H_{46}N_8O_4S_4$ + Na 1045.2417 $[M + Na]^+$, measured 1045.1827 $[M + Na]^+$.

Synthesis of *N*,*N*'-((10,10'-dipropyl-10*H*,10'*H*-[3,3'-biphenothiazine]-7,7'-diyl)bis(1,1,4,4-tetractlobuta-1,3-diene-3,2-diyl))bis(*N*,4-dimethylbenzenesulfonamide) [(PTZ-NTs)$_2$-(TCBD)$_2$, 3]

In a 100 mL round-bottomed flask, TCNE (72 mg, 0.5585 mmol) was added to a solution of **phenothiazine 1** (200 mg, 0.2234 mmol) in CH_2Cl_2 (20 mL) under an argon atmosphere. The mixture was stirred for 24 h at 40 °C. The solvent was removed in a vacuum, and the product was purified by column chromatography with DCM/hexane (3:1, v/v) as eluent to **phenothiazine 3** as a dark blue color solid with 65% yield: m.p. 123–127 °C; ^{1}H NMR (500 MHz, CHLOROFORM-d) δ = 8.30 - 8.28 (m, 1 H), 8.27 - 8.23 (m, 2 H), 7.88 (d, *J* = 8.4 Hz, 1 H), 7.81 (d, *J* = 8.1 Hz, 2 H), 7.76 (d, *J* = 8.4 Hz, 2 H), 7.69 (dd, *J* = 2.3, 8.9 Hz, 1 H), 7.56 - 7.48 (m, 4 H), 7.46 (d, *J* = 8.2 Hz, 3 H), 7.41 (d, *J* = 1.8 Hz, 1 H), 7.36 - 7.31 (m, 1 H), 7.01 - 6.96 (m, 1 H), 6.94 (d, *J* = 9.0 Hz, 1 H), 4.29 - 4.22 (m, 2 H), 3.96 - 3.87 (m, 2 H), 3.56 (s, 3 H), 3.53 (s, 3 H), 2.51 (s, 3 H), 2.50 (s, 3 H), 2.12 - 2.00 (m, 2 H), 1.97 - 1.86 (m, 2 H), 1.15 (t, *J* = 7.3 Hz, 3 H), 1.10 (t, *J* = 7.3 Hz, 3 H); ^{13}C{H} NMR (125 MHz, CHLOROFORM-d) δ = 164.5, 161.4, 150.7, 147.4, 143.5, 141.2, 135.8, 135.6, 132.3, 131.9, 130.8, 129.7, 128.6, 128.3, 127.3, 125.9, 125.3, 125.0, 124.7, 123.3, 116.5, 115.0, 112.9, 112.6, 110.8, 82.5, 79.0, 60.4, 50.1, 41.4, 21.9, 21.5, 20.1, 11.2; HRMS (ESI-TOF) m/z calculated for $C_{62}H_{46}N_{12}O_4S_4$ + Na 1173.2540 $[M + Na]^+$, measured 1173.2838 $[M + Na]^+$.

Synthesis of *N*-(3,3-dicyano-1-(4-(dicyanomethylene)cyclohexa-2,5-dien-1-ylidene)-2-(7'-(((*N*,4-dimethylphenyl)sulfonamido)ethynyl)-10,10'-dipropyl-10*H*,10'*H*-[3,3'-biphenothiazin]-7-yl)allyl)-*N*,4-dimethylbenzenesulfonamide [(PTZ-NTs)$_2$-DCNQ, 4]

In a 100 mL round-bottomed flask, TCNQ (18 mg, 0.0893 mmol) was added to a solution of **phenothiazine 1** (100 mg, 0.1117 mmol) in DCE (20 mL). The mixture was heated at 80 °C for 10 h. After cooling to room temperature, the solvents were removed under vacuum, and the product was purified by column chromatography with DCM/hexane (3:1, v/v) as the eluent to **phenothiazine 4** as a dark green color solid with 50% yield: m.p. 162–165 °C; ^{1}H NMR (500 MHz, CHLOROFORM-d) δ = 7.77 (d, *J* = 8.2 Hz, 2 H), 7.51 - 7.46 (m, 2 H), 7.39 - 7.34 (m, 2 H), 7.33 - 7.27 (m, 7 H), 7.23 (d, *J* = 8.1 Hz, 2 H), 7.16 - 7.11 (m, 3 H), 6.98 - 6.92 (m, 2 H), 6.89 (t, *J* = 8.5 Hz, 2 H), 6.82 (d, *J* = 8.7 Hz, 1 H), 6.06 (s, 1 H), 3.90 (t, *J* = 7.2 Hz, 2 H), 3.83 (t, *J* = 7.0 Hz, 2 H), 3.38 (s, 3 H), 3.03 (s, 3 H), 2.43 - 2.40 (m, 3 H), 2.37 (s, 2 H), 1.92 (s, 3 H), 1.88 - 1.82 (m, 2 H), 1.09 (t, *J* = 7.5 Hz, 3 H), 1.04 (t, *J* = 7.4 Hz, 3 H); ^{13}C{H} NMR (125 MHz, CHLOROFORM-d) δ = 169.1, 167.2, 153.5, 148.6, 146.5, 146.2, 144.7, 144.0, 141.6, 138.5, 136.9, 136.1, 135.9, 135.4, 133.9, 133.7, 132.9, 132.8, 130.3, 130.1, 129.9, 129.8, 129.6, 128.9, 128.0, 127.8, 127.7, 127.3, 126.9, 126.6, 126.2, 125.7, 125.3, 125.3, 125.1, 124.8, 124.0, 123.5, 118.6, 116.3, 115.5, 115.3, 113.7, 112.0, 111.8, 80.3, 49.9, 49.3, 40.5, 36.3, 31.9, 31.4, 30.2, 29.4, 21.7, 21.6, 20.4, 20.1, 20.1, 14.1, 11.3, 11.3; HRMS (ESI-TOF) m/z calculated for $C_{62}H_{50}N_8O_4S_4$ + Na 1121.2730 $[M + Na]^+$, measured 1121.2765 $[M + Na]^+$.

Synthesis of *N*,*N*'-((10,10'-dipropyl-10*H*,10'*H*-[3,3'-biphenothiazine]-7,7'-diyl)bis(3,3-dicyano-1-(4-(dicyanomethylene) cyclohexa-2,5-dien-1-ylidene)prop-2-ene-2,1-diyl))bis(*N*,4-dimethy-benzenesulfonamide) [(PTZ-NTs)$_2$-(DCNQ)$_2$, 5]

In a 100 mL round-bottomed flask, TCNQ (114 mg, 0.5585 mmol) was added to a solution of **phenothiazine 1** (200 mg, 0.2234 mmol) in DCE (20 mL). The mixture was heated at 100 °C for 24 h. After cooling to room temperature, the solvents were removed under vacuum, and the product was purified by column chromatography with DCM/hexane (4:1, v/v) as the eluent to **phenothiazine 5** as a dark green color solid with 60% yield: m.p. 174–178 °C; ^{1}H NMR (500 MHz,

CHLOROFORM-d) δ = 7.51 (d, *J* = 8.4 Hz, 4 H), 7.37 (d, *J* = 2.0 Hz, 1 H), 7.36 (d, *J* = 2.0 Hz, 1 H), 7.33 - 7.29 (m, 5 H), 7.28 (d, *J* = 2.0 Hz, 4 H), 7.18 (d, *J* = 7.0 Hz, 2 H), 7.16 - 7.14 (m, 2 H), 7.13 - 7.10 (m, 3 H), 7.00 (d, *J* = 1.8 Hz, 2 H), 6.95 (d, *J* = 8.5 Hz, 2 H), 6.91 (d, *J* = 8.7 Hz, 2 H), 3.90 (t, *J* = 7.2 Hz, 4 H), 3.38 (s, 6 H), 2.40 (s, 6 H), 1.95 - 1.88 (m, 4 H), 1.09 (t, *J* = 7.4 Hz, 6 H); ^{13}C{H} NMR (125 MHz, CHLOROFORM-d) δ = 167.2, 153.5, 148.4, 146.6, 146.2, 142.1, 136.9, 135.4, 135.2, 133.8, 132.9, 132.8, 130.4, 130.2, 129.0, 128.2, 128.0, 127.0, 126.6, 125.8, 125.3, 125.0, 123.7, 116.3, 115.3, 113.6, 49.9, 40.5, 31.9, 29.4, 21.8, 21.5, 20.1, 14.1, 11.3; HRMS (ESI-TOF) m/z calculated for $C_{74}H_{54}N_{12}O_4S_4$ + Na 1325.3166 $[M + Na]^+$, measured 1325.3716 $[M + Na]^+$.

5.9. Conclusion

In conclusion, we have designed and synthesized symmetrical and unsymmetrical donor-acceptor based phenothiazine derivatives **1–5** by Corey-Fuchs reaction *via* Evano′s conditions followed by [2 + 2] cycloaddition–retroelectrocyclic ring-opening reaction with strong electron acceptors TCNE and TCNQ in good yields. The intramolecular charge transfer (ICT) band of DCNQ functionalized phenothiazine derivatives **4** and **5** was bathochromically shifted by ~105 nm at a longer wavelength region in comparison to phenothiazine derivatives **2** and **3** substituted with TCBD corresponding to strong donor-acceptor (D–A) interaction. The unsymmetrical and symmetrical **1–5** exhibit three oxidation waves on the anodic region, which corresponds to donor phenothiazine and ynamide moiety. The thermogram of phenothiazine derivatives **1–5** exhibited three weight loss stages between 100 and 700 °C, with a residual mass of 40% at 600 °C. The theoretical studies indicate that the ynamides functionalized symmetrical phenothiazine **1** with the highest HOMO–LUMO energy gap exhibits a lower wavelength region in the absorption spectra, while the TCBD/DCNQ substituted phenothiazine **2−5** exhibited red-shifted absorption in the NIR region because of the tunable HOMO–LUMO gap. The reported unsymmetrical and symmetrical phenothiazines **1–5** provide a new

opportunities for the development of donor–acceptor (D–A) based chromophores with low HOMO–LUMO gaps, which are useful in various optoelectronic applications.

5.10. References

[1] Zhang, J., Xu, W., Sheng, P., Zhao, G., & Zhu, D. (2017). Organic Donor-Acceptor Complexes as Novel Organic Semiconductors. *Accounts of Chemical Research*, *50*(7), 1654–1662. (DOI: 10.1021/ACS.ACCOUNTS.7B00124).

[2] Jiao, Y., Liu, S., Shen, Z., Mao, L., Ding, Y., Ren, D., … Grätzel, M. (2021). Carbazol-phenyl-phenothiazine-based sensitizers for dye-sensitized solar cells. *Journal of Materials Chemistry A*, *9*(46), 26311–26322. (DOI: 10.1039/D1TA08020B).

[3] Patil, H., Gupta, A., Bilic, A., Jackson, S. L., Latham, K., & Bhosale, S. V. (2014). Donor-acceptor-donor modular small organic molecules based on the naphthalene diimide acceptor unit for solution-processable photovoltaic devices. *Journal of Electronic Materials*, *43*(9), 3243–3254. (DOI: 10.1007/S11664-014-3243-X).

[4] Patil, H., Chang, J., Gupta, A., Bilic, A., Wu, J., Sonar, P., & Bhosale, S. V. (2015). Isoindigo-Based Small Molecules with Varied Donor Components for Solution-Processable Organic Field Effect Transistor Devices. *Molecules*, *20*(9), 17362–17377. (DOI: 10.3390/MOLECULES200917362).

[5] El-Khouly, M. E., Fukuzumi, S., & D'Souza, F. (2014). Photosynthetic Antenna–Reaction Center Mimicry by Using Boron Dipyrromethene Sensitizers. *ChemPhysChem*, *15*(1), 30–47. (DOI: 10.1002/CPHC.201300715).

[6] Deibel, C., Strobel, T., Dyakonov, V., Deibel,] C, Strobel, T., & Dyakonov, V. (2010). Role of the Charge Transfer State in Organic Donor–Acceptor Solar Cells. *Advanced Materials*, *22*(37), 4097–4111. (DOI: 10.1002/ADMA.201000376).

[7] Rout, Y., Montanari, C., Pasciucco, E., Misra, R., & Carlotti, B. (2021). Tuning the Fluorescence and the Intramolecular Charge Transfer of Phenothiazine Dipolar and Quadrupolar Derivatives by Oxygen Functionalization. *Journal of the American Chemical Society*, *143*(26), 9933–9943. (DOI: 10.1021/JACS.1C04173).

[8] Erden, K., & Dengiz, C. (2022). 3-Alkynylindoles as Building Blocks for the Synthesis of Electronically Tunable Indole-Based Push-Pull Chromophores. *Journal of Organic Chemistry*, *87*(6), 4385–4399. (DOI: 10.1021/ACS.JOC.2C00067).

[9] Bureš, F. (2014). Fundamental aspects of property tuning in push–pull molecules. *RSC Advances*, *4*(102), 58826–58851. (DOI: 10.1039/C4RA11264D).

[10] Rout, Y., Gautam, P., & Misra, R. (2017). Unsymmetrical and Symmetrical Push-Pull Phenothiazines. *Journal of Organic Chemistry*, *82*(13), 6840–6845. (DOI: 10.1021/acs.joc.7b00991).

[11] Dengiz, C., Breiten, B., Gisselbrecht, J. P., Boudon, C., Trapp, N., Schweizer, W. B., & Diederich, F. (2015). Synthesis and optoelectronic properties of janus -dendrimer-type multivalent donor-acceptor systems. *Journal of Organic Chemistry*, *80*(2), 882–896. (DOI: 10.1021/JO502367H).

[12] Randell, N. M., Radford, C. L., Yang, J., Quinn, J., Hou, D., Li, Y., & Kelly, T. L. (2018). Effect of Acceptor Unit Length and Planarity on the Optoelectronic Properties of Isoindigo-Thiophene Donor-Acceptor Polymers. *CHEMISTRY OF MATERIALS*, *30*(14), 4864–4873. (DOI: 10.1021/ACS.CHEMMATER.8B02535).

[13] Poddar, M., Jang, Y., Misra, R., & D'Souza, F. (2020). Excited-State Electron Transfer in 1,1,4,4-Tetracyanobuta-1,3-diene (TCBD)- and Cyclohexa-2,5-diene-1,4-diylidene-Expanded TCBD-Substituted BODIPY-Phenothiazine Donor–Acceptor Conjugates. *Chemistry – A European Journal*, *26*(30), 6869–6878. (DOI: 10.1002/CHEM.202000346).

[14] Revoju, S., Matuhina, A., Canil, L., Salonen, H., Hiltunen, A., Abate, A., & Vivo, P. (2020). Structure-induced optoelectronic properties of phenothiazine-based materials. *Journal of Materials Chemistry C*, *8*(44), 15486–15506. (DOI: 10.1039/D0TC03421E).

[15] Srinivasa Rao, P., Brixi, S., Shaikh, D. B., Al Kobaisi, M., Lessard, B. H., Bhosale, S. V., & Bhosale, S. V. (2021). The Effect of TCNE and TCNQ Acceptor Units on Triphenylamine-Naphthalenediimide Push-Pull Chromophore Properties. *European Journal of Organic Chemistry*, *2021*(18), 2615–2624. (DOI: 10.1002/EJOC.202100198).

[16] Jang, Y., Rout, Y., Misra, R., & D'Souza, F. (2021). Symmetric and Asymmetric Push-Pull Conjugates: Significance of Pull Group Strength on Charge Transfer and Separation. *Journal of Physical Chemistry B*, *125*(16), 4067–4075. (DOI: 10.1021/ACS.JPCB.0C09996).

[17] Poddar, M., Cesaretti, A., Ferraguzzi, E., Carlotti, B., & Misra, R. (2020). Singlet and Triplet Excited-State Dynamics of 3,7-Bis(arylethynyl)phenothiazines: Intramolecular Charge Transfer and Reverse Intersystem Crossing. *Journal of Physical Chemistry C*, *124*(33), 17864–17878. (DOI: 10.1021/ACS.JPCC.0C01786).

[18] Poddar, M., & Misra, R. (2017). NIR-Absorbing Donor–Acceptor Based 1,1,4,4-Tetracyanobuta-1,3-Diene (TCBD)- and Cyclohexa-2,5-Diene-1,4-Ylidene-Expanded TCBD-Substituted Ferrocenyl Phenothiazines. *Chemistry – An Asian Journal*, *12*(22), 2908–2915. (DOI: 10.1002/ASIA.201700879).

[19] Gangadhar, P. S., Reddy, G., Prasanthkumar, S., & Giribabu, L. (2021). Phenothiazine functional materials for organic optoelectronic applications. *Physical Chemistry Chemical Physics*, *23*(28), 14969–14996. (DOI: 10.1039/D1CP01185E).

[20] Krämer, C. S., & Müller, T. J. J. (2003). Synthesis and Electronic Properties of Alkynylated Phenothiazines. *European Journal of*

Organic Chemistry, *2003*(18), 3534–3548. (DOI: 10.1002/EJOC.200300250).

[21] Chandra, B. K. C., & D'Souza, F. (2016). Design and photochemical study of supramolecular donor–acceptor systems assembled via metal–ligand axial coordination. *Coordination Chemistry Reviews*, *322*, 104–141. (DOI: 10.1016/J.CCR.2016.05.012).

[22] Rout, Y., Ekbote, A., & Misra, R. (2021). Recent development on the synthesis, properties and applications of luminescent oxidized phenothiazine derivatives. *Journal of Materials Chemistry C*, *9*(24), 7508–7531. (DOI: 10.1039/D1TC00695A).

[23] Khan, F., Mahmoudi, M., Gupta, P. K., Volyniuk, D., Grazulevicius, J. V., & Misra, R. (2023). Mechanochromic Materials Based on Tetraphenylethylene-Substituted Phenothiazines: Substituent-Dependent Hypsochromic and Bathochromic Switching of Emission. *Journal of Physical Chemistry C*, *127*(3), 1643–1654. (DOI: 10.1021/ACS.JPCC.2C07010).

[24] Tang, G., Sukhanov, A. A., Zhao, J., Yang, W., Wang, Z., Liu, Q., … Jacquemin, D. (2019). Red Thermally Activated Delayed Fluorescence and the Intersystem Crossing Mechanisms in Compact Naphthalimide-Phenothiazine Electron Donor/Acceptor Dyads. *Journal of Physical Chemistry C*, *123*(50), 30171–30186. (DOI: 10.1021/ACS.JPCC.9B09335).

[25] Khan, F., & Misra, R. (2023). Recent advances in the development of phenothiazine and its fluorescent derivatives for optoelectronic applications. *Journal of Materials Chemistry C*, *11*, 2786-2825. (DOI: 10.1039/d2tc04326b).

[26] Hua, Y., Chang, S., Huang, D., Zhou, X., Zhu, X., Zhao, J., … Wong, W. K. (2013). Significant improvement of dye-sensitized solar cell performance using simple phenothiazine-based dyes. *Chemistry of Materials*, *25*(10), 2146–2153. (DOI: 10.1021/CM400800H).

[27] Gu, Y., & Tian, S. K. (2013). N-alkylsulfonamides as useful carbon electrophiles. *Synlett*, *24*(10), 1170–1185. (DOI: 10.1055/S-0033-1338460).

[28] Betou, M., Kerisit, N., Meledje, E., Leroux, Y. R., Katan, C., Halet, J.-F., … Trolez, Y. (2014). High-Yield Formation of Substituted Tetracyanobutadienes from Reaction of Ynamides with Tetracyanoethylene. *Chemistry – A European Journal*, *20*(31), 9553–9557. (DOI: 10.1002/CHEM.201402653).

[29] Betou, M., Durand, R. J., Sallustrau, D. A., Gousset, C., Le Coz, E., Leroux, Y. R., … Trolez, Y. (2017). Reactivity of Functionalized Ynamides with Tetracyanoethylene: Scope, Limitations and Optoelectronic Properties of the Adducts. *Chemistry – An Asian Journal*, *12*(12), 1338–1346. (DOI: 10.1002/ASIA.201700353).

[30] Philippe, C., Bui, A. T., Batsongo-Boulingui, S., Pokladek, Z., Matczyszyn, K., Mongin, O., … Trolez, Y. (2021). 1,1,4,4-Tetracyanobutadiene-Functionalized Anthracenes: Regioselectivity of Cycloadditions in the Synthesis of Small Near-IR Dyes. *Organic Letters*, *23*(6), 2007–2012. (DOI: 10.1021/ACS.ORGLETT.1C00136).

[31] Gupta, P. K., Das, S., Misra, R., & D'Souza, F. (2024). Near-IR Capturing N-Methylbenzene Sulfonamide-Phenothiazine Incorporating Strong Electron Acceptor Push-Pull Systems: Photochemical Ultrafast Carrier Dynamics. *Chemistry – A European Journal*, e202304313. (DOI: 10.1002/CHEM.202304313).

[32] Yadav, I. S., Alsaleh, A. Z., Misra, R., & D'Souza, F. (2021). Charge stabilization via electron exchange: excited charge separation in symmetric, central triphenylamine derived, dimethylaminophenyl–tetracyanobutadiene donor–acceptor conjugates. *Chemical Science*, *12*(3), 1109–1120. (DOI: 10.1039/D0SC04648E).

[33] Michinobu, T. (2008). Click-type reaction of aromatic polyamines for improvement of thermal and optoelectronic

properties. *Journal of the American Chemical Society*, *130*(43), 14074–14075. (DOI: 10.1021/JA8061612).

[34] Khan, F., Jang, Y., Patil, Y., Misra, R., & D'Souza, F. (2021). Photoinduced Charge Separation Prompted Intervalence Charge Transfer in a Bis(thienyl)diketopyrrolopyrrole Bridged Donor-TCBD Push-Pull System. *Angewandte Chemie*, *133*(37), 20681–20690. (DOI: 10.1002/ANGE.202108293).

[35] Srinivasa Rao, P., Brixi, S., Shaikh, D. B., Al Kobaisi, M., Lessard, B. H., Bhosale, S. V., & Bhosale, S. V. (2021). The Effect of TCNE and TCNQ Acceptor Units on Triphenylamine-Naphthalenediimide Push-Pull Chromophore Properties. *European Journal of Organic Chemistry*, *2021*(18), 2615–2624. (DOI: 10.1002/EJOC.202100198).

[36] Zhang, H., Wan, X., Xue, X., Li, Y., Yu, A., & Chen, Y. (2010). Selective tuning of the HOMO-LUMO gap of carbazole-based donor-acceptor-donor compounds toward different emission colors. *European Journal of Organic Chemistry*, (9), 1681–1687. (DOI: 10.1002/EJOC.200901167).

[37] Leliège, A., Blanchard, P., Rousseau, T., & Roncali, J. (2011). Triphenylamine/tetracyanobutadiene-based1 D-A-D π-conjugated systems as molecular donors for organic solar cells. *Organic Letters*, *13*(12), 3098–3101. (DOI: 10.1021/OL201002J).

[38] Kato, S. I., & Diederich, F. (2010). Non-planar push–pull chromophores. *Chemical Communications*, *46*(12), 1994–2006. (DOI: 10.1039/B926601A).

[39] Jayamurugan, G., Gisselbrecht, J. P., Boudon, C., Schoenebeck, F., Schweizer, W. B., Bernet, B., & Diederich, F. (2011). Expanding the chemical space for push-pull chromophores by non-concerted [2+2] and [4+2] cycloadditions: access to a highly functionalised 6,6-dicyanopentafulvene with an intense, low-energy charge-transfer band. *Chemical Communications*, *47*(15), 4520–4522. (DOI: 10.1039/C1CC10247H).

[40] Michinobu, T., Kumazawa, H., Noguchi, K., & Shigehara, K. (2009). One-step synthesis of donor - Acceptor type conjugated polymers from ferrocene-containing poly(aryleneethynylene)s. *Macromolecules*, *42*(16), 5903–5905. (DOI: 10.1021/MA9013324).

[41] Shoji, T., Ito, S., Toyota, K., Iwamoto, T., Yasunami, M., & Morita, N. (2009). Reactions between 1-Ethynylazulenes and 7,7,8,8-Tetracyanoquinodimethane (TCNQ): Preparation, Properties, and Redox Behavior of Novel Azulene-Substituted Redox-Active Chromophores. *European Journal of Organic Chemistry*, *2009*(25), 4316–4324. (DOI: 10.1002/EJOC.200900539).

[42] Michinobu, T., May, J. C., Lim, J. H., Boudon, C., Gisselbrecht, J. P., Seiler, P., … Diederich, F. (2005). A new class of organic donor–acceptor molecules with large third-order optical nonlinearities. *Chemical Communications*, (6), 737–739. (DOI: 10.1039/B417393G).

[43] Kato, S. I., Kijima, T., Shiota, Y., Abe, T., Kuwako, S., Miyauchi, H., … Nakamura, Y. (2020). Chemical transformations of push–pull fluorenones: push–pull dibenzodicyanofulvenes as well as fluorenone– and dibenzodicyanofulvene–tetracyanobutadiene conjugates. *Organic & Biomolecular Chemistry*, *18*(22), 4198–4209. (DOI: 10.1039/C9OB02706H).

[44] Kato, S. ichiro, Noguchi, H., Jin, S., & Nakamura, Y. (2016). Synthesis and Electronic, Optical, and Electrochemical Properties of a Series of Tetracyanobutadiene-Substituted Carbazoles. *Asian Journal of Organic Chemistry*, *5*(2), 246–256. (DOI: 10.1002/AJOC.201500431).

[45] Philippe, C., Bui, A. T., Beau, M., Bloux, H., Riobé, F., Mongin, O., … Trolez, Y. (2022). Synthesis and Photophysical Properties of 1,1,4,4-Tetracyanobutadienes Derived from Ynamides Bearing Fluorophores**. *Chemistry – A European Journal*, *28*(23), e202200025. (DOI: 10.1002/CHEM.202200025).

[46] Bui, A. T., Philippe, C., Beau, M., Richy, N., Cordier, M., Roisnel, T., … Trolez, Y. (2020). Synthesis, characterization and unusual near-infrared luminescence of 1,1,4,4-tetracyanobutadiene derivatives. *Chemical Communications*, *56*(24), 3571–3574. (DOI: 10.1039/C9CC09560H).

[47] Gupta, P. K., Khan, F., & Misra, R. (2023). NIR-Absorbing 1,1,4,4-Tetracyanobuta-1,3-diene- and Dicyanoquinodimethane-Functionalized Donor-Acceptor Phenothiazine Derivatives: Synthesis and Characterization. *The Journal of organic chemistry*, *88*(20), 14308–14322. (DOI: 10.1021/ACS.JOC.3C01029).

[48] Sheokand, M., Ji Tiwari, N., & Misra, R. (2023). Near-IR absorbing 1,1,4,4-tetracyanobutadiene-functionalized phenothiazine sulfones. *Organic & Biomolecular Chemistry*, *21*(18), 3896–3905. (DOI: 10.1039/D3OB00361B).

[49] Yadav, I. S., & Misra, R. (2022). Phenothiazine and phenothiazine-5,5-dioxide-based push–pull derivatives: synthesis, photophysical, electrochemical and computational studies. *New Journal of Chemistry*, *46*(33), 15999–16006. (DOI: 10.1039/D2NJ03089F).

[50] Coste, A., Karthikeyan, G., Couty, F., & Evano, G. (2009). Copper-Mediated Coupling of 1,1-Dibromo-1-alkenes with Nitrogen Nucleophiles: A General Method for the Synthesis of Ynamides. *Angewandte Chemie International Edition*, *48*(24), 4381–4385. (DOI: 10.1002/ANIE.200901099).

[51] Janietz, S., Bradley, D. D. C., Grell, M., Giebeler, C., Inbasekaran, M., & Woo, E. P. (1998). Electrochemical determination of the ionization potential and electron affinity of poly(9,9-dioctylfluorene). *Applied Physics Letters*, *73*(17), 2453–2455. (DOI: 10.1063/1.122479).

[52] Ekbote, A., Mobin, S. M., & Misra, R. (2018). Structure–property relationship in multi-stimuli responsive D–A–A′ benzothiazole functionalized isomers. *Journal of Materials*

Chemistry C, *6*(40), 10888–10901. (DOI: 10.1039/C8TC04310H).

[53] Frisch, M. J.; Trucks, G. W.; Schlegel, G. W.; Scuseria, G. E.; Robb, M. A.; Cheeseman, J. R.; Scalmani, G.; Barone, V.; Petersson, G. A.; Li, Nakatsuji, X.; Caricato, M.; Marenich, A.; Bloino, J.; Janesko, B. G.; Gomperts, R.; Mennucci, B.; Hratchian, H. P.; Ortiz, J. V.; Izmaylov, A. F.; Sonnenberg, J. L.; Williams-Young, D.; Ding, F.; Lipparini, F.; Egidi, F.; Goings, J.; Peng, B.; Petrone, A.; Henderson, T.; Ranasinghe, D.; Zakrzewski, V. G.; Gao, J.; Rega, N.; Zheng, G.; Liang, W.; Hada, M.; Ehara, M.; Toyota, K.; Fukuda, R.; Hasegawa, J.; Ishida, M.; Nakajima, T.; Honda, Y.; Kitao, O.; Nakai, H.; Vreven, T.; Throssell, K.; Montgomery, J. A.; Peralta, J. E., Jr.; Ogliaro, F.; Bearpark, M.; Heyd, J. J.; Brothers, E.; Kudin, K. N.; Staroverov, V. N.; Keith, T.; Kobayashi, R.; Normand, J.; Raghavachari, K.; Rendell, A.; Burant, J. C.; Iyengar, S. S.; Tomasi, J.; Cossi, M.; Millam, J. M.; Klene, M.; Adamo, C.; Cammi, R.; Ochterski, J. W.; Martin, R. L.; Morokuma, K.; Farkas, O.; Foresman, J. B.; Fox, D. J. (2016). Gaussian 09, rev. A.02; Gaussian, Inc.: Wallingford, CT.

[54] Li, Y., Ren, T., & Dong, W. J. (2013). Tuning photophysical properties of triphenylamine and aromatic cyano conjugate-based wavelength-shifting compounds by manipulating intramolecular charge transfer strength. *Journal of Photochemistry and Photobiology A: Chemistry*, *251*, 1–9. (DOI: 10.1016/J.JPHOTOCHEM.2012.10.002).

[55] Wan, Y., Li, J., Peng, X., Huang, C., Qi, Q., Lai, W. Y., & Huang, W. (2017). Intramolecular charge transfer induced emission from triphenylamine-o-carborane dyads. *RSC Advances*, *7*(56), 35543–35548. (DOI: 10.1039/C7RA06237K).

[56] Ahmed, S., Mushahary, B. C., & Kalita, D. J. (2020). Rational Design of Bay-Annulated Indigo (BAI)-Based Oligomers for Bulk Heterojunction Organic Solar Cells: A Density Functional

Theory (DFT) Study. *ACS Omega*, *5*(14), 8321–8333. (DOI: 10.1021/ACSOMEGA.0C00784).

Chapter 6

Synthesis and Characterization of NIR Absorbing Triphenylamine Substituted Donor–Acceptor Phenothiazine and Fulleropyrrolidine Derivatives

6.1. Introduction

In recent years, organic π-conjugated chromophores are an important area of research due to their many applications in materials science, biomedicine, organic photodetectors, organic field-effect transistors (OFETs), organic photovoltaics, organic light-emitting diodes (OLEDs), nonlinear optics, bioimaging and organic solar cells (OSCs).[1–9] A heteroatom-based organic π-conjugated molecule such as phenothiazine, benzothiazole, thiazole, benzothiadiazole, *etc.* in donor–acceptor (D–A) chromophores, play an important role in determining the various applications, such as organic photovoltaics (OPVs), organic light-emitting diodes (OLEDs) and nonlinear optics (NLOs).[10–13] Organic solar cells (OSCs) have been studied as renewable energy sources that are able to effectively transform sunlight into electricity.[14–17] The efficiency of OSCs based on bulk heterojunction (BHJ) with a fullerene derivative as an electron acceptor and conjugated molecules as an electron donor has been reported to greatly improve. [18, 19] However, our group is interested in designing and synthesizing push-pull chromophores by modifying the donor and acceptor moieties to be used in optoelectronics. [20–24]

Fullerene [C_{60}] possesses a remarkable capacity for capturing electrons with a 0.78 diameters, and its tendency to holding six electrons in a solution. [25–27] Fulleropyrrolidines are a form of acceptor that is frequently utilized in the formation of organic photovoltaics (OPVs) and photosynthetic supramolecular model compounds. They are a family of vicinally disubstituted-organo-fullerenes.[28–32] These are formed by 1,3-dipolar cycloaddition of azomethine ylides, and they have a number of properties like small reorganization energy, high electron affinity, and effective charge transfer abilities.[33] The design and development of

novel organofullerenes containing electron donors are fascinating due to their unique optical and electrical characteristics.[34] Triphenylamine derivatives are continuously growing research interest because of their low oxidation potential and hole transport properties.[35] The triphenylamine derivatives have been extensively investigated in organic light-emitting diodes (OLEDs), nonlinear optics (NLO), organic field-effect transistors (OFETs), dye-sensitized solar cells (DSSCs) and bulk heterojunction organic solar cells (BHJ OSCs).[36–39] Phenothiazine can be easily functionalized by the aromatic electrophilic substitution reactions at the 3- & 7- positions and nucleophilic substitution reaction at the *N*-position.[40, 41] The phenothiazine derivatives possess low reversible oxidation potential making them suitable core to be used as an electron donor in various optoelectronic applications.[42, 43] The 1,1,2,2-tetracyanoethylene (TCNE) and 7,7,8,8-tetracyanoquinodimethane (TCNQ) are strong electron acceptors because of they contain four cyano groups,[44, 45] and are highly reactive towards electron-rich alkynes, undergo [2 + 2] cycloaddition reaction to form cyclobutene rings accompanied by retroelectrocyclization reaction to produce 1,1,4,4-tetracyanobutadiene (TCBD) and cyclohexa-2,5-diene-1,4-diylidene-expanded TCBD or DCNQ (DCNQ = dicyanodiquinodimethane) derivatives.[46, 47] The donor-acceptor systems containing TCBD and DCNQ acceptors are interesting possibilities for organic photovoltaic applications.[48] Diederich *et al.* reacted TCNE and TCNQ with various acetylenic donors to produce charge-transfer chromophores using a [2 + 2] cycloaddition-retroelectrocyclization reaction.[49, 50]

In this manuscript, we report the design and synthesis of triphenylamine functionalized phenothiazine derivatives **TPA-PTZ 1–3** by Pd-catalyzed Sonogashira cross-coupling reaction *via* [2 + 2] cycloaddition-electrocyclic ring-opening reaction, and fulleropyrrolidine derivatives **TPA-PTZ-C_{60} 1–3** by 1,3-dipolar cycloaddition reaction (Prato reaction) in good yields (Chart 6.1). In the triphenylamine functionalized phenothiazine derivatives **TPA-PTZ 1–3** and fulleropyrrolidine derivatives **TPA-PTZ-C_{60} 1–3**, we were

investigating the effect of the fullerene moiety and the strong electron acceptors 1,1,4,4-tetracyanobuta-1,3-diene (TCBD) and dicyanodiquinodimethane (DCNQ) moieties on the photophysical, electrochemical, and computational studies.

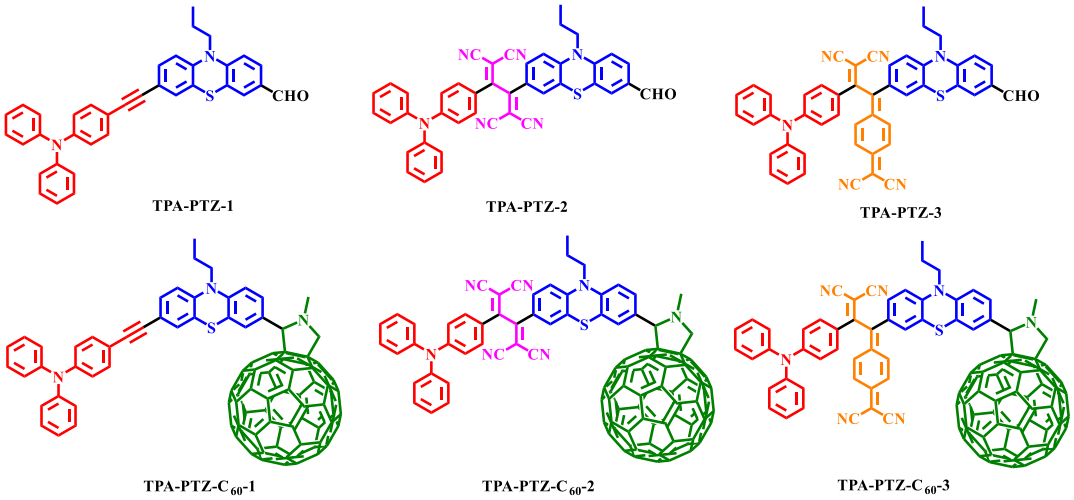

Chart 6.1. Chemical structures of donor−acceptor type triphenylamine-functionalized phenothiazine derivatives **TPA-PTZ 1–3** and fulleropyrrolidine derivatives **TPA-PTZ-C$_{60}$ 1–3**.

6.2. Result and Discussion

Scheme 6.1 illustrates the synthesis of the triphenylamine-functionalized phenothiazine derivatives **TPA-PTZ 1–3** and fulleropyrrolidine derivatives **TPA-PTZ-C$_{60}$ 1–3**. The Pd-catalyzed Sonogashira cross-coupling reaction of 4-ethynyl-*N*,*N*-diphenylaniline **TPA** and 1.1 equivalent of 7-bromo-10-propyl-10*H*-phenothiazine-3-carbaldehyde **Br-PTZ-CHO** using THF:TEA (1:1) under argon conditions in the presence of $Pd(PPh_3)_2Cl_2$/CuI to produce the triphenylamine-functionalized phenothiazine derivative **TPA-PTZ-1** in 85% yield. The TCBD and DCNQ incorporated triphenylamine-functionalized phenothiazine derivatives **TPA-PTZ-2** and **TPA-PTZ-3** were designed and synthesized by the [2 + 2] cycloaddition–retroelectrocyclization reaction. The **TPA-PTZ-1** reacts with 1.1 equivalents of TCNE in dichloromethane at room temperature for 24 h to produce **TPA-PTZ-2** in 75% yield, although the **TPA-PTZ-1** reacts with 1.1 equivalents of TCNQ in dichloroethane (DCE) for 36 h at 60

°C resulting in the formation of **TPA-PTZ-3** in 70% yield. Subsequently, the reaction of the triphenylamine-functionalized phenothiazine derivatives **TPA-PTZ 1–3** with fullerene (C_{60}) using toluene in the presence of excess *N*-methylglycine (sarcosine) and followed by a 1,3-dipolar cycloaddition reaction (Prato reaction)[51, 52] resulted in the formation of fulleropyrrolidine derivatives **TPA-PTZ-C_{60} 1–3** in 30%, 35%, and 33% yield, respectively. All the reported compounds, the triphenylamine-functionalized phenothiazine derivatives **TPA-PTZ 1–3** and fulleropyrrolidine derivatives **TPA-PTZ-C_{60} 1–3** were purified by column chromatography and well-characterized by ^{1}H-NMR, ^{13}C-NMR spectroscopy, HRMS and MALDI-TOF techniques.

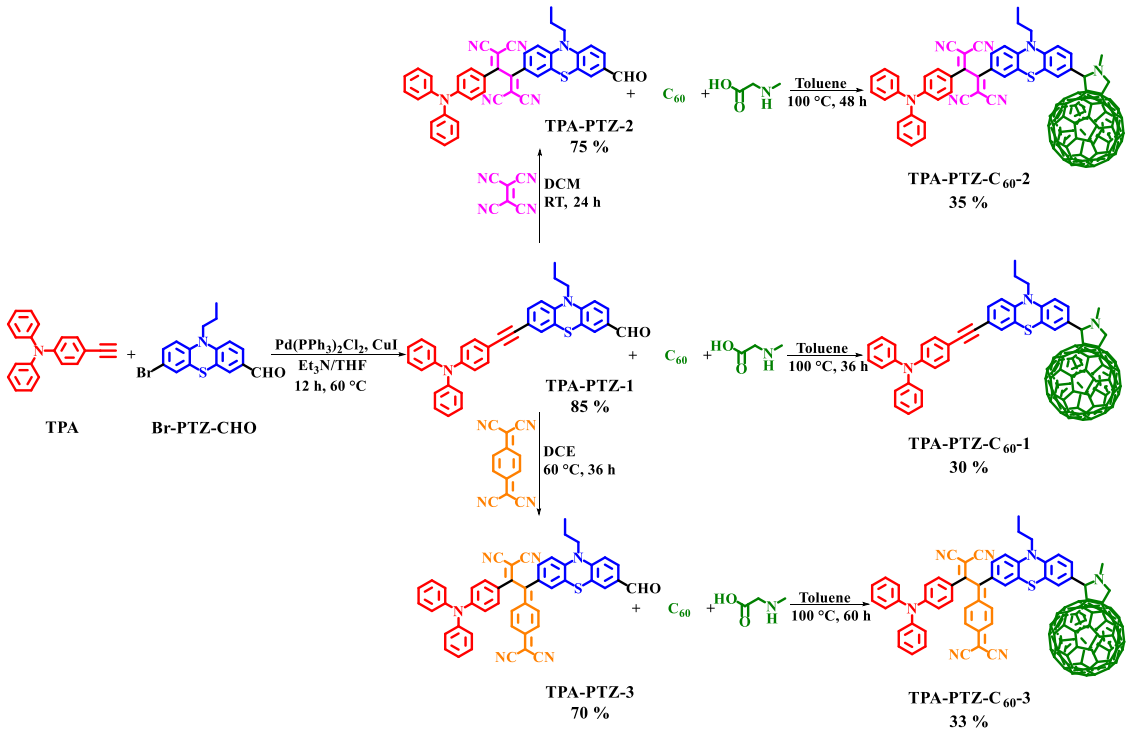

Scheme 6.1. Synthetic route of triphenylamine-functionalized phenothiazine derivatives **TPA-PTZ 1–3** and fulleropyrrolidine derivatives **TPA-PTZ-C_{60} 1–3**.

6.3. Photophysical Properties

The optical properties of the triphenylamine-functionalized phenothiazine derivatives **TPA-PTZ 1–3** and fulleropyrrolidine

derivatives **TPA-PTZ-C_{60} 1–3** were recorded in dilute dichloromethane solutions (1×10^{-5} M) at room temperature. The absorption spectra are depicted in Figure 6.1, and the appropriate data including absorption maxima (λ_{max}), extinction coefficient, and optical bandgap are summarized in Table 6.1.

The triphenylamine-functionalized phenothiazine derivatives **TPA-PTZ 1–3** and fulleropyrrolidine derivatives **TPA-PTZ-C_{60} 1–3** show absorption spectra in the range of ultraviolet to the visible region (300–750 nm). The absorption maxima spectra of triphenylamine-functionalized phenothiazine **TPA-PTZ-1** exhibit absorption maxima at 393 nm due to π–π* transitions and the fulleropyrrolidine **TPA-PTZ-C_{60}-1** shows an absorption band at 374 nm, corresponding to intramolecular charge transfer (ICT) transition from donor to acceptor moiety. The fulleropyrrolidine derivative **TPA-PTZ-C_{60}-1** shows a blue-shifted absorption as compared to **TPA-PTZ-1** because of the acceptor ability of fullerene moiety. The TCBD-incorporated derivative **TPA-PTZ-2** and fulleropyrrolidine **TPA-PTZ-C_{60}-2** exhibit absorption maxima in the visible region at 497 nm and 502 nm, respectively, due to intramolecular charge transfer (ICT) transition. Similarly, DCNQ functionalized derivative **TPA-PTZ-3** and fulleropyrrolidine **TPA-PTZ-C_{60}-3** reveal two prominent absorption maxima at (453 nm, 651 nm) and (459 nm, 656 nm), respectively. The fulleropyrrolidine derivatives **TPA-PTZ-C_{60}-2** and **TPA-PTZ-C_{60}-3** exhibited red-shifted absorption as compared to (TCBD and DCNQ incorporated) **TPA-PTZ-2** and **TPA-PTZ-3** at lower energy regions due to the strong donor–acceptor (D–A) interaction. The optical band gaps for triphenylamine-functionalized phenothiazine derivatives **TPA-PTZ 1–3** and fulleropyrrolidine derivatives **TPA-PTZ-C_{60} 1–3** were evaluated from the onset edge of the absorption band in dichloromethane using equation ($E_g = 1240/\lambda_{onset}$), which was found to be 2.53, 1.78, 1.46, 2.83, 1.75, and 1.44 eV, respectively. The transitions can be explained through theoretical studies using TD-DFT calculations.

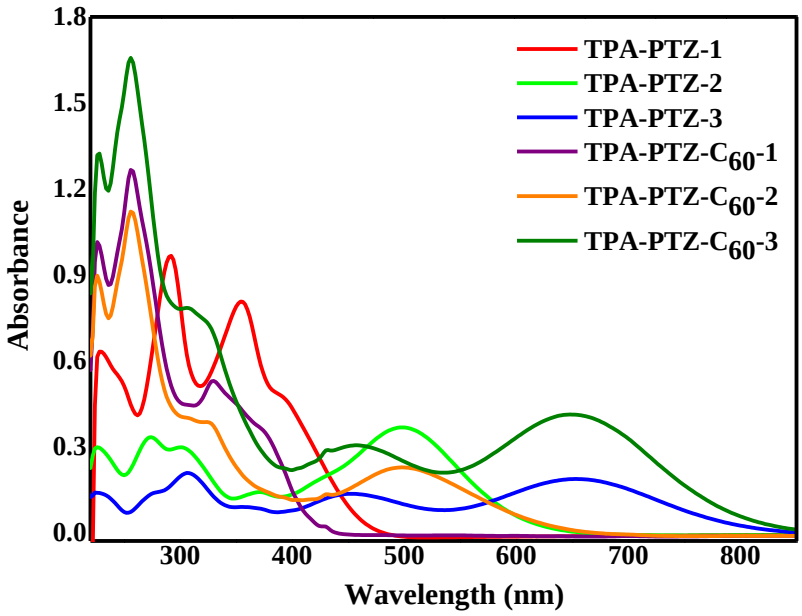

Figure 6.1. Electronic absorption spectra of triphenylamine-functionalized phenothiazine derivatives **TPA-PTZ 1–3** and fulleropyrrolidine derivatives **TPA-PTZ-C$_{60}$ 1–3** in dichloromethane (1×10^{-5} M).

Table 6.1. Photophysical and theoretical data of triphenylamine-functionalized phenothiazine derivatives **TPA-PTZ 1–3** and fulleropyrrolidine derivatives **TPA-PTZ-C$_{60}$ 1–3**.

Compounds	λ_{max} (nm)[a]	ε (M^{-1} cm^{-1})[a]	E_g^{opt} (eV)[a]	HOMO (eV)[b]	LUMO (eV)[b]	band-gap (eV)[b]
TPA-PTZ-1	393	81070	2.53	–4.85	–1.71	3.14
TPA-PTZ-2	497	36660	1.78	–6.00	–3.50	2.50
TPA-PTZ-3	453 651	13460 18645	1.46	–5.96	–4.03	1.93
TPA-PTZ-C$_{60}$-1	374	52730	2.83	–4.73	–3.34	1.39
TPA-PTZ-C$_{60}$-2	502	22780	1.75	–5.29	–3.41	1.88
TPA-PTZ-C$_{60}$-3	459 656	30900 41380	1.44	–5.30	–3.63	1.67

[a]Absorbance measured in dichloromethane at (1×10^{-5} M); λ_{max} = absorption wavelength; ε = extinction coefficient; E_g^{opt} = optical bandgap; [b]Theoretical data obtained from density functional theory (DFT) calculations performed at the B3LYP/6-31G (d,p) basis set level.

6.4. Electrochemical Properties

The redox potentials of triphenylamine-functionalized phenothiazine derivatives **TPA-PTZ 1–3** and fulleropyrrolidine derivatives **TPA-PTZ-C_{60} 1–3** were evaluated by cyclic voltammetry (CV) and differential pulse voltammetry (DPV) using 0.1 M tetrabutylammonium hexafluorophosphate ($TBAPF_6$) as a supporting electrolyte. The electrochemical data are demonstrated in Table 6.2, and the representative cyclic voltammograms and differential pulse voltammograms for **TPA-PTZ 1–3** and **TPA-PTZ-C_{60} 1–3** are shown in Figures 6.2 and 6.3.

The triphenylamine-functionalized phenothiazine derivatives **TPA-PTZ 1-3** and fulleropyrrolidine derivatives **TPA-PTZ-C_{60} 1-3** reveal varying redox waves because of the reduction of fullerene, TCBD, and DCNQ acceptor units on the cathodic side and the oxidation of phenothiazine and triphenylamine donor units on the anodic side. The triphenylamine-functionalized phenothiazine derivatives **TPA-PTZ 1–3** and fulleropyrrolidine derivatives **TPA-PTZ-C_{60} 1-3** exhibit two oxidation waves at (+0.88 V, +1.06 V), (+1.16 V, +1.28 V), (+1.01 V, +1.10 V), (+0.76 V, +1.03 V), (+1.03 V, +1.26 V) and (+0.97 V, +1.21 V) respectively, which is corresponding to the phenothiazine and triphenylamine unit. The fulleropyrrolidine derivative **TPA-PTZ-C_{60}-1** reveals two reduction waves at (–0.76 V, –1.11 V) which are attributed to the fullerene moiety. The TCBD and DCNQ substituted derivatives **TPA-PTZ-2** and **TPA-PTZ-3** show two reduction waves at (–0.50 V, –0.82 V) and (–0.34 V, –1.07 V), respectively due to the TCBD and DCNQ unit. Similarly, TCBD and DCNQ functionalized fulleropyrrolidine derivatives **TPA-PTZ-C_{60}-2** and **TPA-PTZ-C_{60}-3** exhibit four reduction waves at (–0.52 V, –0.63 V, –0.76 V, –1.12 V) and (–0.31 V, –0.42 V, –0.75 V, –1.14 V), respectively because of the

TCBD, DCNQ and fullerene moiety. First, two reduction potentials in the low potential region correspond to the mono and di-anions generation of TCBD and DCNQ unit, while the last two reduction potentials in the higher potential region correspond to fullerene moiety.

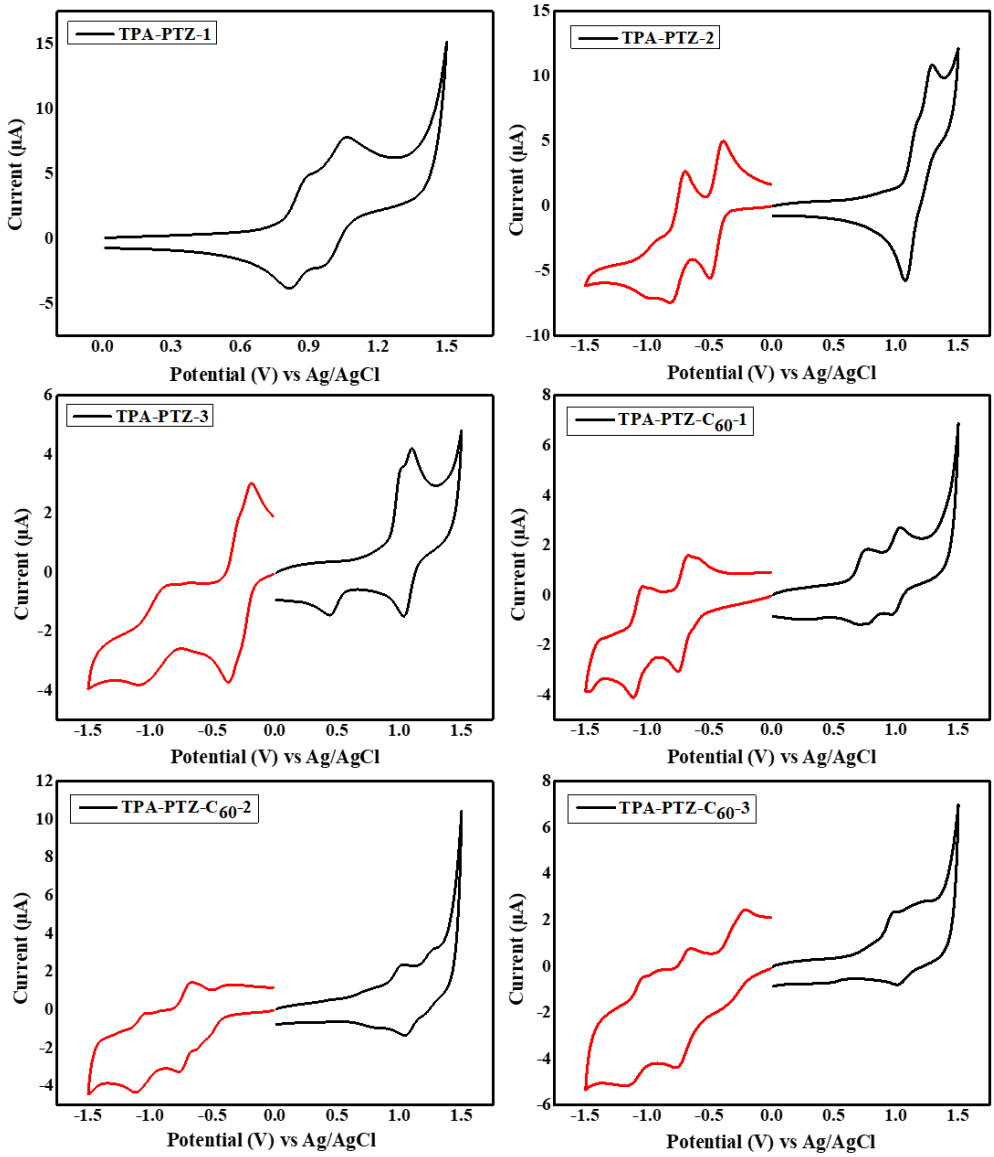

Figure 6.2. Cyclic voltammograms of **TPA-PTZ 1–3** and **TPA-PTZ-C_{60} 1–3** in 0.1 M solution of Bu_4NPF_6 in dichloromethane at 100 mV s^{-1} scan rate *versus* saturated Ag/AgCl at 25 °C.

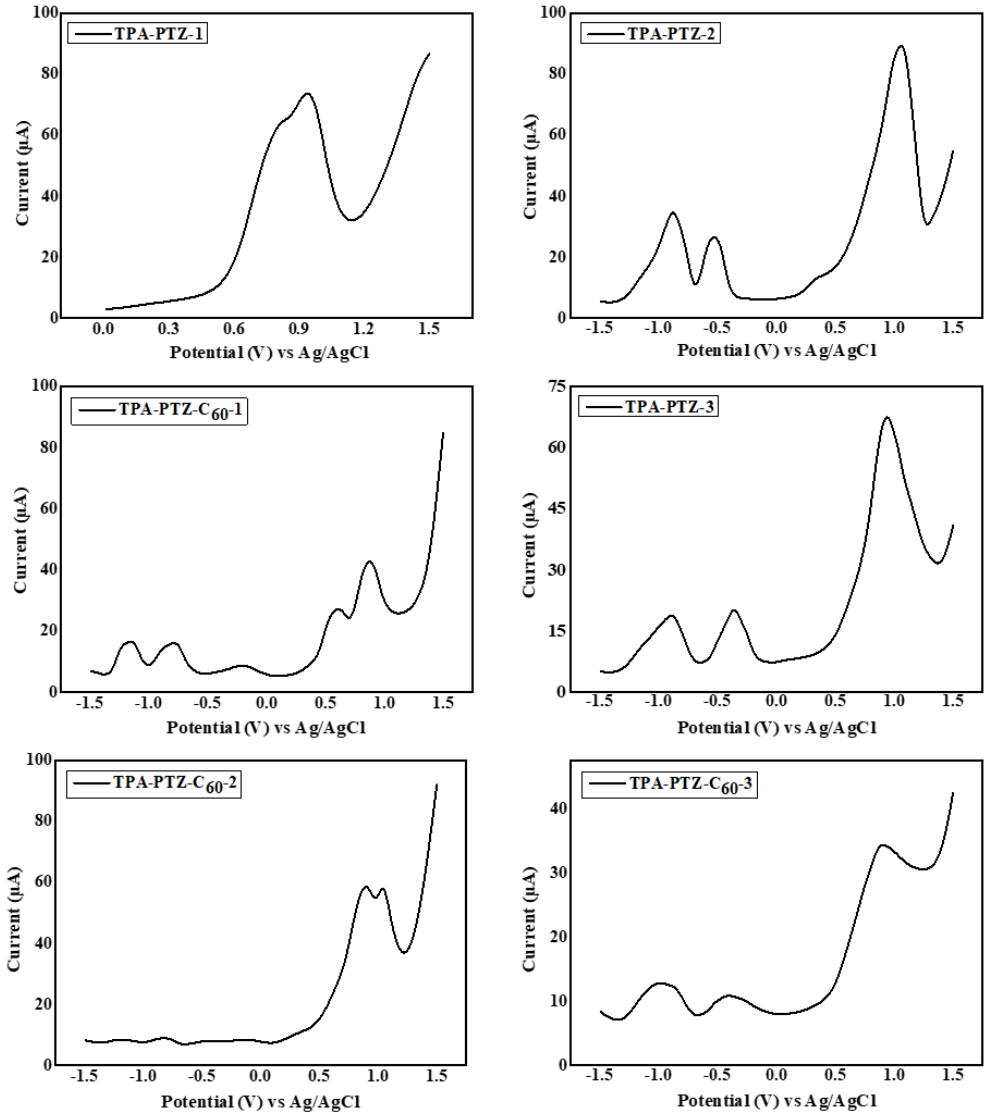

Figure 6.3. Differential pulse voltammograms of **TPA-PTZ 1–3** and **TPA-PTZ-C$_{60}$ 1–3** in 0.1 M solutions of Bu_4NPF_6 in dichloromethane at 100 mV s^{-1} scan rate *versus* saturated Ag/AgCl electrode at 25 °C.

The HOMO and LUMO energy levels as well as the HOMO–LUMO gap of all the triphenylamine-functionalized phenothiazine derivatives **TPA-PTZ 1-3** and fulleropyrrolidine derivatives **TPA-PTZ-C$_{60}$ 1-3** were calculated using the obtained oxidation and reduction onset values. Accordingly, the corresponding HOMO energy levels are −5.68, −5.50, −5.43, −5.66, and −5.61 eV, respectively and the LUMO energy levels are −3.90, −4.06, −3.64, −3.88, and −4.09 eV, respectively. The calculated electrochemical bandgap (E_{gap}) of **TPA-PTZ-2**, **TPA-PTZ-3**, **TPA-PTZ-C$_{60}$-1**, **TPA-PTZ-C$_{60}$-2** and **TPA-**

PTZ-C_{60}-3 were 1.78 eV, 1.44 eV, 1.79 eV, 1.78 eV and 1.52 eV respectively. The electrochemically calculated energy gap values are in good agreement with the theoretically calculated energy gaps.

Table 6.2. Electrochemical data of triphenylamine-functionalized phenothiazine derivatives **TPA-PTZ 1–3** and fulleropyrrolidine derivatives **TPA-PTZ-C_{60} 1–3**.

Compounds	E_{red} **(V)**[a]	E_{ox} **(V)**[a]	E_{HOMO} **(eV)**[a]	E_{LUMO} **(eV)**[a]	E_g **(eV)**[a]
TPA-PTZ-1	–	0.88 1.06	–	–	–
TPA-PTZ-2	–0.50 –0.82	1.16 1.28	–5.68	–3.90	1.78
TPA-PTZ-3	–0.34 –1.07	1.01 1.10	–5.50	–4.06	1.44
TPA-PTZ-C_{60}-1	–0.76 –1.11	0.76 1.03	–5.43	–3.64	1.79
TPA-PTZ-C_{60}-2	–0.52 –0.63 –0.76 –1.12	1.03 1.26	–5.66	–3.88	1.78
TPA-PTZ-C_{60}-3	–0.31 –0.42 –0.75 –1.14	0.97 1.21	–5.61	–4.09	1.52

[a]Electrochemical analysis was estimated by differential pulse voltammetry, in 0.1 M solution of $TBAPF_6$ in DCM at 100 mV s^{-1} scan rate *versus* saturated Ag/AgCl electrode at 25 °C.

6.5. Computational Calculations

The density functional theory calculation was carried out on triphenylamine-functionalized phenothiazine derivatives **TPA-PTZ 1–3** and fulleropyrrolidine derivatives **TPA-PTZ-C_{60} 1–3** to investigate molecular conformations and ground-state geometries at B3LYP/6-31G (d,p) level in the Gaussian 09W program.[53] The energy level diagram and frontier molecular orbitals of **TPA-PTZ 1–3** and **TPA-PTZ-C_{60} 1–3** are displayed in Figure 6.4. The optimized structures of triphenylamine-functionalized phenothiazine derivatives **TPA-PTZ 1–3** and fulleropyrrolidine derivatives **TPA-PTZ-C_{60} 1–3** are nonplanar with a twisted geometry due to the incorporation of the TCBD and DCNQ units. Incorporating a strong DCNQ acceptor unit lowers the LUMO energy level more than TCBD, resulting in a low HOMO–LUMO gap and red-shifted electronic absorption. The HOMOs for all the triphenylamine-functionalized phenothiazine derivatives **TPA-PTZ 1–3** *i.e.* **TPA-PTZ-1**, **TPA-PTZ-2**, **TPA-PTZ-3** and fulleropyrrolidine derivative **TPA-PTZ-C_{60}-1** are localized on the PTZ unit extending to the TPA spacer attached to the C atom of the PTZ unit. Whereas, HOMOs for **TPA-PTZ-C_{60}-2** and **TPA-PTZ-C_{60}-3** are localized on the fullerene moiety. The LUMOs for **TPA-PTZ 1–3** and **TPA-PTZ-C_{60} 1–3** are mainly distributed on the donor PTZ as well as acceptor TCBD, DCNQ and fullerene moiety.

The theoretically calculated HOMO energies for **TPA-PTZ-1**, **TPA-PTZ-2**, **TPA-PTZ-3**, **TPA-PTZ-C_{60}-1**, **TPA-PTZ-C_{60}-2**, and **TPA-PTZ-C_{60}-3** are –4.85 eV, –6.00 eV, –5.96 eV, –4.73 eV, –5.29 eV and –5.30 eV respectively. The theoretically calculated LUMO energies for **TPA-PTZ-1**, **TPA-PTZ-2**, **TPA-PTZ-3**, **TPA-PTZ-C_{60}-1**, **TPA-PTZ-C_{60}-2** and **TPA-PTZ-C_{60}-3** are –1.71 eV, –3.50 eV, –4.03 eV, –3.34 eV, –3.41 eV and –3.63 eV respectively. The calculated HOMO–LUMO gaps in **TPA-PTZ-1**, **TPA-PTZ-2**, **TPA-PTZ-3**, **TPA-PTZ-C_{60}-1**, **TPA-PTZ-C_{60}-2** and **TPA-PTZ-C_{60}-3** are 3.14 eV, 2.50 eV, 1.93 eV, 1.39 eV, 1.88 eV and 1.67 eV respectively and follow the order

TPA-PTZ-1 > **TPA-PTZ-2** > **TPA-PTZ-3** > **TPA-PTZ-C$_{60}$-2** > **TPA-PTZ-C$_{60}$-3** > **TPA-PTZ-C$_{60}$-1** (Table 6.1).

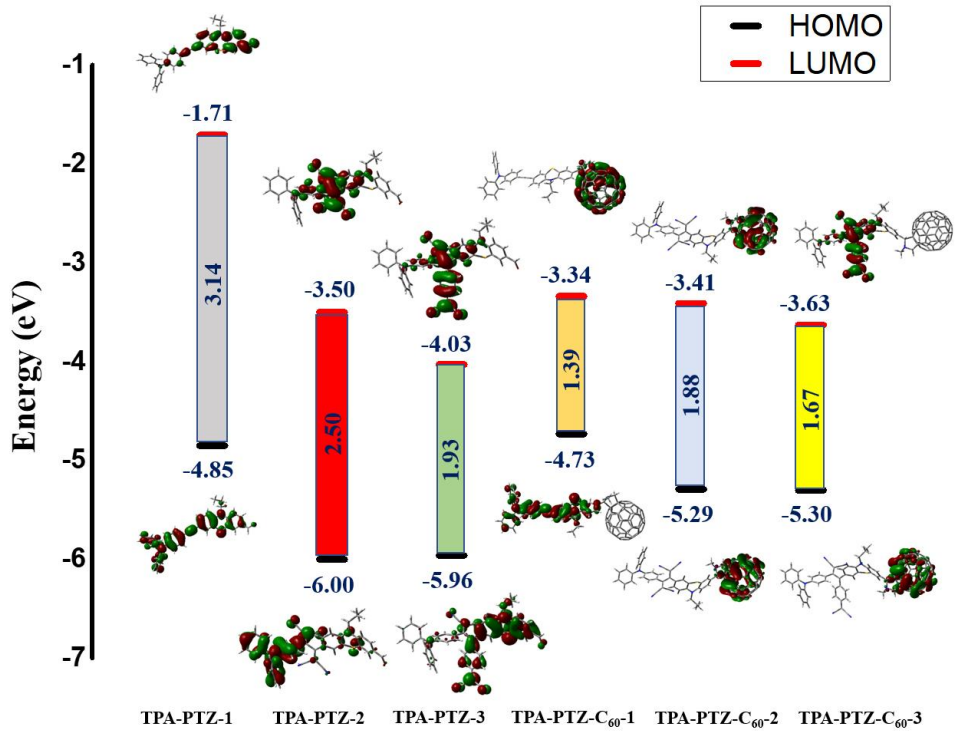

Figure 6.4. Energy level diagram of the HOMO–LUMO frontier orbitals of triphenylamine-functionalized phenothiazine derivatives **TPA-PTZ 1–3** and fulleropyrrolidine derivatives **TPA-PTZ-C$_{60}$ 1–3** calculated by DFT calculations at the B3LYP/6-31G (d,p) level.

The time-dependent density functional theory (TD-DFT) calculations were carried out at the B3LYP/6-31G (d,p) level in DCM solvent to explore the electrical characteristics in the excited state. It was determined that all these results were in good agreement with the absorption investigations. The contribution to the molecular orbitals in the UV/Vis absorption spectra was calculated based on their oscillator strength (*f*). Table 6.3 displays the transitions with oscillator strengths, composition, and molecular contribution. The TD-DFT calculations of the triphenylamine-functionalized phenothiazine derivatives **TPA-PTZ 1–3** and fulleropyrrolidine derivatives **TPA-PTZ-C$_{60}$ 1–3** reveal only one absorption maxima (λ_{max}) for all the molecules. The **TPA-PTZ-1** exhibits absorption maxima at 377 nm which could be attributed to the π–π* transition at the shorter wavelength and the transition occurs from

HOMO→LUMO+1. Other derivatives, such as **TPA-PTZ-2**, **TPA-PTZ-3** and **TPA-PTZ-C$_{60}$ 1–3** show absorption maxima at 468, 776, 426, 635 and 804 nm respectively. These absorption maxima correspond to intramolecular charge transfer (ICT) transitions at a longer wavelength, which occurs from HOMO→LUMO+1, HOMO-1→LUMO, HOMO→LUMO+6, HOMO-1→LUMO+1 and HOMO-1→LUMO. The experimental values of the electronic absorption wavelengths were found to be lower than the theoretical values, which may be caused by a number of things including the solvent effect, the dipole moment, and temperature.

Table 6.3. Calculated electronic transitions for triphenylamine-functionalized phenothiazine derivatives **TPA-PTZ 1–3** and fulleropyrrolidine derivatives **TPA-PTZ-C$_{60}$ 1–3** in dichloromethane.

Compounds	Wavelength (nm)	Composition and Molecular Contribution	f^a	Assignment
TPA-PTZ-1	377	HOMO→LUMO+1 (0.69)	0.74	π–π*
TPA-PTZ-2	468	HOMO→LUMO+1 (0.70)	0.63	ICT
TPA-PTZ-3	776	HOMO-1→LUMO (0.62)	0.25	ICT
TPA-PTZ-C$_{60}$-1	426	HOMO→LUMO+6 (0.60)	0.93	ICT
TPA-PTZ-C$_{60}$-2	635	HOMO-1→LUMO+1 (0.67)	0.26	ICT
TPA-PTZ-C$_{60}$-3	804	HOMO-1→LUMO (0.63)	0.30	ICT

[a]Oscillator strength.

6.6. Experimental section

General methods

The chemicals were used as received unless otherwise indicated. All oxygen or moisture-sensitive reactions were performed under a

nitrogen/argon atmosphere. ^{1}H NMR (400 and 500 MHz) and ^{13}C NMR (100 and 125 MHz) spectra were recorded on Bruker 400 and 500 MHz FT-NMR spectrometers at room temperature. ^{1}H NMR chemical shifts are reported in parts per million (ppm) relative to the solvent residual peak ($CDCl_3$, 7.26 ppm). Multiplicities are given as s (singlet), d (doublet), t (triplet) and m (multiplet) and the coupling constants, *J*, are given in hertz. ^{13}C NMR chemical shifts are reported relative to the solvent residual peak ($CDCl_3$, 77.0 ppm). UV-visible absorption spectra were recorded on a PerkinElmer Lambda 35 instrument. HRMS was recorded with an Agilent 6545A Q-TOF mass spectrometer and on a Bruker-Daltonics micrOTOF-Q II mass spectrometer and MALDI-TOF mass used to measure the mass of the compounds. The voltammograms were recorded on a PalmSens 4 electrochemical analyzer in dichloromethane solvent and 0.1 M $TBAPF_6$ as the supporting electrolyte. The electrodes used were glassy carbon as a working electrode, Pt wire as a counter electrode and Ag/AgCl as a reference electrode, the scan rate was 100 mV s^{-1} for cyclic voltammetry.

Synthesis of TPA-PTZ-1

In a 100 mL round-bottomed flask, 4-ethynyl-*N*,*N*-diphenylaniline **A** (500 mg, 1.857 mmol) and 7-bromo-10-propyl-10*H*-phenothiazine-3-carbaldehyde **B** (683 mg, 2.043 mmol) were purged under nitrogen and bis(triphenylphosphine)palladium(II)dichloride (100 mg) and copper(I) iodide (4 - 5 mg) were added in anhydrous triethylamine (20 mL) and tetrahydrofuran (20 mL), the reaction mixture was stirred and refluxed for 12 h. Then the solvent was evaporated under a vacuum. The residue was dissolved in dichloromethane, and this solution was washed with water for several times, dried with anhydrous Na_2SO_4, and filtered it. The crude was purified by column chromatography using dichloromethane-hexane (1/2 v/v) as eluent to get the desired compound **TPA-PTZ-1** as a yellow color solid with 85 % yield. ^{1}H NMR (500 MHz, CHLOROFORM-d) d = 9.80 (s, 1 H), 7.67 - 7.62 (m, 1 H), 7.58 - 7.56 (m, 1 H), 7.36 - 7.31 (m, *J* = 8.5 Hz, 2 H), 7.31 - 7.26 (m, 4 H), 7.24 (d, *J* = 1.7 Hz, 2 H), 7.11 (d, *J* = 7.8 Hz, 4 H), 7.06 (t, *J* = 7.3 Hz, 2 H), 7.01 - 6.98 (m, *J* = 8.5 Hz, 2 H), 6.89 (d, *J* = 8.5 Hz, 1 H), 6.80 (d,

J = 8.5 Hz, 1 H), 3.88 - 3.83 (m, 2 H), 1.87 - 1.81 (m, 2 H), 1.03 (t, *J* = 7.5 Hz, 3 H). ^{13}C NMR (100 MHz, CHLOROFORM-d) d = 189.9, 150.1, 147.9, 147.2, 143.0, 132.4, 131.3, 130.8, 130.2, 130.2, 130.1, 129.8, 129.4, 128.4, 125.0, 124.5, 123.8, 123.6, 122.3, 118.9, 117.1, 116.0, 115.8, 115.7, 115.1, 115.0, 90.2, 87.6, 49.8, 26.9, 20.0, 20.0, 11.2. HRMS (ESI-TOF) m/z calculated for $C_{36}H_{28}N_2OS$ 536.1922 $[M]^+$, measured 536.1917 $[M]^+$.

Synthesis of TPA-PTZ-2

In a 100 mL round-bottomed flask, TCNE (40 mg, 0.3074 mmol) was added to a solution of **TPA-PTZ-1** (compound 16) (150 mg, 0.2794 mmol) in dichloromethane (20 mL) under an argon atmosphere. The reaction mixture was stirred at RT for 24 h. The solvent was evaporated under vacuum, and the product was purified by column chromatography with DCM/hexane (2:1, v/v) as the eluent to get the desired compound **TPA-PTZ-2** as a dark color solid with 75 % yield. ^{1}H NMR (400 MHz, CHLOROFORM-d) d = 9.83 (s, 1 H), 7.74 (d, *J* = 7.0 Hz, 1 H), 7.70 - 7.61 (m, 3 H), 7.56 (s, 1 H), 7.44 - 7.36 (m, 4 H), 7.33 - 7.28 (m, 2 H), 7.22 (d, *J* = 7.8 Hz, 5 H), 6.99 - 6.89 (m, 4 H), 3.89 (t, *J* = 7.0 Hz, 2 H), 1.92 - 1.81 (m, 2 H), 1.06 (t, *J* = 7.2 Hz, 3 H). ^{13}C NMR (100 MHz, CHLOROFORM-d) d = 189.7, 165.4, 163.7, 153.8, 149.3, 147.7, 144.4, 132.5, 131.9, 130.4, 130.1, 128.5, 127.9, 127.0, 126.8, 126.3, 125.1, 123.7, 121.4, 118.0, 115.9, 113.6, 112.8, 112.6, 111.8, 82.8, 50.3, 20.0, 11.1. HRMS (ESI-TOF) m/z calculated for $C_{42}H_{28}N_6OS$ + Na 687.1943 $[M + Na]^+$, measured 687.1938 $[M + Na]^+$.

Synthesis of TPA-PTZ-3

In a 100 mL round-bottomed flask, TCNQ (55 mg, 0.2664 mmol) was added to a solution of **TPA-PTZ-1** (compound 16) (130 mg, 0.2422 mmol) in dichloroethane (20 mL) under an argon atmosphere. The reaction mixture was stirred at 60 °C for 36 h. The solvent was evaporated under vacuum, and the product was purified by column chromatography with DCM/hexane (3:1, v/v) as the eluent to get the desired compound **TPA-PTZ-3** as a dark color solid with 70 % yield. ^{1}H NMR (400 MHz, CHLOROFORM-d) d = 9.82 (s, 1 H), 7.69 – 7.59 (m, 2H), 7.56 - 7.50 (m, 2 H), 7.40 - 7.33 (m, 4 H), 7.30 (d, *J* = 7.3 Hz,

2 H), 7.24 - 7.14 (m, 9 H), 7.00 - 6.91 (m, 4 H), 6.88 (d, *J* = 8.0 Hz, 1 H), 3.92 – 3.82 (m, 2 H), 1.85 (d, *J* = 6.3 Hz, 2 H), 1.05 (t, *J* = 7.5 Hz, 3 H). ^{13}C NMR (100 MHz, CHLOROFORM-d) d = 189.6, 169.0, 154.0, 151.6, 150.5, 148.6, 147.8, 145.3, 135.2, 134.1, 133.3, 132.5, 132.4, 130.4, 130.3, 129.9, 128.9, 128.4, 126.9, 126.6, 125.9, 125.9, 125.6, 125.0, 123.7, 119.3, 115.8, 114.1, 113.4, 112.7, 83.6, 74.3, 60.4, 50.3, 29.7, 21.0, 20.0, 14.2, 11.1. HRMS (ESI-TOF) m/z calculated for $C_{48}H_{32}N_6OS$ + K 779.1995 $[M + K]^+$, measured 779.1990 $[M + K]^+$.

Synthesis of TPA-PTZ-C$_{60}$-1

In a 100 mL round-bottomed flask, compound **TPA-PTZ-1** (77 mg, 0.1435 mmol), C_{60}-fullerene (206 mg, 0.2869 mmol) and *N*-methylglycine (51 mg, 0.5738 mmol) were dissolved in toluene (20 mL) and refluxed for 36 h. After that, the reaction mixture was extracted with DCM, washed with brine solution and dried over anhydrous sodium sulfate. The solvent was evaporated under vacuum, and the product was purified by column chromatography with DCM/hexane (1:1, v/v) as the eluent to get the desired compound **TPA-PTZ-C$_{60}$-1** as a dark color solid with 30 % yield. ^{1}H NMR (500 MHz, CHLOROFORM-d) d = 7.53 (d, *J* = 7.9 Hz, 1 H), 7.34 - 7.30 (m, *J* = 8.7 Hz, 2 H), 7.29 – 7.26 (m, 4 H), 7.25 (br. s., 2 H), 7.24 - 7.21 (m, 1 H), 7.10 (d, *J* = 7.6 Hz, 4 H), 7.07 - 7.03 (m, 2 H), 7.00 - 6.96 (m, *J* = 8.7 Hz, 2 H), 6.87 (br. s., 1 H), 6.75 (d, *J* = 8.5 Hz, 1 H), 4.96 (d, *J* = 9.5 Hz, 1 H), 4.80 (s, 1 H), 4.22 (d, *J* = 9.5 Hz, 1 H), 3.78 (t, *J* = 7.2 Hz, 2 H), 2.77 (s, 3 H), 1.85 - 1.78 (m, 2 H), 1.00 (t, *J* = 7.4 Hz, 3 H). ^{13}C NMR (100 MHz, CHLOROFORM-d) d = 156.3, 153.5, 147.7, 147.3, 147.2, 146.7, 146.5, 146.3, 146.2, 145.9, 145.6, 145.3, 145.2, 144.7, 144.4, 143.1, 143.0, 142.6, 142.3, 142.1, 142.1, 141.6, 140.2, 135.7, 132.4, 131.3, 130.6, 130.1, 129.4, 124.9, 123.5, 122.4, 117.5, 116.3, 115.0, 89.6, 88.0, 82.9, 70.0, 69.0, 66.7, 49.5, 40.0, 33.4, 31.9, 29.7, 29.4, 22.7, 20.0, 14.1, 11.3. HRMS (ESI-TOF) m/z calculated for $C_{98}H_{33}N_3S$ 1283.2395 $[M]^+$, measured 1283.2390 $[M]^+$.

Synthesis of TPA-PTZ-C$_{60}$-2

In a 100 mL round-bottomed flask, compound **TPA-PTZ-2** (85 mg, 0.1279 mmol), C_{60}-fullerene (184 mg, 0.2559 mmol) and *N*-

methylglycine (91 mg, 1.023 mmol) were dissolved in toluene (20 mL) and refluxed for 48 h. After that, the reaction mixture was extracted with DCM, washed with brine solution and dried over anhydrous sodium sulfate. The solvent was evaporated under vacuum, and the product was purified by column chromatography with DCM/hexane (1:1, v/v) as the eluent to get the desired compound TPA-PTZ-C_{60}-2 as a dark color solid with 35 % yield. ^{1}H NMR (500 MHz, CHLOROFORM-d) d = 7.69 (br. s., 1 H), 7.63 (d, *J* = 9.0 Hz, 2 H), 7.43 - 7.35 (m, 5 H), 7.31 (br. s., 1 H), 7.24 (br. s., 2 H), 7.21 (d, *J* = 7.6 Hz, 5 H), 6.90 (d, *J* = 9.2 Hz, 3 H), 6.81 (d, *J* = 9.0 Hz, 1 H), 4.97 (d, *J* = 9.3 Hz, 1 H), 4.81 (s, 1 H), 4.23 (d, *J* = 9.3 Hz, 1 H), 3.83 - 3.78 (m, 2 H), 2.77 (s, 3 H), 1.84 (d, *J* = 7.5 Hz, 2 H), 1.03 (t, *J* = 7.4 Hz, 3 H). ^{13}C NMR (100 MHz, CHLOROFORM-d) d = 164.9, 164.2, 156.1, 153.7, 153.2, 150.3, 147.4, 146.3, 146.2, 146.2, 146.0, 145.6, 145.4, 145.3, 144.8, 144.5, 144.4, 143.1, 142.7, 142.6, 142.3, 142.1, 142.0, 140.2, 139.7, 137.0, 136.4, 135.7, 133.4, 131.9, 130.6, 130.1, 127.6, 127.0, 126.7, 125.0, 124.7, 121.6, 118.1, 114.8, 113.6, 112.8, 112.2, 111.0, 110.4, 82.6, 80.8, 69.9, 69.0, 50.2, 40.0, 34.3, 30.3, 29.7, 19.9, 14.1, 11.1. MALDI-TOF calculated for $C_{104}H_{33}N_7S$ 1411.2518 $[M]^+$; measured 1410.301.

Synthesis of TPA-PTZ-C_{60}-3

In a 100 mL round-bottomed flask, compound **TPA-PTZ-3** (100 mg, 0.135 mmol), C_{60}-fullerene (195 mg, 0.2701 mmol) and *N*-methylglycine (96 mg, 1.08 mmol) were dissolved in toluene (20 mL) and refluxed for 60 h. After that, the reaction mixture was extracted with DCM, washed with brine solution, and dried over anhydrous sodium sulfate. The solvent was evaporated under vacuum, and the product was purified by column chromatography with DCM/hexane (1:1, v/v) as the eluent to get the desired compound **TPA-PTZ-C_{60}-3** as a dark color solid with 33 % yield. ^{1}H NMR (400MHz, CHLOROFORM-d) d = 7.61 - 7.48 (m, 3 H), 7.41 - 7.30 (m, 6 H), 7.18 (d, *J* = 7.5 Hz, 10 H), 6.95 (d, *J* = 6.5 Hz, 3 H), 6.88 (br. s., 1 H), 6.75 (d, *J* = 8.0 Hz, 1 H), 4.96 (d, *J* = 8.5 Hz, 1 H), 4.80 (s, 1 H), 4.22 (d, *J* = 8.8 Hz, 1 H), 3.78 (br. s., 2 H), 2.76 (s, 3 H), 1.86 - 1.79 (m, 2 H), 1.01 (t, *J* = 7.5 Hz, 3 H). ^{13}C NMR (100 MHz, CHLOROFORM-d) d = 168.6, 156.1, 154.1, 153.9, 153.2,

152.9, 151.6, 151.0, 149.7, 147.4, 147.3, 146.5, 146.4, 146.2, 146.2, 146.0, 145.7, 145.5, 145.4, 145.3, 144.8, 144.5, 144.5, 144.4, 143.2, 143.1, 142.7, 142.6, 142.3, 142.2, 142.2, 142.1, 142.0, 141.8, 141.6, 140.2, 140.0, 139.6, 137.0, 136.4, 135.9, 135.6, 135.2, 134.3, 133.3, 132.3, 130.6, 129.9, 129.0, 128.2, 128.0, 127.5, 126.9, 126.6, 125.9, 125.7, 125.5, 124.5, 119.3, 114.7, 114.2, 114.2, 113.7, 113.0, 82.5, 81.8, 74.0, 69.9, 69.0, 53.4, 50.2, 42.0, 40.0, 29.7, 27.0, 19.9, 14.2, 11.1. MALDI-TOF calculated for $C_{110}H_{37}N_7S$ 1487.2831 $[M]^+$; measured 1488.415.

6.7. Conclusion

In conclusion, we have designed and synthesized the triphenylamine-functionalized phenothiazine derivatives **TPA-PTZ 1–3** *via* Pd-catalyzed Sonogashira cross-coupling reaction followed by [2 + 2] cycloaddition-electrocyclic ring-opening reaction and fulleropyrrolidine derivatives **TPA-PTZ-C_{60} 1–3** also with the help of 1,3-dipole cycloaddition reaction and under the condition described by Preto reaction. The photophysical spectra of fulleropyrrolidine derivatives **TPA-PTZ-C_{60}-2** and **TPA-PTZ-C_{60}-3** exhibit bathochromic shift because of intramolecular charge transfer (ICT) transition in the near-infrared region as compared to **TPA-PTZ-2** and **TPA-PTZ-3**. The electrochemical characteristics showed that the **TPA-PTZ 1–3** and **TPA-PTZ-C_{60} 1–3** produce several redox waves in cyclic voltammetry because of the availability of various acceptor units (Fullerene, TCBD, and DCNQ), and donor units (Phenothiazine and Triphenylamine). According to the computational study, the addition of the fullerene moiety stabilizes the lowest unoccupied molecular orbital (LUMO) energy level more than the TCBD and DCNQ moieties. The reported donor–acceptor based triphenylamine-functionalized phenothiazine derivatives **TPA-PTZ 1–3** and fulleropyrrolidine derivatives **TPA-PTZ-C_{60} 1–3** give up a novel route for the development of NIR-absorbing donor-acceptor chromophores for optoelectronic applications.

6.8. References

[1] Jiao, Y., Liu, S., Shen, Z., Mao, L., Ding, Y., Ren, D., … Grätzel, G. (2021). Carbazol-phenyl-phenothiazine-based sensitizers for dye-sensitized solar cells. *Journal of Materials Chemistry A*, *9*, 26311–26322. (DOI: 10.1039/d1ta08020b).

[2] Patil, H., Gupta, A., Bilic, A., Jackson, S. L., Latham, K., & Bhosale, S. V. (2014). Donor–Acceptor–Donor Modular Small Organic Molecules Based on the Naphthalene Diimide Acceptor Unit for Solution-Processable Photovoltaic Devices. *Journal of Electronic Materials*, *43*(9), 3243–3254. (DOI: 10.1007/s11664-014-3243-x).

[3] Poddar, M., Cesaretti, A., Ferraguzzi, E., Carlotti, B., & Misra, R. (2020). Singlet and Triplet Excited-State Dynamics of 3,7-Bis(arylethynyl)phenothiazines: Intramolecular Charge Transfer and Reverse Intersystem Crossing. *Journal of Physical Chemistry C*, *124*(33), 17864–17878. (DOI: 10.1021/ACS.JPCC.0C01786).

[4] Zhang, J., Xu, W., Sheng, P., Zhao, G., & Zhu, D. (2017). Organic Donor-Acceptor Complexes as Novel Organic Semiconductors. *Accounts of Chemical Research*, *50*(7), 1654–1662. (DOI: 10.1021/ACS.ACCOUNTS.7B00124).

[5] Erden, K., & Dengiz, C. (2022). 3-Alkynylindoles as Building Blocks for the Synthesis of Electronically Tunable Indole-Based Push-Pull Chromophores. *Journal of Organic Chemistry*, *87*(6), 4385–4399. (DOI: 10.1021/ACS.JOC.2C00067).

[6] Srinivasa Rao, P., Brixi, S., Shaikh, D. B., Al Kobaisi, M., Lessard, B. H., Bhosale, S. V., & Bhosale, S. V. (2021). The Effect of TCNE and TCNQ Acceptor Units on Triphenylamine-Naphthalenediimide Push-Pull Chromophore Properties. *European Journal of Organic Chemistry*, *2021*(18), 2615–2624. (DOI: 10.1002/EJOC.202100198).

[7] Poddar, M., Jang, Y., Misra, R., & D'Souza, F. (2020). Excited-State Electron Transfer in 1,1,4,4-Tetracyanobuta-1,3-diene

(TCBD)- and Cyclohexa-2,5-diene-1,4-diylidene-Expanded TCBD-Substituted BODIPY-Phenothiazine Donor–Acceptor Conjugates. *Chemistry - A European Journal*, *26*(30), 6869–6878. (DOI: 10.1002/CHEM.202000346).

[8] Jang, Y., Rout, Y., Misra, R., & D'Souza, F. (2021). Symmetric and Asymmetric Push-Pull Conjugates: Significance of Pull Group Strength on Charge Transfer and Separation. *Journal of Physical Chemistry B*, *125*(16), 4067–4075. (DOI: 10.1021/ACS.JPCB.0C09996).

[9] Kandpal, S., Gupta, P. K., & Misra, R. (2024). Ferrocene-Functionalized Fulleropyrrolidine Derivative: A Performance Enhancer for Solid-State Electrochromic Devices. *ACS Applied Optical Materials*, *2*(1), 158–165. (DOI: 10.1021/ACSAOM.3C00384).

[10] Han, L., Chen, Y., Zhao, ge, Cui, Y., & Jiang, S. (2020). Phenothiazine dyes containing a 4-phenyl-2-(thiophen-2-yl) thiazole bridge for dye-sensitized solar cells. (DOI: 10.1016/j.tet.2020.131102).

[11] Seintis, K., Şahin, Ç., Sigmundová, I., Stathatos, E., Hrobárik, P., & Fakis, M. (2018). Solvent-Acidity-Driven Change in Photophysics and Significant Efficiency Improvement in Dye-Sensitized Solar Cells of a Benzothiazole-Derived Organic Sensitizer. *Journal of Physical Chemistry C*, *122*(35), 20122–20134. (DOI: 10.1021/ACS.JPCC.8B05686).

[12] Sathiyan, G., Chatterjee, S., Sen, P., Garg, A., Gupta, R. K., & Singh, A. (2019). Thiazolothiazole-Based Fluorescence Probe towards Detection of Copper and Iron Ions through Formation of Radical Cations. *ChemistrySelect*, *4*(40), 11718–11725. (DOI: 10.1002/slct.201902994).

[13] Poddar, M., Sivakumar, G., & Misra, R. (2019). Donor–acceptor substituted 1,8-naphthalimides: design, synthesis, and structure–property relationship. *Journal of Materials Chemistry C*, *7*, 14798-14815. (DOI: 10.1039/c9tc02634g).

[14] Ginley, D., Green, M. A., & Collins, R. (2008). Solar Energy Conversion Toward 1 Terawatt. *MRS Bulletin*, *33*(4), 355–364. (DOI: 10.1557/mrs2008.71).

[15] Espinosa, N., H€, M., Angmo, D., & Krebs, F. C. (n.d.). Solar cells with one-day energy payback for the factories of the future. *Energy & Environmental Science*, *5*, 5117–5132. (DOI: 10.1039/c1ee02728j).

[16] Powell, C., Bender, T., & Lawryshyn, Y. (2009). A model to determine financial indicators for organic solar cells. *Solar Energy*, *83*, 1977–1984. (DOI: 10.1016/j.solener.2009.07.009).

[17] Zhang, H., Wan, X., Xue, X., Li, Y., Yu, A., & Chen, Y. (2010). Selective tuning of the HOMO-LUMO gap of carbazole-based donor-acceptor-donor compounds toward different emission colors. *European Journal of Organic Chemistry*, (9), 1681–1687. (DOI: 10.1002/EJOC.200901167).

[18] Lin, Y., Li, Y., & Zhan, X. (2012). Small molecule semiconductors for high-efficiency organic photovoltaics. *Chemical Society Reviews*, *41*(11), 4245–4272. (DOI: 10.1039/c2cs15313k).

[19] Liu, Y., Zhao, J., Li, Z., Mu, C., Ma, W., Hu, H., … Yan, H. (2014). Aggregation and morphology control enables multiple cases of high-efficiency polymer solar cells. *Nature Communications*, *5*(1), 5293. (DOI: 10.1038/ncomms6293).

[20] Gautam, P., Misra, R., Siddiqui, S. A., & Sharma, G. D. (2015). Unsymmetrical donor-acceptor-acceptor-π-donor type benzothiadiazole-based small molecule for a solution processed bulk heterojunction organic solar cell. *ACS Applied Materials and Interfaces*, *7*(19), 10283–10292. (DOI: 10.1021/ACSAMI.5B02250).

[21] Misra, R., Gautam, P., & Mobin, S. M. (2013). Aryl-substituted unsymmetrical benzothiadiazoles: Synthesis, structure, and properties. *Journal of Organic Chemistry*, *78*(24), 12440–12452. (DOI: 10.1021/JO402111Q).

[22] Dhokale, B., Gautam, P., & Misra, R. (2012). Donor-acceptor perylenediimide-ferrocene conjugates: synthesis, photophysical, and electrochemical properties. *Solar Energy*, *83*, 1977–1984. (DOI: 10.1016/j.tetlet.2012.02.107).

[23] Misra, R., Gautam, P., Jadhav, T., & Mobin, S. M. (2013). Donor-acceptor ferrocenyl-substituted benzothiadiazoles: Synthesis, structure, and properties. *Journal of Organic Chemistry*, *78*(10), 4940–4948. (DOI: 10.1021/JO4005734).

[24] Dhokale, B., Jadhav, T., Mobin, S. M., & Misra, R. (2015). Meso Alkynylated Tetraphenylethylene (TPE) and 2,3,3-Triphenylacrylonitrile (TPAN) Substituted BODIPYs. *Journal of Organic Chemistry*, *80*(16), 8018–8025. (DOI: 10.1021/ACS.JOC.5B01117).

[25] Antoniuk-Pablant, A., Kodis, G., Moore, A. L., Moore, T. A., & Gust, D. (2016). Photoinduced Electron and Energy Transfer in a Molecular Triad Featuring a Fullerene Redox Mediator. *Journal of Physical Chemistry B*, *120*(27), 6687–6697. (DOI: 10.1021/ACS.JPCB.6B03470).

[26] Miura, T., Tao, R., Shibata, S., Umeyama, T., Tachikawa, T., Imahori, H., & Kobori, Y. (2016). Geometries, Electronic Couplings, and Hole Dissociation Dynamics of Photoinduced Electron-Hole Pairs in Polyhexylthiophene-Fullerene Dyads Rigidly Linked by Oligophenylenes. *Journal of the American Chemical Society*, *138*(18), 5879–5885. (DOI: 10.1021/JACS.5B13414).

[27] Williams, D. E., Dolgopolova, E. A., Godfrey, D. C., Ermolaeva, E. D., Pellechia, P. J., Greytak, A. B., … Shustova, N. B. (2016). Fulleretic Well-Defined Scaffolds: Donor–Fullerene Alignment Through Metal Coordination and Its Effect on Photophysics. *Angewandte Chemie - International Edition*, *55*(31), 9070–9074. (DOI: 10.1002/ANIE.201603584).

[28] Sánchez, L., Martín, N., & Guldi, D. M. (2005). Hydrogen-bonding motifs in fullerene chemistry. *Angewandte Chemie* -

International Edition, *44*(34), 5374–5382. (DOI: 10.1002/ANIE.200500321).

[29] Fukuzumi, S., Ohkubo, K., Souza, F. D' & Sessler, J. L., (2012). Supramolecular electron transfer by anion binding Supramolecular electron transfer by anion binding. *Chemical Communications*, *48*, 9801–9815. (DOI: 10.1039/c2cc32848h).

[30] Souza, F. D' & Ito, O. (2012). Photosensitized electron transfer processes of nanocarbons applicable to solar cells. *Chemical Society Reviews*, *41*, 86–96. (DOI: 10.1039/c1cs15201g).

[31] Umeyama, T., & Imahori, H. (2008). Carbon nanotube-modified electrodes for solar energy conversion. *Energy and Environmental Science*, 1, 120–133. (DOI: 10.1039/b805419n).

[32] Schuster, D. I., Li, K., & Guldi, D. M. (2006). Porphyrin–fullerene photosynthetic model systems with rotaxane and catenane architectures. *Comptes Rendus Chimie*, *9*(7–8), 892–908. (DOI: 10.1016/j.crci.2005.11.013).

[33] Blanco, G. D., Hiltunen, A. J., Lim, G. N., KC, C. B., Kaunisto, K. M., Vuorinen, T. K., … D'Souza, F. (2016). Syntheses, Charge Separation, and Inverted Bulk Heterojunction Solar Cell Application of Phenothiazine-Fullerene Dyads. *ACS Applied Materials and Interfaces*, *8*(13), 8481–8490. (DOI: 10.1021/ACSAMI.6B00561).

[34] Yin, G., Mao, X., Suo, Z., & Xu, Z. (2001). Synthesis and Photophysical Properties of C_{60} -carbazole Adducts. *Chinese Journal of Chemistry*, *19*(9), 822–828. (DOI: 10.1002/cjoc.20010190903).

[35] Metri, N., Sallenave, X., Plesse, C., Beouch, L., Aubert, P. H., Goubard, F., … Sini, G. (2012). Processable star-shaped molecules with triphenylamine core as hole-transporting materials: Experimental and theoretical approach. *Journal of Physical Chemistry C*, *116*(5), 3765–3772. (DOI: 10.1021/JP2098872).

[36] Szablewski, M., Thomas, P. R., Thornton, A., Bloor, D., Cross, G. H., Cole, J. M., … Goovaerts, E. (1997). Highly dipolar,

optically nonlinear adducts of tetracyano-p-quinodimethane: Synthesis, physical characterization, and theoretical aspects. *Journal of the American Chemical Society*, *119*(13), 3144–3154. (DOI: 10.1021/JA963923W).

[37] Barlow, S., & Marder, S. R. (2000). Electronic and optical properties of conjugated group 8 metallocene derivatives. *Chemical Communications*, 1555–1562 (DOI: 10.1039/b004907g).

[38] Tykwinski, R. R., Gubler, U., Martin, R. E., Diederich, F., Bosshard, C., & Günter, P. (1998). Structure-property relationships in third-order nonlinear optical chromophores. *Journal of Physical Chemistry B*, *102*(23), 4451–4465. (DOI: 10.1021/JP980829O).

[39] Patil, Y., & Misra, R. (2017). Tetracyanobutadiene bridged ferrocene and triphenylamine functionalized pyrazabole dimers. *Journal of Organometallic Chemistry* **2017**, *840*, 23–29. (DOI: 10.1016/j.jorganchem.2017.03.048).

[40] Gupta R. R. & Ojha K. G. (1988). In Phenothiazines and 1,4-Benzothiazines: Chemical and Biochemical Aspects. *Elsevier: Amsterdam*, *p*. 163-269.

[41] Khan, F., Mahmoudi, M., Gupta, P. K., Volyniuk, D., Grazulevicius, J. V., & Misra, R. (2023). Mechanochromic Materials Based on Tetraphenylethylene-Substituted Phenothiazines: Substituent-Dependent Hypsochromic and Bathochromic Switching of Emission. *The Journal of Physical Chemistry C*, *127*(3), 1643–1654. (DOI: 10.1021/acs.jpcc.2c07010).

[42] Hauck, M., Stolte, M., Schönhaber, J., Kuball, H. G., & Müller, T. J. J. (2011). Synthesis, electronic, and electro-optical properties of emissive solvatochromic phenothiazinyl merocyanine dyes. *Chemistry - A European Journal*, *17*(36), 9984–9998. (DOI: 10.1002/CHEM.201100592).

[43] Krämer, C. S., & Müller, T. J. J. (2003). Synthesis and electronic properties of alkynylated phenothiazines. *European Journal of*

Organic Chemistry, (18), 3534–3548. (DOI: 10.1002/EJOC.200300250).

[44] Michinobu, T., Boudon, C., Gisselbrecht, J. P., Seiler, P., Frank, B., Moonen, N. N. P., … Diederich, F. (2006). Donor-substituted 1,1,4,4-tetracyanobutadienes (TCBDs): New chromophores with efficient intramolecular charge-transfer interactions by atom-economic synthesis. *Chemistry - A European Journal*, *12*(7), 1889–1905. (DOI: 10.1002/CHEM.200501113).

[45] Gupta, P. K., Khan, F., & Misra, R. (2023). NIR-Absorbing 1,1,4,4-Tetracyanobuta-1,3-diene- and Dicyanoquinodimethane-Functionalized Donor-Acceptor Phenothiazine Derivatives: Synthesis and Characterization. *The Journal of organic chemistry*, *88*(20), 14308–14322. (DOI: 10.1021/ACS.JOC.3C01029).

[46] Sekita, M., Ballesteros, B., Diederich, F., Guldi, D. M., Bottari, G., & Torres, T. (2016). Intense Ground-State Charge-Transfer Interactions in Low-Bandgap, Panchromatic Phthalocyanine–Tetracyanobuta-1,3-diene Conjugates. *Angewandte Chemie*, *128*(18), 5650–5654. (DOI: 10.1002/ange.201601258).

[47] Gupta, P. K., Das, S., Misra, R., & D'Souza, F. (2024). Near-IR Capturing N-Methylbenzene Sulfonamide-Phenothiazine Incorporating Strong Electron Acceptor Push-Pull Systems: Photochemical Ultrafast Carrier Dynamics. *Chemistry – A European Journal*, *30*(25). (DOI: 10.1002/chem.202304313).

[48] Zhang, H., Wan, X., Xue, X., Li, Y., Yu, A., & Chen, Y. (2010). Selective Tuning of the HOMO–LUMO Gap of Carbazole-Based Donor–Acceptor–Donor Compounds toward Different Emission Colors. *European Journal of Organic Chemistry*, *2010*(9), 1681–1687. (DOI: 10.1002/ejoc.200901167).

[49] Misra, R., & Gautam, P. (2014). Tuning of the HOMO-LUMO gap of donor-substituted symmetrical and unsymmetrical benzothiadiazoles. *Organic & Biomolecular Chemistry*, *12*, 5448. (DOI: 10.1039/c4ob00629a).

[50] Yamada, M., Schweizer, W. B., Schoenebeck, F., & Diederich, F. F. (2010). Unprecedented thermal rearrangement of push-pull-chromophore-[60]fullerene conjugates: formation of chiral 1,2,9,12-tetrakis-adductsw. *Chemical. Communication*, *46*, 5334–5336. (DOI: 10.1039/c0cc00881h).

[51] Luo, H., Fujitsuka, M., Araki, Y., Ito, O., Padmawar, P., & Chiang, L. Y. (2003). Inter- and intramolecular photoinduced electron-transfer processes between C60 and diphenylaminofluorene in solutions. *Journal of Physical Chemistry B*, *107*(35), 9312–9318. (DOI: 10.1021/JP034689G).

[52] Wang, C., Wu, B., Li, Y., Dong, T., Chai, Y., Zhang, Y., & Wang, C. (2023). Regioisomeric Benzidine-Fullerenes: Tuning of the Diverse Hole-Distribution to Influence Charge Separation Patterns. *Angewandte Chemie International Edition*, *62*(15). (DOI: 10.1002/anie.202300377).

[53] Frisch, M. J.; Trucks, G. W.; Schlegel, G. W.; Scuseria, G. E.; Robb, M. A.; Cheeseman, J. R.; Scalmani, G.; Barone, V.; Mennucci, B.; Petersson, G. A.; et al. (2009). Gaussian 09, revision A.02; Gaussian, Inc.: Wallingford, CT.

Chapter 7

Design and Synthesis of TCBD and DCNQ Functionalized Phenothiazine and Fulleropyrrolidine Chromophores: Photophysical, Electrochemical and Computational Studies

7.1. Introduction

In recent years, the π-conjugated organic molecules have played great importance in the fields of organic chemistry, materials science, and electronic devices because of their unique electronic and optical properties.[1–5] π-Conjugated organic molecules form the basis of organic electronic devices, such as organic field-effect transistors (OFETs), organic light-emitting diodes (OLEDs), nonlinear optics (NLOs), and organic photovoltaic cells (OPVs). Due to their tunable electronic and optical properties, they are promising candidates for flexible and affordable electronic applications in optoelectronic devices.[6–13] Additionally, these molecules are employed in the development of organic semiconductors for light-emitting materials and sensors.[14–16] The energy levels of HOMO/LUMO can be fine-tuned using D–A based chromophores by adjusting the strength of the donor or acceptor and incorporating various π-linkers.[17–23] However, our group aims to design and synthesize push-pull chromophores for use in optoelectronics by modifying donor and acceptor moieties.[19–22]

The 10*H*-phenothiazine is a heterocyclic compound that acts as an electron donor. It has a non-planar geometry and a bowl-shaped structure, with electron-rich nitrogen (*N*) and sulphur (*S*) heteroatoms.[24, 25] Phenothiazine and its derivatives are extensively utilized in various fields, such as chemical sensors, photovoltaic devices, and organic light-emitting diodes (OLEDs), owing to their notable characteristics, including high electron density and effective electron-donating capabilities.[26, 27] Fullerene is a unique carbon allotrope with a hollow spherical shape composed completely of carbon atoms arranged in a hexagonal and pentagonal pattern.[28] Fulleropyrrolidines

is a family of vicinally disubstituted-organo-fullerenes. Fulleropyrrolidines are a common form of acceptor used in the development of photosynthetic supramolecular model molecules and organic photovoltaic clouds (OPVs).[29–34] The fulleropyrrolidines are synthesized *via* the 1,3-dipolar cycloaddition of azomethine ylides.[35] These synthesized compounds exhibit noteworthy characteristics, such as high electron affinity, minimal reorganization energy, and excellent charge transport ability.[36] Therefore, fullerene-based D–A systems have potential applications in molecular wires[37], molecular switches[38], nonlinear optical materials[39], and other molecular devices.[40] Ito *et al.* have reported that the fullerene derivatives connected with electron donors play an important role in enhancing the electron-transfer ability.[41, 42] The 1,1,2,2-tetracyanoethylene (TCNE) and 7,7,8,8-tetracyanoquinodimethane (TCNQ) are strong electron acceptors because of they contain four cyano groups,[43, 44] and are highly reactive towards electron-rich alkynes, undergo [2 + 2] cycloaddition reaction to form cyclobutene rings accompanied by retroelectrocyclization reaction to produce 1,1,4,4-tetracyanobutadiene (TCBD) and cyclohexa-2,5-diene-1,4-diylidene-expanded TCBD or DCNQ (DCNQ = dicyanodiquinodimethane) derivatives.[45] The donor-acceptor systems containing TCBD and DCNQ acceptors are interesting possibilities for organic photovoltaics applications.[46] Diederich *et al.* reacted TCNE and TCNQ with various acetylenic donors to produce charge-transfer chromophores using a [2 + 2] cycloaddition-retroelectrocyclization reaction.[47, 48]

In this contribution, we report the phenothiazine chromophores **(PTZ)$_2$ 1–3** which were synthesized by the Pd-catalyzed Sonogashira cross-coupling reaction followed by the [2 + 2] cycloaddition retroelectrocyclization reaction, and fulleropyrrolidine derivatives **(PTZ)$_2$-C$_{60}$ 1–3** by 1,3-dipolar cycloaddition reaction (Prato reaction) in good yields. The phenothiazine chromophore **(PTZ)$_2$-1** was modified by fullerene moiety and cyano-based strong electron acceptors TCNE/TCNQ unit (Chart 7.1). Herein, we investigated the impact of incorporating the fullerene moiety and strong electron acceptors 1,1,4,4-

tetracyanobuta-1,3-diene (TCBD) and dicyanoquinodimethane (DCNQ) moieties on the photophysical, electrochemical, and computational characteristics of donor-acceptor phenothiazine chromophores **$(PTZ)_2$ 1–3** and fulleropyrrolidine chromophores **$(PTZ)_2$-C_{60} 1–3**. The TCBD and DCNQ functionalized chromophores **$(PTZ)_2$-2**, **$(PTZ)_2$-3, $(PTZ)_2$-C_{60}-2**, and **$(PTZ)_2$-C_{60}-3** show intramolecular charge transfer transition bands at lower energy regions correspond to strong D−A interactions. Moreover, the computational studies are performed to investigate the donor-acceptor contributions and molecular geometry of various entities in the derivatives of phenothiazines **$(PTZ)_2$ 1–3** and fulleropyrrolidines **$(PTZ)_2$-C_{60} 1–3**.

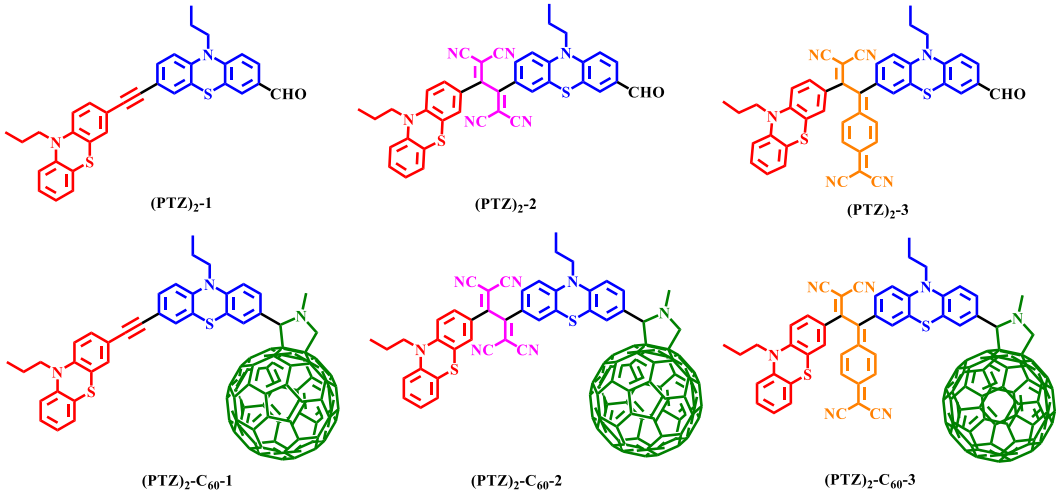

Chart 7.1. Chemical structures of donor−acceptor based phenothiazine chromophores **$(PTZ)_2$ 1–3** and fulleropyrrolidine derivatives **$(PTZ)_2$-C_{60} 1–3**.

7.2. Result and Discussion

The donor–acceptor based phenothiazine chromophores **$(PTZ)_2$ 1–3** and fulleropyrrolidine derivatives **$(PTZ)_2$-C_{60} 1–3** were designed and synthesized by the Sonogashira cross-coupling, [2 + 2] cycloaddition–retroelectrocyclization and 1,3-dipolar cycloaddition reaction using donor phenothiazine (PTZ), and acceptors fullerene (C_{60}), tetracyanoethylene (TCNE) or 7,7,8,8-tetracyanoquino-dimethane (TCNQ) units. The detailed synthetic procedure of the donor–acceptor based phenothiazine chromophores **$(PTZ)_2$ 1–3** and fulleropyrrolidine

derivatives **(PTZ)$_2$-C$_{60}$ 1–3** are shown in Scheme 7.1. The 3-ethynyl-10-propyl-10*H*-phenothiazine **PTZ** react with 1.1 equivalent of 7-bromo-10-propyl-10*H*-phenothiazine-3-carbaldehyde **Br-PTZ-CHO** using THF:TEA (1:1) under N_2 atmosphere in the presence of $Pd(PPh_3)_2Cl_2$/CuI *via* Sonogashira cross-coupling reaction, which resulted in phenothiazine chromophore **(PTZ)$_2$-1** 87% yield. The TCBD and DCNQ incorporated phenothiazine chromophores (**PTZ)$_2$-2** and (**PTZ)$_2$-3** were designed and synthesized by the [2 + 2] cycloaddition–retroelectrocyclization reaction. The **(PTZ)$_2$-1** reacts with 1.1 equivalents of TCNE in dichloromethane at room temperature for 24 h to produce (**PTZ)$_2$-2** in 80% yield. Similarly, (**PTZ)$_2$-1** reacts with 1.1 equivalents of TCNQ in dichloroethane (DCE) for 36 h at 60 °C which results in (**PTZ)$_2$-3** in 60% yield. Subsequently, the donor–acceptor based phenothiazine chromophores **(PTZ)$_2$ 1–3** reacts with fullerene (C_{60}) using toluene in the presence of an excess amount of *N*-methylglycine (sarcosine) and followed by a 1,3-dipolar cycloaddition reaction (Prato reaction)[41, 49] resulted in fulleropyrrolidine derivatives **(PTZ)$_2$-C$_{60}$ 1–3** in 40%, 30% and 35% yields, respectively. The synthesis of the phenothiazine chromophores **(PTZ)$_2$ 1–3** and fulleropyrrolidine derivatives **(PTZ)$_2$-C$_{60}$ 1–3** were purified by column chromatography and well-characterized by ^{1}H-NMR, ^{13}C-NMR spectroscopy, HRMS and MALDI-TOF techniques.

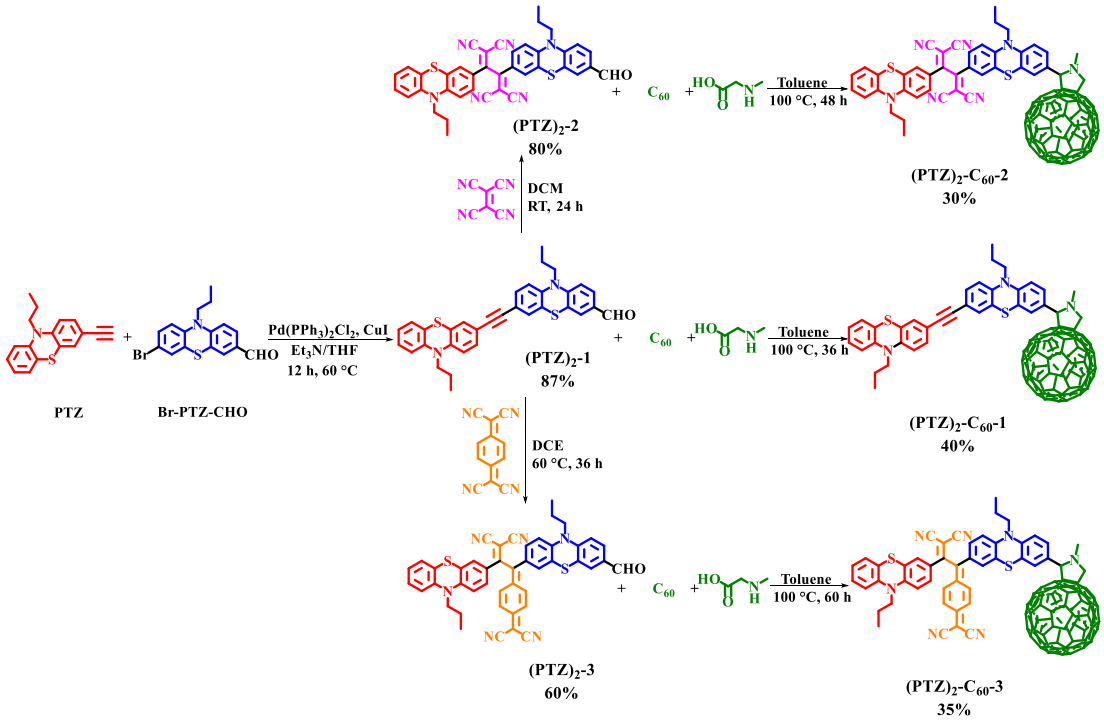

Scheme 7.1. Synthetic route of phenothiazine chromophores **(PTZ)$_2$ 1–3** and fulleropyrrolidine derivatives **(PTZ)$_2$-C$_{60}$ 1–3**.

7.3. Photophysical Properties

The optical properties of the phenothiazine chromophores **(PTZ)$_2$ 1–3** and fulleropyrrolidine derivatives **(PTZ)$_2$-C$_{60}$ 1–3** were recorded in dilute dichloromethane solutions (1×10^{-5} M) at room temperature. The absorption spectra are depicted in Figure 7.1, and the appropriate data including absorption maxima (λ_{max}), extinction coefficient, and optical bandgap are summarized in Table 7.1. The absorption spectra of phenothiazine chromophores **(PTZ)$_2$ 1–3** exhibit an absorption band at 250–430 nm corresponding to $\pi \rightarrow \pi^*$ transitions and 430–800 nm which is due to the intramolecular charge transfer (ICT) transition from donor to acceptor moieties. The absorption band at the higher energy region corresponds to phenothiazine units, and the lower energy region absorption band is due to TCNE/TCNQ moieties. The chromophore **(PTZ)$_2$-1** exhibits absorption maxima at 394 nm (ε = 14400 M^{-1} cm^{-1}), corresponding to the π-π^* transition. The TCBD and DCNQ functionalized chromophores **(PTZ)$_2$-2** and **(PTZ)$_2$-3** have absorption maxima at 533 nm (ε = 20150 M^{-1} cm^{-1}) and 647 nm (ε = 13100 M^{-1} cm^{-}

[1]) respectively, and these longer wavelength transitions are caused by intramolecular charge transfer (ICT) which is attributed to strong donor-acceptor interactions from donor phenothiazine to acceptor TCBD and DCNQ moieties. The absorption spectra of the DCNQ substituted chromophore **(PTZ)$_2$-3** exhibits a bathochromic shift of 114 nm compared to the TCBD functionalized derivative **(PTZ)$_2$-2** due to the stronger electron-accepting character of the DCNQ moiety.

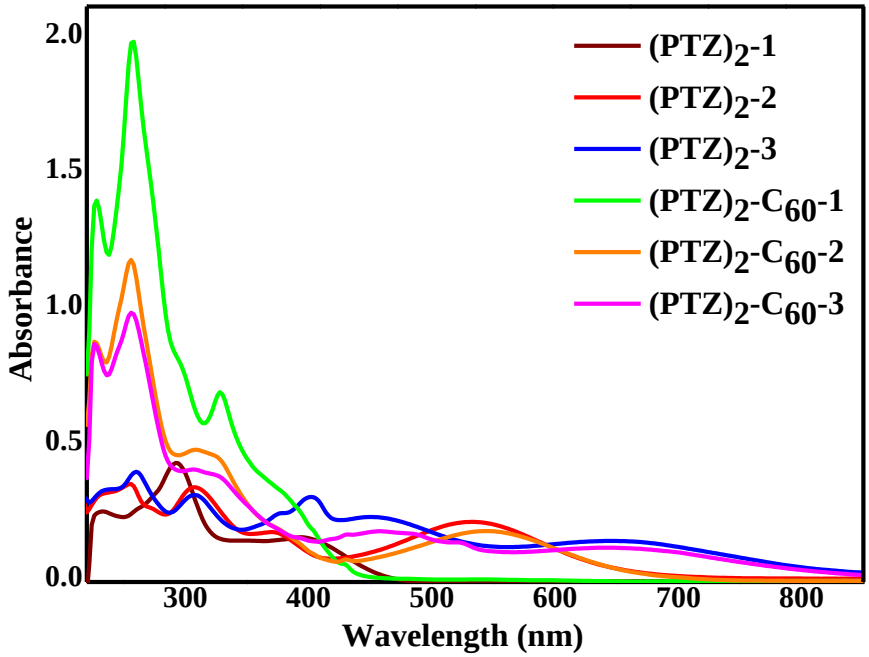

Figure 7.1. Absorption spectra of phenothiazine chromophores **(PTZ)$_2$ 1–3** and fulleropyrrolidine derivatives **(PTZ)$_2$-C$_{60}$ 1–3** in dichloromethane (1×10^{-5} M).

On the other hand, the UV−visible absorption of fulleropyrrolidine derivatives **(PTZ)$_2$-C$_{60}$ 1–3** possesses two shoulder peaks in the range of 220−320 nm corresponding to fullerene moiety. The fulleropyrrolidine derivative **(PTZ)$_2$-C$_{60}$-1** exhibits an absorption maxima at 382 nm (ε = 30000 M^{-1} cm^{-1}), which was attributed to the ICT transition. Whereas, the absorption maxima of fulleropyrrolidines **(PTZ)$_2$-C$_{60}$-2** and **(PTZ)$_2$-C$_{60}$-3** show at 547 nm (ε = 16700 M^{-1} cm^{-1}) and 659 nm (ε = 10500 M^{-1} cm^{-1}) respectively, and these lower-energy region transitions are corresponding to the intramolecular charge transfer (ICT) transition which is attributed to the strong electronic communication between donor (phenothiazine) and acceptor

(TCBD/DCNQ and fullerene) moieties. The DCNQ-functionalized fulleropyrrolidine derivative **(PTZ)$_2$-C$_{60}$-3** reveals a red-shifted ICT band of 112 nm at a lower energy region compared to TCBD-functionalized fulleropyrrolidine **(PTZ)$_2$-C$_{60}$-2** corresponding to strong electronic communication from donor to acceptor unit.

The optical band gaps for phenothiazine chromophores **(PTZ)$_2$ 1–3** and fulleropyrrolidine derivatives **(PTZ)$_2$-C$_{60}$ 1–3** were evaluated from the onset edge of the absorption band in dichloromethane, which was found to be 2.55, 1.67, 1.47, 2.74, 1.69, and 1.46 eV, respectively. The optical band gap values follow the order **(PTZ)$_2$-C$_{60}$-1** > **(PTZ)$_2$-1** > **(PTZ)$_2$-C$_{60}$-2** > **(PTZ)$_2$-2** > **(PTZ)$_2$-3** > **(PTZ)$_2$-C$_{60}$-3**. The trends clearly indicate that the strong electron acceptor DCNQ functionalized donor–acceptor chromophores **(PTZ)$_2$-3** and **(PTZ)$_2$-C$_{60}$-3** resulted in a redshifted band with a low optical bandgap in comparison to TCBD functionalized **(PTZ)$_2$-2** and **(PTZ)$_2$-C$_{60}$-2** which are attributed to intramolecular charge transfer (ICT) transition. All transitions are explained by computational calculations, and their relevant data are included in Table 7.3.

Table 7.1. Photophysical and theoretical data of phenothiazine chromophores **(PTZ)$_2$ 1–3** and fulleropyrrolidine derivatives **(PTZ)$_2$-C$_{60}$ 1–3**.

Compounds	λ_{max} **(nm)**[a]	ε **(M^{-1} cm^{-1})**[a]	E_g^{opt} **(eV)**[a]	**HOMO (eV)**[b]	**LUMO (eV)**[b]	**band-gap (eV)**[b]
(PTZ)$_2$-1	394	14400	2.55	–4.94	–1.72	3.22
(PTZ)$_2$-2	533	20150	1.67	–5.93	–3.59	2.34
(PTZ)$_2$-3	453 647	22100 13100	1.47	–5.97	–4.10	1.87
(PTZ)$_2$-C$_{60}$-1	382	30000	2.74	–4.81	–3.35	1.46
(PTZ)$_2$-C$_{60}$-2	547	16700	1.69	–5.30	–3.42	1.88
(PTZ)$_2$-C$_{60}$-3	463 659	16600 10500	1.46	–5.32	–3.74	1.58

[a]Absorbance measured in dichloromethane at (1×10^{-5} M); λ_{max} = absorption wavelength; ε = extinction coefficient; E_g^{opt} = optical bandgap; [b]Theoretical data obtained from density functional theory (DFT) calculations performed at the B3LYP/6-31G (d,p) level.

7.4. Electrochemical Properties

The redox potentials of phenothiazine chromophores **(PTZ)$_2$ 1–3** and fulleropyrrolidine derivatives **(PTZ)$_2$-C$_{60}$ 1–3** were evaluated by cyclic voltammetry (CV) and differential pulse voltammetry (DPV) using 0.1 M tetrabutylammonium hexafluorophosphate ($TBAPF_6$) as a supporting electrolyte. The electrochemical data are demonstrated in Table 7.2, and the representative cyclic voltammograms and differential pulse voltammograms for phenothiazine **(PTZ)$_2$ 1–3** and fulleropyrrolidine chromophores **(PTZ)$_2$-C$_{60}$ 1–3** are shown in Figures 7.2 and 7.3.

The currently examined phenothiazine chromophores **(PTZ)$_2$ 1–3** and fulleropyrrolidine derivatives **(PTZ)$_2$-C$_{60}$ 1–3** exhibit donor phenothiazine moiety and acceptor fullerene (C_{60}) and tetracyanoethylene (TCNE) and 7,7,8,8-tetracyanoquinodimethane (TCNQ) units. The ability of any moiety to participate in electron transfer activities is mainly determined by the multiple oxidation and reduction waves that it exhibits at different potentials. In general, phenothiazine exhibits one reversible oxidation potential on the anodic side which corresponds to the radical cation formation of $PTZ^{\cdot+}$. The TCBD/DCNQ moieties exhibit two reduction waves at low potential on the cathodic side which is attributed to the formation of radical anions and dianions. The phenothiazine chromophores **(PTZ)$_2$ 1–3** exhibit two oxidation potentials on the anodic side at +0.77 V, +0.99 V; +0.98 V, +1.09 V; and +0.90 V, +1.09 V respectively, and fulleropyrrolidine derivatives **(PTZ)$_2$-C$_{60}$ 1–3** also exhibit two oxidation potentials at +0.72 V, +0.85 V; +0.96 V, +1.39 V; and +0.93 V, +1.34 V respectively. In this case, the initial oxidation potential originates from the terminal phenothiazine unit, while the subsequent oxidation potential is attributed to the centered phenothiazine moiety. The TCBD/DCNQ functionalized chromophores **(PTZ)$_2$-2** and **(PTZ)$_2$-3**

reveal two reduction potentials on the cathodic region at –0.46 V, –0.78 V; and –0.25 V, –0.36 V respectively, which are attributed to radical anions and dianions formation of the TCBD/DCNQ moieties. The fulleropyrrolidine derivative **(PTZ)$_2$-C$_{60}$-1** also shows two reduction potentials on the cathodic side at –0.77 V and –0.98 V, which is due to fullerene moiety. On the other hand, the TCBD/DCNQ functionalized fulleropyrrolidine derivatives **(PTZ)$_2$-C$_{60}$-2** and **(PTZ)$_2$-C$_{60}$-3** show three reduction potentials on the cathodic region at –0.47 V, –0.75 V, –1.16 V; and –0.35 V, –0.74 V, –1.11 V, respectively which is corresponding to the TCBD/DCNQ and fullerene moiety.

The electrochemically HOMO and LUMO energy levels as well as the HOMO–LUMO gap of phenothiazine chromophores **(PTZ)$_2$ 1–3** and fulleropyrrolidine derivatives **(PTZ)$_2$-C$_{60}$ 1–3** were calculated using the obtained oxidation and reduction onset values. Accordingly, the corresponding electrochemically HOMO energy levels of **(PTZ)$_2$ 2–3** and **(PTZ)$_2$-C$_{60}$ 1–3** are −5.38, −5.30, −5.12, −5.36, and −5.33 eV, respectively and the electrochemically LUMO energy levels are −3.94, −4.15, −3.63, −3.93, and −4.02 eV, respectively. The calculated electrochemical bandgap (E_{gap}) of **(PTZ)$_2$-2**, **(PTZ)$_2$-3**, **(PTZ)$_2$-C$_{60}$-1**, **(PTZ)$_2$-C$_{60}$-2** and **(PTZ)$_2$-C$_{60}$-3** were 1.44 eV, 1.15 eV, 1.49 eV, 1.43 eV and 1.31 eV respectively. The E_{gap} values follow the order **(PTZ)$_2$-C$_{60}$-1** > **(PTZ)$_2$-2** > **(PTZ)$_2$-C$_{60}$-2** > **(PTZ)$_2$-C$_{60}$-3** > **(PTZ)$_2$-3**. The electrochemical data demonstrates that integrating cyano-based electron acceptor groups can alter the redox characteristics of phenothiazine and fulleropyrrolidine chromophores. Additionally, the dicyanoquinodimethane (DCNQ) unit stabilizes the LUMO energy level to a greater extent compared to the tetracyanoethylene (TCBD) unit.

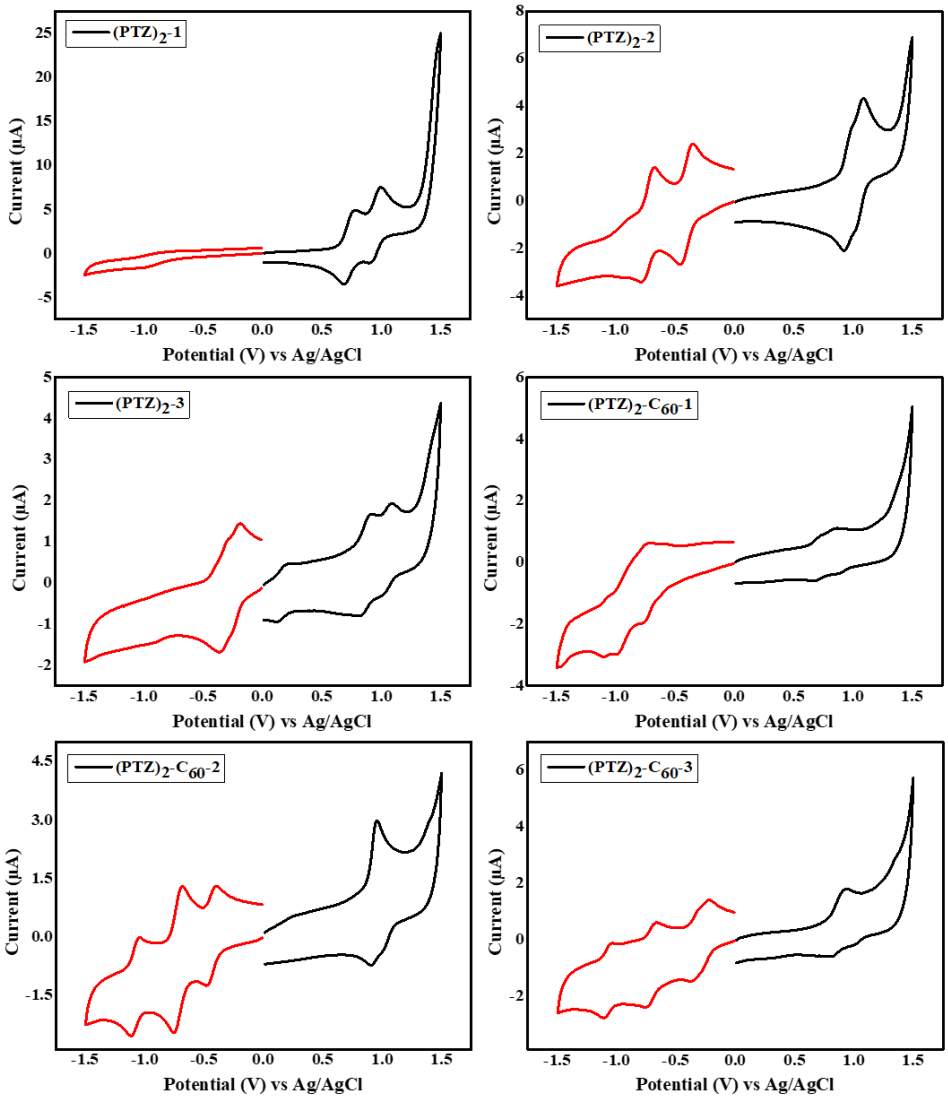

Figure 7.2. Cyclic voltammograms of **(PTZ)$_2$ 1–3** and **(PTZ)$_2$-C$_{60}$ 1–3** in 0.1 M solution of Bu_4NPF_6 in dichloromethane at 100 mV s^{-1} scan rate *versus* saturated Ag/AgCl at 25 °C.

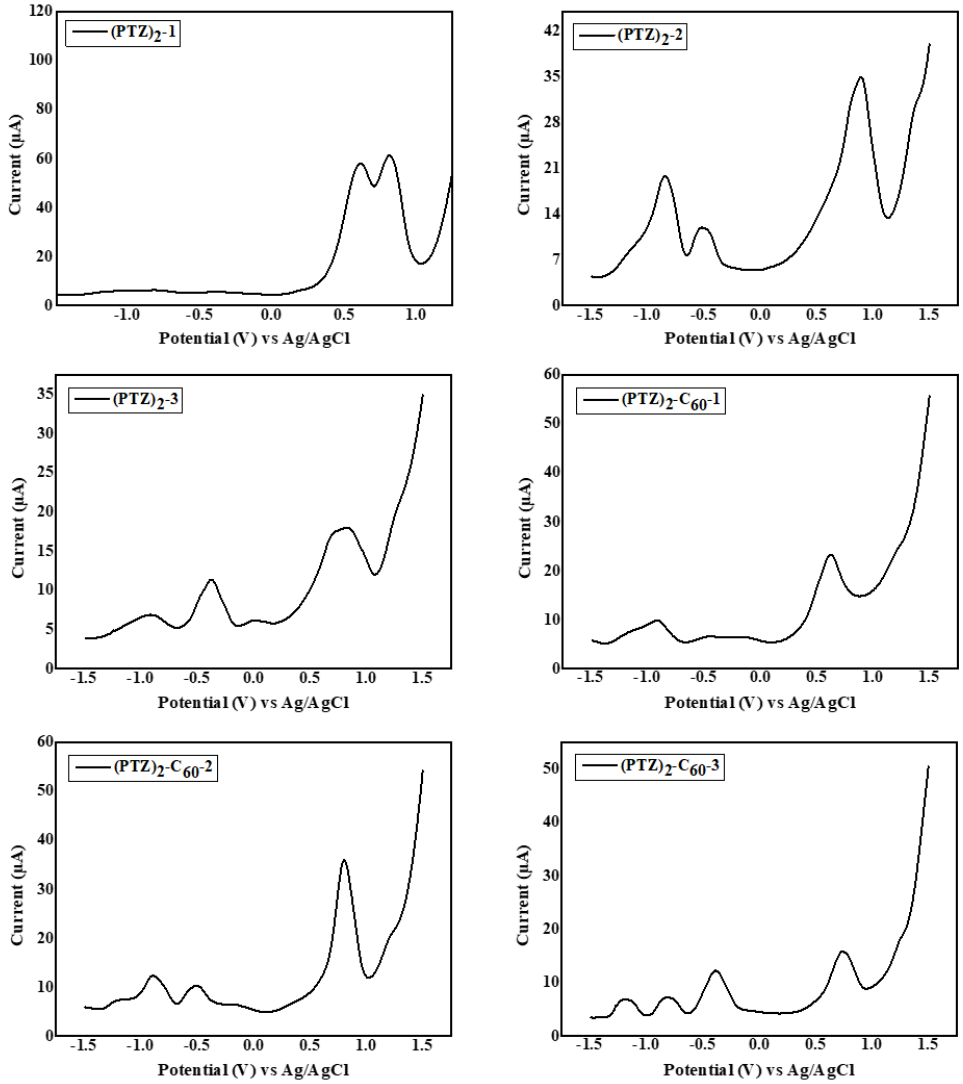

Figure 7.3. Differential pulse voltammograms of **(PTZ)$_2$ 1–3** and **(PTZ)$_2$-C$_{60}$ 1–3** in 0.1 M solutions of Bu_4NPF_6 in dichloromethane at 100 mV s^{-1} scan rate *versus* saturated Ag/AgCl electrode at 25 °C.

Table 7.2. Electrochemical Data of phenothiazine chromophores **(PTZ)$_2$ 1–3** and fulleropyrrolidine derivatives **(PTZ)$_2$-C$_{60}$ 1–3**.

Compounds	E_{red} **(V)**[a]	E_{ox} **(V)**[a]	E_{HOMO} **(eV)**[a]	E_{LUMO} **(eV)**[a]	E_g **(eV)**[a]
(PTZ)$_2$-1	–	0.77 0.99	–	–	–
(PTZ)$_2$-2	–0.46 –0.78	0.98 1.09	–5.38	–3.94	1.44
(PTZ)$_2$-3	–0.25 –0.36	0.90 1.09	–5.30	–4.15	1.15

$(PTZ)_2$-C_{60}-1	–0.77 –0.98	0.72 0.85	–5.12	–3.63	1.49
$(PTZ)_2$-C_{60}-2	–0.47 –0.75 –1.16	0.96 1.39	–5.36	–3.93	1.43
$(PTZ)_2$-C_{60}-3	–0.38 –0.74 –1.11	0.93 1.34	–5.33	–4.02	1.31

[a]Electrochemical analysis was estimated by differential pulse voltammetry, in 0.1 M solution of $TBAPF_6$ in DCM at 100 mV s^{-1} scan rate *versus* saturated Ag/AgCl electrode at 25 °C.

7.5. Computational Calculations

In order to understand the molecular conformations and ground-state geometries in the phenothiazine chromophores **$(PTZ)_2$ 1–3** and fulleropyrrolidine derivatives **$(PTZ)_2$-C_{60} 1–3**, the density functional theory calculation (DFT) was performed at the B3LYP/6-31G (d,p) basis set level for C, H, N, O, and S in the Gaussian 09W program.[50] Figure 7.4 illustrates the energy level diagram and the frontier molecular orbitals, including the Highest Occupied Molecular Orbital (HOMO) and Lowest Unoccupied Molecular Orbital (LUMO) for phenothiazine chromophores **$(PTZ)_2$ 1–3**, along with fulleropyrrolidine derivatives **$(PTZ)_2$-C_{60} 1–3**. The detailed corresponding data for these orbitals are presented in Table 7.1. The studied compounds possessed a nonplanar framework due to the presence of a central phenothiazine (PTZ) with a butterfly shape and substituted TCBD or DCNQ units.[51] The HOMO energy level of **$(PTZ)_2$-1** is mainly localized over the phenothiazine moiety with an extended towards contribution from the alkyne linkage phenothiazine unit, whereas the LUMO is mainly concentrated on the phenothiazine moiety which is bearing with a formyl group. In the case of **$(PTZ)_2$-2** and **$(PTZ)_2$-3** the electron density of HOMO energy levels are mostly delocalized over the phenothiazine unit whereas, the electron density in LUMO energy levels are concentrated over the acceptors TCBD and DCNQ moieties. In case of fulleropyrrolidine derivative

(PTZ)$_2$-C$_{60}$-1 the electron density of HOMO is mainly delocalized over the phenothiazine moiety with an extended towards contribution from the alkyne linkage phenothiazine unit, whereas the LUMO is mainly localized on the fullerene moiety. In case of TCBD and DCNQ functionalized fulleropyrrolidine derivatives **(PTZ)$_2$-C$_{60}$-2** and **(PTZ)$_2$-C$_{60}$-3** the electron density of the HOMO energy level are localized on the fullerene moiety, whereas the LUMOs are concentrated over the fullerene and DCNQ moiety, respectively.

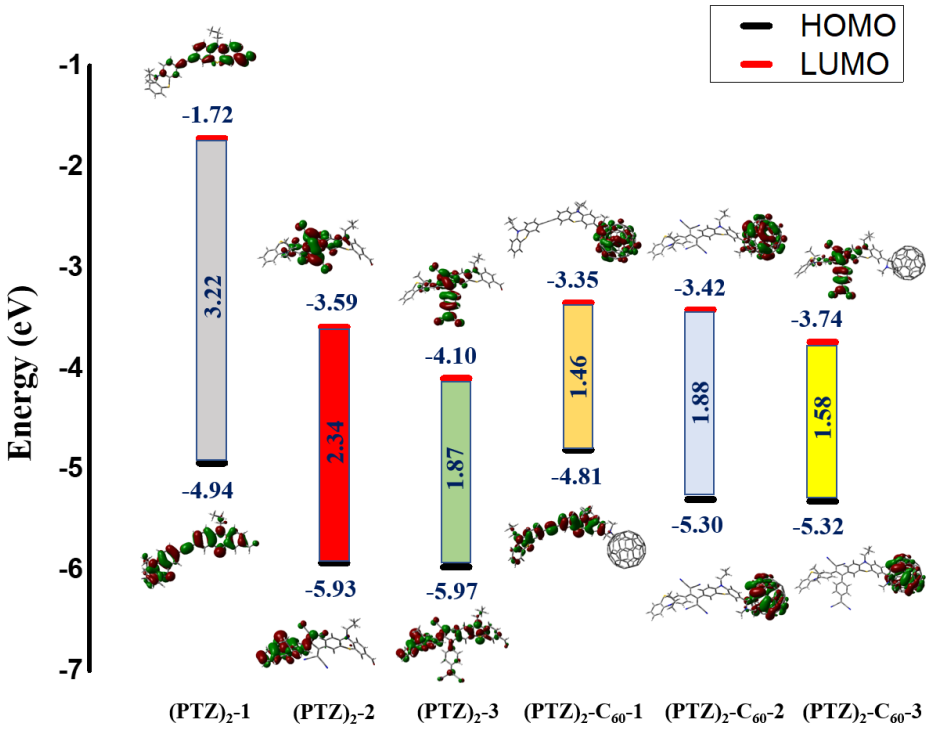

Figure 7.4. Energy level diagram of the HOMO–LUMO frontier orbitals of phenothiazine derivatives **(PTZ)$_2$ 1–3** and fulleropyrrolidine derivatives **(PTZ)$_2$-C$_{60}$ 1–3** calculated by DFT calculations at the B3LYP/6-31G (d,p) level.

The computationally calculated HOMO energy levels of the phenothiazine chromophores **(PTZ)$_2$ 1–3** and fulleropyrrolidine derivatives **(PTZ)$_2$-C$_{60}$ 1–3** are −4.94, −5.93, −5.97, −4.81, −5.30, and −5.32 eV, and the related LUMO energy levels are −1.72, −3.59, −4.10, −3.35, −3.42, and −3.74 eV, respectively. The theoretical HOMO–LUMO gap values for phenothiazine chromophores **(PTZ)$_2$ 1–3** and fulleropyrrolidine derivatives **(PTZ)2-C$_{60}$ 1–3** are 3.22, 2.34, 1.87, 1.46,

1.88 and 1.58 eV respectively, and follow the order **$(PTZ)_2$-1** > **$(PTZ)_2$-2** > **$(PTZ)_2$-C_{60}-2** > **$(PTZ)_2$-3** > **$(PTZ)_2$-C_{60}-3** > **$(PTZ)_2$-C_{60}-1**. From the DFT calculations, the HOMO–LUMO gap values were found to be in good agreement with the values of the optical energy gap (E_{gap}) calculated from the UV/Vis absorption spectrum (Table 7.1). This stabilization consequently induced a red shift in the ICT (Intramolecular Charge Transfer) band observed in the electronic absorption spectra.

The time-dependent density functional theory (TD-DFT) calculations were performed to study the nature of electronic transitions taking place in optimized phenothiazine chromophores **$(PTZ)_2$ 1–3** and fulleropyrrolidine derivatives **$(PTZ)_2$-C_{60} 1–3** using the basis set B3LYP/6-31G (d,p) basis set level in dichloromethane. The transitions with assignments, oscillatory strength, composition and molecular contribution are listed in Table 7.3. The solvent effect in TD-DFT calculation was analyzed using the polarized continuum model (PCM). The phenothiazine chromophores **$(PTZ)_2$-1** and **$(PTZ)_2$-2** exhibit simulated absorption maxima at 394 nm and 503 nm, respectively. These absorption bands in the visible region originate from HOMO–1→LUMO and HOMO→LUMO+1 respectively, which corresponds to π−π* transition for **$(PTZ)_2$-1** and intramolecular charge transfer (ICT) transition for **$(PTZ)_2$-2**. The simulated absorption spectra of phenothiazine chromophores **$(PTZ)_2$-3** and fulleropyrrolidine derivatives **$(PTZ)_2$ 1–3** exhibit absorption maxima at 555 nm, 422 nm, 673 nm, and 822 nm, respectively. These absorption bands in the visible region originate from HOMO–2→LUMO, HOMO→LUMO+5, HOMO–1→LUMO+1, and HOMO–2→LUMO respectively, which are attributed to intramolecular charge transfer (ICT) transition. The theoretical data shows that the fulleropyrrolidine derivatives **$(PTZ)_2$-C_{60}-2** and **$(PTZ)_2$-C_{60}-3** are red-shifted as compared to phenothiazine chromophores **$(PTZ)_2$-2** and **$(PTZ)_2$-3**, respectively. The electronic absorption wavelength values calculated theoretically were in good agreement with the experimental data. However, these values can be affected by various factors such as temperature, solvent, and dipole moment.

Table 7.3. Calculated electronic transitions for phenothiazine chromophores **$(PTZ)_2$ 1–3** and fulleropyrrolidine derivatives **$(PTZ)_2$-C_{60} 1–3** in dichloromethane.

Compounds	Wavelength (nm)	Composition and Molecular Contribution	f^a	Assignment
$(PTZ)_2$-1	394	HOMO-1→LUMO (0.65)	0.13	π–π*
$(PTZ)_2$-2	503	HOMO→LUMO+1 (0.68)	0.13	ICT
$(PTZ)_2$-3	555	HOMO-2→LUMO (0.62)	0.40	ICT
$(PTZ)_2$-C_{60}-1	422	HOMO→LUMO+5 (0.34)	0.18	ICT
$(PTZ)_2$-C_{60}-2	673	HOMO-1→LUMO+1 (0.54)	0.15	ICT
$(PTZ)_2$-C_{60}-3	822	HOMO-2→LUMO (0.62)	0.09	ICT

[a]Oscillator strength.

7.6. Experimental section

General methods

The chemicals were used as received unless otherwise indicated. All oxygen or moisture-sensitive reactions were performed under a nitrogen/argon atmosphere. ^{1}H NMR (400 and 500 MHz) and ^{13}C NMR (100 and 125 MHz) spectra were recorded on Bruker 400 and 500 MHz FT-NMR spectrometers at room temperature. ^{1}H NMR chemical shifts are reported in parts per million (ppm) relative to the solvent residual peak ($CDCl_3$, 7.26 ppm). Multiplicities are given as s (singlet), d (doublet), t (triplet) and m (multiplet) and the coupling constants, *J*, are given in hertz. ^{13}C NMR chemical shifts are reported relative to the solvent residual peak ($CDCl_3$, 77.0 ppm). UV-visible absorption spectra were recorded on a PerkinElmer Lambda 35 instrument. HRMS was recorded with an Agilent 6545A Q-TOF mass spectrometer and on a Bruker-Daltonics micrOTOF-Q II mass spectrometer and MALDI-TOF mass used to measure the mass of the compounds. The voltammograms were recorded on a PalmSens 4 electrochemical analyzer in

dichloromethane solvent and 0.1 M $TBAPF_6$ as the supporting electrolyte. The electrodes used were glassy carbon as a working electrode, Pt wire as a counter electrode and Ag/AgCl as a reference electrode, the scan rate was 100 mV s^{-1} for cyclic voltammetry.

Synthesis of $(PTZ)_2$-1

In a 100 mL round-bottomed flask, 3-ethynyl-10-propyl-10*H*-phenothiazine **PTZ** (550 mg, 2.072 mmol) and 7-bromo-10-propyl-10*H*-phenothiazine-3-carbaldehyde **Br-PTZ-CHO** (761 mg, 2.279 mmol) were purged under nitrogen and bis(triphenylphosphine)palladium(II)-dichloride (100 mg) and copper(I) iodide (4 - 5 mg) were added in anhydrous triethylamine (20 mL) and tetrahydrofuran (20 mL), the reaction mixture was stirred and refluxed for 12 h. Then the solvent was evaporated under a vacuum. The residue was dissolved in dichloromethane, and this solution was washed with water for several times, dried with anhydrous Na_2SO_4, and filtered it. The crude was purified by column chromatography using dichloromethane-hexane (1/2 v/v) as eluent to get the desired compound **$(PTZ)_2$-1** as a yellow color solid with 87 % yield. ^{1}H NMR (500 MHz, CHLOROFORM-d) δ = 9.80 (s, 1 H), 7.64 (dd, *J* = 1.8, 8.5 Hz, 1 H), 7.57 (d, *J* = 1.7 Hz, 1 H), 7.29 - 7.27 (m, 1 H), 7.26 - 7.21 (m, 3 H), 7.14 (s, 1 H), 7.11 (d, *J* = 7.5 Hz, 1 H), 6.94 - 6.91 (m, 1 H), 6.90 (d, *J* = 8.4 Hz, 1 H), 6.85 (d, *J* = 8.1 Hz, 1 H), 6.80 (d, *J* = 8.5 Hz, 1 H), 6.78 (d, *J* = 8.4 Hz, 1 H), 3.89 - 3.83 (m, 2 H), 3.83 - 3.79 (m, 2 H), 1.86 (d, *J* = 7.5 Hz, 2 H), 1.84 - 1.80 (m, 2 H), 1.06 - 1.02 (m, 3 H), 1.02 - 0.99 (m, 3 H); ^{13}C NMR (125 MHz, CHLOROFORM-d) δ = 190.0, 150.1, 145.3, 144.6, 143.1, 131.3, 130.8, 130.6, 130.1, 130.0, 128.5, 127.5, 127.3, 124.8, 124.5, 124.2, 123.8, 122.7, 118.7, 116.9, 115.6, 115.5, 115.1, 115.0, 89.4, 88.1, 49.8, 49.3, 20.1, 20.0, 11.3, 11.2, 11.1; HRMS (ESI-TOF) m/z calculated for $C_{33}H_{28}N_2OS_2$ 532.1638 $[M]^+$, measured 532.1274 $[M]^+$.

Synthesis of $(PTZ)_2$-2

In a 100 mL round-bottomed flask, TCNE (40 mg, 0.3097 mmol) was added to a solution of **$(PTZ)_2$-1** (150 mg, 0.2815 mmol) in

dichloromethane (20 mL) under an argon atmosphere. The reaction mixture was stirred at RT for 24 h. The solvent was evaporated under vacuum, and the product was purified by column chromatography with DCM/hexane (2:1, v/v) as the eluent to get the desired compound **$(PTZ)_2$-2** as a dark color solid with 80 % yield. ^{1}H NMR (500MHz, CHLOROFORM-d) δ = 9.83 (s, 1 H), 7.71 - 7.68 (m, 2 H), 7.68 - 7.65 (m, 1 H), 7.55 (d, *J* = 1.5 Hz, 1 H), 7.34 (d, *J* = 2.4 Hz, 1 H), 7.32 (d, *J* = 2.3 Hz, 1 H), 7.18 (s, 1 H), 7.08 - 7.05 (m, 1 H), 7.01 (d, *J* = 7.3 Hz, 1 H), 6.96 (d, *J* = 8.5 Hz, 1 H), 6.93 (d, *J* = 9.0 Hz, 1 H), 6.88 (t, *J* = 8.7 Hz, 2 H), 3.90 (d, *J* = 7.3 Hz, 2 H), 3.88 - 3.84 (m, 2 H), 1.89 (d, *J* = 7.3 Hz, 2 H), 1.87 - 1.82 (m, 2 H), 1.07 (d, *J* = 7.3 Hz, 3 H), 1.04 (d, *J* = 7.5 Hz, 3 H); ^{13}C NMR (100 MHz, CHLOROFORM-d) δ = 189.7, 164.4, 163.6, 151.3, 149.5, 147.6, 141.9, 132.6, 130.5, 130.4, 130.3, 128.5, 128.0, 127.8, 127.7, 127.6, 125.9, 125.6, 125.3, 124.6, 124.4, 123.6, 122.6, 116.3, 115.9, 115.1, 112.9, 112.6, 112.2, 111.8, 82.7, 80.6, 53.4, 50.4, 50.0, 34.7, 31.6, 25.3, 22.7, 20.1, 20.0, 14.1, 11.1, 11.0; HRMS (ESI-TOF) m/z calculated for $C_{39}H_{28}N_6OS_2$ + Na 683.1658 $[M+Na]^+$, measured 683.4354 $[M+Na]^+$.

Synthesis of $(PTZ)_2$-3

In a 100 mL round-bottomed flask, TCNQ (43 mg, 0.2065 mmol) was added to a solution of **$(PTZ)_2$-1** (100 mg, 0.1877 mmol) in dichloroethane (20 mL) under an argon atmosphere. The reaction mixture was stirred at 60 °C for 36 hours. The solvent was evaporated under vacuum, and the product was purified by column chromatography with DCM/hexane (3:1, v/v) as the eluent to get the desired compound **$(PTZ)_2$-3** as a dark color solid with 60 % yield. ^{1}H NMR (500 MHz, CHLOROFORM-d) δ = 9.80 (s, 1 H), 7.64 (d, *J* = 8.1 Hz, 1 H), 7.57 (d, *J* = 8.7 Hz, 1 H), 7.52 (s, 1 H), 7.47 (d, *J* = 9.6 Hz, 1 H), 7.32 - 7.28 (m, 2 H), 7.22 (d, *J* = 9.5 Hz, 1 H), 7.17 - 7.11 (m, 2 H), 7.08 (d, *J* = 7.5 Hz, 1 H), 6.99 - 6.96 (m, 2 H), 6.95 - 6.90 (m, 2 H), 6.88 - 6.83 (m, 3 H), 3.89 - 3.80 (m, 4 H), 1.84 (dd, *J* = 7.2, 14.4 Hz, 4 H), 1.06 - 1.01 (m, 6 H); ^{13}C NMR (100 MHz, CHLOROFORM-d) δ = 189.6, 168.3, 153.9, 148.9, 148.8, 148.7, 147.8, 142.8, 134.7, 133.9, 133.5, 132.4, 131.8,

130.3, 129.2, 128.9, 128.4, 128.2, 127.8, 127.6, 126.4, 126.2, 125.7, 125.1, 123.9, 123.7, 123.0, 116.0, 115.8, 115.8, 115.4, 113.7, 113.2, 112.7, 83.6, 76.1, 50.3, 49.8, 29.7, 26.9, 20.1, 20.0, 14.1, 11.2, 11.1; HRMS (ESI-TOF) m/z calculated for $C_{45}H_{32}N_6OS_2$ + Na 759.1971 $[M+Na]^+$, measured 759.2002 $[M+Na]^+$.

Synthesis of $(PTZ)_2$-C_{60}-1

In a 100 mL round-bottomed flask, compound **$(PTZ)_2$-1** (90 mg, 0.1689 mmol), C_{60}-fullerene (243 mg, 0.3378 mmol) and *N*-methylglycine (120 mg, 1.352 mmol) were dissolved in toluene (20 mL) and refluxed for 36 h. After that, the reaction mixture was extracted with DCM, washed with brine solution and dried over anhydrous sodium sulfate. The solvent was evaporated under vacuum, and the product was purified by column chromatography with DCM/hexane (1:1, v/v) as the eluent to get the desired compound **$(PTZ)_2$-C_{60}-1** as a dark color solid with 40 % yield. ^{1}H NMR (500 MHz, CHLOROFORM-d) δ = 7.26 - 7.20 (m, 6 H), 7.16 - 7.13 (m, 1 H), 7.13 - 7.09 (m, 1 H), 6.91 (t, *J* = 7.6 Hz, 1 H), 6.84 (d, *J* = 8.1 Hz, 2 H), 6.78 – 6.73 (m, 2 H), 4.96 (d, *J* = 9.5 Hz, 1 H), 4.80 (s, 1 H), 4.22 (d, *J* = 9.5 Hz, 1 H), 3.83 - 3.75 (m, 4 H), 2.76 (s, 3 H), 1.85 - 1.78 (m, 4 H), 1.00 (t, *J* = 7.3 Hz, 6 H); ^{13}C NMR (100 MHz, CHLOROFORM-d) δ = 156.3, 154.0, 153.5, 147.3, 146.3, 145.9, 145.5, 145.3, 144.8, 144.4, 144.3, 143.1, 142.6, 142.3, 142.1, 142.1, 141.7, 140.9, 140.1, 140.1, 136.6, 135.8, 134.7, 131.3, 130.5, 130.1, 129.1, 126.1, 124.2, 123.9, 122.8, 122.5, 120.5, 119.3, 117.9, 115.1, 108.9, 108.8, 82.9, 70.0, 69.0, 49.5, 44.8, 40.1, 34.7, 31.6, 25.3, 22.7, 22.3, 20.1, 14.1, 11.8, 11.3; HRMS (ESI-TOF) m/z calculated for $C_{95}H_{33}N_3S_2$ + H 1280.2189 $[M+H]^+$, measured 1280.1149 $[M+H]^+$.

Synthesis of $(PTZ)_2$-C_{60}-2

In a 100 mL round-bottomed flask, compound **$(PTZ)_2$-2** (110 mg, 0.1665 mmol), C_{60}-fullerene (239 mg, 0.3329 mmol) and *N*-methylglycine (118 mg, 1.332 mmol) were dissolved in toluene (20 mL) and refluxed for 48 h. After that, the reaction mixture was extracted with DCM, washed with brine solution and dried over anhydrous sodium sulfate. The solvent was evaporated under vacuum, and the product was

purified by column chromatography with DCM/hexane (1:1, v/v) as the eluent to get the desired compound **(PTZ)$_2$-C$_{60}$-2** as a dark color solid with 30 % yield. ^{1}H NMR (500 MHz, CHLOROFORM-d) δ = 7.61 (dd, *J* = 2.4, 8.8 Hz, 1 H), 7.55 (d, *J* = 6.6 Hz, 1 H), 7.32 - 7.19 (m, 4 H), 7.09 (t, *J* = 7.7 Hz, 1 H), 6.97 (d, *J* = 7.6 Hz, 1 H), 6.91 (t, *J* = 7.2 Hz, 1 H), 6.80 (s, 1 H), 6.78 (d, *J* = 4.0 Hz, 1 H), 6.77 - 6.70 (m, 2 H), 4.89 (d, *J* = 9.5 Hz, 1 H), 4.73 (s, 1 H), 4.15 (d, *J* = 9.5 Hz, 1 H), 3.75 (td, *J* = 7.5, 15.3 Hz, 4 H), 2.69 (s, 3 H), 1.81 - 1.74 (m, 4 H), 0.96 (t, *J* = 7.3 Hz, 6 H); ^{13}C NMR (100 MHz, CHLOROFORM-d) δ = 165.9, 164.0, 155.1, 152.9, 151.9, 149.4, 146.3, 145.5, 145.3, 145.2, 145.1, 145.0, 144.7, 144.5, 144.3, 144.3, 143.7, 143.5, 143.4, 143.3, 143.0, 142.1, 142.0, 141.7, 141.6, 141.2, 141.1, 141.0, 141.0, 140.8, 140.7, 140.6, 140.4, 139.2, 139.0, 138.6, 136.0, 135.4, 134.9, 134.6, 132.5, 129.8, 126.7, 126.6, 126.5, 124.2, 123.8, 123.2, 122.3, 121.5, 120.9, 120.3, 120.2, 114.8, 113.8, 112.6, 112.1, 111.5, 111.2, 109.2, 108.9, 81.5, 80.0, 79.5, 68.9, 68.0, 49.2, 44.2, 39.0, 28.7, 21.3, 18.9, 13.1, 10.8, 10.1; MALDI calculated for $C_{101}H_{33}N_7S_2$ 1407.2239 $[M]^+$; measured 1407.043.

Synthesis of (PTZ)$_2$-C$_{60}$-3

In a 100 mL round-bottomed flask, compound **(PTZ)$_2$-3** (80 mg, 0.1085 mmol), C_{60}-fullerene (156 mg, 0.2171 mmol) and N-methylglycine (77 mg, 0.8684 mmol) were dissolved in toluene (20 mL) and refluxed for 60 h. After that, the reaction mixture was extracted with DCM, washed with brine solution and dried over anhydrous sodium sulfate. The solvent was evaporated under vacuum, and the product was purified by column chromatography with DCM/hexane (1:1, v/v) as the eluent to get the desired compound **(PTZ)$_2$-C$_{60}$-3** as a dark color solid with 35 % yield. ^{1}H NMR (500 MHz, CHLOROFORM-d) δ = 7.53 (d, *J* = 8.5 Hz, 1 H), 7.48 - 7.44 (m, 1 H), 7.35 (d, *J* = 2.4 Hz, 2 H), 7.31 (br. s., 1 H), 7.28 (d, *J* = 2.0 Hz, 1 H), 7.21 - 7.16 (m, 1 H), 7.16 - 7.11 (m, 2 H), 7.10 - 7.05 (m, 2 H), 6.98 - 6.92 (m, 3 H), 6.86 – 6.80 (m, 2 H), 6.74 (d, *J* = 9.0 Hz, 1 H), 4.95 (d, *J* = 9.5 Hz, 1 H), 4.79 (s, 1 H), 4.21 (d, *J* = 9.5 Hz, 1 H), 3.83 - 3.74 (m, 4 H), 2.77 - 2.73 (m, 3 H), 1.87 - 1.78 (m, 4 H), 1.03 - 0.99 (m, 6 H); ^{13}C NMR (100 MHz, CHLOROFORM-d) δ =

167.9, 156.1, 154.1, 153.9, 153.2, 149.5, 149.2, 149.2, 148.7, 147.4, 147.3, 147.1, 146.5, 146.4, 146.3, 146.2, 146.1, 146.0, 145.7, 145.5, 145.5, 145.4, 145.3, 145.3, 145.2, 144.8, 144.5, 144.4, 144.3, 143.2, 143.0, 142.8, 142.7, 142.6, 142.2, 142.2, 142.2, 142.1, 142.0, 141.7, 141.6, 140.2, 140.0, 139.6, 139.0, 137.0, 135.9, 135.7, 134.7, 134.1, 133.2, 133.2, 131.9, 130.7, 129.2, 129.0, 127.9, 127.8, 127.6, 127.0, 126.2, 126.1, 125.6, 124.6, 124.5, 124.4, 124.0, 123.9, 123.5, 122.9, 119.0, 118.9, 116.0, 115.3, 114.8, 113.8, 113.6, 113.1, 82.5, 81.7, 75.7, 69.9, 69.0, 50.2, 49.8, 40.0, 35.0, 34.9, 34.5, 34.4, 33.5, 31.9, 31.5, 31.5, 30.2, 30.2, 29.7, 29.6, 29.5, 29.4, 29.3, 29.1, 29.1, 24.8, 22.7, 20.1, 19.9, 14.1, 11.3, 11.1; MALDI calculated for $C_{107}H_{37}N_7S_2$ 1483.2552 $[M]^+$; measured 1483.123.

7.7. Conclusion

In summary, a series of donor-acceptor-based phenothiazine chromophores **(PTZ)$_2$ 1–3** were synthesized by Pd-catalyzed Sonogashira cross-coupling and [2 + 2] cycloaddition–electrocyclic ring-opening reaction, and fulleropyrrolidine derivatives **(PTZ)$_2$ 1–3** by 1,3-dipolar cycloaddition reaction (Prato reaction) in good yields. The photophysical properties suggest that the donor–acceptor chromophores **(PTZ)$_2$-2**, **(PTZ)$_2$-3**, **(PTZ)$_2$-C$_{60}$-2**, and **(PTZ)$_2$-C$_{60}$-3** exhibit a strong intramolecular charge transfer (ICT) band at a longer wavelength region due to the strong donor–acceptor (D–A) interactions. The electrochemical properties of phenothiazine and fulleropyrrolidine chromophores display multiple reduction potentials corresponding to the presence of numerous redox-active entities. The electrochemical data shows that incorporating cyano-based electron acceptor groups can change the redox properties of phenothiazine and fulleropyrrolidine chromophores. Furthermore, the dicyanoquinodimethane (DCNQ) unit better stabilizes the LUMO energy level compared to the tetracyanoethylene (TCBD) unit. The theoretical studies show that the LUMO energy level was stabilized by the incorporation of TCBD and DCNQ units. This stabilization resulted in a red shift in the ICT (intramolecular charge transfer) band observed in electronic absorption

spectra. The reported phenothiazine chromophores **(PTZ)$_2$ 1–3** and fulleropyrrolidine derivatives **(PTZ)$_2$-C$_{60}$ 1–3** provide a new opportunities for the development of donor–acceptor systems, which are useful in various optoelectronic applications.

7.8. References

[1] Guo, X., Baumgarten, M., & Müllen, K. (2013). Designing π-conjugated polymers for organic electronics. *Progress in Polymer Science*, *38*(12), 1832–1908. (DOI: 10.1016/J.PROGPOLYMSCI.2013.09.005).

[2] Mateo-Alonso, A. (2023). π-Conjugated Materials: Here, There, and Everywhere. *Chemistry of Materials*, *35*(4), 1467–1469. (DOI: 10.1021/ACS.CHEMMATER.2C03567).

[3] Tuncel, D. (2019). π-Conjugated nanostructured materials: preparation, properties and photonic applications. *Nanoscale Advances*, *1*(1), 19–33. (DOI: 10.1039/C8NA00108A).

[4] Raftani, M., Abram, T., Loued, W., Kacimi, R., Azaid, A., Alimi, K., … Bouachrine, M. (2021). The optoelectronic properties of π-conjugated organic molecules based on terphenyl and pyrrole for BHJ solar cells: DFT / TD-DFT theoretical study. *Current Chemistry Letters*, *10*, 489–502. (DOI: 10.5267/j.ccl.2021.4.002).

[5] Facchetti, A. (2011). π-Conjugated polymers for organic electronics and photovoltaic cell applications. *Chemistry of Materials*, *23*(3), 733–758. (DOI: 10.1021/CM102419Z).

[6] Gangadhar, P. S., Reddy, G., Prasanthkumar, S., & Giribabu, L. (2021). Phenothiazine functional materials for organic optoelectronic applications. *Physical Chemistry Chemical Physics*, *23*(28), 14969–14996. (DOI: 10.1039/D1CP01185E).

[7] Dou, L., Liu, Y., Hong, Z., Li, G., & Yang, Y. (2015). Low-Bandgap Near-IR Conjugated Polymers/Molecules for Organic Electronics. *Chemical Reviews*, *115*(23), 12633–12665. (DOI: 10.1021/ACS.CHEMREV.5B00165).

[8] Zhou, H., Yang, L., & You, W. (2012). Rational design of high performance conjugated polymers for organic solar cells. *Macromolecules*, *45*(2), 607–632. (DOI: 10.1021/MA201648T).

[9] Mahadik, S. S., Garud, D. R., Ware, A. P., Pingale, S. S., & Kamble, R. M. (2021). Design, Synthesis and Opto-electrochemical Properties of Novel Donor–Acceptor Based 2,3-di(hetero-2-yl)pyrido[2,3-b]pyrazine amine derivatives as Blue-Orange Fluorescent Materials. *Dyes and Pigments*, *184*, 108742. (DOI: 10.1016/J.DYEPIG.2020.108742).

[10] Günes, S., Neugebauer, H., & Sariciftci, N. S. (2007). Conjugated polymer-based organic solar cells. *Chemical Reviews*, *107*(4), 1324–1338. (DOI: 10.1021/CR050149Z).

[11] Pathak, A., Justin Thomas, K. R., Singh, M., & Jou, J. H. (2017). Fine-Tuning of Photophysical and Electroluminescence Properties of Benzothiadiazole-Based Emitters by Methyl Substitution. *Journal of Organic Chemistry*, *82*(21), 11512–11523. (DOI: 10.1021/ACS.JOC.7B02127).

[12] Poddar, M., Jang, Y., Misra, R., & D'Souza, F. (2020). Excited-State Electron Transfer in 1,1,4,4-Tetracyanobuta-1,3-diene (TCBD)- and Cyclohexa-2,5-diene-1,4-diylidene-Expanded TCBD-Substituted BODIPY-Phenothiazine Donor–Acceptor Conjugates. *Chemistry – A European Journal*, *26*(30), 6869–6878. (DOI: 10.1002/CHEM.202000346).

[13] Kandpal, S., Gupta, P. K., Kumar, R., & Misra, R. (2024). Ferrocene-Functionalized Fulleropyrrolidine Derivative: A Performance Enhancer for Solid-State Electrochromic Devices. *ACS Applied Optical Materials*, *2*(1), 158–165. (DOI: 10.1021/ACSAOM.3C00384).

[14] Root, S. E., Savagatrup, S., Printz, A. D., Rodriquez, D., & Lipomi, D. J. (2017). Mechanical Properties of Organic Semiconductors for Stretchable, Highly Flexible, and Mechanically Robust Electronics. *Chemical Reviews*, *117*(9), 6467–6499. (DOI: 10.1021/ACS.CHEMREV.7B00003).

[15] Ibanez, J. G., Rincón, M. E., Gutierrez-Granados, S., Chahma, M., Jaramillo-Quintero, O. A., & Frontana-Uribe, B. A. (2018). Conducting Polymers in the Fields of Energy, Environmental Remediation, and Chemical-Chiral Sensors. *Chemical Reviews*, *118*(9), 4731–4816. (DOI: 10.1021/ACS.CHEMREV.7B00482).

[16] Wang, C., Dong, H., Hu, W., Liu, Y., & Zhu, D. (2012). Semiconducting π-conjugated systems in field-effect transistors: A material odyssey of organic electronics. *Chemical Reviews*, *112*(4), 2208–2267. (DOI: 10.1021/CR100380Z).

[17] Han, L., Chen, Y., Zhao, ge, Cui, Y., & Jiang, S. (2020). Phenothiazine dyes containing a 4-phenyl-2-(thiophen-2-yl) thiazole bridge for dye-sensitized solar cells. *Tetrahedron*, *76*, 131102. (DOI: 10.1016/j.tet.2020.131102).

[18] Seintis, K., Şahin, Ç., Sigmundová, I., Stathatos, E., Hrobárik, P., & Fakis, M. (2018). Solvent-Acidity-Driven Change in Photophysics and Significant Efficiency Improvement in Dye-Sensitized Solar Cells of a Benzothiazole-Derived Organic Sensitizer. *Journal of Physical Chemistry C*, *122*(35), 20122–20134. (DOI: 10.1021/ACS.JPCC.8B05686).

[19] Poddar, M., Sivakumar, G., & Misra, R. (2019). Donor–acceptor substituted 1,8-naphthalimides: design, synthesis, and structure–property relationship. *Journal of Materials Chemistry C*, *7*(47), 14798–14815. (DOI: 10.1039/C9TC02634G).

[20] Misra, R., Gautam, P., Jadhav, T., & Mobin, S. M. (2013). Donor-acceptor ferrocenyl-substituted benzothiadiazoles: Synthesis, structure, and properties. *Journal of Organic Chemistry*, *78*(10), 4940–4948. (DOI: 10.1021/JO4005734).

[21] Dhokale, B., Jadhav, T., Mobin, S. M., & Misra, R. (2015). Meso Alkynylated Tetraphenylethylene (TPE) and 2,3,3-Triphenylacrylonitrile (TPAN) Substituted BODIPYs. *Journal of Organic Chemistry*, *80*(16), 8018–8025. (DOI: 10.1021/ACS.JOC.5B01117).

[22] Gautam, P., Misra, R., Siddiqui, S. A., & Sharma, G. D. (2015). Unsymmetrical donor-acceptor-acceptor-π-donor type benzothiadiazole-based small molecule for a solution processed bulk heterojunction organic solar cell. *ACS Applied Materials and Interfaces*, *7*(19), 10283–10292. (DOI: 10.1021/ACSAMI.5B02250).

[23] Misra, R., Gautam, P., & Mobin, S. M. (2013). Aryl-substituted unsymmetrical benzothiadiazoles: Synthesis, structure, and properties. *Journal of Organic Chemistry*, *78*(24), 12440–12452. (DOI: 10.1021/JO402111Q).

[24] Khan, F., & Misra, R. (2023). Recent advances in the development of phenothiazine and its fluorescent derivatives for optoelectronic applications. *Journal of Materials Chemistry C*, *11*(8), 2786–2825. (DOI: 10.1039/D2TC04326B).

[25] Khan, F., Mahmoudi, M., Gupta, P. K., Volyniuk, D., Grazulevicius, J. V., & Misra, R. (2023). Mechanochromic Materials Based on Tetraphenylethylene-Substituted Phenothiazines: Substituent-Dependent Hypsochromic and Bathochromic Switching of Emission. *Journal of Physical Chemistry C*, *127*(3), 1643–1654. (DOI: 10.1021/ACS.JPCC.2C07010).

[26] Hart, A. S., Chandra Bikram, K. C., Subbaiyan, N. K., Karr, P. A., & D'Souza, F. (2012). Phenothiazine-sensitized organic solar cells: effect of dye anchor group positioning on the cell performance. *ACS applied materials & interfaces*, *4*(11), 5813–5820. (DOI: 10.1021/AM3014407).

[27] Gupta, P. K., Khan, F., & Misra, R. (2023). NIR-Absorbing 1,1,4,4-Tetracyanobuta-1,3-diene- and Dicyanoquinodimethane-Functionalized Donor-Acceptor Phenothiazine Derivatives: Synthesis and Characterization. *Journal of Organic Chemistry*, *88*(20), 14308–14322. (DOI: 10.1021/ACS.JOC.3C01029).

[28] Malik, N., Arfin, T., & Khan, A. U. (2019). Graphene nanomaterials: chemistry and pharmaceutical perspectives.

Nanomaterials for Drug Delivery and Therapy, 373–402. (DOI: 10.1016/B978-0-12-816505-8.00002-3).

[29] Matsumoto, F., Iwai, T., Moriwaki, K., Takao, Y., Ito, T., Mizuno, T., & Ohno, T. (2016). Controlling the Polarity of Fullerene Derivatives to Optimize Nanomorphology in Blend Films. *ACS Applied Materials and Interfaces*, *8*(7), 4803–4810. (DOI: 10.1021/ACSAMI.5B11180).

[30] Nagarjuna, P., Bagui, A., Garg, A., Gupta, V., & Singh, S. P. (2017). One-Step Synthesis of New Electron Acceptor for High Efficiency Solution Processable Organic Solar Cells. *Journal of Physical Chemistry C*, *121*(48), 26615–26621. (DOI: 10.1021/ACS.JPCC.7B08167).

[31] Mi, D., Kim, J. H., Kim, H. U., Xu, F., & Hwang, D. H. (2014). Fullerene derivatives as electron acceptors for organic photovoltaic cells. *Journal of Nanoscience and Nanotechnology*, *14*(2), 1064–1084. (DOI: 10.1166/JNN.2014.9007).

[32] Sánchez, L., Martín, N., & Guldi, D. M. (2005). Hydrogen-Bonding Motifs in Fullerene Chemistry. *Angewandte Chemie International Edition*, *44*(34), 5374–5382. (DOI: 10.1002/ANIE.200500321).

[33] Fukuzumi, S., Ohkubo, K., D'souza, F., & Sessler, J. L. (2012). Supramolecular electron transfer by anion binding. *Chemical Communications*, *48*(79), 9801–9815. (DOI: 10.1039/C2CC32848H).

[34] D'souza, F., & Ito, O. (2011). Photosensitized electron transfer processes of nanocarbons applicable to solar cells. *Chemical Society Reviews*, *41*(1), 86–96. (DOI: 10.1039/C1CS15201G).

[35] Maggini, M., Scorrano, G., & Prato, M. (1993). Addition of azomethine ylides to C[sub 60]. Synthesis, characterization, and functionalization of fullerene pyrrolidines. *Journal of the American Chemical Society*, *115:21*(21), 9798–9799. (DOI: 10.1021/JA00074A056).

[36] Blanco, G. D., Hiltunen, A. J., Lim, G. N., KC, C. B., Kaunisto, K. M., Vuorinen, T. K., … D'Souza, F. (2016). Syntheses,

Charge Separation, and Inverted Bulk Heterojunction Solar Cell Application of Phenothiazine-Fullerene Dyads. *ACS Applied Materials and Interfaces*, *8*(13), 8481–8490. (DOI: 10.1021/ACSAMI.6B00561).

[37] Qi, S., Iida, H., Liu, L., Irle, S., Hu, W., & Yashima, E. (2013). Electrical Switching Behavior of a [60]Fullerene-Based Molecular Wire Encapsulated in a Syndiotactic Poly(methyl methacrylate) Helical Cavity. *Angewandte Chemie International Edition*, *52*(3), 1049–1053. (DOI: 10.1002/ANIE.201208481).

[38] Liu, Z. B., Xu, Y. F., Zhang, X. Y., Zhang, X. L., Chen, Y. S., & Tian, J. G. (2009). Porphyrin and fullerene covalently functionalized graphene hybrid materials with large nonlinear optical properties. *Journal of Physical Chemistry B*, *113*(29), 9681–9686. (DOI: 10.1021/JP9004357).

[39] Huang, T., Zhao, J., Feng, M., Popov, A. A., Yang, S., Dunsch, L., & Petek, H. (2011). A molecular switch based on current-driven rotation of an encapsulated cluster within a fullerene cage. *Nano Letters*, *11*(12), 5327–5332. (DOI: 10.1021/NL2028409).

[40] Wang, W., Sun, R., Guo, J., Guo, J., & Min, J. (2019). An Oligothiophene–Fullerene Molecule with a Balanced Donor–Acceptor Backbone for High-Performance Single-Component Organic Solar Cells. *Angewandte Chemie International Edition*, *58*(41), 14556–14561. (DOI: 10.1002/ANIE.201908232).

[41] Luo, H., Fujitsuka, M., Araki, Y., Ito, O., Padmawar, P., & Chiang, L. Y. (2003). Inter- and intramolecular photoinduced electron-transfer processes between C60 and diphenylaminofluorene in solutions. *Journal of Physical Chemistry B*, *107*(35), 9312–9318. (DOI: 10.1021/JP034689G).

[42] Yamanaka, K. ichi, Fujitsuka, M., Araki, Y., Ito, O., Aoshima, T., Fukushima, T., & Miyashi, T. (2004). Intramolecular Photoinduced Electron-Transfer Processes in Tetrathienylethylene-Quaterthiophene-[60]Fullerene Triad in Solutions. *Journal of Physical Chemistry A*, *108*(2), 250–256. (DOI: 10.1021/JP036932H).

[43] Breiten, B., Jordan, M., Taura, D., Zalibera, M., Griesser, M., Confortin, D., … Diederich, F. (2013). Donor-substituted octacyano[4]dendralenes: Investigation of π-electron delocalization in their radical ions. *Journal of Organic Chemistry*, *78*(5), 1760–1767. (DOI: 10.1021/JO301194Y).

[44] Michinobu, T., Boudon, C., Gisselbrecht, J. P., Seiler, P., Frank, B., Moonen, N. N. P., … Diederich, F. (2006). Donor-substituted 1,1,4,4-tetracyanobutadienes (TCBDs): New chromophores with efficient intramolecular charge-transfer interactions by atom-economic synthesis. *Chemistry - A European Journal*, *12*(7), 1889–1905. (DOI: 10.1002/CHEM.200501113).

[45] Sekita, M., Ballesteros, B., Diederich, F., Guldi, D. M., Bottari, G., & Torres, T. (2016). Intense Ground-State Charge-Transfer Interactions in Low-Bandgap, Panchromatic Phthalocyanine–Tetracyanobuta-1,3-diene Conjugates. *Angewandte Chemie*, *128*(18), 5650–5654. (DOI: 10.1002/ange.201601258).

[46] Zhang, H., Wan, X., Xue, X., Li, Y., Yu, A., & Chen, Y. (2010). Selective tuning of the HOMO-LUMO gap of carbazole-based donor-acceptor-donor compounds toward different emission colors. *European Journal of Organic Chemistry*, (9), 1681–1687. (DOI: 10.1002/EJOC.200901167).

[47] Misra, R., & Gautam, P. (2014). Tuning of the HOMO-LUMO gap of donor-substituted symmetrical and unsymmetrical benzothiadiazoles. *Organic & Biomolecular Chemistry*, *12*, 5448. (DOI: 10.1039/c4ob00629a).

[48] Yamada, M., Schweizer, W. B., Schoenebeck, F., & Diederich, F. F. (2010). Unprecedented thermal rearrangement of push-pull-chromophore-[60]fullerene conjugates: formation of chiral 1,2,9,12-tetrakis-adductsw *Chemical. Communication*, *46*, 5334–5336. (DOI: 10.1039/c0cc00881h).

[49] Wang, C., Wu, B., Li, Y., Dong, T., Chai, Y., Zhang, Y., & Wang, C. (2023). Regioisomeric Benzidine-Fullerenes: Tuning of the Diverse Hole-Distribution to Influence Charge Separation

Patterns. *Angewandte Chemie International Edition*, *62*(15). (DOI: 10.1002/anie.202300377).

[50] Frisch, M. J., Trucks, G. W., Schlegel, G. W., Scuseria, G. E., Robb, M. A., Cheeseman, J. R., Scalmani, G., Barone, V., Petersson, G. A., Li, Nakatsuji, X., Caricato, M., Marenich, A., Bloino, J., Janesko, B. G., Gomperts, R., Mennucci, B., Hratchian, H. P., Ortiz, J. V., Izmaylov, A. F., Sonnenberg, J. L., Williams-Young, D., Ding, F., Lipparini, F., Egidi, F., Goings, J., Peng, B., Petrone, A., Henderson, T., Ranasinghe, D., Zakrzewski, V. G., Gao, J., Rega, N., Zheng, G., Liang, W., Hada, M., Ehara, M., Toyota, K., Fukuda, R., Hasegawa, J., Ishida, M., Nakajima, T., Honda, Y., Kitao, O., Nakai, H., Vreven, T., Throssell, K., Montgomery, J. A., Peralta, Jr., J. E., Ogliaro, F., Bearpark, M., Heyd, J. J., Brothers, E., Kudin, K. N., Staroverov, V. N., Keith, T., Kobayashi, R., Normand, J., Raghavachari, K., Rendell, A., Burant, J. C., Iyengar, S. S., Tomasi, J., Cossi, M., Millam, J. M., Klene, M., Adamo, C., Cammi, R., Ochterski, J. W., Martin, R. L., Morokuma, K., Farkas, O., Foresman, J. B. and Fox, D. J. (2016). Gaussian 09, revision A.02; Gaussian, Inc.: Wallingford, CT.

[51] Gupta, P. K., Das, S., Misra, R., & D'Souza, F. (2024). Near-IR Capturing N-Methylbenzene Sulfonamide-Phenothiazine Incorporating Strong Electron Acceptor Push-Pull Systems: Photochemical Ultrafast Carrier Dynamics. *Chemistry – A European Journal*, *30*(25). (DOI: 10.1002/chem.202304313).

Chapter 8

Conclusions and Future Scope

8.1. Conclusions

The 1,1,2,2-tetracyano ethylene (TCNE) and 7,7,8,8-tetracyanoquinodimethane (TCNQ) are strong electron acceptors because they contain four cyano groups, and are highly reactive towards electron-rich alkynes, undergo [2 + 2] cycloaddition reaction to form cyclobutene rings followed by retroelectrocyclization reaction to produce 1,1,4,4-tetracyanobutadiene (TCBD) and cyclohexa-2,5diene-1,4-diylidene-expanded TCBD or DCNQ (DCNQ=dicyanoquinodimethane) derivatives.[1–4] The D–A systems containing TCBD and DCNQ acceptors are promising candidates for organic photovoltaic applications.[5–7] Tuning the photonic properties for donor−acceptor systems can be achieved by changing the strength of donor or acceptor units and the connecting π-linker.[8–10] The cross-conjugated systems with strong electron-acceptor TCBD and DCNQ groups have recently been used in organic electronic devices due to their strong and wide electronic absorption in the visible to near-IR regions and their ability to tune the lowest unoccupied molecular orbital (LUMO) energy levels.[11, 12] The TCBD and DCNQ functionalized donor-acceptor chromophores exhibit good photochemical stability and excellent solubility in wide range of solvents.[13–15] The TCBD and DCNQ functionalized chromophores generally exhibit a strong absorption band at around 400–950 nm range corresponding to intramolecular charge transfer ($S_0 \rightarrow S_1$) transition.[16–18] The photonic properties of the TCBD and DCNQ functionalized chromophores can be modified by varying the type of the donor, acceptor, and spacer substituents. The tuning of optical and electronic properties in TCBD and DCNQ functionalized donor-acceptor chromophores have been investigated to improve the efficiency of a wide range of applications including dye-sensitized solar cells, organic

photovoltaics, nonlinear optics, organic field-effect transistors, organic light-emitting diodes, photodynamic therapy, bioimaging, and single-molecule switches.[19–22] In this context, we have systematically designed and synthesized a series of TCBD and DCNQ functionalized donor-acceptor chromophores and investigated their photophysical, electrochemical, thermal, and computational studies.

In chapter 3, a series of donor-acceptor functionalized symmetrical and unsymmetrical phenothiazine derivatives **1–18** were synthesized by the Pd-catalyzed Sonogashira cross-coupling followed by [2 + 2] cycloaddition electrocyclic ring-opening reaction with TCNE and TCNQ acceptors. The di-DCNQ substituted phenothiazine derivatives **6**, **12**, and **18** show a strong intramolecular charge transfer (ICT) band at a low energy region as compared to mono-DCNQ substituted phenothiazine derivatives **3**, **9**, and **15** due to strong donor-acceptor interaction. The electrochemical analysis reveals reduction waves at low potential due to the TCBD and DCNQ acceptors, whereas oxidation waves at high potential are due to the donor (phenothiazine, thiophene, and carbazole). In comparison to TCBD, the incorporation of DCNQ stabilizes the LUMO energy level considerably. The photophysical and electrochemical data show that the incorporation of TCBD and the DCNQ acceptor into ethynyl phenothiazine derivatives resulted in stronger D–A interactions that led to a lower HOMO–LUMO energy gap. The thermogravimetric analysis (TGA) of phenothiazine derivatives **1–18** shows that the TCBD substituted phenothiazine derivative **2** exhibits the highest thermal stability as compared to other phenothiazine derivatives. The computational studies show that the electron density on HOMO energy level is mainly localized over the donor phenothiazine, thiophene, and carbazole units, whereas the electron density on LUMO energy level is concentrated over the acceptor TCBD and DCNQ units. The proposed symmetrical and unsymmetrical phenothiazine derivatives **1–18** provide a new approach for the development of donor–acceptor chromophores, which are useful for a variety of optoelectronic applications.[23]

In chapter 4, we have designed and synthesized phenothiazine- and ynamide-based chromophores **1–6** by the Corey-Fuchs reaction *via* Evano′s conditions followed by [2 + 2] cycloaddition retroelectrocyclic ring-opening reaction with strong electron acceptors TCNE and TCNQ in good yields. The electronic absorption maxima of the DCNQ substituted **3** and **6** exhibit a significant bathochromic shift of around 100 nm, compared to those of TCBD substituted **2** and **5**, due to the strong electron-accepting nature of the DCNQ moiety. Based on the electrochemical properties, it can be observed that the reduction potential values of **3** and **6** are comparatively lower than those of **2** and **5**. This indicates that the DCNQ unit has a greater impact on the electronic properties and contributes more towards stabilizing the LUMO energy levels in comparison to the TCBD unit. In DFT calculation, the HOMO–LUMO energy gap in DCNQ functionalized **3** and **6** is lower than in TCBD functionalized derivatives **2** and **5**, because of their strong accepting character of the DCNQ unit. The TD-DFT calculations reveal significant donor–acceptor interactions and correspond well with the experimental data.[24]

In chapter 5, we have designed and synthesized symmetrical and unsymmetrical donor-acceptor based phenothiazine derivatives **1–5** by Corey-Fuchs reaction *via* Evano′s conditions followed by [2 + 2] cycloaddition–retroelectrocyclic ring-opening reaction with strong electron acceptors TCNE and TCNQ in good yields. The intramolecular charge transfer (ICT) band of DCNQ functionalized phenothiazine derivatives **4** and **5** was bathochromically shifted by ~105 nm at a longer wavelength region in comparison to phenothiazine derivatives **2** and **3** substituted with TCBD corresponding to the strong donor–acceptor (D–A) interaction. The unsymmetrical and symmetrical **1–5** exhibit three oxidation waves on the anodic region, which corresponds to donor phenothiazine and ynamide moiety. The thermogram of phenothiazine derivatives **1–5** exhibited three weight loss stages between 100 and 700 °C, with a residual mass of 40% at 600 °C. The theoretical studies indicate that the ynamides functionalized symmetrical phenothiazine **1**

with the highest HOMO–LUMO energy gap exhibits a lower wavelength region in the absorption spectra, while the TCBD/DCNQ substituted phenothiazine **2−5** exhibited red-shifted absorption in the NIR region because of the tunable HOMO–LUMO gap. The reported unsymmetrical and symmetrical phenothiazines **1–5** provide a new opportunities for the development of donor–acceptor (D–A) based chromophores with low HOMO–LUMO gaps, which are useful in various optoelectronic applications.[25]

In chapter 6, we have designed and synthesized the triphenylamine-functionalized phenothiazine derivatives **TPA-PTZ 1–3** *via* Pd-catalyzed Sonogashira cross-coupling reaction followed by [2 + 2] cycloaddition-electrocyclic ring-opening reaction and fulleropyrrolidine derivatives **TPA-PTZ-C_{60} 1–3** also with the help of 1,3-dipole cycloaddition reaction and under the condition described by Preto reaction. The photophysical spectra of fulleropyrrolidine derivatives **TPA-PTZ-C_{60}-2** and **TPA-PTZ-C_{60}-3** exhibit bathochromic shift because of intramolecular charge transfer (ICT) transition in the near-infrared region as compared to **TPA-PTZ-2** and **TPA-PTZ-3**. The electrochemical characteristics showed that the **TPA-PTZ 1–3** and **TPA-PTZ-C_{60} 1–3** produce several redox waves in cyclic voltammetry because of the availability of various acceptor units (Fullerene, TCBD, and DCNQ), and donor units (Phenothiazine and Triphenylamine). According to the computational study, the addition of the fullerene moiety stabilizes the lowest unoccupied molecular orbital (LUMO) energy level more than the TCBD and DCNQ moieties. The reported donor–acceptor based triphenylamine-functionalized phenothiazine derivatives **TPA-PTZ 1–3** and fulleropyrrolidine derivatives **TPA-PTZ-C_{60} 1–3** give up a novel route for the development of NIR-absorbing donor-acceptor chromophores for optoelectronic applications.

In chapter 7, a series of donor-acceptor-based phenothiazine chromophores **$(PTZ)_2$ 1–3** were synthesized by Pd-catalyzed Sonogashira cross-coupling and [2 + 2] cycloaddition–electrocyclic

ring-opening reaction, and fulleropyrrolidine derivatives **$(PTZ)_2$ 1–3** by 1,3-dipolar cycloaddition reaction (Prato reaction) in good yields. The photophysical properties suggest that the donor–acceptor chromophores **$(PTZ)_2$-2**, **$(PTZ)_2$-3**, **$(PTZ)_2$-C_{60}-2**, and **$(PTZ)_2$-C_{60}-3** exhibit a strong intramolecular charge transfer (ICT) band at a longer wavelength region due to the strong donor–acceptor (D–A) interactions. The electrochemical properties of phenothiazine and fulleropyrrolidine chromophores display multiple reduction potentials corresponding to the presence of numerous redox-active entities. The electrochemical data shows that incorporating cyano-based electron acceptor groups can change the redox properties of phenothiazine and fulleropyrrolidine chromophores. Furthermore, the dicyanoquinodimethane (DCNQ) unit better stabilizes the LUMO energy level compared to the tetracyanoethylene (TCBD) unit. The theoretical studies show that the LUMO energy level was stabilized by the incorporation of TCBD and DCNQ units. This stabilization resulted in a red shift in the ICT (intramolecular charge transfer) band observed in electronic absorption spectra. The reported phenothiazine chromophores **$(PTZ)_2$ 1–3** and fulleropyrrolidine derivatives **$(PTZ)_2$-C_{60} 1–3** provide a new opportunities for the development of donor–acceptor systems, which are useful in various optoelectronic applications.

8.2. Future Scope

The thesis highlights an important strategy for the design and synthesis of TCBD and DCNQ functionalized donor–acceptor chromophores with tunable photonic properties and low HOMO–LUMO gap. The HOMO–LUMO gap of the TCBD and DCNQ functionalized donor-acceptor chromophores can be modified by (a) varying the number of donor/acceptors attached, (b) enhancing the conjugation length, and (c) changing the π-linker. The variation in the donor/acceptor strength perturbs the HOMO–LUMO gap to a greater extent. The introduction of strong acceptors such as 1,1,4,4-tetracyanobutadiene (TCBD) and cyclohexa-2,5-diene-1,4-diylidene-expanded TCBD or dicyanoquinodimethane (DCNQ) moieties into the phenothiazine

derivatives resulted in systematic variation in their photophysical, electrochemical, and computational studies. The incorporation of strong acceptors like 1,1,2,2-tetracyanoethylene (TCNE) and 7,7,8,8-tetracyanoquinodimethane (TCNQ) can also enhance the donor–acceptor interactions within TCBD and DCNQ functionalized chromophores. This enhancement leads to strong intramolecular charge transfer (ICT) transitions occurring at longer wavelengths which could be extended to the near-infrared (NIR) region. The TCBD and DCNQ functionalized donor–acceptor chromophores with strong absorption and low band gap could be a promising candidate for optoelectronics and are useful in various applications including dye-sensitized solar cells, organic photovoltaics, nonlinear optics, organic field-effect transistors and organic light-emitting diodes.

8.3. References

[1] Sekita, M., Ballesteros, B., Diederich, F., Guldi, D. M., Bottari, G., & Torres, T. (2016). Intense Ground-State Charge-Transfer Interactions in Low-Bandgap, Panchromatic Phthalocyanine–Tetracyanobuta-1,3-diene Conjugates. *Angewandte Chemie*, *128*(18), 5650–5654. (DOI: 10.1002/ange.201601258).

[2] Patil, Y., Butenschön, H., & Misra, R. (2023, January 1). Tetracyanobutadiene Bridged Push-Pull Chromophores: Development of New Generation Optoelectronic Materials. *Chemical Record*. John Wiley and Sons Inc. (DOI: 10.1002/tcr.202200208).

[3] Michinobu, T., Boudon, C., Gisselbrecht, J. P., Seiler, P., Frank, B., Moonen, N. N. P., … Diederich, F. (2006). Donor-substituted 1,1,4,4-tetracyanobutadienes (TCBDs): New chromophores with efficient intramolecular charge-transfer interactions by atom-economic synthesis. *Chemistry - A European Journal*, *12*(7), 1889–1905. (DOI: 10.1002/chem.200501113).

[4] Jordan, M., Kivala, M., Boudon, C., Gisselbrecht, J. P., Schweizer, W. B., Seiler, P., & Diederich, F. (2011). Switching the regioselectivity in cycloaddition-retro-electrocyclizations

between donor-activated alkynes and the electron-accepting olefins TCNE and TCNQ. *Chemistry, an Asian journal*, *6*(2), 396–401. (DOI: 10.1002/ASIA.201000539).

[5] Zhang, H., Wan, X., Xue, X., Li, Y., Yu, A., & Chen, Y. (2010). Selective tuning of the HOMO-LUMO gap of carbazole-based donor-acceptor-donor compounds toward different emission colors. *European Journal of Organic Chemistry*, (9), 1681–1687. (DOI: 10.1002/EJOC.200901167).

[6] Leliège, A., Blanchard, P., Rousseau, T., & Roncali, J. (2011). Triphenylamine/tetracyanobutadiene-based D-A-D π-conjugated systems as molecular donors for organic solar cells. *Organic letters*, *13*(12), 3098–3101. (DOI: 10.1021/OL201002J).

[7] Finke, A. D., Dumele, O., Zalibera, M., Confortin, D., Cias, P., Jayamurugan, G., … Diederich, F. (2012). 6,6-Dicyanopentafulvenes: Electronic structure and regioselectivity in [2 + 2] cycloaddition-retroelectrocyclization reactions. *Journal of the American Chemical Society*, *134*(43), 18139–18146. (DOI: 10.1021/JA309141R).

[8] Bureš, F., Bernd Schweizer, W., May, J. C., Boudon, C., Gisselbrecht, J. P., Gross, M., … Diederich, F. (2007). Property Tuning in Charge-Transfer Chromophores by Systematic Modulation of the Spacer between Donor and Acceptor. *Chemistry – A European Journal*, *13*(19), 5378–5387. (DOI: 10.1002/CHEM.200601735).

[9] Wang, J. L., Xiao, Q., & Pei, J. (2010). Benzothiadiazole-based D-π-A-π-D organic dyes with tunable band gap: Synthesis and photophysical properties. *Organic Letters*, *12*(18), 4164–4167. (DOI: 10.1021/ol101754q).

[10] Zhang, W. W., Mao, W. L., Hu, Y. X., Tian, Z. Q., Wang, Z. L., & Meng, Q. J. (2009). Phenothiazine - anthraquinone donor - acceptor molecules: Synthesis, electronic properties and DFT-TDDFT computational study. *Journal of Physical Chemistry A*, *113*(37), 9997–10004. (DOI: 10.1021/jp903390v).

[11] Michinobu, T., May, J. C., Lim, J. H., Boudon, C., Gisselbrecht, J. P., Seiler, P., … Diederich, F. (2005). A new class of organic donor–acceptor molecules with large third-order optical nonlinearities. *Chemical Communications*, (6), 737–739. (DOI: 10.1039/B417393G).

[12] Breiten, B., Jordan, M., Taura, D., Zalibera, M., Griesser, M., Confortin, D., … Diederich, F. (2013). Donor-substituted octacyano[4]dendralenes: Investigation of π-electron delocalization in their radical ions. *Journal of Organic Chemistry*, *78*(5), 1760–1767. (DOI: 10.1021/jo301194y).

[13] Erden, K., & Dengiz, C. (2022). 3-Alkynylindoles as Building Blocks for the Synthesis of Electronically Tunable Indole-Based Push-Pull Chromophores. *Journal of Organic Chemistry*, *87*(6), 4385–4399. (DOI: 10.1021/ACS.JOC.2C00067).

[14] Misra, R., & Gautam, P. (2014). Tuning of the HOMO–LUMO gap of donor-substituted symmetrical and unsymmetrical benzothiadiazoles. *Organic & Biomolecular Chemistry*, *12*(29), 5448. (DOI: 10.1039/c4ob00629a).

[15] Philippe, C., Melan, J., Barsella, A., Vives, T., Leroux, Y. R., Robin-Le Guen, F., … Trolez, Y. (2023). A comprehensive study of tetracyanobutadiene push-pull chromophores derived from γ-pyranylidene. *Tetrahedron Chem*, *5*, 100036. (DOI: 10.1016/J.TCHEM.2023.100036).

[16] Jang, Y., Sekaran, B., Singh, P. P., Misra, R., & Souza, F. D'. (2023). Accelerated Intramolecular Charge Transfer in Tetracyanobutadiene-and Expanded Tetracyanobutadiene-Incorporated Asymmetric Triphenylamine−Quinoxaline Push−Pull Conjugates. *J. Phys. Chem. A*, *2023*, 4462. (DOI: 10.1021/acs.jpca.3c01732).

[17] Yadav, I. S., Kaswan, R. R., Liyanage, A., Misra, R., & D'Souza, F. (2024). Dimethylaniline-Tetracyanobutadiene and Dimethylaniline-Extended-Tetracyanobutadiene Functionalized BODIPYs Witnessing Ultrafast Charge Transfer. *The Journal of*

Physical Chemistry C, *128*(12), 4934–4945. (DOI: 10.1021/acs.jpcc.4c00072).

[18] Philippe, C., Bui, A. T., Batsongo-Boulingui, S., Pokladek, Z., Matczyszyn, K., Mongin, O., … Trolez, Y. (2021). 1,1,4,4-Tetracyanobutadiene-Functionalized Anthracenes: Regioselectivity of Cycloadditions in the Synthesis of Small Near-IR Dyes. *Organic Letters*, *23*(6), 2007–2012. (DOI: 10.1021/ACS.ORGLETT.1C00136).

[19] Shoji, T., Miura, K., Araki, T., Maruyama, A., Ohta, A., Sekiguchi, R., … Okujima, T. (2018). Synthesis of 2-Methyl-1-azulenyl Tetracyanobutadienes and Dicyanoquinodimethanes: Substituent Effect of 2-Methyl Moiety on the Azulene Ring toward the Optical and Electrochemical Properties. *The Journal of organic chemistry*, *83*(12), 6690–6705. (DOI: 10.1021/ACS.JOC.8B01067).

[20] Yadav, I. S., & Misra, R. (2022). Phenothiazine and phenothiazine-5,5-dioxide-based push–pull derivatives: synthesis, photophysical, electrochemical and computational studies. *New Journal of Chemistry*, *46*(33), 15999–16006. (DOI: 10.1039/D2NJ03089F).

[21] Srinivasa Rao, P., Gupta, A., Bhosale, S. V., Bilic, A., Xiang, W., Evans, R. A., & Bhosale, S. V. (2017). Donor–acceptor–acceptor-based non-fullerene acceptors comprising terminal chromen-2-one functionality for efficient bulk-heterojunction devices. *Dyes and Pigments*, *146*, 502–511. (DOI: 10.1016/j.dyepig.2017.07.047).

[22] Rao, P. S., More, V. G., Jangale, A. D., Bhosale, S. V., Bhosale, R. S., Puyad, A. L., … Sharma, G. D. (2019). A series of V-shaped small molecule non-fullerene electron acceptors for efficient bulk-heterojunction devices. *Dyes and Pigments*, *171*, 107677. (DOI: 10.1016/j.dyepig.2019.107677).

[23] Gupta, P. K., Khan, F., & Misra, R. (2023). NIR-Absorbing 1,1,4,4-Tetracyanobuta-1,3-diene- and Dicyanoquinodimethane-Functionalized Donor-Acceptor

Phenothiazine Derivatives: Synthesis and Characterization. *Journal of Organic Chemistry*, *88*(20), 14308–14322. (DOI: 10.1021/ACS.JOC.3C01029).

[24] Gupta, P. K., Das, S., Misra, R., & D'Souza, F. (2024). Near-IR Capturing N-Methylbenzene Sulfonamide-Phenothiazine Incorporating Strong Electron Acceptor Push-Pull Systems: Photochemical Ultrafast Carrier Dynamics. *Chemistry – A European Journal*, e202304313. (DOI: 10.1002/CHEM.202304313).

[25] Gupta, P. K., Das, S., Misra, R., & D'Souza, F. (2025). Acceptor-Dependent Intervalence Charge Transfer and Separation Dynamics in Broad-Band-Capturing Push–Pull Chromophores. *Journal of Physical Chemistry C*, *129*(14), 6924–6942. (DOI: 10.1021/acs.jpcc.5c01681).